Mathematics scope

Seq.	Title	Authors	Job address
1	Study of G-Bi-shadowing property in Nilpotent Group	Mohammed H. O. Ajam , Samer Adnan Jubair, Hawraa Imad Kadhim	Pathological Analysis Department, College of Science, Al-Qasim Green University, Babylon 51013, Iraq
2	New Results on Fuzzy Banach Space	Shireen Ayed Karim and Noor F. Al-Mayahi	Department of Mathematics College of science, University of AL-Qadisiyah, Diwaniyah-Iraq
3	ON CONVERGENCES IN FUZZY SOFT NORMED SPACES	Qasim Ali Hatif And Noori F. Al-Mayahi	Department of Mathematics College of Science University of Qadisiyah, Diwaniyah, Iraq
4	Some new results related with Fuzzy soft spectrum	Afrah Sadeq Kadhim and Noori F.Al-Mayahi	Department of Mathematics, College of Science, University of Al-Qadisiyah, Diwaniyah-Iraq
5	توليد خماسيّة فيثاغوريّة من خماسيتين فيثاغوريّتين	الدكتور باسل حمدو العرنوس, الأستاذ الدكتور عبد الباسط الخطيب	جامعة البعث , كلية التربية الثانية
6	خوارزمية تشفير متناظرة بمفتاح ثنائي, باستخدام فيثاغوريّات مولّدة بعدد فردي	د. نجوى أحمد نجوم	جامعة البعث (حمص – سوريا)

7	دراسة في بنية الخماسيات الفيثاغورية الجبريّة, واستخدامها في توليد فيثاغوريّات	الدكتور باسل حمدو العرنوس, الأستاذ الدكتور عبد الباسط الخطيب	جامعة كلية التربية الثانية , البعث
8	دراسة لعبة Maker-Breaker الموضعية على بيانات خاصة	د. هديل برباره، د. رياض الحميدو، مالك الخضير	قسم الرياضيات، كلية العلوم، جامعة تشرين، اللاذقية
	Physics scope		
1	Physics of Pulsed Laser Deposition (PLD)	Intesar Dakhel Shakhir Aljenabi	
2	Calculation of The Energies of 1s and 2s shells for (C,N+1,O+2,F+3,Ne+4,Na+5) systems Using Hartree-Fock wave function	Maryam Hakim AL-Quraishi Qassim Shamkhi AL-Khafaji Ameer F. Shamkhi1 shaymaa awad kadhim[d]	Department of Physics//Faculty of Science/ University of Kufa / Najaf/ Iraq
3	Thermoelectric properties of zintl phase antimonite compounds, $Eu_{0.6}Yb_{0.4}Zn_2Sb_2$, $YbCd_{1.6}Zn_{0.4}Sb_2$, $YbZn_{1.6}Mn_{0.4}Sb_2$ prepared by microwave-assisted solid-state technique	IBRAHIM MAJEED JASIM, A. HMOOD	Physics Department, College of Science, University of Basrah, Basrah, Iraq.
4	Heavy Metal Removal from Basrah waste water via Fe2O3 Nanocrystals	Anwar A. Jumaa1, Salwa A.	

		Abduljaleel2, Zuhair A. Abdulnabi1, Abdulzahra A.N. AlHello1,	
Computer scope			
1	Classification of supervised deep learning models for Covid-19 tweets sentiment analysis	Rusul Mohammed alkhafaji[a] shaymaa awad kadhim[b] Humam Adnan Sameer[C] Doaa hadi abid muslim[d]	University of Kufa
2	Accurate Pupil Detection Using the Multi Wavelet Transform (MWT) and the Hough Transform (HT)	Sara Hassan Awad Al-Taee, Ban Hamid Abdul Ridha	Wasit Education Directorate/Al-Rabab High School for Distinguished Grils
3	Drone Management System for Hunting Unauthorized Drones	Suhair Mohammed Zeki Abd Alsammed	Department of Computer Science, University of Technology, Baghdad, Iraq.
4	Survey of Verification Communication Protocol Security using Computational Models	ghadee ribrahima	Technical Institute of Al-Diwaniyah, Al-Furat Al-Awsat Tehnical University (ATU), Al-Diwaniyah, Iraq

Statics scope

1	Estimating the Gini index from Beta-Normal distribution	Waleed Ahmed Hassen Al-Nuaami	Department of Biology, College of Education for Pure Sciences, University of Diyala

المؤتمر العلمي الدولي الثالث عشر
لجمعية الرياضيات العراقية والمنعقد تحت شعار
نحو عالم متقدم : الرياضيات والتقنيات في سباق الابتكار
للمدة 24 - 25 نيسان 2024
الكوفة – النجف الاشرف

Study of G-Bi-shadowing property in Nilpotent Group

Mohammed H. O. Ajam[(1)] , Samer Adnan Jubair[(2)] , Hawraa Imad Kadhim[(3)]

[1,2] Pathological Analysis Department, College of Science, Al-Qasim Green University, Babylon 51013, Iraq.

[3] Medical Biotechnology Department, Biotechnology College, Al-Qasim Green University, Babylon 51013, Iraq.

[1] Corresponding Author: mohammed_ajam@science.uoqasim.edu.iq

Abstract

In this paper, we investigated the property of bi-shadowing for actions of certain finitely generated groups. We have given a definition of the term Bi-Conditions and mentioning some key definitions with example. We have formulated the text of the reductive bi-shadowing theory (through which we set sufficient conditions for the action to have the bi-shadowing property) and we try to prove it by formulating and proving some lemmas that complement one another in order to arrive at proving the main theorem in the paper.

Keywords: group action, shadowing, inverse shadowing, bi-shadowing, virtually nilpotent group.

1- Introduction:

The shadowing property is considered one of the important properties in the study of dynamic systems because it has multiple applications of importance in different fields of life. This is what made scientists continue to study it and develop it into the inverse shadowing property and the bi-shadowing property, as well as studying it in different spaces. This paper aims to study the G-Bi shading property (which means the binary shading property in group space) in the Nilpotent group.

In the second chapter of this paper, we present the basic definitions, including the shadowing property, the inverse shadowing property, and the bi-shadowing property in group space. You can review [1, 2, 3, 4] for more details.

In the third chapter of this paper, we aim to formulate the text of the reductive bi-shadowing theory (through which we set sufficient conditions for the action to have the bi-shadowing property) and we try to prove it by formulating and proving some lemmas that complement each other to arrive at proof of the main theory in the paper. This result will be motivated by a similar results for shadowing and inverse shadowing that was proven in [5, 2].

2- Preliminaries

In this section, we will discuss a set of definitions that we will need in the body of the paper, some of them are basic definitions that you need to form the basic structure of theories, and others we will need to prove those theories.

Considering that the definitions of the group and subgroup are trivial, below we will present the definition of the normal subgroup, commutator, Abelian group, nilpotent group and the virtually nilpotent.

Definitions 2.1 [2, 5]: Assume that $\mathbb{C}$ is a group and $\mathbb{E}$ is a normal subgroup in $\mathbb{C}$ (write $\mathbb{E} \lhd \mathbb{C}$) which satisfy $\mathbb{c}\mathbb{E} = \mathbb{E}\mathbb{c}$, for $\mathbb{c} \in \mathbb{C}$.

And for $\mathbb{c}' \in \mathbb{C}$ then a commutator of $\mathbb{c}$ and $\mathbb{c}'$ satisfy: $[\mathbb{c}, \mathbb{c}'] = \mathbb{c}\mathbb{c}'\mathbb{c}^{-1}\mathbb{c}'^{-1}$

If $\mathbb{E}_1, \mathbb{E}_2$ are subgroups of $\mathbb{C}$, then a commutator of them $[\mathbb{E}_1, \mathbb{E}_2]$ is generated by $[\mathbb{c}_1, \mathbb{c}_2]$, where $\mathbb{c}_1 \in \mathbb{E}_1, \mathbb{c}_2 \in \mathbb{E}_2$.

The group $\mathbb{C}$ is called nilpotent (class n) if there exist n of subgroups $\mathbb{E}_1, \dots, \mathbb{E}_{n+1}$ satisfy

$$\mathbb{C} = \mathbb{E}_1 \rhd \cdots \rhd \mathbb{E}_{n+1} = e, \text{ for } \mathbb{E}_n \neq e, \text{ and } \mathbb{E}_{i+1} = [\mathbb{E}_i, \mathbb{C}].$$

Therefore; the Abelian group is nilpotent (class 1).

Let a group $\mathbb{C}$ is a finitely generated then we called virtually nilpotent if we find subgroup $\mathbb{E}$ of $\mathbb{C}$ which is a normal nilpotent and have finite index (i.e. $\mathbb{C}/\mathbb{E}$ is finite (factor group)).

Example 2.2 [6, 7]: Heisenberg group is nilpotent group, and Polynomial growth group is virtually nilpotent.

In the following definitions, theories and proofs, we will suppose that the group action $\Psi: \mathbb{C} \times \mathbb{S} \to \mathbb{S}$ of a finitely generated group $\mathbb{C}$ on a metric group space $(\mathbb{S}, \mathbb{d})$ and the properties with respect to the generating set $\mathbb{W}$, (any generating set of $\mathbb{C}$) for short we write (w.r.t.).

Definition 2.3 [2]: the continuity of an action Ψ is called a uniform if for some generating set $\mathbb{W}$, any $\Psi(\mathbb{w}, .), \mathbb{w} \in \mathbb{W}$, is uniformly continuous. And in this paper we suppose the continuity of an action Ψ is uniform

Below we mention the shadowing definition, therefore, we need to provide the definition of the pseudo-orbit. For $\rho > 0$, the concept ρ-pseudo-orbit of an action Ψ refers to the sequence $\{y_{\mathbb{c}}: \mathbb{c} \in \mathbb{C}\}$ that satisfies: $\mathbb{d}\left(y_{\mathbb{w}\mathbb{c}}, \Psi_{\mathbb{w}}(y_{\mathbb{c}})\right) < \rho,\ \mathbb{w} \in \mathbb{W}, \mathbb{c} \in \mathbb{C}$. [5]

Definition 2.4 [5]: The concept shadowing property on a set $\mathbb{M} \subset \mathbb{S}$ w.r.t. $\mathbb{W}$ for short we write (S.P.$\mathbb{M}$.$\mathbb{W}$.) refers to an action Ψ that satisfies: if for any $\varepsilon > 0$ there exists $\rho > 0$ such that for any ρ-pseudo-orbit $\{x_{\mathbb{c}} \in \mathbb{M}\}$ w.r.t.$\mathbb{W}$ there exists an exact-orbit $\{p_{\mathbb{c}} = \Psi(\mathbb{c}, p_e): \mathbb{c} \in \mathbb{C}\}$ of Ψ satisfying the inequalities

$$\mathbb{d}(p_{\mathbb{c}}, x_{\mathbb{c}}) < \varepsilon, \qquad \mathbb{c} \in \mathbb{C}. (1)$$

Proposition 2.5 [5]: Assume that $\mathbb{W}$ and $\mathbb{W}'$ are finite, symmetric, generating sets of $\mathbb{C}$. An action Ψ has S.P.$\mathbb{M}$.$\mathbb{W}$., if and only if it has S.P.$\mathbb{M}$.$\mathbb{W}'$.

Below we mention the inverse shadowing definition, therefore, we need to provide the definition of the method and the orbit of it. For $\rho > 0$, the concept ρ-method for Ψ w.r.t. $\mathbb{W}$ refers to a family $\Gamma = \{\gamma_{\mathbb{c}} \in C(\mathbb{S}, \mathbb{S}): \mathbb{c} \in \mathbb{C}\}$ that satisfies:

$$\mathbb{d}\left(\gamma_{\mathbb{w}\mathbb{c}}(x), \Psi\left(\mathbb{w}, \gamma_{\mathbb{c}}(x)\right)\right) < \rho, \qquad \mathbb{c} \in \mathbb{C}, \mathbb{w} \in \mathbb{W}, x \in \mathbb{S};\ (2)$$

And an orbit of the method Γ is a family $\{\chi_{\mathbb{c}} = \gamma_{\mathbb{c}}(x_e) \in \mathbb{S}: \mathbb{c} \in \mathbb{C}\}$. (for $\gamma_e = \mathrm{Id}$)

Definition 2.6 [2]: The concept inverse shadowing property w.r.t. $\mathbb{W}$ for short we write (I.S.P.$\mathbb{W}$.) refers to an action Ψ that satisfies: if for any $\varepsilon > 0$ there exists a $\rho > 0$ such that for any $p \in \mathbb{S}$ and any ρ-method Γ with respect to the generating set $\mathbb{W}$ there exists an orbit $\{\chi_{\mathbb{c}}\}$ of Γ satisfying

$$\mathbb{d}(\Psi(\mathbb{c}, p), \chi_{\mathbb{c}}) < \varepsilon, \qquad \mathbb{c} \in \mathbb{C}.$$

Below we mention the bi-shadowing definition, therefore, we need to provide the definition of distance between two actions. For Ψ and φ are actions, the distance between them is given by:

$$\mathbb{d}_0(\Psi, \varphi) = \sup_{x \in \mathbb{X}} \{\mathbb{d}\left(\Psi(\mathbb{s}, x), \varphi(\mathbb{s}, x)\right)\} \text{ for } \mathbb{s} \in \mathbb{S}.$$

Definition 2.7 [3]: The concept bi-shadowing property w.r.t. $\mathbb{W}$ for short we write (B.S.P.$\mathbb{W}$.) refers to an action Ψ that satisfies: if for any $\varepsilon > 0$ there exists $\alpha > 0$ and $0 < \delta \leq {}^{\varepsilon}/_{\alpha}$ such that for any δ-pseudo-orbit $\{y_{\mathbb{c}} : \mathbb{c} \in \mathbb{C}\}$ of Ψ and any action $\varphi \in C(\mathbb{S}, \mathbb{S})$ satisfying $\mathbb{d}_0(\Psi, \varphi) \leq {}^{\varepsilon}/_{\alpha} - \delta$ then there exists an orbit $\{x_{\mathbb{c}} : \mathbb{c} \in \mathbb{C}\}$ of φ such that

$$\mathbb{d}(x_{\mathbb{c}}, y_{\mathbb{c}}) \leq \alpha\big(\delta + \mathbb{d}_0(\Psi, \varphi)\big) \leq \varepsilon, \text{ for all } \mathbb{c} \in \mathbb{C},$$

Below we mention the expansive definition.

Definition 2.8 [5]: The concept expansive property on a set $\mathbb{M} \subset \mathbb{S}$ for short we write (E.P.$\mathbb{M}$.) refers to an action Ψ that satisfies: if there exists $a > 0$ such that if $\Psi(\mathbb{c}, x), \Psi(\mathbb{c}, y) \in \mathbb{M}$, $\mathbb{d}\big(\Psi(\mathbb{c}, x), \Psi(\mathbb{c}, y)\big) \leq a,\ x, y \in \mathbb{S}, \mathbb{c} \in \mathbb{C}$, then $x = y$.

We now present the main definition in this paper (Bi-Conditions), which brings together the main conditions for achieving it.

Definition 2.9: Consider two sets $\mathbb{M}, \mathbb{N} \subset \mathbb{S}$. We say that an action Ψ satisfies the Bi-Conditions w.r.t. $(\mathbb{M}, \mathbb{N})$ for short we write (B.C.$\mathbb{M}, \mathbb{N}$) if the following conditions are satisfied:

C1- there exists $\gamma > 0$ such that $B(\gamma, \mathbb{N}) \subset \mathbb{M}$;

C2- Ψ has (S.P.$\mathbb{N}$.);

C3- Ψ has (I.S.P.);

C4- Ψ is (E.P.$\mathbb{M}$.).

3- Main Theorem.

The following establish the reductive bi-shadowing theorem (RBST), which will provide sufficient conditions for an action of a virtually nilpotent group to possess the bi-shadowing property.

Theorem. Let Ψ be an action of a finitely generated virtually nilpotent group $\mathbb{C}$. Assume that there exists $\mathbb{c} \in \mathbb{C}$ such that $\Psi|_{\langle \mathbb{c} \rangle}$ satisfies (B.C.$\mathbb{M}, \mathbb{N}$). Then an action Ψ has (B.S.P.).

To prove the above theorem, we will present some interconnected lemmas and prove them to arrive at the final proof. Some results, for brevity, we will refer to in other sources and others we will prove.

Lemma 1. Let $\mathbb{E}$ be finitely generated normal subgroup of $\mathbb{C}$. If $\Psi|_{\mathbb{E}}$ satisfies (B.C.$\mathbb{M}, \mathbb{N}$). Then an action Ψ satisfies (B.C.$\mathbb{M}, \mathbb{N}$).

Proof:

Chose a finitely symmetric generate set $\mathbb{W}_{\mathbb{E}}$ in $\mathbb{E}$ and also it to a finitely symmetric generate set $\mathbb{W}$ in $\mathbb{C}$. By using Proposition 2.5, suppose that the generating set $\mathbb{W}$ was chose in the same way.

To prove an action Ψ satisfies (B.C.$\mathbb{M}, \mathbb{N}$) we must prove an action Ψ satisfies C1, C2, C3, and C4 in Definition 2.9.

C1 is trivial. To prove C2, we must prove an action Ψ has shadowing property, let $\Delta, \gamma > 0$ be the constants from the definitions of (B.C.$\mathbb{M}, \mathbb{N}$) for $\Psi|_{\mathbb{E}}$. Since the continuity of an actions $\{\Psi(\mathbb{w}, .): \mathbb{w} \in \mathbb{W}\}$ are uniform, there exists $\delta < min(\Delta/3, \gamma)$ such that

$$\mathbb{d}\big(\Psi(\mathbb{w}, x), \Psi(\mathbb{w}, y)\big) < \Delta/3 \quad (3)$$

for any $\mathbb{w} \in \mathbb{W}$ and any two points $x, y \in \mathbb{S}$ satisfying $\mathbb{d}(x, y) < \delta$.

Fix $\varepsilon \in (0, \delta)$ and choose $\rho < \varepsilon$ from the definition of shadowing for $\Psi|_{\mathbb{E}}$ for the generating set $\mathbb{W}_{\mathbb{E}}$. Fix a ρ-pseudo-orbit $\{y_{\mathbb{c}} \in \mathbb{N}: \mathbb{c} \in \mathbb{C}\}$ of Ψ.

For each element $q \in \mathbb{C}$ if we take the sequence $\{z_{\mathbb{e}'} = y_{\mathbb{e}'q}: \mathbb{e}' \in \mathbb{E}\}$. We note that this sequence is a ρ-pseudo-orbit of $\Psi|_{\mathbb{E}}$. And since $\Psi|_{\mathbb{E}}$ satisfies (B.C.$\mathbb{M}, \mathbb{N}$), then there exists a unique point $x_q \in \mathbb{M}$ such that

$$\mathbb{d}\left(z_{\mathbb{e}'}, \Psi(\mathbb{e}', x_q)\right) = \mathbb{d}\left(y_{\mathbb{e}'q}, \Psi(\mathbb{e}', x_q)\right) < \varepsilon, \qquad \mathbb{e}' \in \mathbb{E}. \ (4)$$

This existence of x_q can be from (C2), and the uniqueness from (C1), (C4), and the inequality $\varepsilon < \gamma$.

Let us prove the sequence $\{x_q: q \in \mathbb{C}\}$ is an exact-orbit.

Fix $\mathbb{w} \in \mathbb{W}$ and $q \in \mathbb{C}$. Consider an arbitrary element $\mathbb{e} \in \mathbb{E}$. Since $\mathbb{E}$ is a normal subgroup of $\mathbb{C}$, there exists an element $\mathbb{e}' \in \mathbb{E}$ such that

$$\mathbb{w}\mathbb{e}' = \mathbb{e}\mathbb{w}. \quad (5)$$

It follows from (3)–(5) that

$$\mathbb{d}\left(y_{\mathbb{w}\mathbb{e}'q}, \Psi(\mathbb{e}, x_{\mathbb{w}q})\right) < \epsilon \ (6)$$

$$\mathbb{d}\left(\Psi(\mathbb{w}, y_{\mathbb{e}'q}), \Psi\left(\mathbb{e}', (x_q)\right)\right) < \Delta/3. \ (7)$$

Since $\{y_{\mathbb{c}}: \mathbb{c} \in \mathbb{C}\}$ is a ρ-pseudo-orbit for Ψ, it follows from (5)–(7) that

$$\mathbb{d}\left(\Psi(\mathbb{e}, x_{\mathbb{w}q}), \Psi\left(\mathbb{w}, \Psi\left(\mathbb{e}, (x_q)\right)\right)\right)$$

$$\leq \mathbb{d}\big(\Psi(\mathbb{e}, x_{\mathbb{w}q}), y_{\mathbb{w}\mathbb{e}'q}\big) + \mathbb{d}\left(y_{\mathbb{w}\mathbb{e}'q}, \Psi(\mathbb{w}, y_{\mathbb{e}'q})\right)$$

$$+ \mathbb{d}\left(\Psi(\mathbb{w}, y_{\mathbb{e}'q}), \Psi\left(\mathbb{w}, \Psi\left(\mathbb{e}, (x_q)\right)\right)\right) \leq \epsilon + \rho + \Delta/3 < \Delta.$$

Because the expansivity of $\Psi|_{\mathbb{E}}$ on $\mathbb{M}$, we infer

$$x_{\mathbb{w}q} = \Psi(\mathbb{w}, x_q), \qquad \mathbb{w} \in \mathbb{W}, q \in \mathbb{C}.$$

Because $\mathbb{W}$ is a generating set for $\mathbb{C}$, then $x_q = \Psi(q, x_e)$, for all $q \in \mathbb{C}$, and by (4) x_e satisfies inequalities (1).

Hence an action Ψ has shadowing property.

To prove C3, we must prove an action Ψ has inverse shadowing property, let $\rho' = \rho'(\delta) < \Delta/3$ for this δ from the definition of inverse shadowing for $\Psi|_{\mathbb{E}}$. Let Γ be a ρ'-method for Ψ.

Fix an arbitrary point $p \in \mathbb{S}$ and an element $\mathbb{c} \in \mathbb{C}$. By inequalities (2) we get that the following

$$\mathbb{d}\left(\gamma_{\mathbb{w}\mathbb{e}\mathbb{c}}(x), \Psi\left(\mathbb{w}, \gamma_{\mathbb{e}\mathbb{c}}(x)\right)\right) < \rho' \quad (8)$$

are satisfied (for any $\mathbb{w} \in \mathbb{W}$ and $\mathbb{e} \in \mathbb{E}$), that is the set

$$\Gamma|_{\mathbb{E}}(\mathbb{c}) = \{\gamma_{\mathbb{e}\mathbb{c}} : \mathbb{e} \in \mathbb{E}\}$$

is a ρ'-method for $\Psi|_{\mathbb{E}}$ (Note that (8) are satisfied for any $\mathbb{e} \in \mathbb{E}$ and $\mathbb{w} \in \mathbb{W}$ not just for $\mathbb{e} \in \mathbb{E}$ and $\mathbb{w} \in \mathbb{W}_{\mathbb{E}}$, as its application follows.).

By the definitions of inverse shadowing for $\Psi|_{\mathbb{E}}$, there exists a non-empty set $Z(\mathbb{c}, p)$ of $\mathbb{S}$ such that

$$\{\gamma_{\mathbb{e}\mathbb{c}}(z) : \mathbb{e} \in \mathbb{E}, z \in Z(\mathbb{c}, p)\} \text{ satisfying } \rho'\text{-method.} \quad (9)$$

(we shadow the true-orbit of $\Psi(\mathbb{c}, p)$ with respect to the action of $\mathbb{E}$), which means that

$$\mathbb{d}\left(\gamma_{\mathbb{e}\mathbb{c}}(z), \Psi\left(\mathbb{e}, \Psi(\mathbb{c}, p)\right)\right) < \delta, \qquad \mathbb{e} \in \mathbb{E}, \qquad z \in Z(\mathbb{c}, p). \quad (10)$$

Now, we take an arbitrary $\mathbb{w} \in \mathbb{W}$. Let us take $\mathbb{e} \in \mathbb{E}$ and $z \in Z(\mathbb{c}, p)$ and estimate

$$\mathbb{d}\left(\gamma_{\mathbb{e}\mathbb{w}\mathbb{c}}(z), \Psi(\mathbb{e}\mathbb{w}\mathbb{c}, p)\right).$$

Since $\mathbb{E}$ is a normal subgroup of $\mathbb{C}$, there is an element $\mathbb{e}' \in \mathbb{E}$ such that

$$\mathbb{w}\mathbb{e}' = \mathbb{e}\mathbb{w}.$$

Then,

$$\mathbb{d}\left(\gamma_{\mathbb{e}\mathbb{w}\mathbb{c}}(z), \Psi(\mathbb{e}\mathbb{w}\mathbb{c}, p)\right) = \mathbb{d}\left(\gamma_{\mathbb{w}\mathbb{e}'\mathbb{c}}(z), \Psi(\mathbb{e}\mathbb{w}\mathbb{c}, p)\right) \leq$$

$$\leq \mathbb{d}\left(\gamma_{\mathbb{w}\mathbb{e}'\mathbb{c}}(z), \Psi\left(\mathbb{w}, \gamma_{\mathbb{e}'\mathbb{c}}(z)\right)\right) + \mathbb{d}\left(\Psi\left(\mathbb{w}, \gamma_{\mathbb{e}'\mathbb{c}}(z)\right), \Psi\left(\mathbb{w}, \Psi(\mathbb{e}'\mathbb{c}, p)\right)\right) \leq$$

$\leq \rho' + \Delta/3 < \Delta$. (By (9), (10) (with $\mathbb{e} = \mathbb{e}'$) and (3)).

Note that $\Psi\left(\mathbb{w}, (\mathbb{e}'\mathbb{c}, p)\right) = \Psi(\mathbb{w}\mathbb{e}'\mathbb{c}, p) = \Psi(\mathbb{e}\mathbb{w}\mathbb{c}, p)$.

By the definitions of inverse shadowing for $\Psi|_{\mathbb{E}}$,

$$\mathbb{d}\left(\gamma_{\mathbb{e}\mathbb{w}\mathbb{c}}(z), \Psi(\mathbb{e}\mathbb{w}\mathbb{c}, p)\right) < \delta, \qquad \text{for } \mathbb{e} \in \mathbb{E}.$$

This shows that $Z(\mathbb{c},p) \subset Z(\mathbb{wc},p)$. But the above reasoning is symmetric, and we conclude that $Z(\mathbb{wc},p) \subset Z(\mathbb{c},p)$.Hence, the set $Z(\mathbb{c},p)$ is, in fact, independent of $\mathbb{c}$ (let us denote this set by $Z(p)$).

Then, we can take $\mathbb{e} = e$ in (10) to conclude that

$$\mathbb{d}\big(\gamma_{\mathbb{c}}(z), \Psi(\mathbb{c},p)\big) < \delta$$

for any $\mathbb{c} \in \mathbb{C}$, which gives us the definitions of inverse shadowing for Ψ.

The proof of C4 (Expansivity of Ψ) is trivial. ■

Lemma 2: If Ψ is an action of a nilpotent group $\mathbb{C}$ of class n, $\mathbb{c} \in \mathbb{C}$, and $\Psi|_{\mathbb{c}}$ satisfies (B.C.$\mathbb{M},\mathbb{N}$), then also Ψ satisfies (B.C.$\mathbb{M},\mathbb{N}$). Which clear implies that Ψ has bi-shadowing property.

Proof: By induction:

We take $n = 1$, therefore $\mathbb{C}$ is abelian group; and we infer, $\langle \mathbb{c} \rangle$ is a normal subgroup of $\mathbb{C}$, and Therefore, we conclude the above statement from result 1(after compensation $\mathbb{E} = \langle \mathbb{c} \rangle$).

If we take $n > 1$ and suppose that the lemma 2 statement proved for nilpotent groups when the class not exceed $n-1$.

We will need to use the helper text below to complete the proof using the same assumptions in Lemma 2.

Lemma 3 [5]: Let $Q = [\mathbb{C},\mathbb{C}]$, let $\mathbb{c} \in \mathbb{C}$, and let $\mathcal{M} = \langle Q, \mathbb{c} \rangle$ (i.e. $\mathcal{M}$ is the minimal subgroup of $\mathbb{C}$ containing Q and $\mathbb{c}$), then

1. $\mathcal{M}$ is a normal subgroup of a group $\mathbb{C}$.
2. $\mathcal{M}$ is a nilpotent group of class not exceed n – 1.

Now we continue to proof Lemma 2.

Clear that any normal subgroup of a finite generating nilpotent group is finite generating. Therefore, $\mathcal{M}$ is a finite generating nilpotent group of class not exceed $n - 1$, $\mathbb{c} \in \mathcal{M}$, and $\Psi|_{\langle \mathbb{c} \rangle}$ satisfy the conditions of (B.C.$\mathbb{M},\mathbb{N}$).

Now our induction assumption implies that $\Psi_{\mathcal{M}}$ satisfy the conditions of (B.C.$\mathbb{M},\mathbb{N}$). And by the Lemma 3:1 and Lemma 1 we get that Ψ satisfy the conditions of (B.C.$\mathbb{M},\mathbb{N}$). ■

Below we complete the proof of main Theorem (RBST).

Proof: where the group $\mathbb{C}$ is a virtually nilpotent, we can find a normal nilpotent subgroup $\mathbb{E}$ of finite index of group $\mathbb{C}$. Let $\mathfrak{c} \in \mathbb{C}$ that satisfy the conditions of (B.C.$\mathbb{M}$, $\mathbb{N}$). Because that $\mathbb{E}$ has finite index, we can there exists $k > 0$ such that $\mathfrak{c}^k \in \mathbb{E}$. And the action $\Psi|_{\langle \mathfrak{c} \rangle}$ satisfy the conditions of (B.C.$\mathbb{M}$, $\mathbb{N}$); hence, the action $\Psi|_{\langle \mathfrak{c}^k \rangle}$ also satisfy the conditions of (B.C.$\mathbb{M}$, $\mathbb{N}$). By Lemma 2, $\Psi|_{\mathbb{E}}$ satisfies (B.C.$\mathbb{M}$, $\mathbb{N}$). Thus, by apply Lemma 1 to $\mathbb{C}$ and $\mathbb{E}$, we complete the proof. ■

References:

1- Pilyugin, S. Y., & Tikhomirov, S. B. (2003). Shadowing in actions of some abelian groups. *Fundamenta Mathematicae*, *179*(1), 83-96.
2- Pilyugin, S. Y. (2017). Inverse shadowing in group actions. *Dynamical Systems*, *32*(2), 198-210.
3- Ajam, M. H. O., & Al-Shara'a, I. M. T. (2021). Study of Chaotic Behaviour with G-Bi-Shadowing Property. *Journal of the College of Basic Education*, *2*(SI), 110-122.
4- Ajam, M. H. O., & Al-Sharaa, I. M. T. (2022). Some of the sufficient conditions to get the G-Bi-shadowing action. *International Journal of Nonlinear Analysis and Applications*, *13*(1), 1105-1112.
5- Osipov, A. V., & Tikhomirov, S. B. (2014). Shadowing for actions of some finitely generated groups. *Dynamical Systems*, *29*(3), 337-351.
6- de La Harpe, P. (2000). *Topics in geometric group theory*. University of Chicago Press.
7- Gromov, M. (1981). Groups of polynomial growth and expanding maps (with an appendix by Jacques Tits). *Publications Mathématiques de l'IHÉS*, *53*, 53-78.

New Results on Fuzzy Banach Space

Shireen Ayed Karim and Noor F. Al- Mayahi
Department of Mathematics,
College of science
University of AL-Qadisiyah,Diwaniyah-Iraq,
E-mail: nafm60@yahoo.com
sci.math.mas.22.12@qu.edu.iq

Abstract

In this paper the ideas of fuzzy soft spectrum ,fuzzy soft condition spectrum, fuzzy soft condition spectrum and fuzzy soft spectral radius of fuzzy a soft element over fuzzy soft Banach space are introduced. Then we define the notions of fuzzy soft multiplicative linear functional, almost fuzzy soft multiplicative linear functional, fuzzy soft Jordan multiplicative linear functional and almost fuzzy soft Jordan multiplicative linear functional in fuzzy soft Banach space. Finally some new results and theorems about them over fuzzy soft Banach space are investigated.

Keywords: fuzzy soft spectrum ,fuzzy soft Condition Spectrum, fuzzy Soft Spectral Radius, Almost fuzzy Soft Multiplicative Linear Functional ,fuzzy Soft Jordan Functional.

1.Introduction

Due to uncertain data in real world, various problems in mathematics, engineering, environmental sciences, economics and medical sciences cannot be solved by the usual mathematical methods. The difficulty of the usual mathematical method is the lack of the parameterization tools for descriptions of problems arising in the fields of ambiguities and uncertainties.

To dealing with such problems Molodtsov [1] introduced the concept of soft set theory. Soft set theory is an innovative mathematical method which has the capability for dealing with uncertainties. Furthermore it has the parameterization tool which is more flexible than the customary mathematical methods through the vagueness and uncertainties of day to day problems in real world.

Das and Samanta [2] introduced the idea of soft linear functional over soft linear spaces. They studied some basic properties of such operators and extended some fundamental theorems of functional analysis in soft set settings.

Thakur and Samanta [3]introduced the concept of soft Banach algebras and studied some of its preliminary properties.For more information about soft set theory and some of its applications one can see [4-5] and[6-7].

This study introduces of fuzzy soft spectrum, fuzzy soft condition spectrum and fuzzy soft spectral radius of fuzzy soft element over fuzzy soft Banach space. We define fuzzy soft multiplicative linear functional, almost fuzzy soft multiplicative linear functional,fuzzy soft Jordan multiplicative linear functional and almost fuzzy soft Jordan multiplicative linear functional in fuzzy soft space. The paper explores new discoveries and theorems in fuzzy soft Banach space.

2.1 Preliminaries

Throughout this work. Let X be an universe set and E be the set of parameter, I^X denote the set of all fuzzy set over X and A $\subseteq E$.

Definition(2.1.1) [8]: Assume that A be a subset of E . A pair $(\overline{\Gamma}, A)$ is referred to as a fuzzy soft set over (X, E) , if $\overline{\Gamma}: A \to I^X$ is a mapping from A into I^X .The collection of all fuzzy soft sets over (X, E) is represents by $\overline{\Gamma}(X, E)$.

Definition(2.1.2) [8]: For two fuzzy soft sets$(\overline{\Gamma}, A)$ and (μ, B) in $\overline{\Gamma}(U, E)$ we state that $(\overline{\Gamma}, A) \subseteq (\mu, B)$ if $A \subseteq B$ and $\overline{\Gamma}(e)(x) \leq \mu(e)(x)$.

Definition(2.1.3)[8]: *In* $\Gamma(U, E)$,two fuzzy soft sets $(\overline{\Gamma}, A)$ and(μ, B) are equal if $\overline{\Gamma} \subseteq \mu$ and $\mu \subseteq \overline{\Gamma}$.

Definition(2.1.4)[9]: Let $(\overline{\Gamma}, A)$ and (μ, B) be two fuzzy soft sets in **F**(X , E) with A $\tilde{\cap}$ B $\neq \Phi$, then:

a) their intersection ($\overline{\Gamma} \tilde{\cap} \mu$, C) is a fuzzy soft set , where C = A $\tilde{\cap}$ B and $(F \tilde{\cap} \overline{\Gamma})(e) =$ F (e) $\tilde{\cap}$ $\overline{\Gamma}$ (e)for each e $\in$ C,$(F \tilde{\cap} \overline{\Gamma})(e)(x) = \min\{(e, F_e(x)), (e, \overline{\Gamma}_e(x))$

b)their union (F $\tilde{\cup}$ $\overline{\Gamma}$, C) is a fuzzy soft set , where C = A $\tilde{\cup}$ B and $(F \tilde{\cup} \overline{\Gamma})e =$ F(e) $\tilde{\cup}$ $\overline{\Gamma}$ (e)for each e $\in$ C $(F \tilde{\cup} \overline{\Gamma})(e)(x) = \max\{F(e)(x), \overline{\Gamma}(e)(x)\}$

Definition(2.1.5)[8]: The complement of a fuzzy soft set ($\overline{\Gamma}$, E) is a fuzzy soft set(Γ^c, E) defined by Γ^c(e)=$1/\overline{\Gamma}(e)$ for each $e \in E$,

$(\Gamma^c(e))(x) = 1 - \overline{\Gamma}(e)(x)$ $\forall x \in X$.

Definition(2.1.6) [8]: A fuzzy soft set $(\overline{\Gamma}, A)$ is said to be a null fuzzy soft set , denoted by Φ, if $\overline{\Gamma}(e) = \bar{0}$ for all $e \in A, \overline{\Gamma}(e)(x) = 0$ $\forall x \in X$. where , $\bar{0}$ is the null fuzzy soft subset of X .

Definition(2.1.7) [8]: A fuzzy soft set $(\overline{\Gamma}, A)$ is said to be an absolute fuzzy soft set , denoted by $\tilde{A}$, if $\overline{\Gamma}(e) = \bar{1}$ for all $e \in A$. where , $\bar{1}$ is the absolute fuzzy soft subset of X .

3.1 fuzzy soft spectrum

Definition (3.1.1): Let $\mathbb{C}$ be the set of complex numbers and $\mathcal{G}(\mathbb{C})$ be the collection of all nonempty bounded subsets of the set of complex numbers. Also let A be a set of parameters. Then a mapping $\Gamma: A \longrightarrow \mathcal{G}(\mathbb{C})$ is called a fuzzy soft complex set. It is denoted by Γ_A . If in particular Γ_A is a singleton set, then after identifying Γ_A with the corresponding fuzzy soft element, it will be called a fuzzy soft complex number. The set of all fuzzy soft complex numbers is denoted by $\mathbb{C}(f)$.

Definition (3.1.2): Let $\hat{\Gamma}_B$ be fuzzy soft Banach space with fuzzy soft unit element $\hat{e}$.we denote the fuzzy soft spectrum of an element x ∈ A by $\hat{\Gamma}_S$ and define it by

$\hat{\Gamma}_S=\{\lambda \in \mathbb{C}(f): \lambda e - x \notin \mathcal{G}(x)\}$

Where $\mathcal{G}(x)$ is the set of all fuzzy soft invertible element,of fuzzy soft Banach space $\hat{\Gamma}_B$.

We denoted the fuzzy soft spectral radius of x $\hat{r}(x)$ and define it by $\hat{r}(x)=\text{Sup}\{|\lambda|: \lambda \in \hat{\Gamma}_S\}$.

Definition (3.1.3): Let $0 < \varepsilon < 1$ .We denote the fuzzy soft condition spectrum of x in G by $\hat{\Gamma}_C(x)$ and define it by:

$\hat{\Gamma}_C(x) = \{\lambda \in \mathbb{C}(f): \|(\lambda e - x)\|\|(\lambda e - x)^{-1}\| > \frac{1}{\varepsilon}\}$

We denote the fuzzy soft condition spectral radius of x by $\hat{r}_C(x)$ and define it by:

$$\hat{r}_C(x) = \text{Sup}\{|\lambda|: \lambda \in \hat{\Gamma}_C(x)\}.$$

Proposition(3.1.4) : Let $\hat{\Gamma}_B$ be a fuzzy soft Banach space. If x ∈Γ satisfies ||x||<1,

then $(e - \hat{x})$ is is invertible and $(e - \hat{x})^{-1} = e+\sum_{n=1}^{\infty} \hat{x}n$.

Proof. Since $\hat{\Gamma}_B$ is fuzzy soft Banach space , so we have $\|\hat{x}^j\| \leq \|\hat{x}\|^j$ for any positive integer j, so that the infinite series $\sum_{n=1}^{\infty}\|\hat{x}\|^n$ is fuzzy soft convergent because ||$\hat{x}$||<1. So the sequence of partial sum $\hat{s}_k = \sum_{n=1}^{k} \hat{x}_n$ is a fuzzy soft Cauchy sequence since $\left\|\sum_{n=1}^{k+p} \hat{x}^n\right\| < \sum_{n=k}^{k=p}\|\hat{x}\|^n$.

Since $\hat{\Gamma}_B$ is fuzzy soft complete so $\sum_{n=1}^{\infty} \hat{x}^n$ is fuzzy soft convergent.

Now let $s = e + \sum_{n=1}^{\infty} \hat{x}^n$.

Now it is only we have to show that $s = (e - \hat{x})^{-1}$.

We have

(1) $$(e - \hat{x})(e + \hat{x} + \hat{x}^2 + \ldots \hat{x}^n) = (e + \hat{x} + x^2 + \ldots \hat{x}^n)(e - \hat{x}) = e - \hat{x}^{n+1}$$

Now again since $\|\hat{x}\| < 1$ so $\hat{x}^{n+1} \to \theta$ as $n \to \infty$. Therefore letting $n \to \infty$ in and remembering that multiplication in Γ is continuous we get, $(e-\hat{x})s=s(e-\hat{x})=e$
So that $s = (e - \hat{x})^{-1}$. This proves the proposition.

Lemma (3.1.5): Let $\hat{\Gamma}_B$ be a fuzzy soft Banach space with fuzzy soft with identity element e

Let x ∈ G such that $\|\hat{x}\| \leq 1$ then (e-x) invertible and $(e-\hat{x})^{-1} = e + \sum_{n=1}^{\infty} \hat{x}^n$ Furthermore we have $\|(e-\hat{x})^{-1}\| \leq \frac{\|e\|}{\|e\|-\|\hat{x}\|}$.

Proof. For the proposition (4). Now let $S_n = e + \hat{x} + \hat{x}^2 + \cdots + \hat{x}^n$ and y= $e + \sum_{n=1}^{\infty} \hat{x}^n$ Then by the first part we know that $(e-x)^{-1} = y$. Also we have

$$\|y\| = \lim_{n\to\infty} \|S_n\| = \lim_{n\to\infty} \left\|e + \sum_{k=1}^{n} \hat{x}^k\right\| \leq \|e\| + \sum_{k=1}^{\infty} \|\hat{x}\|^k = \frac{\|e\|}{\|e\| - \|\hat{x}\|}.$$

If $\hat{\Gamma}_B$ is fuzzy soft with identity (i.e.,$\|e\| = 1$) then we have $\|(e-\hat{x})^{-1}\| \leq \frac{1}{1-\|\hat{x}\|}$

Corollary (3.1.6): Let $\hat{\Gamma}_B$ be a fuzzy soft Banach space. Let $\hat{x} \in \hat{\Gamma}$ and $\hat{\mu}$ be a fuzzy soft scalar such that $|\hat{\mu}|>\|\hat{x}\|$. Then $(\hat{\mu}e- \hat{x})^{-1}$ exists and $(\hat{\mu}e- \hat{x})^{-1}=\sum_{n=1}^{\infty} \hat{\mu}^{-n}\, \hat{x}^{n-1} (x^0 = e)$

Proof. y ∈ $\hat{\Gamma}$ be such that y^{-1}exists in $\hat{\Gamma}$ and α be afuzzy soft scalar such that α(λ) ≠0, ∀λ ∈ A. Then it is clear that

$(\alpha y)^{-1} = \alpha^{-1} y^{-1}$.

Having noted this we can write

$\hat{\mu}e-\hat{x} = \hat{\mu}(e - \hat{\mu}^{-1}\hat{x})$

and now we show that $(e - \hat{\mu}^{-1}\hat{x})^{-1}$ exists. We have $\|e- (e - \hat{\mu}^{-1}\hat{x})\| = \|\hat{\mu}^{-1}\hat{x}\| = |\hat{\mu}|^{-1}\|\hat{x}\|$ <1 by hypothesis. So, By Corollary 10 $(e - \hat{\mu}^{-1}\hat{x})^{-1}$ exists and hence $(\hat{\mu}e- \hat{x})^{-1}$ exists. For the infinite series representation, using the Proposition 9 we have

$(\hat{\mu}e- \hat{x})^{-1} = \hat{\mu}^{-1}(e - \hat{\mu}^{-1}\hat{x})^{-1}$

$=\hat{\mu}^{-1}(e + \sum_{n=1`}^{\infty} \quad [e - (e - \hat{\mu}^{-1}\hat{x})]^n$

$=\hat{\mu}^{-1}(e + \sum_{n=1}^{\infty} (\hat{\mu}^{-1}\hat{x})^n)$

$$=\sum_{n=1}^{\infty} \hat{\mu}^{-n}\hat{x}^{n-1}.$$

This proves the corollary.

Corollary (3.1.7) :Let $\hat{\Gamma}_B$ be a fuzzy soft Banach space with fuzzy soft unit element $\hat{e}$ such that $\|\hat{e}\|= \check{1}$ and $\widetilde{x} \in \mathcal{G}(x)$. Let $\lambda \in \widetilde{\mathbb{C}(f)} - \{0\}$ such that $\|\hat{x}\| \ddot{<} \check{\lambda}$ Then $(\lambda e - \hat{x})$ is invertible and $(\hat{\mu}e - \hat{x})^{-1} = \sum_{n=1}^{\infty} \check{\mu}^{-n}\, \hat{x}_n{}^{n-1} : (\hat{x}^0 = \check{e})$ .Furthermore we have

$$\|(\widetilde{\lambda e} - 1)^{-1}\| \acute{\leq} \frac{\bar{1}}{|\bar{\lambda}| - \|\hat{x}\|}$$

Proof. For the corollary (6) To prove the last statement we need only to substitute $\frac{\hat{x}}{\lambda}$ with $\check{x}$ in Lemma (5) and we get the result

Theorem (3.1.8): Let $\hat{\Gamma}_B$ be a fuzzy soft Banach space with fuzzy soft with identity element e such that $\|e\| = 1$ and x ∈ A. Then we have $\hat{r}$(x)≤ $r_C(x) \leq \frac{1+\varepsilon}{1-\varepsilon}\|\hat{x}\|$.

Proof. Since $\hat{\Gamma}_S \subseteq \Gamma_C(x)$, so we have r(x)≤ $\hat{r}_C(x)$. Suppose that $\lambda \in \Gamma_C(x)$. If $|\lambda| \leq \|\hat{x}\|$, then we can easily prove that $|\lambda| \leq \frac{1+\varepsilon}{1-\varepsilon}\|\hat{x}\|$ Thus we have $r_\varepsilon(x) \leq \frac{1+\varepsilon}{1-\varepsilon}\|\hat{x}\|$. Now suppose that $|\lambda| > \|\hat{x}\|$. Then $(\lambda e - \hat{x})$ is invertible and by corollary (3.5) we have $\|(\lambda e - \hat{x})^{-1}\| \leq \frac{1}{|\lambda| - \|\hat{x}\|}$. Consequently by some computations we get $|\lambda| \leq \frac{1+\varepsilon}{1-\varepsilon}\|\hat{x}\|$.

Thus we conclude that $r_\varepsilon(x) \leq \frac{1+\varepsilon}{1-\varepsilon}\|\hat{x}\|$

Definition (3.1.9): Let $\hat{\Gamma}_B$ be a fuzzy soft Banach space and T: $\Gamma_G \to \mathbb{C}(A)$ be a fuzzy soft linear functional. We say that T is almost fuzzy soft multiplicative if there exists an $\delta > 0$such that for all x,y ∈ G:

$|T(xy) - T(x)T(y)| \leq \delta\|x\|\|y\|$.

Proposition (3.1.10): Let $\hat{\eta}$ is a fuzzy soft linear functional on a fuzzy soft Banach space $\hat{\Gamma}_B$ with identity element e such that $\hat{\eta}(e) = 1$. Then the following conditions are equivalent.

i) $\hat{\eta}(x) = 0$ implies $\hat{\eta}(x^2) = 0$ $for\ all\ x \in G$,
ii) $\hat{\eta}(x^2) = (\hat{\eta}(x))^2, x \in G$,
iii) $\hat{\eta}(x) = 0$ implies $\hat{\eta}(xy) = 0$ $for\ all\ x, y \in G$
iv)$\hat{\eta}(xy) = \hat{\eta}(x)\hat{\eta}(y)$ $for\ all\ x, y \in G$

proof: (i)→ (ii)

$\hat{\eta}(e) = 1$ implies

$\hat{\eta}\big(x - \hat{\eta}(x)\big)(\lambda) = \hat{\eta}(ex - \hat{\eta}(x))(\lambda\hat{\eta}(e)(\lambda)\hat{\eta}(x)(\lambda) - \hat{\eta}(x)(\lambda) = 0\ ; \forall\lambda \in A.$

So we have 0=$\hat{\eta}\big(x - \hat{\eta}(x)\big) = 0$. By (i) we have

0=$\hat{\eta}\left(\big(x - \hat{\eta}(x)\big)^2\right) = \hat{\eta}(x^2 - 2x\hat{\eta}(x) + \big(\hat{\eta}(x)\big)^2 = \hat{\eta}(x^2) - \big(\hat{\eta}(x)\big)^2$.

Thus we deduce that $\hat{\eta}(x)^2 = \left(\hat{\eta}(x)\right)^2$.

(ii)$\Longrightarrow$ (iii)

By replacing u+v with (x) in (ii) we get $\hat{\eta}(uv + vu) = 2\hat{\eta}(u)\hat{\eta}(v); u, v \in G, (1)$

Let x,y be in G with $\hat{\eta}(x) = 0$. According to (1) we have $\hat{\eta}(xy + yx) = 0. (2)$

Hence by (ii) we obtain $\hat{\eta}(xy + yx)^2) = 0$. Since $(xy + yx)^2$=$2\hat{\eta}(x(yxy) + (yxy)x) = 4\hat{\eta}(x)\hat{\eta}(yxy) = 0$.

According to (ii) we have $\hat{\eta}(xy - yx) = 0, (3)$. If we add two equalities (2) and (3) we conclude that $\hat{\eta}(xy) = 0$.

(iii)$\Longrightarrow$(iv)

Let x,y $\in G. we\ have\ \hat{\eta}\left(x - \hat{\eta}(x)\right) = 0$. Hence for each $\lambda \in A$ we have

$\hat{\eta}\left(x - \hat{\eta}(x)\right)(\lambda) = 0$. Thus by (iii) we have $\hat{\eta}\left(\left(x - \hat{\eta}(x)\right)y\right)(\lambda) = 0$.

Then we get

0=$\hat{\eta}\left(\left(x - \hat{\eta}(x)\right)y\right)(\lambda) = \hat{\eta}(xy - \hat{\eta}(x)y)(\lambda) = \hat{\eta}(xy)(\lambda) - \hat{\eta}(x)(\lambda)\hat{\eta}(y)(\lambda); \forall\lambda \in A.$

Thus we have 0=$\hat{\eta}(xy) - \hat{\eta}(x)\hat{\eta}(y)$. Consequently we get $\hat{\eta}(xy) = \hat{\eta}(x)\hat{\eta}(y)$.

(iv)$\Longrightarrow$ (i)

From (iv) we have$\hat{\eta}(xy)(\lambda) = \hat{\eta}(x)(\lambda)\hat{\eta}(y)(\lambda)$. If $\hat{\eta}(x) = 0, then\ \hat{\eta}(x)(\lambda) = 0; \forall \in A$ so we have $\hat{\eta}(xy)(\lambda) = \hat{\eta}(x)(\lambda)(y)(\lambda) = 0. \hat{\eta}(y)(\lambda) = 0$

Therefore $\hat{\eta}(xy) = 0$.

Clearly if $\hat{\eta}$ is fuzzy soft multiplicative linear functional then $\hat{\eta}$ is fuzzy soft Jordan multiplicative functional. Now we have the following corollary.

Corollary(3.1.11)

Let $\hat{\eta}$ is a fuzzy soft Jordan multiplicative linear functional on fuzzy soft Banach space $\hat{\Gamma}_B$ with identity element e such that $\phi(e) = 1$. Then $\hat{\eta}$ is fuzzy soft multiplicative.

Lemma (3.1.12): Let $\hat{\eta}$ is a fuzzy soft multiplicative linear functional on soft fuzzy Banach space $\hat{\Gamma}_B$ Then we have $\hat{\eta}(x) \in \hat{\Gamma}_B$; x $\in G$.

Proof: For x $\in G$ we set z= $\hat{\eta}(x)e - x$ Then we have $\hat{\eta}(z)(\lambda) = \hat{\eta}(x)(\lambda)\hat{\eta}(e)(\lambda) - \hat{\eta}(x)(\lambda) = \hat{\eta}(x)(\lambda) - \hat{\eta}(x)(\lambda) = 0$

Hence we have $\hat{\eta}(z) = 0$. Therefore z$\in ker\hat{\eta}$. So we have z $\in sing(G)$. Consequently $\hat{\eta}(x) \in \hat{\Gamma}_B$.

Remark (3.1.13): Now suppose that $\hat{\eta}$ is fuzzy soft multiplicative linear functional and let z $\in \hat{\Gamma}_B$, for some x $\in G$. Then ze-xis not invertible and so we have $\hat{\eta}(ze - x) = 0$. We know that, for invertible element y we have $\hat{\eta}(y) = 0$.

Thus $z\hat{\eta}(e) - \hat{\eta}(x) = 0$. So we have z=$\hat{\eta}(x)$. . Consequently we have the following theorem.

Theorem (3.1.14): Let $\hat{\Gamma}_B$ be a commutative fuzzy soft Banach space and let x $\in G$ then

$\hat{\Gamma}_B = \{\hat{\eta}(x) : \hat{\eta}$ is a fuzzy soft multiplicative linear functional$\}$

Proof. It follows from lemma (3.12) and last statement.

Lemma(3.1.15): Let T:$\Gamma_E(A) \longrightarrow \mathbb{C}(f)$ be a fuzzy soft bounded linear functional. ThenT is almost fuzzy soft multiplicative.

Proof: For each $\hat{x}, \hat{y} \in A$ we have

$$|T(\hat{x}\check{y}) - T(\hat{x})T(\check{y})| \leq |T(\hat{x}\check{y})| + |T(\hat{x})T(\check{y})| \leq \|T\|\|\hat{x}\check{y}\| + \|T\|^2\|\hat{x}\|\|\check{y}\|$$
$$= (\|T\| + \|T\|^2)\|\hat{x}\|\|\check{y}\|$$

Thus T is almost soft multiplicative where $\bar{\bar{\delta}}$ =$(\|T\| + \|T\|^2)$

Proposition (3.1.16): Let $\hat{\Gamma}_B$ is a fuzzy soft Banach space and T_1:$\Gamma_E(A) \longrightarrow \mathbb{C}(f)$ is a fuzzy soft multipicactive linear functional and T_2:$\Gamma_E(A) \longrightarrow \mathbb{C}(f)$ is a soft bounded linear functional. Then$T_1 + T_2$ is almost fuzzy soft multiplicative functional but not multiplicative.

Proof: For each $\hat{x}, \check{y} \in A$ we have

$|(T_1 + T_2)(\hat{x}\check{y}) - (T_1 + T_2)(\hat{x})(T_1 + T_2)(\check{y})|$=

$|T_1(\hat{x}\check{y}) + T_2(\hat{x}\check{y}) - (T_1(\hat{x}) + T_2(\check{y}))(T_1(\check{y}) + T_2(\check{y})|$=

$$|T_1(\hat{x}\check{y}) + T_2(\hat{x}\check{y}) - T_1(\hat{x})T_1(\check{y}) - T_2(\hat{x})T_2(\check{y}) - T_1(\hat{x})T_2(\check{y}) - T_2(\hat{x})T_1(\check{y})| \leq$$

$$|T_1(\hat{x}\check{y}) - T_1(\hat{x})T_1(\check{y})| + |T_2(\hat{x}\check{y}) - T_2(\hat{x})T_2(\check{y})| + |T_1(\hat{x})T_2(\check{y})| + |T_2(\hat{x})T_1(\check{y})|$$

So by lemma(14) we get

$$|(T_1+T_2)(\hat{x}\check{y})-(T_1+T_2)(\hat{x})(T_1+T_2)(\check{y})|\leq$$

$$(\|T_2\|+\|T_2\|^2)\|\hat{x}\|\|\check{y}\|+\acute{2}\|T_1\|\|\hat{x}\|\|T_2\|\|\check{y}\|=$$

$$(\|T_2\|+\|T_2\|^2)\|\hat{x}\|\|\check{y}\|+\acute{2}\|T_1\|\|T_2\|\|\hat{x}\|\|\check{y}\|.$$

Thus(T_1+T_2) is almost fuzzy soft multiplicative. Clearly$(T_1+T_2)$is not multiplicative.

Definition(3.1.17):Let $\hat{\Gamma}_B$ be a fuzzy soft Banach space. We say that fuzzy soft linear functional $\hat{\eta}$:$\Gamma_E(A)\longrightarrow\mathbb{C}(f)$ is almost fuzzy soft Jordan multiplicative functional if there exist $\bar{\bar{\delta}}\gtrsim\bar{0}$such that: $\left|\hat{\eta}(\hat{X}^2)-\hat{\eta}(\hat{X})^2\right|\leq\bar{\bar{\delta}}\left\|\hat{X}\right\|^2$,$\forall\check{x}\in A$

Corollary(3.1.18): Let $\hat{\Gamma}_B$ be a fuzzy soft Banach space and T_1:$\Gamma_E(A)\longrightarrow\mathbb{C}(f)$ is a fuzzy soft Jordan multiplicative linear functional and T_2:$\Gamma_E(A)\longrightarrow\mathbb{C}(f)$ is fuzzy soft bounded linear functional. Then $T_1+T_2$is almost fuzzy soft Jordan multiplicative linear functional.
Proof: It can be proved by similar method which we stated in theorem (13).

Definition(3.1.19): Let $\hat{\Gamma}_B$ be fuzzy soft Banach space with identity element $\check{e}$ and let $\bar{\bar{\varepsilon}}\gtrsim\bar{0}$ We denote the fuzzy soft ε_ condition spectrum of an element$\hat{X}\in\check{A}$ by $\Gamma_{\bar{\varepsilon}}(\check{X})$and define it by: $\Gamma_{\bar{\varepsilon}}=\{\check{\lambda}\in\mathbb{C}(F):\|\check{\lambda}\,\check{e}-\check{x})^{-1}\|\cong\frac{\check{1}}{\varepsilon}\}$.

Theorem(3.1.20): Let $\hat{\Gamma}_B$ be a fuzzy soft Banach space with identity element $\check{e}$ and let $\bar{\bar{\varepsilon}}\gtrsim\bar{0}$. Let $\hat{\eta}$:$\Gamma_E(A)\longrightarrow\mathbb{C}(f)$ be a fuzzy soft linear functional such that $\hat{\eta}(\check{e})=\check{1}$ and $\hat{\eta}(e)\bar{\bar{\in}}\Gamma_{\check{\varepsilon}}$ for$\hat{X}\in\check{A}$ .Then is fuzzy soft multiplicative functional.

Proof: We prove that for all $\hat{X}\in\check{A}$ we have $T(\check{x})\in\Gamma_x$.We put $\bar{\lambda}=\hat{\eta}(\check{x})$. If $\bar{\bar{\lambda}}\in\Gamma_x$ then $\hat{\eta}$ is multiplicative. If $\bar{\bar{\lambda}}\notin\Gamma_x$ then $\bar{\bar{\lambda}}\check{e}-\check{x}$ is invertible and so$\bar{\bar{\lambda}}\check{e}-\check{x}\bar{\in}\mathcal{G}(x)$.Suppose that $\acute{z}\bar{\supset}\check{\varepsilon}\|(\bar{\bar{\lambda}}\check{e}-\check{x})^{-1}\|$ Then we have $\|(\bar{\bar{\lambda}}\check{e}-\check{x})^{-1}\|\bar{<}\frac{\check{1}}{\varepsilon}$.Thus we get $\|(\bar{\bar{\lambda}}\check{e}\acute{z}-\check{x}\acute{z})^{-1}\|\bar{<}\frac{\check{1}}{\varepsilon}$ Consequently we have $\bar{\bar{\lambda}}\,\acute{z}=\hat{\eta}(\check{x})\acute{z}=\hat{\eta}(\check{x}\acute{z})\notin\Gamma_{\check{\varepsilon}}(\acute{z}\check{x})$ which is a contradiction. So $\hat{\eta}$ is fuzzy soft multiplicative.

Lemma(3.1.21). Let $\overline{\overline{\delta}} \gtrsim \bar{\bar{0}}$ and $\check{X} \in \check{A}$ Then $\Gamma_x \subseteq \Gamma_{\delta\check{x}}$

Proof: It can be proved easily by definition.

Theorem(3.1.22): Let $\hat{\Gamma}_B$ be a fuzzy soft Banach space with identity $\check{e}$ element and $\hat{\eta}$ be an almost fuzzy soft multiplicative linear functional on A If $\hat{\eta}$ $(\check{e})=\check{1}$ Then for every element $\check{x} \ \bar{\bar{\in}} A$ we have $\hat{\eta}$ $(\check{x}) \bar{\bar{\in}} \Gamma_{\delta x}$

Proof: Let $\hat{x} \ \bar{\bar{\in}} A$ and $\bar{\bar{\lambda}} = \hat{\eta}$ $(\hat{x})$ .If $\bar{\bar{\lambda}}\check{e} - \check{x}$ is not invertible then $\bar{\bar{\lambda}} \in \Gamma_x \subseteq \Gamma_{\delta\check{x}}$ So $\overline{\bar{\lambda}} \in T_\varepsilon(\hat{x})$. Now assume that is invertible. Then

$$\bar{\bar{1}} = |\hat{\eta}(\check{e})| = \left|\hat{\eta}(\hat{x}) - \check{0}\right| =$$

$$\left|\hat{\eta}(\check{e}) - \hat{\eta}\left(\bar{\bar{\lambda}}\check{e} - \hat{x}\right)\mathrm{T}((\bar{\bar{\lambda}}\check{e} - \hat{x}))^{-1}\right|$$

$$\check{\leq} \ \bar{\bar{\delta}}\left\|(\bar{\bar{\lambda}}\check{e} - \hat{x})((\bar{\bar{\lambda}}\check{e} - \hat{x}))^{-1}\right\|$$

Thus we have

$$\left\|(\bar{\bar{\lambda}}\check{e} - \hat{x})((\bar{\bar{\lambda}}\check{e} - \hat{x}))^{-1}\right\| \bar{\bar{\geq}} \frac{\check{1}}{\varepsilon}$$

So we conclude that $\bar{\bar{\lambda}} \in \Gamma_{\varepsilon x}$. Consequently we have $\hat{\eta}$ $(\hat{x}) \bar{\bar{\in}} \Gamma_{\delta x}$.

References

[1] D. Molodtsov, Soft set theory first results, Comput. Math. Appl. 37(1999) 19-31.

[2] S. Das and S. K. Samanta, Soft linear functionals in soft normed linear.

[3] R. Thakur, S. K. Samanta, Soft Banach Algebra, Ann. Fuzzy Math.Inform. 10 (3) (2015) 397-412.bers, J. Fuzzy Math. 21 (1) (2013) 195-216.

[4] H. Aktas and N. Cagman, Soft sets and soft groups, Inform. Sci. 177(2007) 2226-2735.

[5] S. Das, P. Majumdar and S. K. Samanta, On Soft linear spaces and softnormed linear spaces, Ann. Fuzzy Math Inform. 9 (1) (2015) 91-109.

[6] P. K. Maji, R. Biswas and A. R. Roy, An application of soft sets in adecision making problem,Comput. Math. Appl. 44 (2002) 1077-1083

[7] S. H. J. Petroudi, S. A. Sadati, A. Yaghobi, Almost Soft multiplicativelinear functional, The first national conference on Applied mathematicsin engineering and basic science. (2017), Shiraz, Iran.

[8] Maji, P.K. , Biswas, R. and Roy, A.R., Fuzzy Soft Set ,Journal of Fuzzy Mathematics 9,589-602 , (3) (2001)-8843

[9] Kamel, A. and Mirzavaziri, M., Closability of farthest point in fuzzy normed spaces, Bulletin of Mathematical Analysis and Applications, Vol.2,140-145, (2010).

Some new results related with Fuzzy soft spectrum

Afrah Sadeq Kadhim and Noori F.Al-Mayahi

Department of Mathematics,

College of Science

University of Al-Qadisiyah,Diwaniyah-Iraq,

E-mail:sci.math.mas.22.7@qu.end.iq E-mail: nafm60@yahoo.comi

Abstract-

In this paper the ideas of fuzzy soft spectrum, fuzzy soft condition spectrum ,fuzzy soft condition spectrum and fuzzy soft spectral radius of a fuzzy soft element over fuzzy soft Banach algebras are introduced. Some basic properties of these ideas in fuzzy soft Banach algebras are studied. Then we define the notions of fuzzy soft multiplicative linear functional, almost fuzzy soft multiplicative linear functional,fuzzy soft Jordan multiplicative linear functional and almost fuzzy soft Jordan multiplicative linear functional in fuzzy soft Banach algebras. Finally some new results and theorems about them over fuzzy soft Banach algebra are investigated.

Keywords- Condition Spectrum ,fuzzy Soft Spectral Radius, fuzzy Soft Normed Linear Space, Almost fuzzy Soft Multiplicative Linear Functional, fuzzy Soft Jordan Functional

I.Introduction

Due to uncertain data in real world, various problems in mathematics, engineering, environmental sciences, economics and medical sciences cannot be solved by the usual mathematical methods. The difficulty of the usual mathematical method is the lack of the parameterization tools for descriptions of problems arising in the fields of ambiguities and uncertainties.To dealing with such problems Molodtsov [14] introduced the concept of soft set theory. Soft set theory is an innovative mathematical method which has the capability for dealing with uncertainties. Furthermore it has the parameterization tool which is more flexible than the customary mathematical methods through the vagueness and uncertainties of day to day problems in real world.Das and Samanta [4] introduced the idea of soft linear functional over soft linear spaces. They studied some basic properties of such operators and extended some fundamental theorems of functional analysis in soft set settings. Thakur and Samanta [20] introduced the concept of soft Banach algebras and studied some of its preliminary properties. For more information about soft set theory and some of its applications one can see [2,5,11] and[13,14,17,18,19].

In this paper we introduce a definition fuzzy soft spectrum and study some of its properties. In section 2, preliminary results are given, In section 3, we introduce the concept of fuzzy soft spectrum Banach algebra and some of its preliminary properties are studied. Section 4 concludes the paper.

2.1 preliminaries

Throughout this work. Let X be an universe set and E be the set of parameter, I^X denote the set of all fuzzy set over X and A⊆ E

Definition (2.1)[11] :

A pair (Γ , A) denote by $\Gamma_A$is said to be a fuzzy soft set over X, where Γ is a function given by $\Gamma: A \to I^X$.

Definition (2.2)[11]:

A Fuzzy soft set (Γ ,A) over X is said to be an absolute fuzzy soft set, if for all $\check{e} \in E$, *F(e)* is a fuzzy universal set $\tilde{1}$ over X and is denoted by.$\check{E}$

Definition (2.3)[11]:

A fuzzy soft set (Γ, E) over X is said to be a null fuzzy soft set, if for all $\check{e} \in E$, *F(e)* is the null fuzzy set $\tilde{0}$ over X. It is denoted by $\check{\emptyset}$.

Definition (2.4)[7]:

Into two fuzzy soft sets (Γ, A) and (Λ, B) in $\Gamma(X, E)$ is said to be $(\Gamma, A) \tilde{\subseteq} (\Lambda, B)$ if $A \subseteq B$ and $\Gamma(e)(x) \leq \Lambda(e)(x)$.

Definition (2.5)[11]:

Two fuzzy soft sets (Γ, A) and (Λ, B) in $\Gamma(X, E)$ are equal if $\Gamma \tilde{\subseteq} \Lambda$ and $\Lambda \tilde{\subseteq} \Gamma$.

Definition (2.6)[7]:

The different between two fuzzy soft sets (Γ, A) and (Λ, B) in $\Gamma(X, E)$ is a fuzzy soft set $(\Gamma/\Lambda, E)$ (say) defined by $(\Gamma/\Lambda)(e)=\Gamma(e)/\Lambda(e)$ for each $\check{e} \in E$. $(\Gamma/\Lambda)(e): X \to I$, $(\Gamma/\Lambda)(e)(x) = \Gamma(e)(x) \tilde{\cap} \left(\Lambda(e)(x)\right)^c = \min\{\Gamma(e)(x), \Lambda^c(e)(x)\} \forall x \in X$.

Definition (2.7)[11] :

The complement of a fuzzy soft set (Γ, E) is a fuzzy soft set(Γ^c, E) defined by $\Gamma^c(e)=1/\Gamma(e)$ for each $\check{e} \in E$, $\left(\Gamma^c(e)\right)(x) = 1 - \Gamma(e)(x)\ \forall x \in X$.

Definition (2.8)[7]:

Let (Γ, A) and (Λ, B) be two fuzzy soft sets in $\Gamma(X, E)$ with $A \tilde{\cap} B \neq \Phi$, then:

a) their intersection $(\Gamma \tilde{\cap} \Lambda, C)$ is a fuzzy soft set , where $C = A \tilde{\cap} B$ and $(\Gamma \tilde{\cap} \Lambda)(e) = \Gamma(e) \tilde{\cap} \Lambda(e)$ for each $e \in C$, $(\Gamma \tilde{\cap} \Lambda)(e)(x) = \min\{(e, \Gamma_e(x)), (e, \Lambda_e(x))$

b)their union $(\Gamma \tilde{\cup} \Lambda, C)$ is a fuzzy soft set , where

$C = A \tilde{\cup} B$ and $(\Gamma \tilde{\cup} \Lambda)e = \Gamma(e) \tilde{\cup} \Lambda(e)$for each $e \in C$

$(\Gamma \tilde{\cup} \Lambda)(e)(x) = \max\{\Gamma(e)(x), \Lambda(e)(x)\}$

Definition (2.9)[11]:
A fuzzy soft set Γ_A over X is called a fuzzy soft point if for the element $e^* \in E$

$$f_e(x)= \begin{cases} \lambda_x & \text{if } e = e^* \\ 0 & \text{otherwise} \end{cases} \quad \text{for every } e \in E$$

Otherwise, for the element $x^* \in X$,

$$f_e(x)= \begin{cases} \lambda & \text{if } x = x^* \\ 0 & \text{otherwise} \end{cases} \quad \text{for every } x \in X \text{ ,where } \lambda \in (0,1].$$

The set of all fuzzy soft points is denoted as $\tilde{x}_E$.

Definition (2.10)[11]:

Let R be the set of real numbers and $\check{E}$ be the parameter set. The set of all fuzzy soft real number is a mapping f from $\check{E}$ to I^R and is denoted by R_E , where for all $\check{e} \in E$, *f (e)"s* are fuzzy real numbers.

Definition (2.11)[7]:

A linear space is a set X over a field F together with two operations + and • satisfying the following axioms

(i) An operation called vector addition that associates a sum $u+ v \in X$ with each pair of vector u v , $\in X$ such that it is associative with identity 0.

(ii) An operation called multiplication by a scalar that associates with each scalar $a \in F$ and vector $u \in X$ vector $au \in X$, called the product of a and u , such that it is distributive with identity 1.

Definition (2.12)[14]:

Let X be a linear space over a field f and A be a parameter set . A soft set G is said to be a soft linear space of X over f if G(e) is a linear subspace of X, $\forall e \in A$.

Definition (2.13)[12]:

Suppose that X be a linear space over f. A soft set G_A is called a soft subspace of F if (i) for each e $\in$ *A*, *G*(e) is a linear subspace of X over f and (ii) F*(e)* $\supseteq$ G*(e), $\forall e \in A$.*

Theorem (2.14)[12]:

A soft subset $\check{G}$ of a soft linear space X is a soft linear sub-space of X if and only if for all scalar $\alpha,\beta \in f$,$\alpha\check{G}+\beta\check{G} \subseteq \check{G}$.

Definition (2.15): [10]

Suppose that X be a linear space over a field f and $\check{E}$ be a parameter set . A fuzzy set F over X is said to be a fuzzy linear space of X over f if F(e) is a linear subspace of X, $\forall \check{e} \in E$.

Definition (2.16): [8]

Suppose that X be a linear space over f. A fuzzy set $\check{A}$ in X is said to be a fuzzy subspace if $\alpha\check{A}+\beta$B $\subseteq \check{A}$ for all $\alpha,\beta \in f$

Or equivalent

$\check{A}(\alpha x+\beta y) \geq \min\{\check{A}(x),B(y)\}$ for all x ,y ∈ X and all x ∈ X.

Definition (2.17):

Let X be a linear space over a field F and A be a parameter set. A fuzzy soft set Γ_A over F is called a fuzzy soft linear space of X over F if Γ(e) is a fuzzy subspace of X, ∀e ∈ A.

Definition (2.18):[9]

Let X linear space over F ,where F is the field of real number or the field of complex number

A norm on X is function $\|.\|: X \to R$ having the following properties

(1) $\|\check{x}\| \geq 0$,for all $\check{x} \in X$

(2) $\|\check{x}\| = 0$ if and only if $\check{x}$=0

(3) $\|\hat{\lambda}\check{x}\| = |\hat{\lambda}|\|\check{x}\|$,for all $\check{x} \in X$ and $\hat{\lambda} \in f$

(4) $\|\check{x} + \check{y}\| \leq \|\check{x}\| + \|\check{y}\|$,for all $\check{x},\check{y} \in X$

The linear space X over ƒ together with $\|.\|$ is said to be a normed space and is denoted by (X, $\|.\|$) .

Definition (2.19):[12]

A binary operation T on I=[0,1] (i.e. T:$I \times I \to I$ is a function) is called triangular Norm (write t-norm), if it satisfies the following axioms.

(i) T is boundary ,(i.e. T($\check{a}$,1)=a for all $\check{a} \in I$

(ii) T is associative, i.e. T($\check{a}$,T($\check{b}$,$\check{c}$))=T(T($\check{a}$,$\check{b}$),$\check{c}$) for all $\check{a},\check{b} \in I$

(iii) T is commutative , i.e. T($\check{a}$,$\check{b}$)=T($\check{b}$,$\check{a}$) for ll $\check{a},\check{b} \in I$

(iv) T is monotone, If $\check{b},\check{c} \in I$ with $\check{b} \leq \check{c}$, then T($\check{a}$,$\check{b}$)≤T($\check{a}$,$\check{c}$) for all a ∈ I

Definition (2.20):[12]

Let X be a linear space over the field f (real or complex) and T a continuous t-norm ″A fuzzy norm″ on X × R̈ , R̈ -set of all real numbers is said to be ″a fuzzy norm″ on X if and only if for $\check{x},\check{y} \in$ X and $\check{c} \in f$

(i) for all t ∈R̈ with t ≤ 0, N ($\check{x}$, t) = 0 .

(ii) for all t ∈R̈ with t > 0, N ($\check{x}$,t) = 1 if and only if $\check{x}$ = 0 .

(iii) for all t $\in \grave{R}$ with t > 0, N ($\check{c}\check{x}$,t) =$\left(\check{x}, \frac{t}{|\check{c}|}\right)$ if $\check{c}\neq 0$

.)) for all s ,t $\in \grave{R}$, $\check{x}$,$\check{y}\in$ X ($\check{x}$ +$\check{y}$,t + s) $\geq$ N ($\check{x}$,t) *N ($\check{y}$,s iv (

(v) N ($\check{x}$,.) is a continuou non- decreasing function of $\grave{R}$ and

$$\lim_{x\to\infty} N(x,t) = 1$$

The triplet (X,N, T) will be referred to as a ″fuzzy normed linear space″.

Definition (2.21)[16]:

Let SL($\tilde{X}$) be a soft linear space. The mapping $\|\ .\ \|$: SL($\tilde{X}$) $\rightarrow \grave{R}^{+}$(E) is called a soft norm($\tilde{X}$), if it satisfies the following conditions:

(i) $\|\ \tilde{x}_e\ \| \geq \tilde{0}$ for all $\tilde{x}_e \in$ SL (x˜) and $\|\ \tilde{x}_e\ \| = \tilde{0} \leftrightarrow \tilde{x}_e \quad \tilde{\theta}_0$.

ii) $\|\tilde{r}.\ \tilde{x}_e\| = |\tilde{r}|\ \|\tilde{x}_e\|$ for all $\tilde{x}_e \in$ SL (˜X) For every soft scalar $\tilde{r}$.(

iii) $\|\ \tilde{x}_e + \tilde{y}_e\| \leq \|\ \tilde{x}_e\ \| + \|\ \tilde{y}_e\|$ for all $\tilde{x}_e, \tilde{y}_e \in$ SV $(\widetilde{X})$(

The soft linear space SL ($\tilde{X}$) with a soft norm $\|\ .\|$ on $\tilde{X}$ is said to be a soft normed linear space and is denoted by ($\tilde{X}$, $\|\ .\|$)

Definition (2.22):

Let X be a vector space field F and let E be the set of parameters .The fuzzy soft norm $\|.\|$ over X is defined as the map $\tilde{X}$ to R*E Such that

. i) $\tilde{x}_E = \tilde{0}_E \leftrightarrow \|\ \tilde{x}_E\ \| = \tilde{0}_E$(

ii) $\|\tilde{r}.\ \tilde{x}_E\| = |r| \otimes \|\ \tilde{x}_E\ \|$.(

iii) $\|\tilde{x}_E + \tilde{y}_E\| = \|\ \tilde{x}_E\ \| \oplus \|\tilde{y}_E\ \|$ for all $\tilde{x}_E, \tilde{y}_E \in$ SV ($\tilde{X}$)(

Definition(2.23):[3]

An algebra X over a field F is a linear space X over F such that for each ordered pair of elements x,y∈ X a unique product xy ∈ X is defined with the properties
1- x∘ (y∘z)=(x∘y)∘z for all x,y,z ∈ X

2- x∘(y+z)=x∘y+x∘z and (x+y)∘z=x∘z+y∘z for all x, y,z ∈ X

3-λ (x∘y)=(λx)∘y=x∘(λy) for all x,y ∈ X and for all λ∈ F

A non empty set X is called an algebra over a field F if
1- (X,+,.) is a linear space over a filed F

2- (X,+,∘) is a ring

3- λ (x∘y)= (λx)∘y =x∘(λy) for all x,y ∈X and for all λ∈ F

Usually we write xy instead of x∘y for notational convenience .Thus an algebra is a linear space that is also a ring in which (3) holds.

Definition(2.24):[16]

Let X be an algebra over a field F and A be the parameter set. A soft set G_A is called a soft algebra of X over F if G(e) is a subalgebra of X , ∀e ∈ A.

Definition (2.25):
Let X be an algebra over a field F and A be a parameter set. A fuzzy soft set Γ_A is called a fuzzy soft algebra X over F if Γ(e) is a fuzzy subalgebra of X,
∀e ∈ A.

Definition (2.26):

Let X be a linear space over a field F , X is called fuzzy soft linear algebra , if there exists an operation which is called multiplication satisfying that for all x,y,z ∈ X and λ∈F

(i) λ(xy)=(λx)y=x(λy) .
(ii) (xy)z=x(yz) .
(iii) (x+y)z=(xz+yz), and x(y+z)=xy+xz .

Definition(2.27):[17]
An algebra norm is a norm ‖.‖ on an algebra X such that $\|x \circ y\| \leq \|x\| \, \|y\|$ for all x, y ∈ X .i.e. A real valued function on a nonempty set X is called a algebra norm over a field F if
1. X is an algebra
2. ‖.‖ is a norm on X
3. $\|x \circ y\| \leq \|x\| \, \|y\|$ for all x, y∈ X.

Definition(2.28): [12]

A quadruplet (X,N,*,#) is called a fuzzy normed algebra X , if satisfies the following axioms,

(i) * and # are continuous t-norm .
(ii) X is an algebra
(iii) (X,N,*) is a fuzzy normed space.
(iv) $N(xy,ts) \geq N(x,t) \# N(y,s)$ for all $x,y \in X$ and for all $t,s \geq 0$

Definition(2.29)[21]:

A sequence of soft elements $\{\check{x}_N\}$ in a soft normed linear space $(X, \|.\|, A)$ is said to be convergent and converges to a soft element $\tilde{x}$ if $\|\tilde{x}_n - \tilde{x}\| \to 0$ as $n \to \infty$.This means for every $\varepsilon > 0$, chosen arbitrarily, $\exists$ a natural number $N = N(\varepsilon)$, such that $0 \leq \|\tilde{x}_n - \tilde{x}\| < \varepsilon$, whenever $n > N$.
i.e., $n > N \Rightarrow \check{x}_N \in B(\tilde{x}, \varepsilon)$. We denote this by $\check{x}_N \to \tilde{x}$ as $n \to \infty$ or by $\lim n\to\infty \check{x}_N = \tilde{x}$. $\tilde{x}$ is said to be the limit of the sequence $\check{x}_N$ as $n \to \infty$.

Definition(2.30) [21]:

Let $\{\check{x}_N\}$ be a sequence of soft elements of a soft normed space $(X, \|.\|)$ such that $\{\check{x}_N\}$ is said to be a Cauchy sequence if for every $\in \geq 0$, there is $k \in N$ such that $\|\tilde{x}_i - \tilde{x}_j\| < \in$, for all $i, j \geq k$. That is $\|\tilde{x}_i - \tilde{x}_j\| \to 0$ as $i, j \to \infty$.

Definition(2.31): [12]

A normed space is called A complete normed space , if every Cauchy sequence in X is converge to a point of X .

3.1 fuzzy soft spectrum

Definition (3.1): Let $\mathbb{C}$ be the set of complex numbers and $\wp(\mathbb{C})$ be the collection of all nonempty bounded subsets of the set of complex numbers. Also let A be a set of parameters. Then a mapping $\Gamma: A \to \wp(\mathbb{C})$ is called a fuzzy soft complex set. It is denoted by Γ_A . If in particular Γ_A is a singleton set, then after identifying Γ_A with the corresponding fuzzy soft element, it will be called a fuzzy soft complex number. The set of all fuzzy soft complex numbers is denoted by $\mathbb{C}(f)$.

Definition (3.2): Let $\Gamma_A$be fuzzy soft Banach algebra with fuzzy soft unit element $\tilde{e}$.we denote the fuzzy soft spectrum of an element $x \in A$ by Γ_x and define it by

$\Gamma_x = \{\lambda \in \mathbb{C}(f) : \lambda e - x \notin \mathcal{G}(x)\}$

Where $\mathcal{G}(x)$ is the set of all fuzzy soft invertible element,of soft Banach algebra Γ_A.

We denoted the fuzzy soft spectral radius of x r(x) and define it by $r(x) = \text{Sup}\{|\lambda| : \lambda \in \Gamma_x\}$.

Definition (3.3): Let $0 < \varepsilon < 1$ .We denote the fuzzy soft condition spectrum of x in G by $\Gamma_\varepsilon(x)$ and define it by:

$\Gamma_\varepsilon(x) = \{\lambda \in \mathbb{C}(f): \|(\lambda e - x)\|\|(\lambda e - x)^{-1}\| > \frac{1}{\varepsilon}\}$

We denote the fuzzy soft condition spectral radius of x by $r_\varepsilon(x)$ and define it by:

$$r_\varepsilon(x) = \text{Sup}\{|\lambda|: \lambda \in \Gamma_\varepsilon(x)\}.$$

Proposition(3. 4) : Let $\Gamma_A$be a fuzzy soft Banach algebra. If x $\in\Gamma$ satisfies ||x||<1,

then $(e - x)$ is is invertible and $(e - x)^{-1} = e+\sum_{n=1}^{\infty} xn$.

Proof. Since Γ_A is fuzzy soft algebra, so we have $||x^j||\leq||x||^j$ for any positive integer j, so that the infinite series$\sum_{n=1}^{\infty}\|x\|^n$ is fuzzy soft convergent because ||x||<1. So the sequence of partial sum $s_k = \sum_{n=1}^{k} x_n$ is a fuzzy soft Cauchy sequence since $\left\|\sum_{n=1}^{k+p} x^n\right\| < \sum_{n=k}^{k=p}\|x\|^n$.
Since Γ_A is fuzzy soft complete so $\sum_{n=1}^{\infty} x^n$ is fuzzy soft convergent.

Now let $s = e + \sum_{n=1}^{\infty} x^n$.

Now it is only we have to show that $s = (e - x)^{-1}$.

We have

(1) $$(e - x)(e + x+ x^2+ ...x^n) = (e + x + x^2 + ...x^n)(e- x) = e - x^{n+1}$$

Now again since ||x||<1 so $x^{n+1} \to \theta$ as $n\to \infty$. Therefore letting $n\to \infty$ in and remembering that multiplication in Γ is continuous we get, (e−x)s=s(e−x)=e
So that $s = (e - x)^{-1}$. This proves the proposition.

Lemma (3.5): Let Γ_A be a fuzzy soft Banach algebra with fuzzy soft with identity element e

Let $x \in G$ such that $\|x\| \leq 1$ then (e-x) invertible and $(e - x)^{-1} = e + \sum_{n=1}^{\infty} x^n$ Furthermore we have $\|(e - x)^{-1}\| \leq \frac{\|e\|}{\|e\|-\|x\|}$.

Proof. For the proposition (4).

Now let $S_n = e + x + x^2 + \cdots + x^n$ and $y= e + \sum_{n=1}^{\infty} x^n$ Then by the first part we know that $(e - x)^{-1} = y$. Also we have

$$\|y\| = \lim_{n\to\infty}\|S_n\| = \lim_{n\to\infty}\left\|e + \sum_{k=1}^{n} x^k\right\| \leq \|e\| + \sum_{k=1}^{\infty}\|x\|^k = \frac{\|e\|}{\|e\| - \|x\|}.$$

If Γ_A is fuzzy soft with identity (i.e.,$\|e\| = 1$) then we have $\|(e-x)^{-1}\| \leq \frac{1}{1-\|x\|}$

Corollary (3.6): Let Γ be a fuzzy soft Banach algebra. Let x∈ Γ and μ be a fuzzy soft scalar such that |μ|>||x||. Then (μe− x)$^{-1}$ exists and$(\mu e - x)^{-1}$=$\sum_{n=1}^{\infty} \mu^{-n} x^{n-1}(x^0 = e)$.

Proof. y ∈ Γ be such that y^{-1}exists in Γ and α be afuzzy soft scalar such that α(λ) ≠0, ∀λ ∈ A. Then it is clear that

$(\alpha y)^{-1} = \alpha^{-1} y^{-1}$.

Having noted this we can write

$\mu e - x = \mu(e - \mu^{-1}x)$

and now we show that $(e- \mu^{-1}x)^{-1}$ exists. We have $\|e- (e -\mu^{-1}x)\| = \|\mu^{-1}x\| = |\mu|^{-1}\|x\|$ <1 by hypothesis. So, By Corollary 10 $(e - \mu^{-1}x)^{-1}$ exists and hence $(\mu e- x)^{-1}$ exists. For the infinite series representation, using the Proposition 9 we have

$(\mu e- x)^{-1} = \mu^{-1}(e - \mu^{-1}x)^{-1}$

$=\mu^{-1}(e + \sum_{n=1`}^{\infty} [e - (e - \mu^{-1}x)]^n$

$=\mu^{-1}(e + \sum_{n=1}^{\infty}(\mu^{-1}x)^n)$

$$=\sum_{n=1}^{\infty} \mu^{-n} x^{n-1}.$$

This proves the corollary.

Corollary (3.7) :LetΓ_A be a fuzzy soft Banach algebra with fuzzy soft unit element $\check{e}$ such that $\|\check{e}\|= \check{1}$ and $\widetilde{x} \in \mathcal{G}(x)$. Let $\lambda \in \widetilde{\mathbb{C}(f)} - \{0\}$ such that $\|\check{x}\| \lesssim \check{\lambda}$ Then $(\lambda e - x)$ is invertible and $(\mu e - x)^{-1} = \sum_{n=1}^{\infty} \check{\mu}^{-n} \check{x}_n{}^{n-1} : (\check{x}^0 = \check{e})$ .Furthermore we have

$$\|(\widetilde{\lambda e} - 1)^{-1}\| \lesssim \frac{\bar{1}}{|\bar{\lambda}| - \|\check{x}\|}$$

Proof. For the corollary (6) To prove the last statement we need only to substitute $\frac{\ddot{x}}{\ddot{\lambda}}$ with $\check{x}$ in Lemma (5) and we get the result

Theorem (3.8): Let Γ_A be a fuzzy soft Banach algebra with fuzzy soft with identity element e such that $\|e\| = 1$ and x ∈ A. Then we have r(x)≤ $r_\varepsilon(x) \leq \frac{1+\varepsilon}{1-\varepsilon}\|x\|$.

Proof. Since $\Gamma_x \subseteq \Gamma_\varepsilon(x)$, so we have r(x)≤ $r_\varepsilon(x)$. Suppose that $\lambda \in \Gamma_\varepsilon(x)$. If $|\lambda| \leq \|x\|$, then we can easily prove that $|\lambda| \leq \frac{1+\varepsilon}{1-\varepsilon}\|x\|$ Thus we have $r_\varepsilon(x) \leq \frac{1+\varepsilon}{1-\varepsilon}\|x\|$.

Now suppose that $|\lambda| > \|x\|$. Then $(\lambda e - x)$ is invertible and by corollary (3.5) we have $\|(\lambda e - x)^{-1}\| \leq \frac{1}{|\lambda| - \|x\|}$. Consequently by some computations we get $|\lambda| \leq \frac{1+\varepsilon}{1-\varepsilon} \|x\|$.

Thus we conclude that $r_\varepsilon(x) \leq \frac{1+\varepsilon}{1-\varepsilon} \|x\|$

Definition (3.9): Let Γ_A be a fuzzy soft Banach algebra and T: $\Gamma_G \to \mathbb{C}(A)$ be a fuzzy soft linear functional. We say that T is almost fuzzy soft multiplicative if there exists an $\delta > 0$such that for all x,y $\in G$:

$|T(xy) - T(x)T(y)| \leq \delta\|x\|\|y\|$.

Proposition (3.10): Let φ is a fuzzy soft linear functional on a fuzzy soft Banach algebraΓ_A with identity element e such that $\varphi(e) = 1$. Then the following conditions are equivalent.

v) $\varphi(x) = 0$ implies $\varphi(x^2) = 0$ $for\ all\ x \in G$,
vi) $\varphi(x^2) = (\varphi(x))^2, x \in G$,
vii) $\varphi(x) = 0$ implies $\varphi(xy) = 0$ $for\ all\ x, y \in G$
viii) $\varphi(xy) = \varphi(x)\varphi(y)$ $for\ all\ x, y \in G$

proof: (i)→ (ii)

$\varphi(e) = 1$ implies

$\varphi\big(x - \varphi(x)\big)(\lambda) = \varphi(ex - \varphi(x))(\lambda\varphi(e)(\lambda)\varphi(x)(\lambda) - \varphi(x)(\lambda) = 0\ ; \forall \lambda \in A.$

So we have 0=$\varphi\big(x - \varphi(x)\big) = 0$. By (i) we have

$0=\varphi\left(\big(x - \varphi(x)\big)^2\right) = \varphi(x^2 - 2x\varphi(x) + \big(\varphi(x)\big)^2 = \varphi(x^2) - \big(\varphi(x)\big)^2.$

Thus we deduce that $\varphi(x)^2 = \big(\varphi(x)\big)^2$.

(ii)⟹ (iii)

By replacing u+v with (x) in (ii) we get $\varphi(uv + vu) = 2\varphi(u)\varphi(v); u, v \in G, (1)$

Let x,y be in G with $\varphi(x) = 0$. According to (1) we have $\varphi(xy + yx) = 0. (2)$

Hence by (ii) we obtain $\varphi(xy + yx)^2) = 0$. Since $(xy + yx)^2$=$2\varphi(x(yxy) + (yxy)x) = 4\varphi(x)\varphi(yxy) = 0$.

According to (ii) we have $\varphi(xy - yx) = 0, (3)$. If we add two equalities (2) and (3) we conclude that $\varphi(xy) = 0$.

(iii)⟹(iv)

Let x,y ∈ $G. we\ have\ \varphi\big(x - \varphi(x)\big) = 0$. Hence for each $\lambda \in A$ we have

$\varphi\big(x - \varphi(x)\big)(\lambda) = 0$. Thus by (iii) we have $\varphi\left(\big(x - \varphi(x)\big)y\right)(\lambda) = 0$.

Then we get

$0=\varphi\left(\big(x - \varphi(x)\big)y\right)(\lambda) = \varphi(xy - \varphi(x)y)(\lambda) = \varphi(xy)(\lambda) - \varphi(x)(\lambda)\varphi(y)(\lambda); \forall \lambda \in A.$

Thus we have $0=\varphi(xy) - \varphi(x)\varphi(y)$. Consequently we get $\varphi(xy) = \varphi(x)\varphi(y)$.

(iv)⟹ (i)

From (iv) we have $\varphi(xy)(\lambda) = \varphi(x)(\lambda)\varphi(y)(\lambda)$. If $\varphi(x) = 0, then\ \varphi(x)(\lambda) = 0; \forall \in A$ so we have $\varphi(xy)(\lambda) = \varphi(x)(\lambda)(y)(\lambda) = 0.\varphi(y)(\lambda) = 0$

Therefore $\varphi(xy) = 0$.

Clearly if φ is fuzzy soft multiplicative linear functional then φ is fuzzy soft Jordan multiplicative functional. Now we have the following corollary.

Corollary(3.11)
Let φ is a fuzzy soft Jordan multiplicative linear functional on fuzzy soft Banach algebra Γ_A with identity element e such that $\phi(e) = 1$. Then φ is fuzzy soft multiplicative.

Lemma (3.12): Letφ is a fuzzy soft multiplicative linear functional on soft fuzzy Banach algebra Γ_G Then we have $\varphi(x) \in \Gamma_G$; x ∈ G.
Proof: For x ∈ G we set z=$\varphi(x)e - x$ Then we have $\varphi(z)(\lambda) = \varphi(x)(\lambda)\varphi(e)(\lambda) - \varphi(x)(\lambda) = \varphi(x)(\lambda) - \varphi(x)(\lambda) = 0$
Hence we have $\varphi(z) = 0$. Therefore z∈ $ker\varphi$. So we have z∈ $sing(G)$. Consequently $\varphi(x) \in \Gamma_G$.

Remark (3.13): Now suppose thatφ is fuzzy soft multiplicative linear functional and let z ∈ Γ_G , for some x ∈ G. Then ze-xis not invertible and so we have $\varphi(ze - x) = 0$.

We know that, for invertible element y we have $\varphi(y) = 0$. Thus $z\varphi(e) - \varphi(x) = 0$. So we have $z=\varphi(x)$. .
Consequently we have the following theorem.

Theorem (3.14): Let Γ_A be a commutative fuzzy soft Banach algebra and let $x \in G$ then
$\Gamma_G = \{\varphi(x): \varphi \text{ is a fuzzy soft multiplicative linear functional}\}$
Proof. It follows from lemma (3.12) and last statement.

Lemma(3.15): Let $T:\Gamma_E(A) \longrightarrow \mathbb{C}(f)$ be a fuzzy soft bounded linear functional. ThenT is almost fuzzy soft multiplicative.
Proof: For each $\check{x}, \check{y} \in A$ we have
$$|T(\check{x}\check{y}) - T(\check{x})T(\check{y})| \leq |T(\check{x}\check{y})| + |T(\check{x})T(\check{y})| \leq \|T\|\|\check{x}\check{y}\| + \|T\|^2\|\check{x}\|\|\check{y}\|$$
$$= (\|T\| + \|T\|^2)\|\check{x}\|\|\check{y}\|$$
Thus T is almost soft multiplicative where $\bar{\bar{\delta}} = (\|T\| + \|T\|^2)$

Proposition (3.16): LetΓ_A is a fuzzy soft Banach algebra and $T_1:\Gamma_E(A) \longrightarrow \mathbb{C}(f)$ is a fuzzy soft multipicactive linear functional and $T_2:\Gamma_E(A) \longrightarrow \mathbb{C}(f)$ is a soft bounded linear functional. Then$T_1 + T_2$ is almost fuzzy soft multiplicative functional but not multiplicative.
Proof: For each $\check{x}, \check{y} \in A$ we have
$|(T_1 + T_2)(\check{x}\check{y}) - (T_1 + T_2)(\check{x})(T_1 + T_2)(\check{y})|=$

$|T_1(\check{x}\check{y}) + T_2(\check{x}\check{y}) - (T_1(\check{x}) + T_2(\check{y}))(T_1(\check{y}) + T_2(\check{y})|=$

$$|T_1(\check{x}\check{y}) + T_2(\check{x}\check{y}) - T_1(\check{x})T_1(\check{y}) - T_2(\check{x})T_2(\check{y}) - T_1(\check{x})T_2(\check{y}) - T_2(\check{x})T_1(\check{y})| \leq$$

$$|T_1(\check{x}\check{y}) - T_1(\check{x})T_1(\check{y})| + |T_2(\check{x}\check{y}) - T_2(\check{x})T_2(\check{y})| + |T_1(\check{x})T_2(\check{y})| + |T_2(\check{x})T_1(\check{y})|$$

So by lemma(14) we get

$$|(T_1 + T_2)(\check{x}\check{y}) - (T_1 + T_2)(\check{x})(T_1 + T_2)(\check{y})| \leq$$

$$(\|T_2\| + \|T_2\|^2)\|\check{x}\|\|\check{y}\| + \acute{2}\|T_1\|\|\check{x}\|\|T_2\|\|\check{y}\| =$$

$(\|T_2\| + \|T_2\|^2)\|\check{x}\|\|\check{y}\| + \acute{2}\|T_1\|\|T_2\|\|\check{x}\|\|\check{y}\|$.

Thus$(T_1 + T_2)$ is almost soft multiplicative. Clearly$(T_1 + T_2)$is not multiplicative.

Definition(3.17):LetΓ_A be a fuzzy soft Banach algebra. We say that fuzzy soft linear functional $\varphi:\Gamma_E(A) \longrightarrow \mathbb{C}(f)$ is almost soft Jordan multiplicative functional if there exist $\bar{\bar{\delta}} \gtrsim \bar{0}$such that:

$$\left|\varphi(\check{X}^2)-\varphi(\check{X})^2\right| \leq \bar{\bar{\delta}}\|\check{X}\|^2, \forall \check{x} \in A$$

Corollary(3.18): Let be a fuzzy soft Banach algebra and T_1:$\Gamma_E(A) \longrightarrow \mathbb{C}(f)$ is a fuzzy soft Jordan multiplicative linear functional and T_2:$\Gamma_E(A) \longrightarrow \mathbb{C}(f)$ is a soft bounded linear functional. Then $T_1 + T_2$is almost fuzzy soft Jordan multiplicative linear functional.
Proof: It can be proved by similar method which we stated in theorem (13).

Definition(3.19): Let Γ_A be a soft Banach algebra with identity element $\check{e}$ and let $\bar{\bar{\varepsilon}} \acute{>} \bar{0}$ We denote the fuzzy soft ε_ condition spectrum of an element $\check{X} \in \check{A}$ by $\Gamma_{\bar{\varepsilon}}(\check{X})$and define it by: $\Gamma_{\bar{\varepsilon}} = \left\{\check{\lambda} \breve{\in} \mathbb{C}(F): \left\|\check{\lambda}\, \check{e} - \check{x})^{-1}\right\| \breve{\geq} \frac{\check{1}}{\varepsilon}\right\}$.

Theorem(3.20): Let Γ_A be a fuzzy soft Banach algebra with identity element $\check{e}$ and let $\bar{\bar{\varepsilon}} \acute{>} \bar{0}$. Let φ:$\Gamma_E(A) \longrightarrow \mathbb{C}(f)$ be a fuzzy soft linear functional such that $\varphi(\check{e})=\check{1}$ and $\varphi(e) \bar{\bar{\in}} \Gamma_{\check{\varepsilon}}$ for $\check{X} \in \check{A}$. Then is fuzzy soft multiplicative functional.

Proof: We prove that for all $\check{X} \in \check{A}$ we have $T(\check{x}) \in \Gamma_x$.We put $\bar{\lambda} = \varphi(\check{x})$. If $\bar{\bar{\lambda}} \in \Gamma_x$ then φ is multiplicative. If $\bar{\bar{\lambda}} \notin \Gamma_x$ then $\bar{\bar{\lambda}}\check{e} - \check{x}$ is invertible and so$\bar{\bar{\lambda}}\check{e} - \check{x} \in \mathcal{G}(x)$.Suppose that $\acute{z} \breve{>} \check{\varepsilon}\left\|(\bar{\bar{\lambda}}\check{e} - \check{x})^{-1}\right\|$ Then we have $\left\|(\bar{\bar{\lambda}}\check{e} - \check{x})^{-1}\right\| \breve{<} \frac{\check{1}}{\varepsilon}$.Thus we get $\left\|(\bar{\bar{\lambda}}\check{e}\acute{z} - \check{x}\acute{z})^{-1}\right\| \breve{<} \frac{\check{1}}{\varepsilon}$ Consequently we have $\bar{\bar{\lambda}}\, \acute{z} = \varphi(\check{x})\acute{z} = \varphi(\check{x}\acute{z}) \notin \Gamma_{\check{\varepsilon}}(\acute{z}\check{x})$ which is a contradiction. So φ is fuzzy soft multiplicative.

Lemma(3.21). Let$\bar{\bar{\delta}} \acute{>} \bar{0}$ and $\check{X} \in \check{A}$ Then$\Gamma_x \subseteq \Gamma_{\widetilde{\delta x}}$

Proof: It can be proved easily by definition.

Theorem(3.22): Let Γ_A be a fuzzy soft Banach algebra with identity $\check{e}$ element and φ be an almost fuzzy soft multiplicative linear functional on A If $\varphi(\check{e})=\check{1}$ Then for every element $\check{x} \bar{\bar{\in}} A$ we have $\varphi(\check{x}) \bar{\bar{\in}} \Gamma_{\delta x}$

Proof: Let $\check{x} \bar{\bar{\in}} A$ and $\bar{\bar{\lambda}} = \varphi(\check{x})$ .If $\bar{\bar{\lambda}}\check{e} - \check{x}$ is not invertible then $\bar{\bar{\lambda}} \in \Gamma_x \subseteq \Gamma_{\widetilde{\delta x}}$ So $\bar{\bar{\lambda}} \in T_\varepsilon(\check{x})$. Now assume that is invertible. Then

$$\bar{\bar{1}} = |\varphi(\check{e})| = \left|\varphi(\check{x}) - \check{0}\right| =$$

$$\left|\varphi(\check{e}) - \varphi\left(\bar{\bar{\lambda}}\check{e} - \check{x}\right)T((\bar{\bar{\lambda}}\check{e} - \check{x}))^{-1}\right|$$

$$\lesseqgtr \bar{\bar{\delta}}\left\|(\bar{\bar{\lambda}}\check{e} - \check{x})((\bar{\bar{\lambda}}\check{e} - \check{x}))^{-1}\right\|$$

Thus we have

$$\left\|(\bar{\bar{\lambda}}\check{e} - \check{x})((\bar{\bar{\lambda}}\check{e} - \check{x}))^{-1}\right\| \lesseqgtr \frac{\check{1}}{\varepsilon}$$

So we conclude that $\bar{\bar{\lambda}} \in \Gamma_{\varepsilon x}$. Consequently we have $\varphi\,(\check{x}) \bar{\bar{\in}} \Gamma_{\delta x}$.

4.CONCLUSION

In this paper we introduced the ideal of fuzzy soft spectrum. we studied some basic properties of these ideal in fuzzy soft Banach algebras. Finally some new result and theorems about them over fuzzy soft Banach algebra have investigated.

References

1. H. Aktas and N. Cagman, Soft sets and soft groups, Inform. Sci. 177 (2007) 2226-2735.

2. N. Cagman, S. Karatas and S. Enginoglu, Soft topology, Comput. Math. Appl. 62 (2011) 351-358.

3.F.F.Bonsall.J.Duncan,Complete Normed Algebras,1973.

4. S. Das and S. K. Samanta, Soft linear functionals in soft normed linear

5. S. Das, P. Majumdar and S. K. Samanta, On Soft linear spaces and soft normed linear spaces, Ann. Fuzzy Math Inform. 9 (1) (2015) 91-109.

6.Y.B.JUN,Soft BCK/BCI-algebras, Comput.Math.Appl.56(2008),1408-1413.

7. Kamel, A. and Mirzavaziri, M., Closability of farthest point in fuzzy normed spaces, Bulletin of Mathematical Analysis and Applications, Vol.2,140-145, (2010).

8.A.K.Katsaras and D.B.Liu, fuzzy vector and fuzzy topological vector space, J.Math.Anal.Appl.58(1977), 135-146.

9.J.R.Kider,On fuzzy normed spaces,EnTech.Journal,Vol.29,no.9,(2011),1790-1795.

10.P.Lubczonok,Fuzzy vector space,Fuzzy set and Systems, 38(1990).

11. Maji, K., Biswas, R., and Roy, A., Fuzzy Soft Set, Journal of Fuzzy Mathematics 9,589-602, (3) (2001).

12. P. K. Maji, R. Biswas and A. R. Roy, An application of soft sets in a decision making problem,Comput. Math. Appl. 44 (2002) 1077-1083.

13. P. K. Maji, R. Biswas and A. R. Roy, Soft set theory, Comput. Math. Appl. 45 (2003) 555-562.

14. D. Molodtsov, Soft set theory first results, Comput. Math. Appl. 37 (1999) 19-31.

15. M.A.NAIMARK, Normed algebras ,1972

16.Pabitra,M.,RoyRanjit,B.,Bayrawov, and Cigdem G.,An Application of soft set in A Decision Making problem,Comput.Math.Appl.44,pp.1077-1038,(2002).

17. S. H. J. Petroudi, S. A. Sadati, A. Yaghobi, Almost Soft multiplicative linear functional, The first national conference on Applied mathematics in engineering and basic science. (2017), Shiraz, Iran

18. S. H. J. Petroudi, S. A. Sadati, Z. Nabati, From soft set theory to a decision making problem, The first conference on modeling mathematics and statistics in applied studies. (2017), Chalos, Iran..

19.Sujoy,D.,Pinaki,M.,Syamal,On soft Linear space and soft Normed Linear space ,Ann.fuzzy Math .Inform.9,pp.91-109,(2015).

20. R. Thakur, S. K. Samanta, Soft Banach Algebra, Ann. Fuzzy Math. Inform. 10 (3) (2015) 397-412.

21.Tudor, B.,Ftaavius,P.,Sorin N.,On fuzzy normed algebra,J.Nonlinear Sci.Appl.9(2016).

المؤتمر العلمي الدولي الثالث عشر
لجمعية الرياضيات العراقية والمنعقد تحت شعار
نحو عالم متقدم : الرياضيات والتقنيات في سباق الابتكار
للمدة 24 - 25 نيسان 2024
الكوفة – النجف الاشرف

توليد خماسيّة فيثاغوريّة من خماسيتين فيثاغوريّتين

الدكتور باسل حمدو العرنوس الأستاذ الدكتور عبد الباسط الخطيب
عميد كلية التربية الثانية رئيس جامعة البعث

ملخّص البحث

قمنا في هذا البحث بتعريف عمليّة مغلقة $*$ على مجموعة الخماسيّات الفيثاغوريّة PP_5, على النحو الآتي:

ليكن $(a_1,a_2,a_3,a_4,a_5),(b_1,b_2,b_3,b_4,b_5)\in PP_5$, نعرّف على PP_5 العمليّة الثّنائيّة الآتية:

$$(a_1,a_2,a_3,a_4,a_5)*(b_1,b_2,b_3,b_4,b_5)=(c_1,c_2,c_3,c_4,c_5)$$

حيث:

$$\begin{aligned} c_1 &= a_1b_1-a_2b_2-a_3b_3-a_4b_4\\ c_2 &= a_1b_2+a_2b_1+a_3b_4-a_4b_3\\ c_3 &= a_1b_3+a_3b_1+a_4b_2-a_2b_4\\ c_4 &= a_1b_4+a_4b_1+a_2b_3-a_3b_2 \end{aligned} \quad , \quad c_5=a_5b_5$$

عندئذٍ $(PP_5,*)$ بنية جبريّة.

ثمّ أثبتنا أنّ هذه البنية, هي نصف زمرة.

الكلمات المفتاحيّة: خماسيّة فيثاغوريّة, رباعيّة فيثاغوريّة, ثلاثيّة فيثاغوريّة, بنية, نصف زمرة, محايد, نصف مقلوب.

استخدام قانون التحويل التنسوري في التشفير

1.مقدّمة

لتكن R حلقة صحيحة معرّفة فوق الحقل العددي K, تكون الثلاثيّة (a,b,c) والتي عناصرها من R ثلاثيّة فيثاغوريّة إذا كانت $a^2+b^2=c^2$.

في العام 1984 عرّف إيكيرت Eckert عمليّة جمع بين الثلاثيّات الفيثاغوريّة عندما $R=\mathbf{Z}$, على النحو الآتي:

$$(a_1,b_1,c_1)+(a_2,b_2,c_2)=(a_1a_2-b_1b_2,a_1b_2+b_1a_2,c_1c_2)$$

بحيث تشكّل مجموعة كلّ الثّلاثيّات الفيثاغوريّة الصحيحة بالإضافة إلى $(1,0,1)$ مع العمليّة $+$ زمرة تبديلية [1] .

بعد ذلك وتحديداً في العام 1991 قام زناردو Zanardo و زانيير Zannier بتعميم المجال من $\mathbf{Z}$ إلى أي حلقة من الأعداد الصحيحة R [2] .

في العام 1996 قام بيوريجارد Beauregard و سوريانريان Suryanarayan بتعريف عمليّة مغلقة * على مجموعة كل الثلاثيّات الفيثاغوريّة الصحيحة, على النحو الآتي [3]:

$$(a_1,b_1,c_1)*(a_2,b_2,c_2)=(a_1a_2,b_1c_2,c_1b_2+b_1b_2+c_1c_2)$$

في هذا البحث, قمنا بتعريف الخماسيّات الفيثاغوريّة, ومن ثمّ تعريف عمليّة مغلقة * على مجموعة كل الخماسيّات الفيثاغوريّة PP_5, وأثبتنا أنّ البنية $(PP_5,*)$ هي نصف زمرة, وأوجدنا العنصر المحايد بالنسبة للعمليّة *.

استخدمنا في ذلك الأعداد فوق العقديّة (الكواترنيون)

2. هدف البحث

يهدف البحث إلى إيجاد عمليّة مغلقة على مجموعة كل الخماسيّات الفيثاغوريّة الصحيحة, وبالتالي توليد خماسيات فيثاغوريّة من خماسيتين فيثاغوريّتين.

3. المناقشة و النّتائج

أوّلاً: مجموعة الأعداد فوق العقدية [4] :

تعريف1:

تعرّف مجموعة الأعداد فوق العقديّة (الكواتيرنيون) H, بأنّها مجموعة كلّ الأعداد التي لها الشّكل:

$$q=q_0+q^*=q_0+q_1i+q_2j+q_3k$$

حيث: $q_0,q_1,q_2,q_3\in\mathbb{R}$ و i,j,k وحدات تحقّق:

$$i^2=j^2=k^2=ijk=-1$$
$$ij=k=-ji$$
$$jk=i=-kj$$
$$ki=j=-ik$$

مثال 1: الأعداد الآتية فوق عقديّة:

$$4+2i-2j+3k\quad,\quad -5\quad,\quad 2i-3j+3k\quad,\quad 5-4i$$

لكل عدد فوق عقدي, قسمين, قسم حقيقي (سلّمي) وجزء متّجهي, فمن أجل العدد فوق العقدي:

$$q=q_0+q^*=q_0+q_1i+q_2j+q_3k$$

فإنّ الجزء الحقيقي: q_0, أمّا الجزء المتّجهي: $q^*=q_1i+q_2j+q_3k$

ثانياً: جبر الأعداد فوق العقديّة [5] :

ليكن لدينا $p,q\in\mathrm{H}$ حيث:

$$p = p_0 + p^* = p_0 + p_1 i + p_2 j + p_3 k$$
$$q = q_0 + q^* = q_0 + q_1 i + q_2 j + q_3 k$$

تعريف2:

تُعرّف عمليّة جمع الأعداد فوق العقديّة $(+)$ على النّحو الآتي:

$$p + q = (p_0 + q_0) + \left(p^* + q^*\right)$$
$$= \left(p_0 + q_0\right) + \left(p_1 + q_1\right) i + \left(p_2 + q_2\right) j + \left(p_3 + q_3\right) k$$

واضح أنّ الصّفر هو محايد بالنّسبة لعمليّة الجمع, وكذلك فإنّ لكل عدد p من H نظير جمعي, هو:

$$-p = -p_0 - p^* = -p_0 - p_1 i - p_2 j - p_3 k$$

تعريف3:

تُعرّف عمليّة ضرب الأعداد فوق العقديّة $(.)$ على النّحو الآتي:

$$p.q = (p_0.q_0) - \left(p_1.q_1 + p_2.q_2 + p_3.q_3\right) +$$
$$+ p_0\left(q_1 i + q_2 j + q_3 k\right) + q_0\left(p_1 i + p_2 j + p_3 k\right) +$$
$$+ \left(p_2.q_3 - p_3.q_2\right) i + \left(p_3.q_1 - p_1.q_3\right) j + \left(p_1.q_2 - p_2.q_1\right) k$$

وهي تكتب بالشّكل:

$$p.q = (p_0.q_0) - p^* q^* + p_0 q^* + q_0 p^* + p^* \times q^*$$

حيث:

$$p^*.q^* = p_1.q_1 + p_2.q_2 + p_3.q_3$$
$$p^* \times q^* = \begin{vmatrix} i & j & k \\ p_1 & p_2 & p_3 \\ q_1 & q_2 & q_3 \end{vmatrix}$$

ولأنّ: $p^* \times q^* \neq q^* \times p^*$ فإنّ الضّرب ليس عمليّة تبديليّة.

ثالثاً: المرافق, النّظيم, المقلوب [6] **:**

ليكن $q = q_0 + q^* = q_0 + q_1 i + q_2 j + q_3 k$ عدد فوق عقديّ.

تعريف4:

يُعرّف مرافق العدد q بانّه العدد $\bar{q}$ من H المعطى بالعلاقة:

$$\bar{q} = q_0 - q^* = q_0 - q_1 i - q_2 j - q_3 k$$

من التّعريف ينتج أنّ:

1. $\overline{(\bar{q})} = q$ لأنّ: $\overline{(\bar{q})} = \overline{(q_0 - q^*)} = q_0 - (-q^*) = q_0 + q^* = q$
2. $q + \bar{q} = 2q_0$.
3. $q.\bar{q} = \bar{q}.q$ وعلاوةً على ذلك فإنّ:
$$q.\bar{q} = \bar{q}.q = {q_0}^2 + {q_1}^2 + {q_2}^2 + {q_3}^2$$
4. $\overline{(q.p)} = \bar{p}.\bar{q}$ حيث: $p \in \mathrm{H}$.

تعريف5:

يُعرّف نظيم العدد q بانّه العدد $|q|$ من $\mathbb{H}$ المعطى بالعلاقة:

$$|q| = \sqrt{q.\bar{q}} = \sqrt{{q_0}^2 + {q_1}^2 + {q_2}^2 + {q_3}^2}$$

نتائج: ينتج من التّعريف أنّ:

1. $|q| = |\bar{q}|$.
2. $|p.q| = |p|.|q|$ حيث $p \in \mathrm{H}$ لأنّ:

$$|p.q|^2 = p.q.(\overline{p.q}) = p.q.\bar{q}.\bar{p} = p.|q|^2.\bar{p} = p.\bar{p}.|q|^2 = |p|^2.|q|^2$$

رابعاً: أعداد ليبشتز الصّحيحة [7] :

تعريف 6:

أعداد ليبشتز الصّحيحة هي مجموعة كلّ الأعداد فوق العقديّة التي مكوّناتها أعداد صحيحة, ونرمز لها بالرمز $\mathbb{L}$, أي أنّ:

$$\mathbb{L} = \{a + bi + cj + dk \in \mathrm{H};\ a,b,c,d \in \mathbb{Z}\}$$

خامساً: الخماسيّات الفيثاغوريّة $\mathbb{Z}$:

نعلم من نظريّة الأعداد, أنّ الثّلاثيّات الفيثاغوريّة في $\mathbb{Z}$ هي مجموعة كلّ الثّلاثيّات $\{x, y, z\}$ التي تحقّق معادلة ديوفانتس الآتية:

$$x^2 + y^2 = z^2 \ ;\ x,y,z \in \mathbb{Z}$$

وعليه فإنّ الخماسيّات الفيثاغوريّة, هي مجموعة كلّ الخماسيّات $\{x, y, z, w, r\}$ والتي تحقّق معادلة ديوفانتس الآتية:

$$x^2 + y^2 + z^2 + w^2 = r^2 \ ;\ x,y,z,w,r \in \mathbb{Z}^+$$

تعريف 7:

تسمّى خماسيّة فيثاغوريّة, كلّ خماسيّة (a,b,c,d,e), حيث $a,b,c,d,e \in \mathbb{Z}$, وتحقّق:

$$a^2 + b^2 + c^2 + d^2 = e^2$$

سنرمز لمجموعة كلّ الخماسيّات الفيثاغوريّة بالرّمز PP_5 وبالتّالي يكون:

$$PP_5=\left\{(a,b,c,d,e);\ a^2+b^2+c^2+d^2=e^2 : a,b,c,d,e\in \square\right\}$$

مبرهنة 1 وتعريف 8:

ليكن $(a_1,a_2,a_3,a_4,a_5),(b_1,b_2,b_3,b_4,b_5)\in PP_5$, نعرّف على PP_5 العمليّة الثّنائيّة الآتية:

$$(a_1,a_2,a_3,a_4,a_5)*(b_1,b_2,b_3,b_4,b_5)=(c_1,c_2,c_3,c_4,c_5)$$

حيث:

$$\begin{aligned} c_1&=a_1b_1-a_2b_2-a_3b_3-a_4b_4\\ c_2&=a_1b_2+a_2b_1+a_3b_4-a_4b_3\\ c_3&=a_1b_3+a_3b_1+a_4b_2-a_2b_4\\ c_4&=a_1b_4+a_4b_1+a_2b_3-a_3b_2 \end{aligned} \quad , \quad c_5=a_5b_5$$

عندئذٍ $(PP_5,*)$ بنية جبريّة.

الإثبات:

إنّ: $(0,0,0,0,0)\in PP_5$ وبالتّالي فإنّ: $PP_5\neq\{\ \}$

ليكن $(a_1,a_2,a_3,a_4,a_5),(b_1,b_2,b_3,b_4,b_5)\in PP_5$, ولنعرّف العددين:

$$p_1=\frac{a_1}{a_5}+\frac{a_2}{a_5}i+\frac{a_3}{a_5}j+\frac{a_4}{a_5}k\ ,\quad p_2=\frac{b_1}{b_5}+\frac{b_2}{b_5}i+\frac{b_3}{b_5}j+\frac{b_4}{b_5}k$$

ويكون:

$$|p_1|=\sqrt{\frac{{a_1}^2+{a_2}^2+{a_3}^2+{a_4}^2}{{a_5}^2}}=\sqrt{\frac{{a_5}^2}{{a_5}^2}}=1,$$

$$|p_2|=\sqrt{\frac{{b_1}^2+{b_2}^2+{b_3}^2+{b_4}^2}{{b_5}^2}}=\sqrt{\frac{{b_5}^2}{{b_5}^2}}=1$$

وبالتّالي يكون:

$$|p_1.p_2|=|p_1|.|p_2|=1$$

في الحقيقة فإنّ:

$$p_1.p_2=\frac{a_1b_1}{a_5b_5}-\left(\frac{a_2b_2+a_3b_3+a_3b_3}{a_5b_5}\right)+\frac{a_1}{a_5}\left(\frac{b_2}{b_5}i+\frac{b_3}{b_5}j+\frac{b_4}{b_5}k\right)$$
$$+\frac{b_1}{b_5}\left(\frac{a_2}{a_5}i+\frac{a_3}{a_5}j+\frac{a_4}{a_5}k\right)+\begin{vmatrix} i & j & k \\ \frac{a_2}{a_5} & \frac{a_3}{a_5} & \frac{a_4}{a_5} \\ \frac{b_2}{b_5} & \frac{b_3}{b_5} & \frac{b_4}{b_5} \end{vmatrix}$$

بإصلاح العلاقة, يكون:

$$p_1.p_2=\left(\frac{a_1b_1-a_2b_2-a_3b_3-a_3b_3}{a_5b_5}\right)+\left(\frac{a_1b_2+a_2b_1+a_3b_4-a_4b_3}{a_5b_5}\right).i$$

وبحسب

$$=+\left(\frac{a_1b_3+a_3b_1+a_4b_2-a_2b_4}{a_5b_5}\right).j+\left(\frac{a_1b_4+a_4b_1+a_2b_3-a_3b_2}{a_5b_5}\right).k$$

فرضيات المبرهنة يكون:

$$p_1.p_2=\left(\frac{c_1}{c_5}\right)+\left(\frac{c_2}{c_5}\right).i+\left(\frac{c_3}{c_5}\right).j+\left(\frac{c_4}{c_5}\right).k$$

ولأنّ $|p_1.p_2|=1$ فإنّ:

$$\left(\frac{c_1}{c_5}\right)^2+\left(\frac{c_2}{c_5}\right)^2+\left(\frac{c_3}{c_5}\right)^2+\left(\frac{c_4}{c_5}\right)^2=1$$

ومنه فإنّ:

$$c_1{}^2+c_2{}^2+c_3{}^2+c_4{}^2=c_5{}^2$$

وهذا يعني أنّ: $(c_1,c_2,c_3,c_4,c_5)\in PP_5$.

أي أنّ العمليّة $*$ هي قانون تشكيل داخلي على PP_5, وبالتّالي $(PP_5,*)$ هي بنية.

مثال 2:

إنّ: $(1,2,4,10,11),(1,2,8,10,13)\in PP_5$ ويكون:

$$(1,2,4,10,11)*(1,2,8,10,13)=(-135,-36,12,28,143)$$

إنّ:

$$(-135)^2+(-36)^2+(12)^2+(28)^2=20449$$
$$(143)^2=20449$$

وبالتّالي فإنّ: $(-135,-36,12,28,143)\in PP_5$.

مبرهنة 2:

تقبل العمليّة $*$ في البنية الجبريّة $(PP_5,*)$ عنصراً محايداً, هو $(1,0,0,0,1)$.

الإثبات:

لنفرض وجود عنصر محايد يميني (e_1,e_2,e_3,e_4,e_5) للعمليّة $*$, عندئذٍ يكون:

مهما يكن (a_1,a_2,a_3,a_4,a_5) من $PP_5\setminus\{(0,0,0,0,0)\}$, فإنّ:

$$(a_1,a_2,a_3,a_4,a_5)*(e_1,e_2,e_3,e_4,e_5)=(a_1,a_2,a_3,a_4,a_5)$$

وبالتّالي يكون:

$$\begin{aligned}
a_1e_1-a_2e_2-a_3e_3-a_4e_4&=a_1\\
a_1e_2+a_2e_1+a_3e_4-a_4e_3&=a_2\\
a_1e_3+a_3e_1+a_4e_2-a_2e_4&=a_3\\
a_1e_4+a_4e_1+a_2e_3-a_3e_2&=a_4\\
a_5e_5&=a_5
\end{aligned}\qquad(1)$$

من العلاقة الأخيرة ينتج أنّ $e_5=1$, ولأنّ $(e_1,e_2,e_3,e_4,e_5)\in PP_5$ فإنّ إحدى الأعداد e_1,e_2,e_3,e_4 يساوي 1 أو -1 والباقي أصفاراً. بالعودة إلى الجملة (1), تُـكتب المعادلات الأربع الأولى منها بالشّكل:

$$\begin{aligned}
a_1e_1-a_2e_2-a_3e_3-a_4e_4&=a_1\\
a_2e_1+a_1e_2-a_4e_3+a_3e_4&=a_2\\
a_3e_1+a_4e_2+a_1e_3-a_2e_4&=a_3\\
a_4e_1-a_3e_2+a_2e_3+a_1e_4&=a_4
\end{aligned}\qquad(2)$$

نضرب الأولى بـ a_2 والثانية بـ $-a_1$ ونجمع المعادلتين الناتجتين, ثمّ نضرب الأولى بـ a_3 والثالثة بـ $-a_1$ ونجمع المعادلتين الناتجتين, وأخيراً نضرب الأولى بـ a_4 والرابعة بـ $-a_1$ ونجمع المعادلتين الناتجتين, نحصل على:

$$\begin{aligned}
&-(a_1^{\,2}+a_2^{\,2})e_2+(a_1a_4-a_2a_3)e_3-(a_1a_3+a_2a_4)e_4=0\\
&-(a_1a_4+a_2a_3)e_2-(a_1^{\,2}+a_3^{\,2})e_3+(a_1a_2-a_3a_4)e_4=0 \qquad (3)\\
&(a_1a_3-a_4a_2)e_2-(a_1a_2+a_3a_4)e_3-(a_1^{\,2}+a_4^{\,2})e_4=0
\end{aligned}$$

الجملة (3) هي جملة متجانسة, وحيث أنّ اثنين من e_2,e_3,e_4 على الأقل تساوي الصفر, فإنّ $e_2=e_3=e_4=0$, بالتعويض في الجملة (2) نحصل على:

$$a_1e_1=a_1,\ \ a_2e_1=a_2,\ \ a_3e_1=a_3,\ \ \ a_4e_1=a_4$$

وهي تكافئ: $e_1=1$, وعلى هذا يكون:

$$(e_1,e_2,e_3,e_4,e_5)=(1,0,0,0,1)$$

وبنفس الطريقة نصل إلى أنّ: $(1,0,0,0,1)$ محايد يساري للعمليّة $*$.

مبرهنة 3:

إنّ العمليّة $*$ في البنية الجبريّة $(PP_5,*)$ هي عمليّة تجميعيّة.

الإثبات:

ليكن: $(a_1,a_2,a_3,a_4,a_5),(b_1,b_2,b_3,b_4,b_5),(c_1,c_2,c_3,c_4,c_5)\in PP_5$ لنفرض أنّ:

$$\begin{aligned}
&(d_1,d_2,d_3,d_4,d_5)=\\
&=(a_1,a_2,a_3,a_4,a_5)*\left[(b_1,b_2,b_3,b_4,b_5)*(c_1,c_2,c_3,c_4,c_5)\right]
\end{aligned}$$

عندئذٍ يكون:

$$\begin{aligned}
(d_1,d_2,d_3,d_4,d_5)=(a_1,a_2,a_3,a_4,a_5)*\\
(b_1c_1-b_2c_2-b_3c_3-b_4c_4,b_1c_2+b_2c_1+b_3c_4-b_4c_3,\\
b_1c_3+b_3c_1+b_4c_2-b_2c_4,b_1c_4+b_4c_1+b_2c_3-b_3c_2,b_5c_5)
\end{aligned}$$

وبالتالي:

$$\begin{aligned}
d_1=a_1(b_1c_1-b_2c_2-b_3c_3-b_4c_4)-a_2(b_1c_2+b_2c_1+b_3c_4-b_4c_3)\\
-a_3(b_1c_3+b_3c_1+b_4c_2-b_2c_4)-a_4(b_1c_4+b_4c_1+b_2c_3-b_3c_2)
\end{aligned}$$

وكذلك:

$$d_2 = a_1(b_1c_2 + b_2c_1 + b_3c_4 - b_4c_3) + a_2(b_1c_1 - b_2c_2 - b_3c_3 - b_4c_4) +$$
$$+ a_3(b_1c_4 + b_4c_1 + b_2c_3 - b_3c_2) - a_4(b_1c_3 + b_3c_1 + b_4c_2 - b_2c_4)$$
$$d_3 = a_1(b_1c_3 + b_3c_1 + b_4c_2 - b_2c_4) + a_3(b_1c_1 - b_2c_2 - b_3c_3 - b_4c_4) +$$
$$+ a_4(b_1c_2 + b_2c_1 + b_3c_4 - b_4c_3) - a_2(b_1c_4 + b_4c_1 + b_2c_3 - b_3c_2)$$
$$d_4 = a_1(b_1c_4 + b_4c_1 + b_2c_3 - b_3c_2) + a_4(b_1c_1 - b_2c_2 - b_3c_3 - b_4c_4) +$$
$$+ a_2(b_1c_3 + b_3c_1 + b_4c_2 - b_2c_4) - a_3(b_1c_2 + b_2c_1 + b_3c_4 - b_4c_3)$$
$$d_5 = a_5(b_5c_5) = a_5b_5c_5$$

الآن بفرض أنّ:

$$(f_1, f_2, f_3, f_4, f_5) =$$
$$= \left[(a_1, a_2, a_3, a_4, a_5) * (b_1, b_2, b_3, b_4, b_5)\right] * (c_1, c_2, c_3, c_4, c_5)$$

عندئذٍ يكون:

$$(f_1, f_2, f_3, f_4, f_5) = (a_1b_1 - a_2b_2 - a_3b_3 - a_4b_4,$$
$$a_1b_2 + a_2b_1 + a_3b_4 - a_4b_3, a_1b_3 + a_3b_1 + a_4b_2 - a_2b_4,$$
$$a_1b_4 + a_4b_1 + a_2b_3 - a_3b_2, a_5b_5) * (c_1, c_2, c_3, c_4, c_5)$$

وبالتالي:

$$f_1 = (a_1b_1 - a_2b_2 - a_3b_3 - a_4b_4)c_1 - (a_1b_2 + a_2b_1 + a_3b_4 - a_4b_3)c_2 -$$
$$-(a_1b_3 + a_3b_1 + a_4b_2 - a_2b_4)c_3 - (a_1b_4 + a_4b_1 + a_2b_3 - a_3b_2)c_4$$
$$= a_1(b_1c_1 - b_2c_2 - b_3c_3 - b_4c_4) - a_2(b_2c_1 + b_1c_2 - b_4c_3 + b_3c_4) -$$
$$-a_3(b_3c_1 + b_1c_3 + b_4c_2 - b_2c_4) - a_4(b_4c_1 + b_1c_4 - b_3c_2 + b_2c_3)$$

وبالمثل نجد:

$$f_2 = a_1(b_1c_2 + b_2c_1 + b_3c_4 - b_4c_3) + a_2(b_1c_1 - b_2c_2 - b_3c_3 - b_4c_4) +$$
$$+ a_3(b_1c_4 + b_4c_1 + b_2c_3 - b_3c_2) - a_4(b_1c_3 + b_3c_1 + b_4c_2 - b_2c_4)$$
$$f_3 = a_1(b_1c_3 + b_3c_1 + b_4c_2 - b_2c_4) + a_3(b_1c_1 - b_2c_2 - b_3c_3 - b_4c_4) +$$
$$+ a_4(b_1c_2 + b_2c_1 + b_3c_4 - b_4c_3) - a_2(b_1c_4 + b_4c_1 + b_2c_3 - b_3c_2)$$
$$f_4 = a_1(b_1c_4 + b_4c_1 + b_2c_3 - b_3c_2) + a_4(b_1c_1 - b_2c_2 - b_3c_3 - b_4c_4) +$$
$$+ a_2(b_1c_3 + b_3c_1 + b_4c_2 - b_2c_4) - a_3(b_1c_2 + b_2c_1 + b_3c_4 - b_4c_3)$$
$$f_5 = (a_5b_5)c_5 = a_5b_5c_5$$

واضح أنّ: $(f_1,f_2,f_3,f_4,f_5)=(d_1,d_2,d_3,d_4,d_5)$, وبالتّالي فإنّ العمليّة $*$ هي عمليّة تجميعيّة.

4المراجع العلمية.

1. Ernest J. Eckert, The Group of Primitive Pythagorean Triangles, Mathematics Magazine, 57 (Jan., 1984
2. P. Zanardo and U. Zannier, The group of pythagorean triples in number fields, Annali di Matematica pura ed applicata (IV), CLIX (1991)
3. Raymond A. Beauregard and E. R. Suryanarayan, Pythagorean Triples: The Hyperbolic View, The College Mathematics Journal, 27 (May, 1996)
4. Ant_onio Machiavelo and Lu__s Ro_cadas, Some connections between the arithmetic and geometry of Lipschitz integers,(2011)
5. John H. Conway and Derek Smith, On Quaternions and Octonions, AK Peters (2003)
6. J. B. Kuipers. Quaternions and Rotation Sequences. Princeton University Press, (1999).
7. S. L. Altmann. “Hamilton, Rodrigues, and the Quaternion Scandal,” *Mathematics Magazine* 62(5), (December 1989).

خوارزمية تشفير متناظرة بمفتاح ثنائي, باستخدام فيثاغوريّات مولّدة بعدد فردي

A symmetric Binary-key Encryption Algorithm Using Pythagoreans That Generates an Odd Number.

د. نجوى أحمد نجوم
دكتوراه في الرياضيات البحتة
جامعة البعث
(حمص – سوريا)

Dr. Najwa Ahmad Najjom
PhD in pure mathematics
Al Baath University
(Homs – Syria)

المؤتمر العلمي الدولي الثالث عشر
لجمعية الرياضيات العراقية والمنعقد تحت شعار
نحو عالم متقدم : الرياضيات والتقنيات في سباق الابتكار
للمدة 24 - 25 نيسان 2024
الكوفة – النجف الاشرف

الملخّص

يستند هذا البحث إلى بناء ثلاثيّات, رباعيات, خماسيّات, ... فيثاغوريّة, انطلاقاً من عدد فردي λ ولتكن هذه الفيثاغوريّات:

$$(x_0,x_1,x_2),(x_3,x_4,x_5,x_6),(x_7,x_8,x_9,x_{10},,x_{11}),...$$

ومن ثمّ تطوير خوارزميّة **Luma and Raufi** للتشفير بالاعتماد على الفيثاغوريّات المنشأة وبمفتاح تشفير ثنائي $K(\lambda,m)$ حيث λ عدد صحيح فردي و m عدد طبيعي لا يساوي الصفر.

الكلمات المفتاحيّة

ثلاثيّة فيثاغوريّة – رباعيّة فيثاغوريّة - خماسيّة فيثاغوريّة– تشفير – فك التشفير

1. المقدّمة:

في الوقت الذي يعتبر التشفير علماً قائماً بحد ذاته, إلّا أنّه يعتبر فنّاً يظهر روعة الرياضيّات, ولا سيّما نظريّة الأعداد. ربما لم يكن الاهتمام في هذه الأوراق هو التشفير بحد ذاته, وإنّما قضايا في نظريّة الأعداد وإظهار أهميّتها من خلال التشفير.

التّشفير هو تحويل البيانات من شكلها القابل للفهم, إلى شكل آخر لا يمكن إلا لمن يمتلك المفتاح والخوارزميّة بقراءتها من خلال فك التشفير.

يُعد علم التشفير من أقدم العلوم المستخدمة, فقد استخدم منذ 1900 سنة قبل الميلاد تقريباً لفك رموز الحضارة الهيروغليفية في مصر [1], وقد استخدم التشفير بشكل كبير لنقل المعلومات المشفّرة لحماية الرسائل السريّة وخصوصاً حماية الأسرار العسكريّة أثناء الحروب.

في العام 2014 قام كل من **Luma and Raufi** [2] بإيجاد طريقتين لتوليد ثلاثيّات فيثاغوريّة بوسيطين طبيعيّين p,q بحيث يكون $p>q$ وقاما باستخدام نتائجهما بإيجاد طريقة للتشفير.

استخدم الباحثان (العرنوس – شراباتي 2023) [5] نتائج **Luma and Raufi** في إيجاد صيغتين جديدتين لتوليد رباعيّات فيثاغوريّة وقاما باستخدام العلاقات في تشفير نص محرفي.

ثم قام الباحث (العرنوس 2023) [6] بتطبيق الخوارزميّة باستخدام خماسيّة فيثاغوريّة مولّدة من ثلاثيّتين فيثاغوريّتين.

عمدنا في هذه الأوراق إلى بناء ثلاثيّات, رباعيات, خماسيّات, ... فيثاغوريّة, انطلاقاً من عدد فردي λ, ومن ثمّ تطوير خوارزميّة **Luma and Raufi** للتشفير بالاعتماد على الفيثاغوريّات المنشأة وبمفتاح تشفير ثنائي $K(\lambda,m)$ حيث λ عدد صحيح فردي و m عدد طبيعي لا يساوي الصفر.

2. هدف البحث:

يهدف البحث إلى بناء ثلاثيّات, رباعيات, خماسيّات, ... فيثاغوريّة, انطلاقاً من عدد فردي λ, واستخدام النتائج في تشفير نص محرفي, من خلال بناء خوارزميّة للتشفير وآليّة لفك التشفير.

3. النتائج والمناقشة:

أوّلاً: بناء فيثاغوريّات انطلاقاً من عدد فردي

المؤتمر العلمي الدولي الثالث عشر
لجمعية الرياضيات العراقية والمنعقد تحت شعار
نحو عالم متقدم : الرياضيات والتقنيات في سباق الابتكار
للمدة 24 - 25 نيسان 2024
الكوفة – النجف الاشرف

تعريف1: [3]

تسمّى ثلاثيّة فيثاغوريّة كل ثلاثيّة مرتّبة (x,y,z) عناصرها من $\mathbb{N}$ وتحقّق:

$$x^2+y^2=z^2$$

وكمثال على ذلك: الثّلاثيّة $(3,4,5)$.

وقد تمّ إيجاد طرائق عدّة لتوليد ثلاثيّات فيثاغوريّة من أهمّها صيغة إقليدس, وهي الصيغة الأساسيّة لثلاثيّات فيثاغوريّة, وتنص على أنّه من أجل زوج اختياري من الأعداد الصحيحة m,n حيث $m>n$ والذي أحدهما زوجي والأخر فردي, فإنّ الثّلاثيّة الآتية تكون فيثاغوريّة:

$$\left(m^2-n^2,\ 2mn,\ m^2+n^2\right)$$

تمهيديّة: [7]

ليكن $\lambda\in\mathbb{N}$ وبحيث λ عددٌ فرديّ عندئذٍ تكون الثّلاثيّة الآتية فيثاغوريّة:

$$\left(\lambda,\ \frac{\lambda^2-1}{2},\ \frac{\lambda^2+1}{2}\right)$$

تعريف 2:

نسمّي رباعيّة فيثاغوريّة كل رباعيّة مرتّبة (x,y,z,w) عناصرها من $\mathbb{N}$ وتحقّق:

$$x^2+y^2+z^2=w^2$$

تعريف 3:

نسمّي خماسيّة فيثاغوريّة كل خماسيّة مرتّبة (x,y,z,w,t) عناصرها من $\mathbb{N}$ وتحقّق:

$$x^2+y^2+z^2+w^2=t^2$$

تمهيدية 2:

ليكن $\lambda\in\mathbb{N}$ عدداً فرديّاً, والثّلاثيّة المولّدة بالتمهيديّة 1 هي:

$$\left(\lambda,\ \frac{\lambda^2-1}{2},\ \frac{\lambda^2+1}{2}\right)$$

عندئذٍ فإنّ الثالث الفيثاغوري هو فردي.

الإثبات:

بما أنّ λ فرديّ, عندئذٍ يوجد $n\in\mathbb{N}$ بحيث: $\lambda=2n+1$, وبالتالي يكون:

$$\frac{\lambda^2+1}{2}=\frac{(2n+1)^2+1}{2}=\frac{4n^2+4n+2}{2}=2n^2+2n+1$$

واضح إنّ: $\frac{\lambda^2+1}{2}$ فرديّ.

مبرهنة 1 :

ليكن $\lambda \in \mathbb{Z}$ عدداً فردياً, عندئذٍ الرّباعيّة الآتية هي رباعيّة فيثاغوريّة:

$$\left(\lambda,\ \frac{\lambda^2-1}{2},\ \frac{\lambda^4+2\lambda^2-3}{8},\frac{\lambda^4+2\lambda^2+5}{8}\right)$$

والرّابع الفيثاغوريّ, هو عددٌ فرديّ.

الإثبات:

ليكن $\lambda \in \mathbb{Z}$ عدداً فردياً, عندئذٍ الثّلاثيّة الآتية فيثاغوريّة:

$$\left(\lambda,\ \frac{\lambda^2-1}{2},\ \frac{\lambda^2+1}{2}\right)$$

أي:

$$(\lambda)^2+\left(\frac{\lambda^2-1}{2}\right)^2=\left(\frac{\lambda^2+1}{2}\right)^2 \qquad (6)$$

ولأنّ: $\frac{\lambda^2+1}{2}$ فرديّ, فإنّ الثّلاثيّة الآتية فيثاغوريّة:

$$\left(\frac{\lambda^2+1}{2},\ \frac{\left(\frac{\lambda^2+1}{2}\right)^2-1}{2},\ \frac{\left(\frac{\lambda^2+1}{2}\right)^2+1}{2}\right)$$

أي:

$$\left(\frac{\lambda^2+1}{2},\ \frac{\lambda^4+2\lambda^2-3}{8},\ \frac{\lambda^4+2\lambda^2+5}{8}\right)$$

وبالتالي:

$$\left(\frac{\lambda^2+1}{2}\right)^2+\left(\frac{\lambda^4+2\lambda^2-3}{8}\right)^2=\left(\frac{\lambda^4+2\lambda^2+5}{8}\right)^2$$

ومنه:

$$\left(\frac{\lambda^2+1}{2}\right)^2=\left(\frac{\lambda^4+2\lambda^2+5}{8}\right)^2-\left(\frac{\lambda^4+2\lambda^2-3}{8}\right)^2$$

بالتعويض في (6) نجد:

$$(\lambda)^2+\left(\frac{\lambda^2-1}{2}\right)^2=\left(\frac{\lambda^4+2\lambda^2+5}{8}\right)^2-\left(\frac{\lambda^4+2\lambda^2-3}{8}\right)^2$$

وبالتالي:

$$(\lambda)^2+\left(\frac{\lambda^2-1}{2}\right)^2+\left(\frac{\lambda^4+2\lambda^2-3}{8}\right)^2=\left(\frac{\lambda^4+2\lambda^2+5}{8}\right)^2$$

وبهذا يتم المطلوب.

الآن, وحيث إنّ λ فردي, فيوجد $n\in\mathbb{Z}$ بحيث: $\lambda=2n+1$, وبالتالي:

$$\frac{(2n+1)^4+2(2n+1)^2+5}{8}=\frac{16n^4+32n^3+32n^2+16n+8}{8}=$$
$$=2n^4+4n^3+4n^2+2n+1$$

واضح انّ هذا العدد فردي.

مبرهنة 2 :

ليكن $\lambda\in\mathbb{Z}$ عدداً فرديّاً, عندئذٍ الخماسيّة (x,y,z,t,w) هي خماسيّة فيثاغوريّة, حيث:

$$x=\lambda,$$
$$y=\frac{\lambda^2-1}{2},$$
$$z=\frac{\lambda^4+2\lambda^2-3}{8},$$
$$t=\frac{\lambda^8+4\lambda^6+14\lambda^4+20\lambda^2-39}{128},$$
$$w=\frac{\lambda^8+4\lambda^6+14\lambda^4+20\lambda^2+89}{128}$$

و w عددٌ فرديّ.

الإثبات:

يتم بنفس طريقة إثبات المبرهنة 1.

نتيجة 1:

من أجل $\lambda\in\mathbb{Z}$, و λ عدد فردي, تم بناء ثلاثية فيثاغوريّة, ورباعيّة فيثاغوريّة, وخماسية فيثاغوريّة, نرمز لها بالرمز:

$$(x_0,x_1,x_2)=\left(\lambda,\ \tfrac{\lambda^2-1}{2},\ \tfrac{\lambda^2+1}{2}\right)$$
$$(x_3,x_4,x_5,x_6)=\left(\lambda,\ \tfrac{\lambda^2-1}{2},\ \tfrac{\lambda^4+2\lambda^2-3}{8},\ \tfrac{\lambda^4+2\lambda^2+5}{8}\right)$$
$$(x_7,x_8,x_9,x_{10},x_{11})=\left(\lambda,\ \tfrac{\lambda^2-1}{2},\ \tfrac{\lambda^4+2\lambda^2-3}{8},x_{10},x_{11}\right)$$

حيث:

$$x_{10}=\frac{\lambda^8+4\lambda^6+14\lambda^4+20\lambda^2-39}{128},$$

$$x_{11}=\frac{\lambda^8+4\lambda^6+14\lambda^4+20\lambda^2+89}{128}$$

ويمكن بالطريقة ذاتها إيجاد سداسية فيثاغوريّة, سباعية فيثاغوريّة, ...

مثال 1:

من أجل $\lambda=3$ نجد:

الثلاثيّة الفيثاغوريّة: $(3,4,5)$

الرّباعيّة الفيثاغوريّة: $(3,4,12,13)$

الخماسيّة الفيثاغوريّة: $(3,4,12,84,85)$

السداسيّة الفيثاغوريّة: $(3,4,12,84,3612,3613)$

السباعيّة الفيثاغوريّة: $(3,4,12,84,3612,6526884,6526885)$

.....

ويمكن توضيح طريقة البناء من خلال:

الثّلاثيّة	λ	$\frac{\lambda^2-1}{2}$	$\frac{\lambda^2+1}{2}$
$(3,4,5)$	3	4	5
	5	12	13
	13	84	85
	85	3612	3613
	3613	6526884	6526885

الرّباعيّة	λ	$\frac{\lambda^2-1}{2}$	$\frac{\lambda^2+1}{2}$
$(3,4,12,13)$	3	4	5
	5	12	13
	13	84	85
	85	3612	3613

	3613	6526884	6526885

الخماسيّة	λ	$\frac{\lambda^2-1}{2}$	$\frac{\lambda^2+1}{2}$
$(3,4,12,84,85)$	3	4	5
	5	12	13
	13	84	85
	85	3612	3613
	3613	6526884	6526885

السداسيّة	λ	$\frac{\lambda^2-1}{2}$	$\frac{\lambda^2+1}{2}$
$(3,4,12,84,3612,3613)$	3	4	5
	5	12	13
	13	84	85
	85	3612	3613
	3613	6526884	6526885

السباعية	λ	$\frac{\lambda^2-1}{2}$	$\frac{\lambda^2+1}{2}$
$(3,4,12,84,3612,6526884,6526885)$	3	4	5
	5	12	13
	13	84	85
	85	3612	3613
	3613	6526884	6526885

وهكذا ..

ثانياً: تشفير نص بمفتاح ثنائي $K(\lambda,m)$.

تعريف 3: (مفتاح التشفير)

ليكن $\lambda \in \mathbb{Z}$ و λ فرديّ, وليكن m عدد طبيعي لا يساوي الصفر, بحيث:
$m=1$ عندما نبني ثلاثيّة, بحسب النتيجة 1.
$m=2$ عندما نبني ثلاثيّة ورباعيّة, بحسب النتيجة 1.
$m=3$ عندما نبني ثلاثيّة ورباعيّة وخماسيّة, بحسب النتيجة 1.
وهكذا ...
نسمّي الثّنائيّة المرتّبة (λ, m) مفتاح تشفير باستخدام فيثاغوريّات مولّدة بعدد فردي.
وكمثال على ذلك:
المفتاح $(3,2)$ يعني أنّ سيتم بناء ثلاثيّة فيثاغوريّة ورباعيّة فيثاغوريّة مولّدة بالعدد الفردي 3.

تعريف 4:

ليكن $\lambda \in \mathbb{Z}$ و λ فرديّ, وليكن m عدد طبيعي لا يساوي الصفر, و x_i معرّفة وفق النتيجة 1, لنعرّف المجموعة التي χ_m على النحو:

- من أجل $m=1$ فإنّ: $\chi_1=\{x_0,x_1,x_2\}$ وعدد عناصرها 3.
- من أجل $m=2$ فإنّ: $\chi_2=\{x_0,x_1,x_2,x_3,x_4,x_5,x_6\}$ وعدد عناصرها $3+4=7$.
- من أجل $m=3$ فإنّ: $\chi_3=\{x_0,x_1,\dots,x_{11}\}$ وعدد عناصرها $3+4+5=12$.

نتيجة 2:

ليكن $\lambda \in \mathbb{Z}$ و λ فرديّ, وليكن m عدد طبيعي لا يساوي الصفر, عدد عناصر المجموعة χ_m يساوي:

$$3+4+5+\dots+(m+2)=\frac{m}{2}(3+m+2)=\frac{m}{2}(m+5)$$

تعريف 5: (متتالية مفتاح التشفير)

ليكن $\lambda \in \mathbb{Z}$ و λ فرديّ, وليكن m عدد طبيعي لا يساوي الصفر, عندئذٍ نعرّف المتتالية $\{k_i\}$ على النّحو الآتي:

$$\begin{aligned} k_i &= x_i \pmod{256} \quad ; \quad i \in \left\{0,1,\dots,\tfrac{m}{2}(m+5)-1\right\} \\ k_i &= k_{i \left(\bmod \frac{m}{2}(m+5)\right)} \quad ; \quad i \in \left\{\tfrac{m}{2}(m+5),\tfrac{m}{2}(m+5)+1,\dots\right\} \end{aligned} \qquad (7)$$

حيث x_i معرّفة وفق النتيجة 1.

مثال 2 :

من أجل مفتاح التشفير $(3,2)$ تكون العناصر x_i:

$$x_0=3, x_1=4, x_2=5, x_3=3, x_4=4, x_5=12, x_6=13$$

وتكون متتالية مفتاح التشفير:

$$\{k_i\}=\left\{\boxed{3,4,5,3,4,12,13},3,4,5,3,4,12,13,\dots\right\}$$

تعريف 6: (متتالية النص الواضح) [5]

ليكن M النص الواضح المراد تشفيره, نشكّل المتتالية $\{m_i\}$ التي تنتج عن النص الواضح باستبدال كل محرف بمقابله في جدول ASCII, بحيث يكون m_0 هو المقابل العددي للمحرف الأوّل من النص الواضح في جدول ASCII, و m_1 هو المقابل العددي للمحرف الثاني من النص الواضح, وهكذا ...

تعريف 7: (متتالية النص المشفّر) [5]

ليكن C النص المشفّر المراد توضيحه, نشكّل المتتالية $\{c_i\}$ التي تنتج عن النص المشفّر باستبدال كل محرف بمقابله في جدول ASCII, بحيث يكون c_0 هو المقابل العددي للمحرف الأوّل من النص المشفّر في جدول ASCII, و c_1 هو المقابل العددي للمحرف الثاني من النص الواضح, وهكذا ...

خوارزميّة التشفير باستخدام المفتاح $K(\lambda,m)$

ليكن M النص الواضح المراد تشفيره باستخدام مفتاح التشفير $K(\lambda,m)$ حيث λ عدد صحيح فردي, و m عدد طبيعي لا يساوي الصفر. وليكن n عدد محارفه.

لتشفير النص M نتّبع الخطوات الآتية:

أوّلاً: نوجد عناصر متتالية النص الواضح $\{m_i\}_{i=0}^{n-1}$.

ثانياً: نوجد عناصر متتالية مفتاح التشفير $\{k_i\}_{i=0}^{n-1}$.

ثالثاً: نحسب عناصر متتالية النص المشفّر $\{c_i\}_{i=0}^{n-1}$ وفق العلاقة الآتية:

$$c_i = m_i + k_i \pmod{256} \;;\; i \in \{0,1,...,n-1\}$$

رابعاً: نوجد المحارف التي تقابل متتالية النص المشفّر من جدول ASCII, فنحصل على النص المشفّر C.

<u>وبالعكس</u> لفك تشفير النص C والذي عدد محارفه n, نتّبع الخطوات الآتية:

أوّلاً: نوجد عناصر متتالية النص المشفّر $\{c_i\}_{i=0}^{n-1}$.

ثانياً: نوجد عناصر متتالية مفتاح التشفير $\{k_i\}_{i=0}^{n-1}$.

ثالثاً: نحسب عناصر متتالية النص الواضح $\{m_i\}_{i=0}^{n-1}$ وفق العلاقة الآتية:

$$m_i = c_i - k_i \pmod{256} \;;\; i \in \{0,1,...,n-1\}$$

رابعاً: نوجد المحارف التي تقابل متتالية النص الواضح من جدول ASCII, فنحصل على النص الواضح M.

مبرهنة 3:

إنّ تشفير كل نص واضح M طوله n محرفاً, باستخدام فيثاغوريّات مولّدة بعدد فردي, باستخدام المفتاح $K(\lambda,m)$ يتم بشكلٍ وحيد.

الإثبات :

بطريقة مشابهة لما ورد في [6].

مبرهنة 4:

إنّ فك تشفير نص مشفّر C طوله n محرفاً, باستخدام فيثاغوريّات مولّدة بعدد فردي, باستخدام المفتاح $K(\lambda,m)$ يتم بشكلٍ وحيد.

(الإثبات بنفس طريقة إثبات المبرهنة 3)

مثال 3 :

نهدف في هذا المثال إلى تشفير كلمة mathematics-is-life باستخدام فيثاغوريّات مولّدة بعدد فردي, والمفتاح $K(3,3)$.

باستخدام المفتاح $K(3,3)$ واستناداً إلى النتيجة 1 فإنّ:

(x_0,x_1,x_2)	(x_3,x_4,x_5,x_6)	$(x_7,x_8,x_9,x_{10},x_{11})$
$(3,4,5)$	$(3,4,12,13)$	$(3,4,12,84,85)$

وحيث إنّ طول النص الواضح هو 19 فبحسب العلاقة (7) تكون متتالية مفتاح التشفير هي:

$$\{k_i\}_{i=0}^{18}=\{\boxed{3,4,5,3,4,12,13,3,4,12,84,85},3,4,5,3,4,12,13\}$$

وتكون عمليّة التشفير موضّحة من خلال الجدول الآتي:

M	m_i	k_i	m_i+k_i	c_i	C
m	109	3	112	112	p
a	97	4	101	101	e
t	116	5	121	121	y
h	104	3	107	107	k
e	101	4	105	105	i
m	109	12	121	121	y
a	97	13	110	110	n
t	116	3	119	119	w
i	105	4	109	109	m
c	99	12	111	111	o
s	115	84	199	199	ا
–	175	85	260	4	¬

i	105	3	108	108	l
s	115	4	119	119	w
¯	175	5	180	180	´
l	108	3	111	111	o
i	105	4	109	109	m
f	102	12	114	114	r

ويكون النص المشفّر هو:

¬lw´omr|peykiynwmo

مثال 4 :

إنّ فك تشفير الجملة:

|ªdxnow»`rgu¹ÌLvftm»Zdxt¹

باستخدام فيثاغوريّات مولّدة بعدد فردي, والمفتاح $K\left(3,3\right)$, يُعطي النص الواضح:

Iraqi_Mathematics_Sosiety

4. الاستنتاجات والتوصيات:

من خلال هذا البحث تمّ إيجاد طريقة لتوليد فيثاغوريّات من عدد فردي, ثلاثيّة فيثاغوريّة, رباعيّة فيثاغوريّة, وخماسيّة فيثاغوريّة, ... ومن ثمّ تمّ بناء متتالية من الأعداد الصحيحة مكوّنة من ثلاثيّة فرباعيّة فخماسيّة ... فيثاغوريّة, واستخدمنا ذلك في بناء متتالية مفتاح التشفير.

بيّنا أنّ التشفير باستخدام فيثاغوريّات مولّدة بعدد فردي يتم بشكل وحيد, وكذلك فك التشفير.

من توصيات البحث بناء كود برمجي يقوم وبشكل آلي بعمليّة التشفير لمجرد إدخال النص ومفتاح التشفير, وكذلك لعمليّة فك التشفير.

6. المراجع العلميّة:

[1] History of Cryptography, 2013- **AN Easy to understand History of Cryptography**

[2] Luma A, RAUFI B., 2014- **Data Encryption and Decryption Using New Pythagorean Triple Algorithm.** *Proceedings of the World Congress on Engineering*, Vol I, London, U.K.

[3] SPARKS J., 2008- **The Pythagorean Theorem Crown Jewel of Mathematics**. Author House, USA, 176P

, **دراسة تحليلية معمّقة في التشفير الكلاسيكي والحديث.** كليّة 2017 صطيف أحمد, الخطيب عبد الباسط, شمّه محمد نور, [4] صفحة.109العلوم, جامعة البعث,

, **تشفير نص بواسطة خوارزميّة الرّباعيّات الفيثاغوريّة.** مؤتمر الرياضيّات 2023 العرنوس باسل, شراباتي محمد, [5] صفحة.18وتطبيقاتها بجامعة الفرات,

, **توليد خماسيّة فيثاغوريّة بوسيطين طبيعيّين واستخدامها في التشفير.** المؤتمر الحادي عشر لجمعيّة 2023 العرنوس باسل, [6] صفحة.14الرياضيّات العراقيّة,

دراسة في بنية الخماسيات الفيثاغورية الجبريّة, واستخدامها في توليد فيثاغوريّات

الدكتور باسل حمدو العرنوس **الأستاذ الدكتور عبد الباسط الخطيب**
عميد كلية التربية الثانية **رئيس جامعة البعث**

ملخّص البحث

قمنا في هذا البحث بدراسة في بنية الخماسيات الفيثاغوريّة $(PP_5,*)$ حيث بيّنا أنّ هذه البنية تقبل عنصراً محايداً, وأوجدنا العناصر القابلة للقلب بالنّسبة للعمليّة $*$, واستخدمنا مفهوم شبه المقلوب لحل معادلات تتضمّن العمليّة $*$.

أوجدنا طرقاً لتوليد خماسيّات فيثاغوريّة من رباعيّات فيثاغوريّة, وتوليد خماسيّات من ثلاثيّات فيثاغوريّة, وأخيراً طرقاً لتوليد ثلاثيّات فيثاغوريّة من ثلاثيّات فيثاغوريّة من خلال عملية مغلقة .

الكلمات المفتاحيّة:

خماسيّة فيثاغوريّة, رباعيّة فيثاغوريّة, ثلاثيّة فيثاغوريّة, بنية, نصف زمرة, محايد, نصف مقلوب.

دراسة في بنية الخماسيات الفيثاغورية الجبريّة, واستخدامها في توليد فيثاغوريّات

1.مقدّمة

تهدف دراسة الفيثاغوريّات في معظم حالاتها إلى إيجاد طرائق توليد لهذه الفيثاغوريّات, بدءاً من صيغة إقليدس لتوليد الثلاثيات الفيثاغوريّة إلى طريقة الأشجار الثلاثية, وهكذا.

ثمّ ظهرت طرائق توليد جديدة تعتمد على الفيثاغوريّات نفسها, وذلك من خلال تعريف عمليّات مغلقة على الفيثاغوريّات.

ففي العام 1984 عرّف إيكيرت Eckert عمليّة جمع بين الثلاثيّات الفيثاغوريّة التي عناصرها من $\mathbf{Z}$, على النحو الآتي:

$$(a_1,b_1,c_1)+(a_2,b_2,c_2)=(a_1a_2-b_1b_2,a_1b_2+b_1a_2,c_1c_2)$$

بحيث تشكّل مجموعة كلّ الثّلاثيّات الفيثاغوريّة الصحيحة بالإضافة إلى $(1,0,1)$ مع العمليّة $+$ زمرة تبديلية [1] .

بعد ذلك في العام 1991 قام زناردو Zanardo و زانيير Zannier بتعميم المجال من $\mathbf{Z}$ إلى أي حلقة من الأعداد الصحيحة R [2] .

في العام 1996 قام بيوريجارد Beauregard و سوريانريان Suryanarayan بتعريف عمليّة مغلقة $*$ على مجموعة كل الثلاثيّات الفيثاغوريّة الصحيحة, على النحو الآتي [3]:

$$(a_1,b_1,c_1)*(a_2,b_2,c_2)=(a_1a_2,b_1c_2,c_1b_2+b_1b_2+c_1c_2)$$

في العام 2024 قمنا بتعريف الخماسيّات الفيثاغوريّة, ومن ثمّ تعريف عمليّة مغلقة $*$ على مجموعة كل الخماسيّات الفيثاغوريّة PP_5, وأثبتنا أنّ البنية $(PP_5,*)$ هي نصف زمرة, وأوجدنا العنصر المحايد بالنسبة للعمليّة $*$.

ندرس في هذا البحث خواص هذه البنية من حيث العناصر القابلة للقلب, وطرائق أخرى لتوليد الخماسيات الفيثاغوريّة وكذلك الثلاثيات الفيثاغوريّة.

2. هدف البحث

يهدف البحث إلى إيجاد العناصر القابلة للقلب في بنية الخماسيات الفيثاغوريّة الجبريّة. وإيجاد طرائق أخرى لتوليد الخماسيات الفيثاغوريّة وكذلك الثلاثيات الفيثاغوريّة.

3. المناقشة و النّتائج

أوّلاً: الخماسيّات الفيثاغوريّة $\mathbb{Z}$:

نعلم من نظريّة الأعداد, أنّ الثّلاثيّات الفيثاغوريّة في $\mathbb{Z}$ هي مجموعة كلّ الثّلاثيّات $\{x,y,z\}$ التي تحقّق معادلة ديوفانتس الآتية:

$$x^2+y^2=z^2 \;;\; x,y,z\in\mathbb{Z}$$

وعليه فإنّ الخماسيّات الفيثاغوريّة, هي مجموعة كلّ الخماسيّات $\{x,y,z,w,r\}$ والتي تحقّق معادلة ديوفانتس الآتية:

$$x^2+y^2+z^2+w^2=r^2 \;;\; x,y,z,w,r\in\mathbb{Z}^+$$

تعريف 1:

تسمّى خماسيّة فيثاغوريّة, كلّ خماسيّة (a,b,c,d,e), حيث $a,b,c,d,e\in\mathbb{Z}$, وتحقّق:

$$a^2+b^2+c^2+d^2=e^2$$

سنرمز لمجموعة كلّ الخماسيّات الفيثاغوريّة بالرّمز PP_5 وبالتّالي يكون:

$$PP_5=\{(a,b,c,d,e);\, a^2+b^2+c^2+d^2=e^2 : a,b,c,d,e\in\mathbb{Z}\}$$

مبرهنة 1 وتعريف 2:

ليكن $(a_1,a_2,a_3,a_4,a_5),(b_1,b_2,b_3,b_4,b_5)\in PP_5$, نعرّف على PP_5 العمليّة الثّنائيّة الآتية:

$$(a_1,a_2,a_3,a_4,a_5)*(b_1,b_2,b_3,b_4,b_5)=(c_1,c_2,c_3,c_4,c_5)$$

حيث:

$$\begin{aligned} c_1 &= a_1b_1-a_2b_2-a_3b_3-a_4b_4 \\ c_2 &= a_1b_2+a_2b_1+a_3b_4-a_4b_3 \\ c_3 &= a_1b_3+a_3b_1+a_4b_2-a_2b_4 \\ c_4 &= a_1b_4+a_4b_1+a_2b_3-a_3b_2 \end{aligned} \quad , \quad c_5=a_5b_5$$

عندئذٍ $(PP_5,*)$ بنية جبريّة.

مبرهنة 2:

تقبل العمليّة $*$ في البنية الجبريّة $(PP_5,*)$ عنصراً محايداً, هو $(1,0,0,0,1)$.

مبرهنة 3:

إنّ العمليّة $*$ في البنية الجبريّة $(PP_5,*)$ هي عمليّة تجميعيّة.

مبرهنة 4: العناصر القابلة للقلب في $(PP_5,*)$

إنّ عدد العناصر القابلة للقلب في $(PP_5,*)$ هو 16.

الإثبات:

بفرض $(a_1,a_2,a_3,a_4,a_5)\in PP_5\setminus\{(0,0,0,0,0)\}$ ولنفرض أنّه قابلاً للقلب بالنسبة للعمليّة $*$, وبالتالي يوجد $(b_1,b_2,b_3,b_4,b_5)\in PP_5$, بحيث:

$$(a_1,a_2,a_3,a_4,a_5)*(b_1,b_2,b_3,b_4,b_5)=(1,0,0,0,1) \qquad (4)$$

$$(b_1,b_2,b_3,b_4,b_5)*(a_1,a_2,a_3,a_4,a_5)=(1,0,0,0,1) \qquad (5)$$

من $(4),(5)$ يتّضح أنّ:

$$a_5b_5=1 \qquad (6)$$

لنعرّف العددين:

$$p_1=\frac{a_1}{a_5}+\frac{a_2}{a_5}i+\frac{a_3}{a_5}j+\frac{a_4}{a_5}k, \qquad p_2=\frac{b_1}{b_5}+\frac{b_2}{b_5}i+\frac{b_3}{b_5}j+\frac{b_4}{b_5}k$$

وليكن $p_1.p_2=1$ عندئذٍ فإنّ:

$$p_2=\frac{1}{p_1}=\frac{\bar{p}_1}{|p_1|^2}=\frac{a_1}{a_5}-\frac{a_2}{a_5}i-\frac{a_3}{a_5}j-\frac{a_4}{a_5}k$$

وبالتّالي نضع:

$$(b_1,b_2,b_3,b_4,b_5)=(a_1,-a_2,-a_3,-a_4,a_5) \qquad (7)$$

وبملاحظة أنّ:

$$\begin{aligned}(a_1,a_2,a_3,a_4,a_5)*(a_1,-a_2,-a_3,-a_4,a_5)&=({a_5}^2,0,0,0,{a_5}^2)\\(a_1,-a_2,-a_3,-a_4,a_5)*(a_1,a_2,a_3,a_4,a_5)&=({a_5}^2,0,0,0,{a_5}^2)\end{aligned} \qquad (8)$$

من العلاقة (6) ومن العلاقتين الأخيرتين يتّضح أنّ (a_1,a_2,a_3,a_4,a_5) يكون قابلاً للقلب إذا وفقط إذا كان:

$a_5=+1$ أو $a_5=-1$. وعليه فإنّ العناصر في $(PP_5,*)$ القابلة للقلب, استناداً إلى (7) هي:

م	العنصر من $(PP_5,*)$	مقلوبه
1	$(1,0,0,0,1)$	$(1,0,0,0,1)$
2	$(-1,0,0,0,1)$	$(-1,0,0,0,1)$
3	$(1,0,0,0,-1)$	$(1,0,0,0,-1)$
4	$(-1,0,0,0,-1)$	$(-1,0,0,0,-1)$
5	$(0,1,0,0,1)$	$(0,-1,0,0,1)$
6	$(0,1,0,0,-1)$	$(0,-1,0,0,-1)$
7	$(0,-1,0,0,1)$	$(0,1,0,0,1)$
8	$(0,-1,0,0,-1)$	$(0,1,0,0,-1)$
9	$(0,0,1,0,1)$	$(0,0,-1,0,1)$

$(0,0,-1,0,-1)$	$(0,0,1,0,-1)$	10
$(0,0,1,0,1)$	$(0,0,-1,0,1)$	11
$(0,0,1,0,-1)$	$(0,0,-1,0,-1)$	12
$(0,0,0,-1,1)$	$(0,0,0,1,1)$	13
$(0,0,0,-1,-1)$	$(0,0,0,1,-1)$	14
$(0,0,0,1,1)$	$(0,0,0,-1,1)$	15
$(0,0,0,1,-1)$	$(0,0,0,-1,-1)$	16

تعريف 3:

ليكن $A=(a_1,a_2,a_3,a_4,a_5)\in PP_5$ حيث $a_5\notin\{1,-1\}$ فإنّنا نسمّي العنصر:

$$\tilde{A}=(a_1,-a_2,-a_3,-a_4,a_5)$$

شبه مقلوب العنصر A.

نتيجة 1:

إنّ البنية $(PP_5,*)$ هي نصف زمرة, تقبل الخماسيّة $(1,0,0,0,1)$ عنصراً محايداً, ويوجد لـ16عنصراً منها مقلوباً بالنّسبة للعمليّة $*$, أمّا بقيّة العناصر ما عدا $(0,0,0,0,0)$ فلكلّ عنصر شبه مقلوب.

نتيجة 2:

من العلاقة (8) يتّضح أنّه إذا كان $A,B\in PP_5$, وكانت المعادلة:

$$A*X=B$$

قابلة للحل في PP_5 فإنّ:

$$X=\frac{1}{a_5^{\,2}}\tilde{A}*B \qquad (9)$$

وإذا كانت المعادلة: $X*A=B$ قابلة للحل في PP_5 فإنّ:

$$X=\frac{1}{a_5^{\,2}}B*\tilde{A} \qquad (10)$$

مثال 3:

ليكن: $A=(1,4,8,12,15), B=(2,4,5,6,9)$, وبما أنّ:

$$A*B=(-126,0,45,18,135)$$

فإنّ المعادلة $A*X=(-126,0,45,18,135)$ قابلة للحل في PP_5, وحلّها بحسب العلاقة (9), هو:

$$X=\frac{1}{225}\tilde{A}*(-126,0,45,18,135)=$$
$$=\frac{1}{225}(1,-4,-8,-12,15)*(-126,0,45,18,135)$$
$$=\frac{1}{225}(450,900,1125,1350,2025)=(2,4,5,6,9)$$

وهذا منطقي.

سادساً: توليد خماسيّات فيثاغوريّة من رباعيّات فيثاغوريّة أو ثلاثيّات فيثاغوريّة.

1 . التوليد من رباعيّات فيثاغوريّة

يمكن استخدام العمليّة $*$ لتعريف عمليّات غرضها توليد خماسيّات فيثاغوريّة, وذلك بتمديد الرباعيّات الفيثاغوريّة لتصبح خماسيّات.

فالرباعيّة الفيثاغوريّة (a,b,c,e) تحقّق:

$$a^2+b^2+c^2=e^2 \qquad (11)$$

ويمكن تمديدها بأربعة طرق لتصبح خماسيّة, على النّحو:

$$(a,b,c,0,e),(a,b,0,c,e),(a,0,b,c,e),(0,a,b,c,e)$$

وبالتّالي بتطبيق العمليّة $*$ على خماسيّتين ممدّدتين من رباعيّات فيثاغوريّة نحصل على خماسيّة فيثاغوريّة.

فمن أجل الرباعيّتين: $(a,b,c,e),(x,y,z,r)$ يمكن توليد خماسيّات فيثاغوريّة بتطبيق العلاقة $*$ بعدّة طرق, وذلك تبعاً لاختلاف طرق تمديد الرباعيّة الفيثاغوريّة إلى خماسيّة فيثاغوريّة, نضع مثلاً:

$$(a,b,0,c,e)*(x,y,z,0,r)=$$
$$=(ax-by,ay+bx-cz,az+cy,cx+bz,er)$$

بأخذ كلّ طرق التمديد وتطبيق العلاقة $*$ نحصل من الرباعيّتين:

$$(a,b,c,e),(x,y,z,r)$$

على الخماسيّات الآتية:

$$(ax-by-cz\ ,ay+bx\ ,az+cx\ ,bz-cy\ ,er) \quad (12)$$

$$(ax-by\ ,ay+bx-cz\ ,az+cy\ ,cx+bz\ ,er) \quad (13)$$

$$(ax-bz\ ,ay-cz\ ,az+bx+cy\ ,cx-by\ ,er) \quad (14)$$

$$(-ay-bz\ ,ax-cz\ ,bx+cy\ ,cx+az-by\ ,er) \quad (15)$$

$$(ax-by\ ,ay+bx+cz\ ,cx-bz\ ,az-cy\ ,er) \quad (16)$$

$$(ax-by-cz\ ,ay+bx\ ,cy-bz\ ,az+cx\ ,er) \quad (17)$$

$$(ax-cz\ ,ay+bz\ ,bx+cy\ ,az+cx-by\ ,er) \quad (18)$$

$$(-ay-cz\ ,ax+bz\ ,bx+cy-az\ ,cx-by\ ,er) \quad (19)$$

$$(ax-cy\ ,bx+cz\ ,ay+cx-bz\ ,az+by\ ,er) \quad (20)$$

$$(ax-cz\ ,bx-cy\ ,ay-bz\ ,az+cx+by\ ,er) \quad (21)$$

$$(ax-by-cz\ ,bz-cy\ ,ay+bx\ ,az+cx\ ,er) \quad (22)$$

$$(-by-cz\ ,ax+bz-cy\ ,bx-az\ ,cx+ay\ ,er) \quad (23)$$

$$(-bx-cy\ ,ax+cz\ ,ay-bz\ ,az+by-cx\ ,er) \quad (24)$$

$$(-bx-cz\ ,ax-cy\ ,ay+cx-bz\ ,az+by\ ,er) \quad (25)$$

$$(-by-cz\ ,ax+bz-cy\ ,ay+cx\ ,az-bx\ ,er) \quad (26)$$

$$(-ax-by-cz\ ,bz-cy\ ,cx-az\ ,ay-bx\ ,er) \quad (27)$$

مثال 4:

عند تطبيق العلاقات من (12) إلى (27) على الرباعيتين $(2,6,3,7)$, $(8,1,4,9)$ نحصل على الخماسيات:

العلاقة	الخماسيّة	العلاقة	الخماسيّة
(12)	$(-2,50,32,21,63)$	(20)	$(13,60,2,14,63)$

$(4,45,-22,38,63)$	(21)	$(10,38,11,48,63)$	(13)
$(-2,21,50,32,63)$	(22)	$(-8,-10,59,18,63)$	(14)
$(-18,37,40,26,63)$	(23)	$(-26,4,51,26,63)$	(15)
$(-51,28,-22,-10,63)$	(24)	$(10,62,0,5,63)$	(16)
$(-60,13,2,14,63)$	(25)	$(-2,50,-21,32,63)$	(17)
$(-18,37,26,-40,63)$	(26)	$(4,26,51,26,63)$	(18)
$(-34,21,16,-46,63)$	(27)	$(-14,40,43,18,63)$	(19)

2 . التوليد من ثلاثيّات فيثاغوريّة

بنفس الطريقة يمكن توليد خماسيّات فيثاغوريّة من ثلاثيّات فيثاغوريّة, فإذا أهملنا إشارة وترتيب المركّبات الأربع الأولى في الخماسيّة, فإنّ الثلاثيّتين $(a,b,e),(x,y,r)$ تولّدان الخماسيّة:

$$(ax\ ,ay\ ,bx\ ,by\ ,er)$$

مثال 5:

من أجل الثّلاثيّتين $(3,4,5)$, $(5,12,13)$ نحصل بتطبيق (28) على الخماسيّة الفيثاغوريّة:

$$(15\ ,\ 36\ ,\ 20,\ 48\ ,\ 65)$$

3 . توليد ثلاثيّات فيثاغوريّة من ثلاثيّات فيثاغوريّة

لدى تطبيق العمليّة $*$ على كلّ الخماسيّات الفيثاغوريّة التي تمّ توليدها من الثّلاثيّتين (a,b,e), (x,y,e) فإنّنا نحصل على خماسيّات فيها مركّبات صفريّة, وبالنّتيجة نحصل على ثلاثيّات فيثاغوريّة, وبالتّالي نحصل على توليد لثلاثيّات فيثاغوريّة من ثلاثيّات فيثاغوريّة.

لتوضيح الأمر, نلاحظ أنّ:

$$(0,a,0,b,e)*(x,0,y,0,r)=(0\ ,\ ax\ -by\ ,0,bx\ +ay\ ,er)$$

وبالتّالي يمكن تعريف عمليّة مغلقة على الثّلاثيّات الفيثاغوريّة على النّحو:

$$(a,b,e)\square\ (x,y,r)=(ax\ -by\ \ ,bx\ +ay\ ,er)$$

مثال 6: نلاحظ أنّ:

$$(3,4,5)\square(5,12,13)=(-33,56,65)$$

في الحقيقة بالإضافة إلى العلاقة (29) يمكن برصد كلّ نتائج العمليّة $*$ على الخماسيّات الممدّدة من الثّلاثيّتين (a,b,e), (x,y,e), أن نعرّف العمليّات المغلقة الآتية على الثّلاثيّات الفيثاغوريّة:

$$(a,b,e)\square(x,y,r)=(ax+by,bx-ay,er) \quad (30)$$

$$(a,b,e)\square(x,y,r)=(-ax-by,bx-ay,er) \quad (31)$$

$$(a,b,e)\square(x,y,r)=(ax+by,ay-bx,er) \quad (32)$$

$$(a,b,e)\square(x,y,r)=(-ax-by,ay-bx,er) \quad (33)$$

4المراجع العلمية.

1. Ernest J. Eckert, The Group of Primitive Pythagorean Triangles, Mathematics Magazine, 57 (Jan., 1984
2. P. Zanardo and U. Zannier, The group of pythagorean triples in number fields, Annali di Matematica pura ed applicata (IV), CLIX (1991)
3. Raymond A. Beauregard and E. R. Suryanarayan, Pythagorean Triples: The Hyperbolic View, The College Mathematics Journal, 27 (May, 1996)

دراسة لعبة Maker-Breaker الموضعية على بيانات خاصة

د. هديل بربارة[1]، د. رياض الحميدو[2]، مالك الخضير[3]

الملخص

ترتبط نظرية الألعاب الموضعية بعلوم الحاسب النظرية ارتباطاً وثيقاً، فهي تبنى على بنى نظرية البيان ولها علاقة وثيقة بالخوارزميات ونظريتي التعقيد والحوسبة. نقدم في هذه الورقة دراسة للعبة Maker-Breaker القياسية الموضعية، إذ لا وجود لحالة التعادل هنا، تم فرض شرط على تحركات Maker وهو الحركة ضمن مسلك (Walk) ثم ضمن مسار (path) بينما اللاعب الثاني يتحرك بدون قيود وتمت الدراسة على بيانات تامة وبيانات تكعيبة، وقدمنا أمثلة توضيحية لفهم المبرهنات بشكل أفضل.

المؤتمر العلمي الدولي الثالث عشر
لجمعية الرياضيات العراقية والمنعقد تحت شعار
نحو عالم متقدم : الرياضيات والتقنيات في سباق الابتكار
للمدة 24 - 25 نيسان 2024
الكوفة – النجف الاشرف

الكلمات المفتاحية: ألعاب الباني_الهادم، ألعاب توافقية، ألعاب موضعية، بيان تام، بيان تكعيبي.

Study of the positional Maker-Breaker game on special graphs

Key words: Maker-Breaker games, combinatorial games, Positional games, Complete graph, Cube graph.

Abstract:

Positional game theory is closely related to theoretical computer science, as it is built on the constructs of graph theory and has a close relationship with algorithms, complexity and computation. In this paper, we present a study of the standard Maker-Breaker game where there is no draw. A restriction was imposed on Maker's moves, which is moves within a walk, while Breaker moves without restrictions. The study was conducted on complete graphs and cubes, and we provided illustrative examples to better understand the theorems.

المقدمة:

قُدمت ألعاب Maker-Breaker من قبل Erdös و Selfridge [1] على أنها تعميم للعبة Tic-tac-toe. ومن ثمَّ توالت العديد من النتائج على أنواع من هذا النمط. وفي نسخة قياسية لهذه اللعبة، لتكن X مجموعة منتهية و $\mathcal{F}$ عائلة من المجموعات الجزئية من X، ولتكن a و b أعداد صحيحة موجبة معطاة، في لعبة Maker-Breaker(الباني_الهادم) (a: b) التوافقيّة الموضعيّة والتي يرمز لها بالرمز $(X,\mathcal{F})$، يوجد لاعبَين، أحدهما يدعى Maker (الباني أو الصانع) والآخر يدعى Breaker (الهادم أو المخرب) يأخذ الباني دوره في استدعاء a عنصر من المجموعة X ويأخذ الهادم دوره في استدعاء b عنصر من المجموعة ذاتها. ومن الطبيعي جداً أن تُلعب ألعاب (الباني_الهادم) على أضلاع لبيان معطى G، أي عندما تكون المجموعة X ممثلة بأضلاع البيان المعطى، أي أنَّ $X = E(G)$، ومجموعات الربح هي بُنى معينة في نظرية البيان، كأن تكون أشجار مولدة أو حلقات هاملتونية أو غير ذلك من البنى حسب مقتضيات الدراسة. وبالتالي إذا أخذنا نسخة قياسية تُلعب على بيان تام K_n، فإن كلاً من الباني والهادم يأخذان دورهما في استدعاء أضلاع من الرسم البياني المعطى، حيث يحاول الباني (قد يكون فريق أو مؤسسة أو جيش ...) بناء بنية خاصة من الأضلاع التي استطاع الحصول عليها، بينما ينصب هدف الهادم (أيضاً، قد يكون فريق أو مؤسسة أو جيش ...) على منع الأول من الوصول إلى هدفه.

نعتبر النوع التالي من لعبة Maker-Breaker القياسية، في هذا النوع يقوم Maker، عند حلول دوره في التحرك سواء كان هو من يبدأ اللعبة أم لا، باستدعاء الأضلاع وفقاً لمسلك (Walk) على التوالي، أي أنه عند أي لحظة من اللعبة إذا كان Maker عند رأس v من البيان G وحان دوره في التحرك، فإنه يتحرك على امتداد ضلع $e \in G$ بحيث أنه يحقق شرطين أولهما أن يكون هذا الضلع واقعاً على الرأس v ، وثانيهما أن هذا الضلع لم يتم الاستيلاء عليه من قبل Breaker.

وفي بعض الأحيان يسمح للاعب Breaker القيام بالاستيلاء على أكثر من ضلع في الحركة الواحدة، نرمز لهذه الحالة المتحيزة بالرمز $(1:\alpha)$.

نعتبر في هذا البحث بأن لعبة Maker-Breaker ضمن الشرط الموضح أعلاه، أن هدف Maker هو الحصول على العديد من الرؤوس ما استطاع إلى ذلك سبيلا، بينما يهدف Breaker إلى تقليل عدد الرؤوس الممكن زيارتها من قبل Maker وذلك من خلال الاستيلاء عليها، وتنتهي اللعبة عندما لا يوجد مسلك (ممر) من موضع Maker الحالي إلى أي رأس غير مزار على طول الأضلاع غير المُستدعاة من قبل Breaker.

ومن المسلم به عند دراسة تحرك Maker ضمن مسلك فلا بد من دراسة حركته ضمن مسار، وبالتالي سنعتبر ذلك تنوع آخر من هذه اللعبة، حيث أنَّ Maker لا يستطيع إعادة زيارة رؤوس قد زارها مسبقاً على حين كان يستطيع فعل ذلك عندما كان يتحرك وفق مسلك، وهنا تنتهي اللعبة عندما لا يوجد مسار من موضع Maker الحالي إلى أي رأس غير مزار على طول الأضلاع التي لم يستولي عليها Breaker والرؤوس غير المُزارة مسبقاً من قبل Maker.

ولتجنب الالتباس بين النوعين سنرمز للنوع الأول (الحركة ضمن مسلك) بـِ WMaker-Breaker، وللنوع الثاني (الحركة ضمن مسار) بـِ PMaker-Breaker.

علماً أنَّه قد تمت معالجة ألعاب Maker-Breaker في كتاب Beck[2] وكذلك الدراسة الأخيرة لـِ Hefetz و Krivelevich وآخرون [6].

1. هدف البحث:

ينصب تركيز البحث عموماً في دراسة لعبة Maker-Breaker وذلك عندما تتقيد حركة Maker ضمن مسلك أو مسار على بيان مترابط، بينما حركة Breaker غير مقيدة بشرط، والبيانات المترابطة التي تم العمل عليها هي البيانات التامة K_n $(n \geq 6)$، والنوع الآخر هي البيانات التكعيبية (n-cube)، ونريد معرفة كم عدد الرؤوس التي يستطيع Maker الحصول عليها.

2. طرق ومواد البحث:

التعاريف والمفاهيم الأساسية [6],[5],[2]:

[1] اللعبة التوافقية (Combinatorial Game): تتعامل اللعبة التوافقية مع نوع محدد من الألعاب الثنائية، ويمكن وصفها على النحو التالي:

- هناك لاعبان يتبادلان التحرك.
- لا توجد أدوات حظ مثل حجر النرد أو البطاقات العشوائية.
- هناك معلومات كاملة، أي كلا اللاعبين يعرفان جميع الحركات المتاحة لكلا اللاعبين.
- تنتهي اللعبة في النهاية، حتى ولم يتبادل اللاعبان التحركات.
- تنتهي اللعبة عندما يجد أحد اللاعبين نفسه غير قادر على القيام بأي حركة قانونية.

[2] اللعبة الموضعية (Positional Game) : لاعبَين يتبادلان بشغل نقاط جديدة. اللاعب الذي يستطيع أولاً شغل مجموعة ربح (winnig set) هو الفائز، أما إذا لم توجد مجموعة ربح فيعلن عن اللعبة أنها تعادل.

[3] لعبة Maker-Breaker: يتبادل اللاعبان Maker و Breaker بشغل نقاط جديدة. يربح Maker في نهاية اللعبة إذا ما استطاع شَغِل كافة العناصر لأغلب مجموعات الربح، ويربح Breaker إذا ما استطاع شغل عنصر واحد على الأقل من كل مجموعة ربح.(هنا لا يوجد تعادل بين اللاعبين، إما رابح أو خاسر، وبالتالي لعبة Maker-Breaker هي حالة خاصة من الألعاب الموضعية.)

[4] البيان التام ($\mathbf{K_n}$): نقول عن البيان $G(V,E)$ ، حيث V مجموعة الرؤوس و E مجموعة الأضلاع، أنه بيان تام (Complete graph) إذا كان كل رأس في البيان يجاور جميع رؤوس البيان الأخرى، وبالتالي لكل رأس الدرجة n-1.

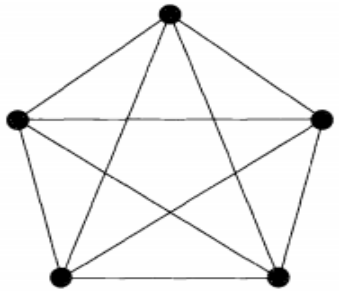

[5] البيان التكعيبي ($\mathbf{Q_n}$): هو بيان منتظم من المرتبة 2^n والدرجة n ، كما أن رؤوس البيان مرتبة وفق متجه $(a_1, a_2, \dots, a_n)$ حيث $(a_i = 0 \text{ or } 1)$ لأجل $(i = 1,2, \dots, n)$ ويكون الرأسان متجاورين إذا اختلفا بمركبة واحدة فقط من مركبات متجهي الرأسين. ولهذه البيانات أهمية خاصة وهي تنتج من تعريف الجداء الديكارتي للبيانات ويرمز له بـِ $Q_n . Q_n$ (n-cube) يكون K_2 عندما $n = 1$، أي أن $Q_1 = K_2$. إذا كان $n > 1$ نعرف Q_n بشكل متتابع، أي أنَّ $Q_n = Q_{n-1} \times K_2$. حيث أن البيان التكعيبي هو البيان كما في الشكل التالي:

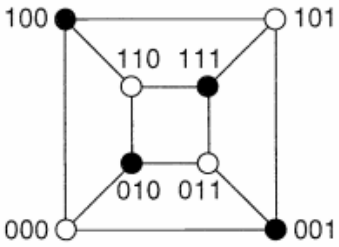

[6] الشجرة (Tree): هي بيان مترابط خالٍ من الحلقات، والبيان غير المترابط الذي لا يحوي حلقات يسمى غابة (forest) وبناءً على تعريف الغابة فإن الشجرة غابة مؤلفة من مركبة وحيدة.

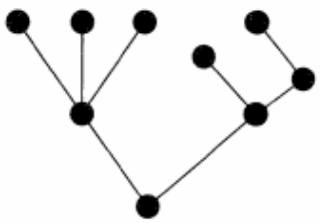

[7] المسلك (Walk): ليكن البيان $G(V, E)$، وليكن u و v رأسين من البيان G (ليس بالضرورة متمايزان). نسمي $W=u-v$ مسلك (walk) من الرأس u إلى الرأس v ، إذا كان W متتالية متناوبة من الرؤوس والأضلاع بالشكل التالي:

$$u = v_0, e_0, v_1, e_1, v_2, \dots, v_{k-1}, e_{k-1}, v_k = v$$

من الممكن تكرار الرؤوس والأضلاع في المسلك.

[8] المسار (Path): هو مسلك شريطة عدم تكرار الرؤوس أو الأضلاع.

مثال: ليكن لدينا البيان التالي:

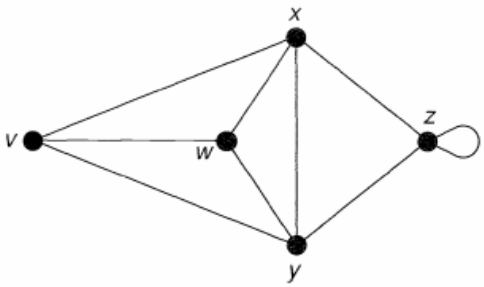

لدينا المتتالية $v \longrightarrow w \longrightarrow x \longrightarrow y \longrightarrow z \longrightarrow z \longrightarrow y \longrightarrow w$ عبارة عن مسلك (ممر) أما المتتالية $w \longrightarrow x \longrightarrow y \longrightarrow z$ فهي عبارة عن مسار.

3. النتائج والمناقشات:

المبرهنة (1): ليكن البيان $G(V, E)$ عبارة عن بيان تام، حيث أن عدد الرؤوس n يحقق $n \geq 6$ ، وضمن عملية لعب مثالية في لعبة PMaker-Breaker (1:1)، فإنَّ اللاعب Maker يزور كل الرؤوس باستثناء اثنين منها.

المبرهنة (2): ليكن البيان $G(V, E)$ عبارة عن بيان تام، وضمن عملية لعب مثالية في لعبة WMaker-Breaker $(1: \alpha)$ على البيان G بحيث $(n \geq 2\alpha^2)$، فإن Maker يزور $n - 2\alpha + 1$ رأس، حيث $(\alpha \geq 1)$.

المبرهنة (3): ليكن البيان $G(V, E)$ عبارة عن بيان تكعيبي، فإنه ضمن عملية لعب مثالية في لعبة WMaker-Breaker، فإنّ Maker يزور على الأقل 2^{n-2} رأس وعلى الأكثر 2^{n-1} رأس.

بعض الرموز:

لتكن V_t تشير إلى مجموعة الرؤوس التي تمت زيارتها من Maker، ولتكن U_t تشير إلى خلاف ذلك، وذلك بعد قيام Maker بالحركة t. حيث أنَّ Maker يكون عند الرأس v_t وذلك بعد قيامه بالحركة t. نشير إلى البيان المحدث بأضلاع Breaker بـِ Γ_B ، وإلى البيان المحدث بأضلاع Maker بـِ Γ_M.

إثبات المبرهنة (1): من الواضح أنه في اللحظة t سيكون البيان Γ_M عبارة عن مسار. علماً أن المسألة ليست مسألة من يبدأ أولاً بالتحرك، ولإظهار ذلك نفرض أن Maker يبدأ أولاً من أجل أي حد أدنى على عدد الرؤوس التي تمت زيارتها، ويبدأ Breaker من أجل أي حد أدنى على عدد الرؤوس التي تمت زيارتها.

الحد الأدنى: يتبع Maker الاستراتيجية التالية: إذا كان $|U_t| > 2$ وقام Breaker باختيار f_t حيث $f_t \cap V_{t-1} = \emptyset$، فإنّ Maker يتحرك إلى $v_t \in f_t$. بخلاف ذلك، فإن Maker يتحرك إلى رأس كيفي. وطالما أن Maker قادر على اتباع هذه الاستراتيجية، سيكون لدينا بعد كل تحرك لـ Maker ما يلي:

كل ضلع لـ Breaker يحتوي على عنصر من V_t . (1)

نتحقق الآن فيما إذا كانت هذه الاستراتيجية مجدية لـ $|U_t| > 2$. نبدأ مع النوع الأول من أضلاع Breaker، والتي تكون منفصلة عن V_t. في الحركة t، ليكن $v_{t-1} = x$ و $v_t = y$. بفرض أن Breaker اختار الضلع (b_1, b_2) حيث $b_1, b_2 \notin V_t$، ومن أجل $i = 1,2$ فإن (y, b_i) هو ضلع لـ Breaker. ونعتبر هذه هي المرة الأولى التي يحدث فيها هذا الوضع. ثمَّ نفرض أنَّ (y, b_i) هو الضلع المختار من Breaker (حيث $s_1 < s_2$) s_i. فإننا نحصل على تعارض مع العلاقة (1) بعد اختيار الرأس x. وإذا ما تم اختيار الرأس x ، فإنَّ (y, b_i) هو ضلع لـ Breaker والذي لا يحتوي على عناصر من V_{t-1}.

نعتبر الآن الحالة التي يكون فيها ضلع لـ Breaker واقع على عنصر في V_t. العلاقة (1) تشير إلى أنَّ اختيار Breaker هو في الغالب الضلع الثاني بين الرأس v_t والمجموعة U_t. وعلى وجه الخصوص، $|U_t| > 2$ تشير إلى أن Maker بإمكانه التحرك إلى رأس لم تتم زيارته. وبالتالي سينجح Maker بزيارة كل الرؤوس باستثناء اثنين منها.

الحد الأعلى: يلعب Breaker بشكل كيفي لغاية حركته عند الدور $n - 4$، عندما $|U_{n-4}| > 4$. يختار في حركتيه التاليتين ضلعين من تجزئة مستقلة من U_{n-4}. وبعد هاتين الحركتين (مع حركة لـMaker بينهما)، يحين دور Maker، ويتبقى ثلاثة رؤوس غير مُزارة. وأيّاً يكن الرأس من U_{n-3} فإن Maker ربما يختار التحرك إلى الرأس التالي، وهذا الرأس سيكون متجاوراً مع رأس في U_{n-2} على طول أحد ضلعي التجزئة المستقلة لـ Breaker؛ وبالتالي مع وجود حركة إضافية، فإنَّ Breaker سيضمن أنَّ كلاً من الضلعين من الرأس v_{n-2} إلى المجموعة U_{n-2} تكون مشغولة من قِبَلِهِ.

مثال (1): ليكن لدينا البيان K_6، ولنقم بتطبيق استراتيجية Maker كما يلي:

الشكل (4-1)

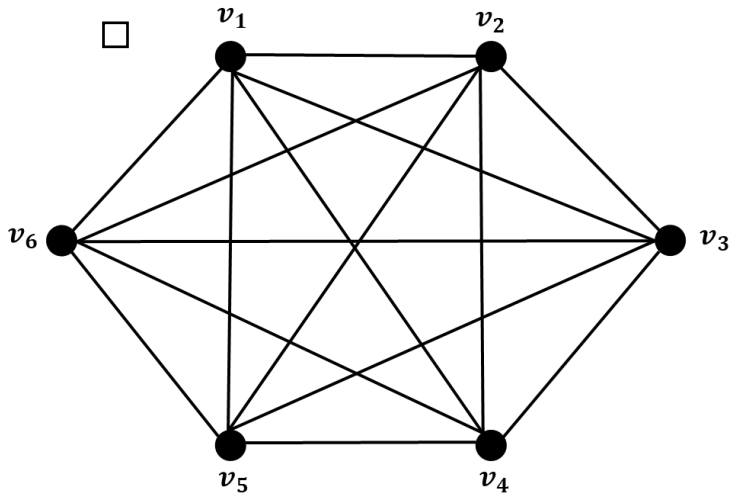

في بداية اللعبة يكون $|U_t| > 2$، ويكون $f_t \cap U_t = \phi$، لذا بمقدور Maker تطبيق استراتيجيتها. يبدأ Breaker اللعب ويختار ضلعاً كيفياً وليكن v_1v_2، وبالتالي على Maker أن تتحرك من موضعها الحالي وليكن من v_3 إلى v_2، ثم يحين دور Breaker ثانية ويختار ضلعاً كيفياً (باستثناء v_2v_3) وليكن v_4v_5، والآن لا تزال Maker قادرة على تطبيق استراتيجيتها وتتحرك من الرأس v_2

إلى الرأس v_5 (أي الضلع v_2v_5)، بعدها يتحرك Breaker ويختار الضلع v_1v_6، ويتوجب على Maker التحرك من موضعها الحالي v_5 إلى الرأس v_6، ويقوم Breaker بإنهاء اللعبة واختيار الضلع v_4v_6، وهنا لا يوجد مسار من موضع Maker الحالي إلى رأس لم تقوم بزيارته سابقاً على طول ضلع لم يتم اختياره من Breaker، وبالتالي استطاعت Maker أن تزور أربعة رؤوس من ستة، ويأخذها بيانها الشكل التالي:

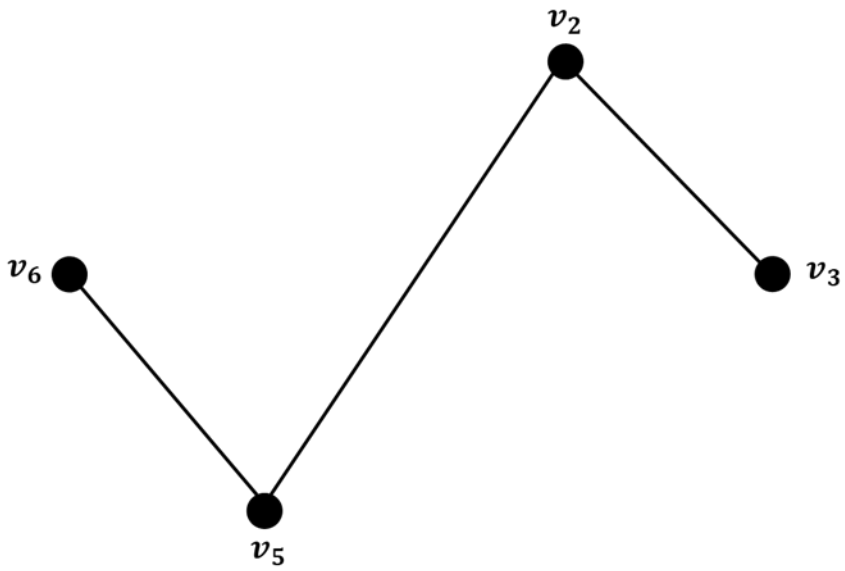

الشكل (2-4)

إثبات المبرهنة (2): هنا اللاعب Maker غير مقيد بمسار، وإنما تتم حركته وفقاً لمسلك إذ بمقدوره تكرار الرؤوس والأضلاع.

الحد الأدنى: تقوم Maker ببناء شجرة T في جولتها الأولى (وهذا طبيعي؛ لأن البيان مترابط)، وليكن الجذر هو الرأس v_1 عند المستوى 0. ومن المعلوم إن التعابير (مستوى/أب/ ابن) تتعلق بالجذر. ليكن $v \in T$ وليكن $w = \pi(v)$ (أي أن الرأس w هو أب للرأس v). إذا كانت Maker عند رأس، وليكن x، وَوُجِدَ رأس $y \in U_t$ بحيث أنَّ Breaker لم يستدعي بعد الضلع (x, y) فإنَّ Maker ستتحرك إلى الرأس y. وليكن $x = \pi(y)$. وبخلاف ذلك، إذا لم توجد حركة ممكنة مثل هذه فإنَّ Maker ستتحرك إلى $\pi(x)$ وتُعيد البحث من جديد عن $y \in U_t$ في حركتها التالية. اللعبة تنتهي عندما يجد Maker نفسه عند v_1 وكل الأضلاع بين v_1 و U_t تم أخذها من قبل Breaker.

بفرض أنَّ اللعبة تنتهي عندما $|U_t| = k$. وبالتالي فإن اللاعب Maker يكون قد صنع $2(n - k - 1)$ حركة. وذلك لأن كل ضلع من الشجرة T قد تم عبوره مرتين، الأولى من الجهة الأمامية، أما الثانية فمن الجهة الخلفية. كما انَّ Breaker يكون قد كَسِبَ على الأقل $k(n - k)$ ضلع وذلك بين T و U_t. وبالتالي لدينا:

$$k(n - k) \leq 2\alpha(n - k - 1)$$

وينتج من هذا أنَّ $k < 2\alpha$. وهذا يبين أنَّ Maker يزور على الأقل $n - 2\alpha + 1$ رأس.

الحد الأعلى: معطيات استراتيجية Breaker على النحو التالي: بفرض أنَّ Maker يستهل التحرك أولاً ويستدعي ضلع $\{v_1, v_2\}$، أما اللاعب Breaker فيختار رأس w_1 بحيث $w_1 \notin \{v_1, v_2\}$. سيستهلك Breaker، $\frac{n-1}{\alpha}$ حركة مما يجعلنا نتأكد بأن Maker

ليس بمقدوره زيارة w_1. وفي حركة ما، سيقوم Breaker باستدعاء الضلع من الرأس w_1 إلى الرأس v_t، وهذا عند الضرورة، بالإضافة إلى $\alpha - 1$ ضلع آخر تقع على w_1. وهذا يأخذ ما يقارب $\frac{n-1}{\alpha}$ حركة. بعد ذلك يقوم Breaker باختيار الرأس، غير المزار، ويعمل على حمايته لئلا تتم زيارته مرة ثانية بنفس الطريقة. وهو يفعل هذا لأجل $w_{\alpha-1}, \dots, w_2, w_1$. وبالإجمال، هذا يصنع على الأقل $(\alpha - 1)\lfloor(n-1)/\alpha\rfloor$ حركة، ويترك على الأقل $1 + \left\lfloor\frac{n-1}{\alpha}\right\rfloor$ رأس غير مزار. بعدها يقوم Breaker باختيار α رأس غير مزار $y_\alpha, \dots, y_2, y_1$ $(n > 2\alpha^2)$، وكل حركة له تتألف من اكتساب ضلع من الأضلاع (v_t, y_i)، $i = 1,2, \dots, \alpha$. وهذا يحمي الرؤوس $y_\alpha, \dots, y_2, y_1$ وبالتالي فإن Maker يزور على الأكثر $n - 2\alpha + 1$ رأس. ■

مثال (2.3): ليكن لدينا البيان k_9، ولنقم بلعب WM-Br (1: 2) على هذا البيان على النحو التالي:

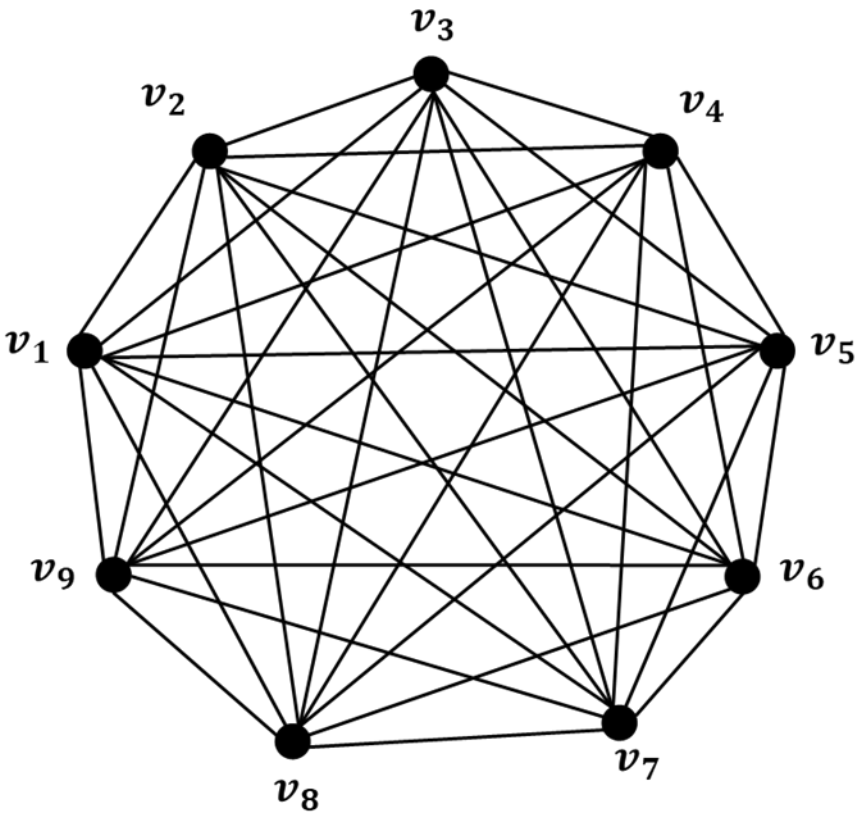

الشكل (3-4)

يبدأ Breaker اللعب ويختار في كل حركة له ضلعين بشكل كيفي، بينما تختار Maker ضلع واحد فقط في كل حركة، وتكون حركتها مقيدة وفق مسلك، تحاول Maker بناء شجرة T وزيارة أكبر عدد ممكن من الرؤوس وتتبع الاستراتيجية الموضحة في الحد الأدنى.

والجدول التالي يبين كامل تحركات اللاعبَين حتى الوصول إلى نهاية اللعبة، وتمكن Maker من زيارتها لسبعة رؤوس من اللوحة اللعبة (K_9).

تحركات Maker	تحركات Breaker
v_1v_4	v_1v_2, v_1v_3
v_4v_7	v_4v_5, v_4v_6
v_7v_2	v_7v_8, v_7v_9
v_2v_6	v_2v_5, v_2v_3
v_6v_5	v_6v_8, v_6v_9
v_5v_3	v_5v_8, v_5v_9
	v_3v_8, v_3v_9

ويصبح بيان Maker على النحو التالي:

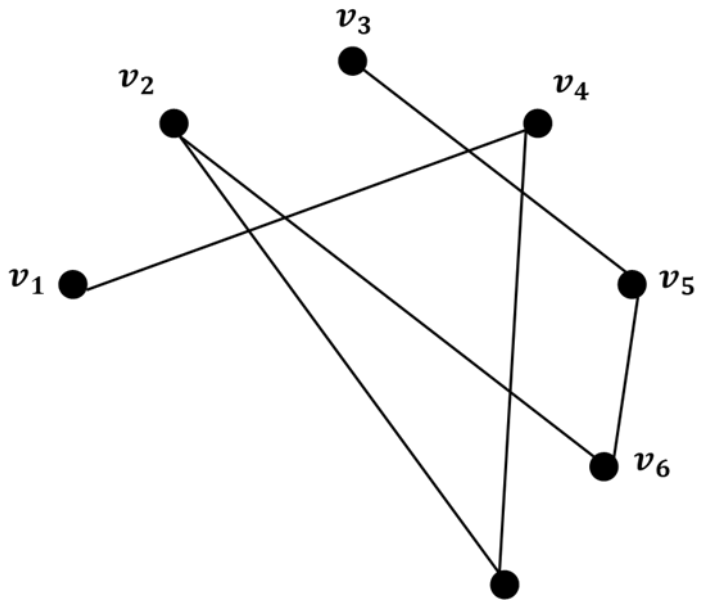

الشكل (4-4)

إثبات المبرهنة (3):

الحد الأدنى: نستهل المناقشة هنا بأسلوب مشابه لما رأيناه في القسم الأول من المبرهنة السابقة. يبني Maker شجرة T على مدار جولته الأولى. وللمرة الثانية فإنَّ الأضلاع بين T و U_t ستكون لِـ Breaker . والآن لنفرض أنَّ T لديه k رأس، وبالتالي:

$$2(k-1) \geq e(T, U_t) \geq k(n - \log_2 k)$$

الحد الأدنى ينتج من مبرهنة Harber[7]، وعليه فإن:

$$\log_2 k \geq n - 2 + \frac{2}{k}$$

وبالتالي 2^{n-2} رأس على الأقل تكون مأخوذة من قبل Maker.

الحد الأعلى: بفرض أن Maker يبدأ أولاً، وبفرض أنه يبدأ من الرأس $(0,0,\dots,0)$ وبعجها يتحرك إلى الرأس $(0,1,\dots,0)$. حيث ان Breaker لن يسمح لخصمه من أخذ أي رأس تكون مركبته الأولى هي 1. عندما يتحرك Maker إلى $(0,x_2,x_3,\dots,x_n)$، فإن Breaker يستولي على الضلع $(0,x_2,x_3,\dots,x_n)(1,x_2,x_3,\dots,x_n)$. ويستطيع Maker اكتساب الضلع $(0,0,\dots,0)(1,0,\dots,0)$ في حركته الأخيرة، أو ما قبل الأخيرة. وهذا يوضح بأن 2^{n-1} رأس على الأكثر تمت زيارتها من قبل Maker.

مثال (3): ليكن لدينا البيان Q_3 الموضح في الشكل (3-5).

وفقاً للمبرهنة الأخيرة تستطيع Maker زيارة $2^{n-1} = 2^2 = 4$ رأس على الأكثر، ولتكن Maker هي من يبدأ اللعب ستختار في حركتها الأولى التحرك من الرأس $(0,0,0)$ إلى الرأس $(0,1,0)$، ويعمل Breaker على منعها من زيارة أي رأس يبدأ بالمركبة 1، فيختار التحرك من الرأس $(0,1,0)$ إلى الرأس $(1,1,0)$، ثم تتحرك Maker من موضعها الأخير إلى الرأس $(0,1,1)$، عندها يختار Breaker التحرك من الرأس $(0,1,1)$ إلى الرأس $(1,1,1)$، بعد ذلك تتحرك Maker إلى الرأس $(0,0,1)$، عندها يختار Breaker التحرك من $(0,0,1)$ إلى $(1,0,1)$، ولا تستطيع Maker التحرك إلى الرأس $(0,0,0)$ لأنها تتحرك لبناء شجرة من أضلاعها، وتنهي اللعبة بزيارتها لأربعة رؤوس من ثمانية رؤوس.

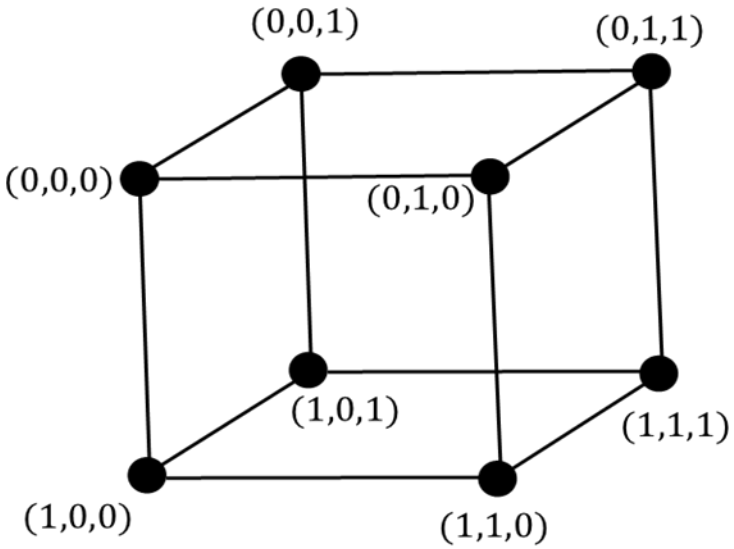

الشكل (3-5)

ويصبح بيان Maker على النحو التالي:

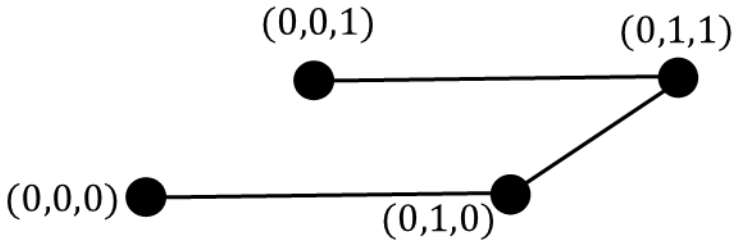

الشكل (3-6)

المراجع:

[1]. P. Erdös AND J. Selfridge, On a combinatorial game, J. Combinatorial Theory Ser. A, 14(1973), pp. 298-301.

[2]. J. Beck, Combinatorial Games: Tic- Tac- Toe Theory, Cambridge Press, Cambridge, UK, 2008.

[3]. D. Clemens, T. Tran, Creating in Walker-Breaker games, Discrete Mathematics 339 (8) (2016), 2113-2126.

[4]. D. Hefetz, M. Krivelevich, M. Stojakovič and and T.Szabó, Fast winning strategies in Maker-Breaker games, Journal of Combinatorial Theory Series B 99 (2009), 39-47.

[5]. D. Hefetz, M. Krivelevich, M. Stojakovič and and T.Szabó, Positional Games, Oberwalfach Seminars 44, Birkhäuser/Springer Basel, 2014.

[6]. D. B. West, Introduction to Graph Theory, Prentice Hall, 2001.

[7] L. Harper, Optimal numberings and isoperimetric problems on graphs, J. Combinatorial Theory, 1(1966), pp. 385-394.

[8] L. Espig, A. Frieze, M. Krivelevich, W. Pegden, Walker-Breaker Games, society for Industrial and Applied Mathematics, 29(2015), pp. 1476-1485.

المؤتمر العلمي الدولي الثالث عشر
لجمعية الرياضيات العراقية والمنعقد تحت شعار
نحو عالم متقدم : الرياضيات والتقنيات في سباق الابتكار
للمدة 24 - 25 نيسان 2024
الكوفة – النجف الاشرف

Physics scope

Physics of Pulsed Laser Deposition (PLD)

Intesar Dakhel Shakhir Aljenabi

babylove123hrw123@gmail.com

Abstract

In both academia and industry, pulsed laser deposition (PLD) is a frequently used technique for creating thin films. The PLD offers more superior benefits than other deposition methods, including flexibility, growth rate control, stoichiometric transfer, and an infinite degree of freedom in the ablation geometry. The process of pulsed deposition and growth was demonstrated in this study. In addition, the form of lazar employed in the PLD. The benefits and drawbacks noted in this research as well as any PLD application[1].

1- pulsed Laser Deposition (PLD) Process

The pulsed laser deposition process can be divided into four steps, each having a significant impact on the crystallinity, uniformity, and stoichiometry of the created thin film (Read more about Thickness Uniformity).

- Laser absorption on the target surface, including contact with the material, ablation, and generation of plasma
- Interactions between laser and plume dynamics
- The material that has been separated from the target is deposited on the substrate.
- The material's nucleation and development into a thin film on the substrate surface.

2- Laser-Target Interaction

The laser beam is adsorbed on the target surface during the first stage. By applying a high enough energy density and a brief pulse length, all of the elements in the target surface are abruptly heated to their evaporation temperature. At this point, they are instantly ablated out with the same stoichiometry as the target and separated from it by exfoliation, collisional, thermal, and electronic excitation [2].

-Plasma Plume Formation

In the second stage, the ablated materials exhibit the forward peaking phenomena and have a propensity to migrate towards the substrate in accordance with the dynamic laws of gases, producing a plasma plume[3].

-Deposition on the Substrate

Through the third stage, the high-energy species in the plasma plume impinge on the substrate surface. A zone where the incident flow and the sputtering atoms collide is formed when these energetic species sputter part of the atoms placed on the substrate surface. Directly adjacent to this collision or thermalized area is where film growth occurs. In order for the energetic particles to be deposited on the substrate, this region condenses them (Figure 2).

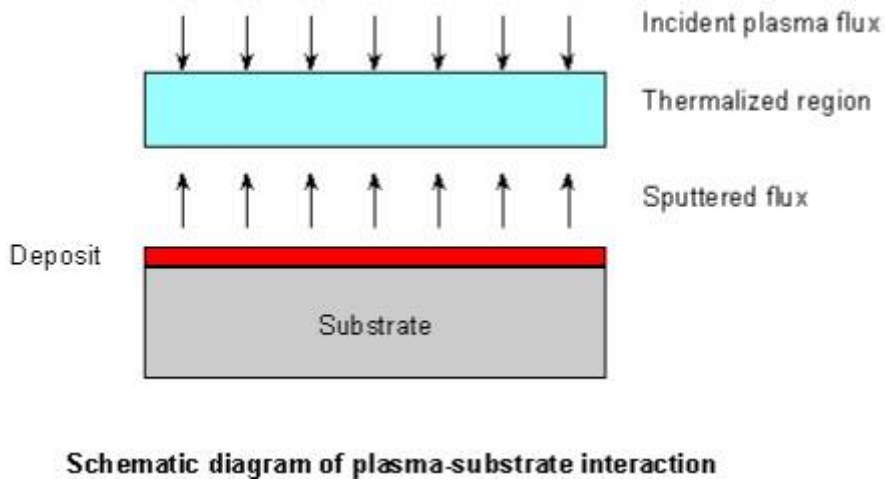

Figure 2. Schematic Diagram of Plasma-Substrate Interaction

3 -Nucleation and Growth

Numerous variables, including temperature, the kind of condensing material, energy, density, and substrate characteristics, influence the nucleation and development of crystalline thin films during the fifth stage. The interfacial energies between the substrate, condensing substance, and vapor affect the nucleation process. The essential size of the nucleus is significantly influenced by the substrate temperature and the rate of deposition. On the substrates, large nuclei form isolated film islands that expand and unite (Figure 3). The deposited atoms' surface mobility, which diffuses on the surface before stabilizing in a position that is strongly dependent on substrate temperature, governs the formation of the crystalline layer. While deposition on a low temperature substrate may result in poor crystalline or even amorphous structural properties, high temperatures can promote defect-free crystal development [4].

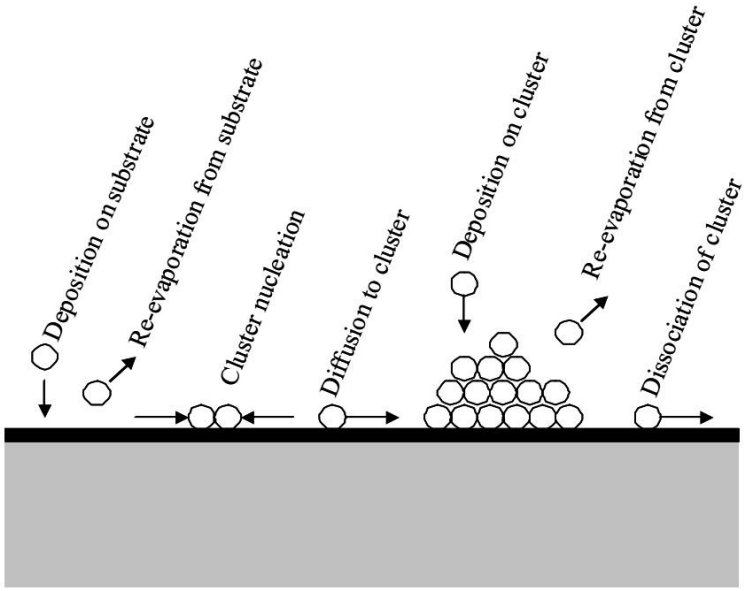

Figure 3. Thin Film Growth Steps

4-Which Laser is Used in PLD?

Target material, laser characteristics such as wavelength, fluence, and pulse width, substrate, temperature, and deposition geometry affect every stage of the PLD process. The laser wavelengths employed in PLD research span from the mid-infrared (e.g., CO2 laser, 10.6 μm) to the ultraviolet, near-infrared, and visible (e.g., Nd-YAG laser, with output wavelengths of 1064 nm and 532 nm). Excimer lasers operating at various UV wavelengths, such as 308 nm (XeCl), 248 nm (KrF), 193 nm (ArF), and 157 nm (F2), are used in the majority of PLD work conducted today.

The target material's surface should be penetrated by the laser pulse to a predetermined depth. The refractive index of the target material at the laser wavelength and the laser wavelength determine the penetration depth. Typically, this depth is around 10 nm for most materials. The electrons detach from the bulk due to the laser beam's strong electric field. This process happens because of nonlinear processes like multi-photon ionization and is carried out in a pulse of 10 picoseconds or nanoseconds[5].

The advantages of excimer lasers are stability and high power output. Compared to an excimer laser, the Nd:YAG (neodymium-doped yttrium-aluminum-garnet) laser offers a compact system and easy maintenance.
PLD applications using excimers include the following:

- Production of copper oxide films using rare earth elements for multilayer high-temperature superconductor tapes

- Production of DLC layers devoid of hydrogen that adhere well to a variety of materials
- Enabling the fabrication of scandium-doped aluminum nitride thin films for radiofrequency filters
- Manufacturing crystalline thin films for application in micro-nano devices on big wafers (up to 300 mm)[6].

The deposition parameters are influenced by the laser properties in multiple ways. The deposition flux (deposition rate), film quality, and stoichiometry are all influenced by the laser pulse energy, repetition rate, fluence [Joule/cm2], and ionization degree of the ablated material. These parameters also affect the nucleation process and the film's growth kinetics; a higher deposition flux results in a bigger nucleation density.

5-PLD Targets

Since storing the stoichiometry is the primary characteristic of the PLD process, it can be used to deposit a wide variety of elemental and compound targets. YBa2Cu3O7 (YBCO), Yttrium Iron Garnet (Y3Fe5O12, YIG), Zinc Gallate (ZnGa2O4), Strontium Titanate SrTiO3, Barium Ferrite (BaFeO3), Bismuth Vanadate (BiVO4), and other compounds are common metal elements utilized as targets for PLD[7].

PLD: Advantages and Disadvantages

PLD technique has several advantages that make it straightforward for thin film deposition, such as:

- Target stoichiometry is maintained in the deposited film. Only a few laser-related parameters, such as laser energy density and pulse repetition rate, need to be controlled during the deposition process. In comparison to conventional sputtering procedures, fewer targets are needed.
- Capacity to sequentially ablate many targets to create multi-layered films of distinct materials.
- Reducing the thickness of the film to an atomic monolayer by varying the pulse count
- Lower substrate temperature needed compared to other deposition techniques

Main Disadvantages of Pulsed Laser Deposition Technique

However, several limitations in producing large area uniform thin films by pulsed laser deposition method have been identified that are listed below[8]:

- Splashing or deposition of micrometer-sized particulates on the films because of sub-surface boiling, expulsion of the liquid layer, and exfoliation of the target

- Narrow angular distribution of the ablated species by the laser

Although these problems can be rectified by rotating the target and substrate to create larger, more uniform films or by introducing a shadow mask to block off the larger particulates, these drawbacks have prevented PLD from being completely utilized in industry. PLD Methods Scanning Multi-Component Pulsed Laser Deposition By adjusting the scan line with respect to the target geometry, it is possible to deposit a desired composition of distinct target segments made of different materials using this approach. Multicomponent coatings are deposited uniformly over a vast area as a result (Figure 4) [9]

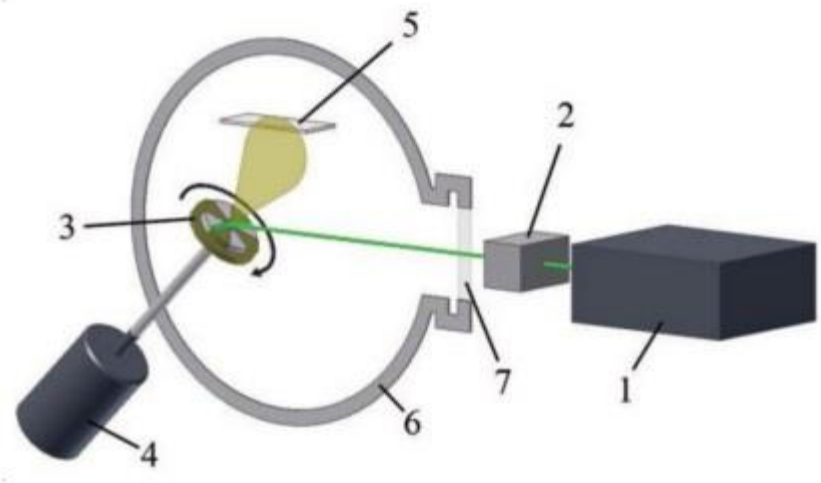

Figure 4. Scanning Multi-Component Pulsed Laser Deposition

Combined PLD and Magnetron Sputtering PLD and magnetron sputtering (MS) can be combined to achieve greater deposition rates and direct deposition of clusters and neutral atomic species by PLD, while maintaining the magnetron discharge at lower pressures than in a standard MS system (Figure 5)[10].

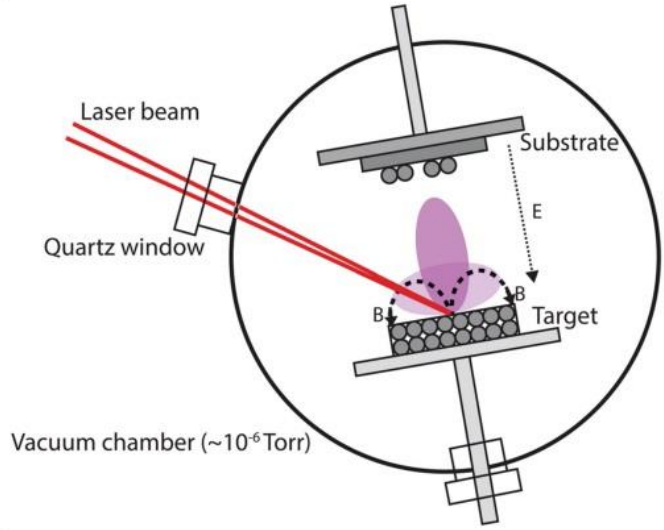

Figure 5. Combined PLD and Magnetron Sputtering

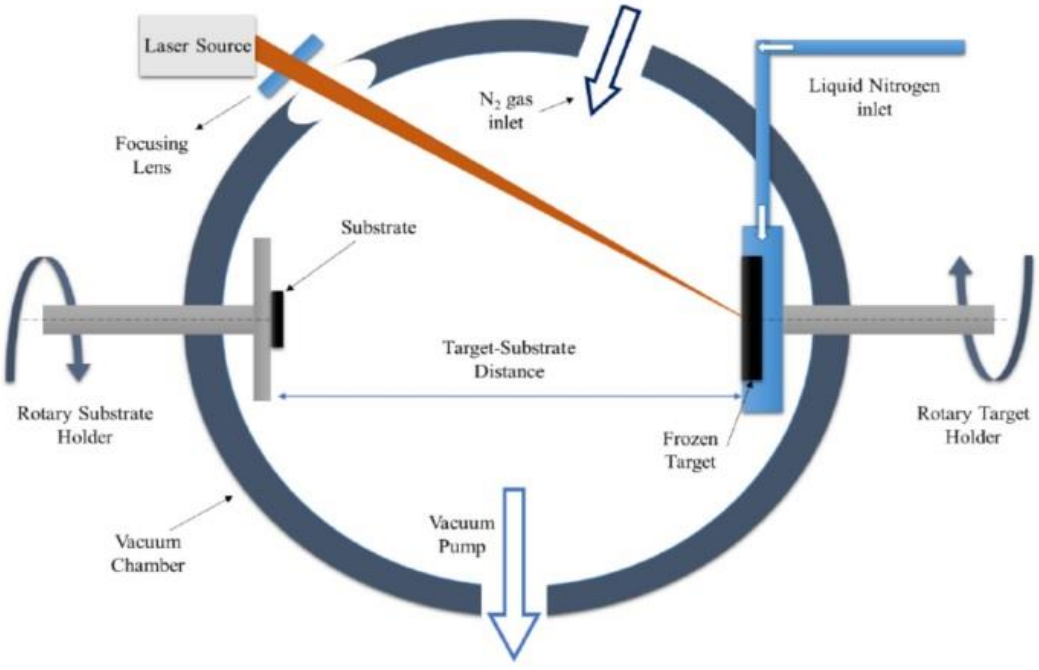

Figure 6. Matrix Assisted Pulsed Laser Evaporation

6-Matrix Assisted Pulsed Laser Evaporation (MAPLE)

Depositing frozen targets comprising inorganics, polymers, and biomaterials immersed in a volatile solvent is a helpful technique because it adsorbs high energy laser beams and shields the material

molecules from harm. As a result of their decreased adhesion coefficient, solvent vapor may be easily pumped out of target molecules once they have heated up through collisions with solvent molecules (Figure 6)[11].

Multi-Beam PLD

By combining multiple plasma plumes during thin film deposition, the PLD method is primarily utilized to deposit a thin layer from multiple targets of various materials (Figure 7)[12].

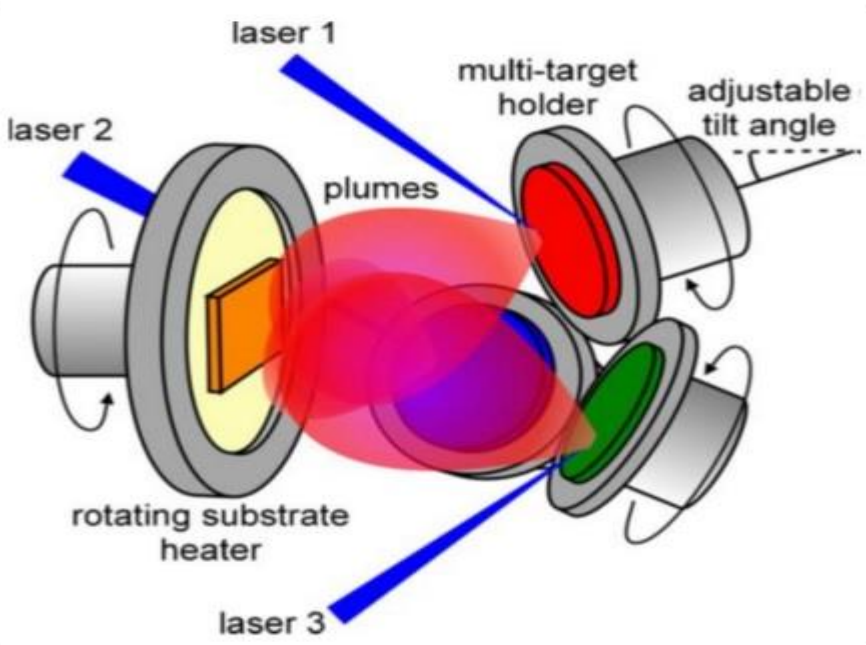

Figure 7. Multi-Beam PLD

Off-Axis PLD

When the substrate is positioned parallel to the plasma plume in the off-axis PLD approach, thinner and more uniform coatings are deposited on the substrate than on the on-axis substrate (Figure 8) [13].

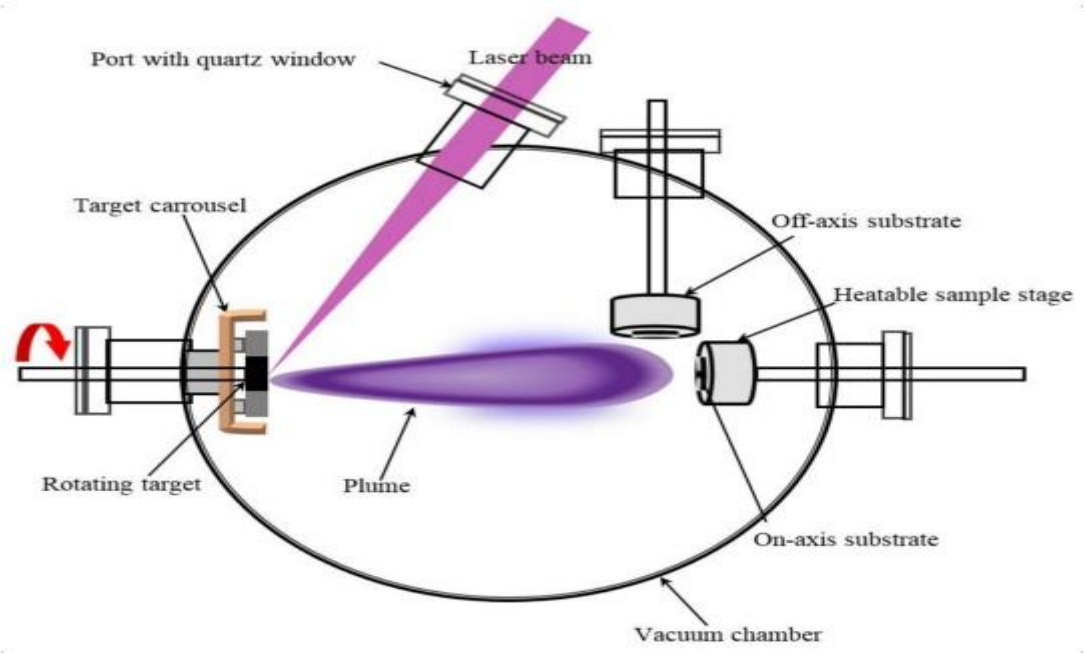

Figure 8. Off-axis PLD

Pulsed Laser Deposition Applications Since the successful development of high-temperature superconducting films in 1987, pulsed laser deposition has garnered much attention. This method has been used to create a variety of materials, such as[14]:

- Epitaxy crystalline thin films
- Nitride films
- Metallic multilayers

  Ceramic oxides
- Superlattices
- Nanotubes
- Nanopowders
- And quantum dots

Because of the high heating rate and lower substrate temperature in PLD compared to other deposition methods, semiconductors, and the underlying integrated circuits can be deposited through PLD [15]

7- Conclusions

Due to the technique's simplicity, PLD is commonly utilized in research laboratories to develop thin films, ablation, deposition, etc. Additionally, it shows great promise for various commercial applications such as coated-conductor, microwave filter, solar cell, sensors, and satellite communication. PLD has a high-power density laser with a narrow, wide bandwidth to vaporize the appropriate substance. This procedure is mainly employed when previous techniques such as LPCVD, PECVD, and ALD have proven difficult or have failed to deposit the material

References:

1. S.M. Metev and V.P. Veiko, Laser Assisted Microtechnology, Springer, Berlin, Heidelberg (1994)
2. D.B. Chrisey and G.K. Hubler, Pulsed Laser Deposition of Thin Film, John Wiley & Sons, Inc., New York (1994)
3. F. Breech and L. Cross, Appl. Spect.16, 59 (1962)
4. H.M. Smith and A.F. Tuner, Appl. Opt. 4, 147 (1965)
5. C.K.N. Patel, Phys. Rev. Lett.12, 588 (1964)
6. J.E. Geusic, H.M. Marcos and L.G. Uitert, Appl. Phys. Lett. 4, 182 (1964)
7. Y. Zhang, H. Gu, and S. Iijima, Appl. Phys. Lett. 73, 3827 (1998)
8. D.B. Geohegan, A.A. Puretzky, and D.L. Rader, Appl. Phys. Lett. 74, 3788 (1999)
9. T.J. Goodwin, V.L. Leppert, S.H. Risbud, I.M. Kennedy, and H.W.H. Lee, Appl. Phys. Lett. 10, 3122 (1997)
10. J.T. Cheung, I.M. Gergis, J. James and R.E. DeWames, Appl. Phys. Lett. 60, 3180 (1992)
11. J.A. Greer and H.J. Van Hook, Mater. Res. Soc. Symp. Proc. 191, 171 (1990)
12. A. Namiki, T. Kawai, K. Ichige, Surf. Sci. 166, 129 (1986)
13. R.K. Sing, SPIE 2945, 10
14. M. Hanabusa, Mater. Res. Soc. Symp. Proc. 285, 447 (1993)
15. S. Metev, K. Meteva, Appl. Surf. Sci. 43, 402 (1989)

المؤتمر العلمي الدولي الثالث عشر
لجمعية الرياضيات العراقية والمنعقد تحت شعار
نحو عالم متقدم : الرياضيات والتقنيات في سباق الابتكار
للمدة 24 - 25 نيسان 2024
الكوفة – النجف الاشرف

Calculation of The Energies of 1s and 2s shells for (C,N+1,O+2,F+3,Ne+4,Na+5) systems Using Hartree-Fock wave function

Maryam Hakim AL-Quraishi[a] Qassim Shamkhi AL-Khafaji[b] Ameer F. Shamkhi1[c] shaymaa awad kadhim[d]

Department of Physics//Faculty of Science/ University of Kufa / Najaf/ Iraq

ABSTRACT

In this research the Hartree- Fock energies were calculated of the 1s and 2s shells for($C,N^{+1},O^{+2},F^{+3},Ne^{+4},Na^{+5}$) systems Using Hartree-Fock wave function are obtained by an account the atomic properties by using the Hartree- Fock method and Mathcad 14 program, the total expectation value energy $\langle E_{HF} \rangle$ is important property account in this research and when comparing the result with published results. It was found that there is a good agreement.

Keywords: Hartree- Fock, atomic units, atomic properties, Hamiltonian operator

1. Introduction

Bohr model of the hydrogen atom invoked quantum theory, it was still primarily based on classical physics, and the picture of the atom in concrete terms involving particles. An electron orbiting around a nucleus is like Earth orbiting the Sun. In contrast, the treatment of atomic structure, especially the wave properties of the electron is called either quantum mechanics or wave mechanics .In 1926 Erwin Schrödinger developed an equation, called a wave equation, to describe the behavior of matter waves. An acceptable solution to Schrödinger's wave equation is called a wave function. By using Schrödinger's equation scientists can find the wave function which solves a particular problem in quantum mechanics. Unfortunately, it is usually impossible to find an exact solution to this equation, so certain assumptions are used in order to obtain an approximate answer for the particular problem. Both Erwin Schrödinger and Werner Heisenberg (1927) independently formulated general quantum theory. At first sight, the two methods appeared to be different because Heisenberg's method is formulated in terms of matrices whereas Schrödinger's method is formulated in terms of partial differential equations. Just a year later, however, Schrödinger was able to show that the two formulations are mathematically equivalent A wave function, denoted by the Greek letter ψ, the square of the wave function $|\psi|^2$ gives the probability of finding an electron in a particular infinitesimally

small volume of space [1].The central feature of which is a partial differential equation known as the Schrödinger equation [2]:

$\grave{H}\psi = E\psi$ (1)

Where ψ represents the wave function and determines the behaviour of the electron.

When the Schrödinger equation has written as in equation(1), it has seen to be an eigen value equation, an equation in the form:

(operator) (function) = (constant factor) × (same function)

E is called the eigen value of the operator $\hat{H}$.

2. Theory

In 1928, Hartree introduced the self-consistent field (SCF) method. This method may be used to calculate the ground state wave function and energy for any atom in this state. If interaction repulsion terms in Schrödinger equation are ignored, the Schrödinger equation for an n-electron atom may be separated into n-electron hydrogen like equations. The wave function obtained in this way is the product of n one-electron function that is hydrogen like wave functions (orbitals). The results of such a calculation are only approximate. Hydrogen like orbitals use the full nuclear charge +Ze, but the outer electrons of an atom shielded from the nucleus.

The Pauli principle putting no more than two electrons in each orbital, but in Hartree wave function did not involve spin and were not made to be antisymmetric with respect to the interchange of electrons, and Hartree function incorrectly describes the electron-electron interaction.

Hartree-Fock is usually defined as ″ uncorrelated″ .However, the electron motion are no longer completely independent (for two electrons with the same spin) [3].

The Hartree-Fock wave function for N-particles can be written as a single normalized determination (Slater determinant)

$$\Psi_{HF}(123\cdots N) = \frac{1}{\sqrt{N!}} \begin{vmatrix} \phi_1(1)\phi_1(2) & \ldots & \ldots & \phi_1(N) \\ \phi_2(1)\phi_2(2) & \ldots & \ldots & \phi_2(N) \\ .. \quad .. & .. & .. & .. \\ .. \quad .. & .. & .. & .. \\ \phi_N(1)\phi_N(2) & .. & .. & \phi_N(N) \end{vmatrix} \quad (2)$$

Where $\phi_i(i)$ refer to spin-orbital .Any spin-orbital may be written as the product of a space function ϕ and a spin function α or β .

The number in the parentheses denote the number associated to the particle, and the subscripts 1, 2,….,*N* denote the eigen state, and the multiplying factor $\frac{1}{\sqrt{N!}}$ arising from the fact that there are *N*! permutations of the electron coordinates(1,2,3,….., *N*), and $\frac{1}{\sqrt{N!}}$ introduced to ensure that the wave function Ψ is normalized after integrating over all the space and spin coordinates such that[4]:

$$\int \Psi \Psi^* d\tau = 1 \qquad \ldots\ldots (3)$$

$$\int d\tau = \int_0^{\infty} \int_0^{\pi} \int_0^{2\pi} d\tau$$

Where Ψ^* represent the complex conjugate of the wave function Ψ

$$D(r_1) = \int_0^{\infty} D(r_1, r_2) dr_2 \qquad (4)$$

The radial electron-electron distribution function $f(r_{12})$, which describes the probability of locating two electrons separated by distance r_{12} from each other, [5,6].

The pair distribution function can be written as [7]:

$$f(r_{12}) = 8\pi^2 r_{12} \left[\int_0^{r_{12}} r_1 d\, r_1 \int_{r_1 - r_{12}}^{r_1 + r_{12}} \Gamma(r_1, r_2) r_2 dr_2 + \int_{r_{12}}^{\infty} r_1 dr_1 \int_{r_{12} - r_1}^{r_{12} + r_1} \Gamma(r_1, r_2) r_2 dr_2 \right] \qquad (5)$$

The one-electron expectation value $\langle {r_1}^n \rangle$ is determined by the expression [7]:

$$\langle r_1^n \rangle = \int_0^{\infty} D(r_1) r_1^n \, dr_1 \qquad (6)$$

The inter-electron expectation values $\langle r_{12}^n \rangle$ is given by the relation [8]:

$$\langle r_{12}^n \rangle = \int_0^{\infty} f(r_{12}) r_{12}^n \, dr_{12} \qquad (7)$$

The virial theorem is a necessary condition for any stationary state. From the theorem, one is led to [9]:

$$\langle E \rangle = \langle T \rangle + \langle V \rangle \qquad (8)$$

$$\langle E \rangle = -\langle T \rangle = {}^{\langle V \rangle}/_{2} \qquad (9)$$

The expectation value of potential energy is proportional to the expectation values of $\langle r_1^{-1} \rangle$ and $\langle r_{12}^{-1} \rangle$ respectively, where [10]:

$$\langle V_{en} \rangle = -Z. \langle r_1^{-1} \rangle \qquad (10)$$

$$\langle V_{ee} \rangle = \langle r_{12}^{-1} \rangle \qquad (11)$$

Where $\langle T \rangle$ is the expectation value of kinetic energy ,$\langle V_{ee} \rangle$ is the Coulomb repulsion between electron-electron, and $\langle V_{en} \rangle$ is an attraction energy between electron-nucleus.

4. Results:

Table (1): show the relation between the maximum values for D(r1) with .5 corresponding position

Shell	Atom or ion	r1		D_{max}
1s	C	0.17		3.0134
	N^{+1}	0.15		3.5505
	O^{+2}	0.13		4.0876
	F^{+3}	0.11		4.6176
	Ne^{+4}	0.1		5.1593
	Na^{+5}	0.09		5.695
2s	C	First peak	0.14	0.11172
		Second peak	1.22	0.66736
	N^{+1}	First peak	0.12	0.15603
		Second peak	0.99	0.85852
	O^{+2}	First peak	0.1	0.20312
		Second peak	0.83	1.0513
	F^{+3}	First peak	0.09	0.25191
		Second peak	0.72	1.2448

	Ne^{+4}	First peak	0.08	0.30131
		Second peak	0.63	1.4375
	Na^{+5}	First peak	0.07	0.35071
		Second peak	0.56	1.6303

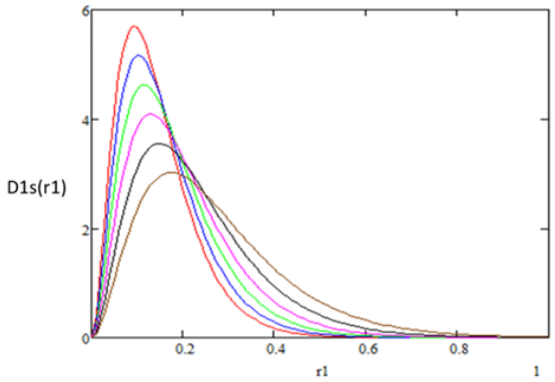

Figure 1. Relation between the radial density distribution function $D(r_1)$ and the position(r_1) for 1s shell

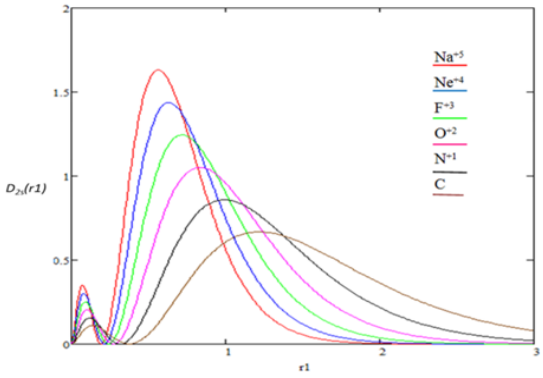

Figure 2. Relation between the radial density distribution function $D(r_1)$ and the position(r_1) for 2s shell

Table 2. show the relation between the maximum values for f(r12) with corresponding inter position.

Shell	Atom or ion	r12	$f(r12)_{max}$
1s	C	0.3	**2.2093**
	N^{+1}	0.25	**2.6032**
	O^{+2}	0.22	**2.9972**
	F^{+3}	0.19	**3.3912**

	Ne^{+4}	0.17	**3.7864**
	Na^{+5}	0.16	**4.1821**
2s	C	1.93	**0.41982**
	N^{+1}	1.55	**0.53475**
	O^{+2}	1.29	**0.64969**
	F^{+3}	1.11	**0.76428**
	Ne^{+4}	0.97	**0.87791**
	Na^{+5}	0.86	**0.99154**

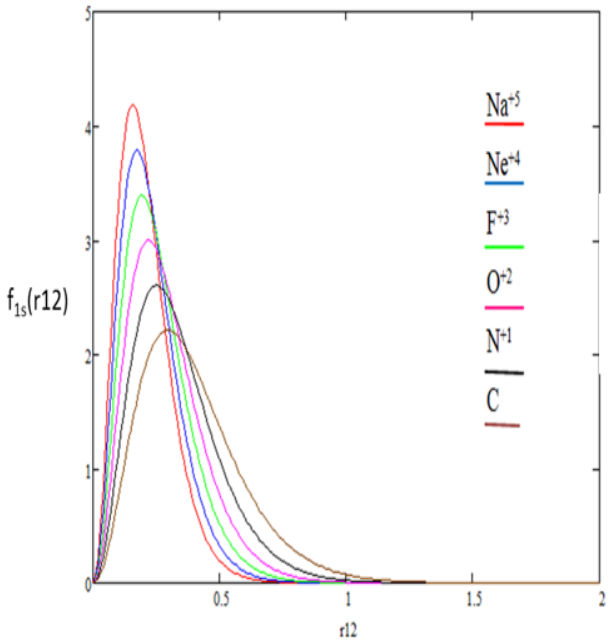

Figure 3. Relation between the inter-particle distribution function $f(r_{12})$ and the position($r12$) for 1s shell

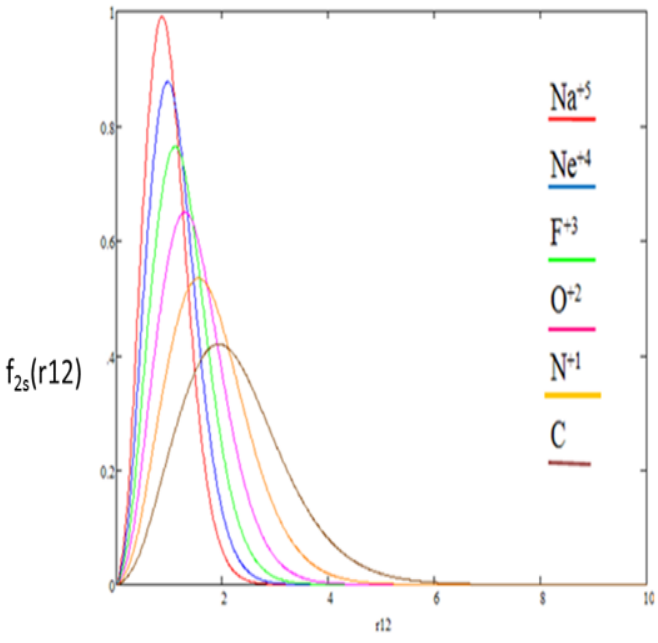

Figure 4. Relation between the inter-particle distribution function $f(r_{12})$ and the position($r12$) for 2s shell

Table 3. Expectation Values<r1^n> of 1s and 2s shells for studied systems

Atom or ion	n=-2		n=-1	n=0	n=1	n=2
C	1s	65.247991	5.664884	1	0.268396	0.097151
	2s	3.287347	0.900968	1	1.582306	3.024067
N^{+1}	1s	89.925624	6.657056	1	0.228049	0.070067
	2s	5.309914	1.143419	1	1.250261	1.866598
O^{+2}	1s	118.589505	7.650879	1	0.198185	0.052868
	2s	7.866053	1.390418	1	1.032477	1.264882
F^{+3}	1s	151.249933	8.645799	1	0.175207	0.041285
	2s	10.936092	1.639073	1	0.879387	0.913859
Ne^{+4}	1s	187.908601	9.641733	1	0.156979	0.033118

	2s	14.516125	1.888179	1	0.766 28	0.692272
Na^{+5}	1s	228.558121	10.638293	1	0.142 174	0.027149
	1s	18.598188	2.137785	1	0.678 917	0.542414

Table 4. Expectation Value<r_{12}^n> of 1s and 2s shells for studied systems

Atom or ion	Shell	n=-2	n=-1	n=0	n=1	n=2
C	1s	21.189057	3.509465	1	0.392361	**0.194302**
	2s	0.540875	0.57542	1	2.246568	**6.048232**
N^{+1}	1s	29.295567	4.128275	1	0.333293	**0.14013**
	2s	0.861276	0.725996	1	1.770719	**3.733232**
O^{+2}	1s	38.731215	4.748475	1	0.289587	**0.105733**
	2s	1.260842	0.87762	1	1.460288	**2.52974**
F^{+3}	1s	49.494948	5.369552	1	0.255969	**0.082569**

	2s	1.737954	1.02936	1	1.242754	**1.827719**
Ne^{+4}	1s	61.591625	5.991455	1	0.229306	**0.066236**
	2s	2.290879	1.180573	1	1.082423	**1.384535**
Na^{+5}	1s	75.019905	6.613852	1	0.207655	**0.054298**
	2s	2.920974	1.33189	1	0.958691	**1.084826**

Figure 5. Expectation Values of potential , kinetic and total energy of 1s and 2s shells for studied systems

Atom or ion	Shell	$\langle V_{ee} \rangle$	$\langle V_{en} \rangle$	< V >	< T >	< E >
C	1s	3.50947	-67.979	-64.46909	32.234545	**-32.234545**
	2s	0.57542	-10.808	-10.23298	5.11649	**-5.11649**
N^{+1}	1s	4.128275	-91.9884	-87.86012	43.93006	**-43.93006**
	2s	0.725996	-16.008	-15.28187	7.64093	**-7.64093**
O^{+2}	1s	4.748475	-122.414	-117.6655	58.832794	**-58.8327945**
	2s	0.87762	-22.247	-21.369068	10.68453	**-10.68453**
F^{+3}	1s	5.369552	-155.624	-150.2548	75.12741	**-75.12741**
	2s	1.02936	-29.503	-28.47395	14.23698	**-14.23698**

Ne^{+4}	1s	5.991455	-192.835	-186.84320	186.8432	**-186.8432**
	2s	1.180573	-37.764	-36.583007	18.2915	**-18.2915**
Na^{+5}	1s	6.613852	-234.042	-227.429	113.7142	**-113.7142**
	2s	1.33189	-47.031	-45.69938	22.84969	**-22.84969**

3. Discussion:

In table (1) the maximum values of one-particle radial density distribution function increase as atomic number increase in specific shell, that mean the probability of finding electron near nucleus increasing when atomic number increase because of the attraction force between the electron and nucleus depends upon the atomic number, also notice the maximum value of one-particle radial density distribution for 1s shell is larger than 2s shell , that means the probability of finding electron increasing whenever electron approached to nucleus because the electron cloud of 1s is smaller than 2s .

The corresponding position of maximum values of D(r1) decreases when atomic number increase for specific shell in atoms because of the attractive force between electron-nucleus increase.

in figures (1) and (2)also we notice in these figure. When r1 o , $D(r_1)=0$ that mean the electrons are dropping in the nucleus and the probability to find these electrons is zero. When ∞ , $D(r_1)=0$ that mean the electrons escape from the atom and the probability of finding these electrons is zero . figures (2) shows us there are two peak of one particle radial density function of 2s shell according to effect called penetration.

In table (2) , we notice the maximum values of the inter-particle distribution function in 1s shell which is bigger than the maximum values of the inter-particle distribution function in 2s shell ,because of the concentrate of electron

in the electron cloud of specific shell increase whenever the intra shell approached from the nucleus then the probability of finding the pair be bigger

,and we notice from the table the increasing in atomic number make the maximum values of the inter-particle distribution function for specific shell increase, because of the increasing in atomic number makes the intra shell approached to the nucleus according to Coulomb 's law .from figure (3)and (4) we notice when r12=0 , $f(r_{12})=0$ it is means is impossible to find two electrons in the same position and the same time and when r12=∞ , $f(r_{12})=0$ it refer one of the electron is not founded.

When K=0 , the one-particle expectation value equal to unity for each shell in all atoms and this represents the normalization condition for one-particle radial distribution function D(r1) ,also we notice in this table(3) when K=-2 , it is used to calculate the correlation coefficient where the one-particle expectation value increases as the atomic number increases for each individual shells ,also $<r_1^{-2}>$ of 1s shell is larger than 2s shell ,and $<r_1^{-1}>$ of 1s shell is larger than 2s shell ,

Also we notice when K=1,2 , one-particle expectation value decrease as the atomic number increases for each individual shells , that mean for K=1 the distance between nucleus and electron is decreases when atomic number increasing because of attraction force between them increase also $<r_1^{1}>$ and $<r_1^{2}>$ of 2s shell is larger than 1s shell

When K=0 , the inter -particle expectation values equal to unity for intra shells in all atoms and this represents the normalization condition for inter-particle radial distribution function D(r1) , when K=1 represented the distance between two electrons in specific shell, the inter -particle expectation values decrease when atomic number increasing because of increasing in atomic number create more attraction force between nucleus and electron ,so the distance between two electrons in 1s shell is smaller than 2s shell .

The behavior of K=1,2 takes the opposite for K=1,2 as repulsion force between the electrons when K= -1 where the increasing in inter -particle expectation values $<r_{12}^{-1}>$ create more repels between the electrons according to the atomic number increase From table (5)contain five expectation values determine the behavior of studied atoms where those expectation values are attraction potential (nucleus-electron),repulsion potential (electron- electron),total potential kinetic energy and Hartree-Fock energy, we observed from table(5) the total attraction energy for intra – shell increase with atomic number , also when we compare between the attraction energy of intra – shells for each studied atom , we not the 1s shell has a bigger attraction energy than 2s shell.

from table (5) we notice the repulsion energy of each intra – shells increase with atomic number because the increasing in electronic density of each individual shell making more repel between the electrons according to Coulomb's law. The dominate factors on kinetic energy of intra shell are the number mass and velocity of electron, when atomic number increase the kinetic energy increases for each individual shell.

Conclusions

1. When the atomic number Z increases , the one-particle radial density distribution function $D(r_1)$ and the inter-particle distribution function $f(r_{12})$ are increased in 1s shell which is bigger than the maximum values of the inter-particle distribution function in 2s shell.

2. the one-particle expectation value increases as the atomic number increases for each individual shells ,also $<r_1^{-2}>$ of 1s shell is larger than 2s shell ,and $<r_1^{-1}>$ of 1s shell is larger than 2s shell ,

Also we notice when K=1,2 , one-particle expectation value decrease as the atomic number increases for each individual shells.

3. the inter -particle expectation values decrease when atomic number increasing because of increasing in atomic number create more attraction force between nucleus and electron ,so the distance between two electrons in 1s shell is smaller than 2s shell.

4.All the expectation values of the energies $\langle V_{en} \rangle$, $\langle V_{ee} \rangle$, $\langle V \rangle$, $\langle T \rangle$, $\langle E \rangle$ are increased when the atomic number increases for each individual shell.

Acknowledgements

We would like to extend our sincere gratitude and admiration to the University of Kufa/Iraq for the assistance and resources it offers researchers. Particularly, the physics department laboratory at the scientific college to support them.

Ethical Approval: The study protocol was approved by local ethics committee.

Disclaimer: None

Conflict of interest: There are no conflicts of interest to declare.

Funding disclosure: support by ourselves.

References

[1] J.W. Hill, R. H. Petrucci, T. W. Mccreay, and S. S. Perry. " General Chemistry " Pearson Prentice Hall , Pearson Education , Inc. ,Upper Saddle River ,New Jersey P. 282 ,Forth Edition (2005).

[2] A. Levin "Solid State Quantum Chemistry" ,Me GRAY-HILL INTERNATIONAL BOOK COMPANY, New York (1976).

[3] M.N.Murshed,Ph.D.Sc.,Thesis"Evaluation of x-ray scattering factor for closed shell atoms using hartree-fock and correlated wave function ",College of Education (Ibn Al-Haithem),Baghdad University (2004).

[4] AlaaHafedh Al-Hayani, Tikrit Journal of Pure Science Vol. 11 No. 1(2006)89-92.

[5] P. Dressel and F. King , J. Chemical physics, V. 100, No. 10 ,p7515–7522, (1994).

[6] R . Benesch and Vedene H. Smith , J. Chemical Physics, V. 55, No. 2 ,p 482-488, (1971).

[7] N.Moiseyev, J.Katriel and R. Boyd , J. Theoretica Chimica Acta, V. 45, p61 –67, (1977).

[8] A. Gupta and R. J. Boyd , J. Chemical physics, V. 68, No. 4 ,p1951 –1957, (1978).

[9] R . Jaber. and Q. shamkhi 2014. " Study of Energy and some atomic properties for electronic shells at ground state of three electron systems by analysis Hartree-Fock- Roothaan wavefunction".J. Of Kufa –Physics.V.5.No.1.P.91-102,2013.

[10] K. Sen and V. Reddy , J. Chemical Physics, V. 81, No. 5213 . p5213-5214, (1984).

Heavy Metal Removal from Basrah waste water via Fe2O3 Nanocrystals

Anwar A. Jumaa1, Salwa A. Abduljaleel2, Zuhair A. Abdulnabi1, Abdulzahra A.N. AlHello1,

ABSTRACT

In this study, the co-precipitation method were used to synthesize α-Fe2O3 nanocrystals, that were then used as an adsorbent to remove Cu^{2+}, Zn^{2+}, Cd^{2+} , and Pb^{2+} from wastewater at room temperature. The prepared sample's structural and morphological properties are assessed using XRD, BET surface area, and FESEM. The development of a pure hematite structure with an average particle size of about 48 nm is confirmed by the XRD patterns and is further corroborated by the 70 nm nanocrystals' FESEM pictures. The BET specific surface area of the nanocrystals is determined to be approximately 39.89 $m^2\ g^{-1}$. Adsorption experiments are conducted for a range of solution pH values, contact times, and initial metal ion concentrations The maximum adsorption capacities of Fe2O3 nanocrystals related to Cu^{2+}, Zn^{2+}, Cd^{2+} , and Pb^{2+} are found to be 96.56 ppm for Pb^{2+} ions for a contact time 120 min. At pH 3, 6, and 9, high efficiency removal of Cu^{2+}, Zn^{2+}, Cd^{2+} , and Pb^{2+} takes place for zinc ions of 99.79 ppm. These results clearly suggest that the synthesized Fe2O3 nanocrystals can be considered as potential nano-adsorbents for future environmental and health related applications.

Keywords: water treatment, heavy metal removing, Iron oxide nanoparticles; Fe2O3.

1.Introduction

The growing population and industrialization are closely linked to the health and environmental problems associated with water pollution. Because wastewater contaminates soil and water resources with heavy metals and other contaminants, it poses a serious risk to the environment [1]. Cadmium, lead, and copper are ranked in the top eleven hazardous pollutants [2]. Wastewater from the battery, steel, paint pigment, fuel, photo materials, engineering and manufacturing, and coating industries are the main sources of lead pollution [3,4]. The second most toxic metal is lead (Pb), which makes up 0.002% of the Earth's crust. Lead is found naturally in very small amounts, but most of the lead that is produced is used in human-made industries, cars, batteries, and other products, which pollutes the environment and affects people. The main routes for human contact with lead salts and oxides are dust, battery vents, lead paint, and contaminated food [5]. Paint pigments and Ni-Cd batteries both make extensive use of the heavy and toxic metal cadmium. It has been reported that cadmium is a potent

carcinogen and hemopoietic [6]. Conventional environmental and biological processes do not effectively remove or reduce a large number of organic pollutants and heavy metals from wastewater. Common techniques for removing heavy metal ions from wastewater include adsorption, chemical precipitation, ion exchange, reverse osmosis, and electrochemical treatment. Copper can be found in nature as native copper, as well as in sulfide and oxide ores and salt minerals. It represents the second most of the non-ferrous metal that industry uses [7,8]. No review that covers the most recent reports on copper smelter-related air, soil, and water pollution has been published in the past ten years. Monitoring and testing the harmful effects of hazardous waste is still important because the quantity and variety of pollutants are too great for the environment to be able to clean itself [9]. Common techniques for removing heavy metal ions from wastewater include adsorption, chemical precipitation, ion exchange, reverse osmosis, and electrochemical treatment.[10]. Of these, adsorption is a popular and reasonably priced method.9) Silica gel, activated alumina, molecular sieve zeolites, activated carbon, and polymeric adsorbents are commonly utilized adsorbents in this technique. These sorbents do, however, have a number of drawbacks, including their high cost and poor adsorption capacities [10]. Iron oxide nanoparticles with a large surface area have the highest number of reactive surface sites among the inorganic materials found in the environment, along with organic contaminants such as cations and anions[6]. Metal ions from solution can scatter onto the active sites of the adsorbent's surface due to iron oxide's small size[12]. Hematite, or α-Fe2O3, is thought to be the most environmentally safe and stable iron oxide.

In this work, the co-precipitation method were used to synthesize Fe2O3. Both chemical and physical methods were used to characterize the synthetic sample. As nano-adsorbents, the α-Fe2O3 nanocrystals were employed to extract the heavy metal ions Cu^{2+}, Zn^{2+}, Cd^{2+} ,and Pb^{2+} from water. We looked into the ideal pH, adsorption capacity, and equilibrium parameters. The present study's results unequivocally indicate that hematite nanocrystals can be an affordable and practical material for recovering heavy metal ions from wastewater.

Synthesis of Fe2O3 MNPs: Fe2O3 nanoparticles were synthesized by simple co- precipitation procedure as follows: solution A contains 10 g of FeCl3.4H2O was dissolved in 150 ml of pure water and left under stirred at room temperature for ten minutes, Solution B included ammonium hydroxide, this solution was added drop wise to solution A under continuous stirred for one hours and left at room temperature about thirty minutes , finally the brown powder precipitate was formed, the product was filtered, washed several times by deionized water and dried in oven at 90 °C for 6 hours

2. Results and discussions

2.1. Grain size analysis of Fe3O4 and Fe2O3 by Scanning electron microscopy(SEM).

The nonhomogeneous outer surface characteristics of agglomerated plates with a cubic-like shape as a result of particle magnetostatic interactions and humidity are depicted in the images of Fe2O3 Figure 1. In the SEM micrograph, numerous channels and grooves that provide a good adsorbent surface are

visible. For Fe2O3 nanoparticles falling within the nanoscale range, the mean particle size within the range was calculated to be 71 nm. following the collection of grain diameter statistical data using the Image-J Log Normal function as the best fit. Tables 1 displays the results.

Table 1. Statistical results of particle size distribution for the Fe_2O_3 sample fitted with Log-Normal function.

Sample			Mean (nm)	Standard deviation	Minimum (nm)	Median (nm)	Maximum (nm)
Fe_2O_3	70.958	4.195	61	71.4		81.2	

Figure 1. (Left Panel) The SEM Image and (right Panel) grain size analysis of Fe2O3

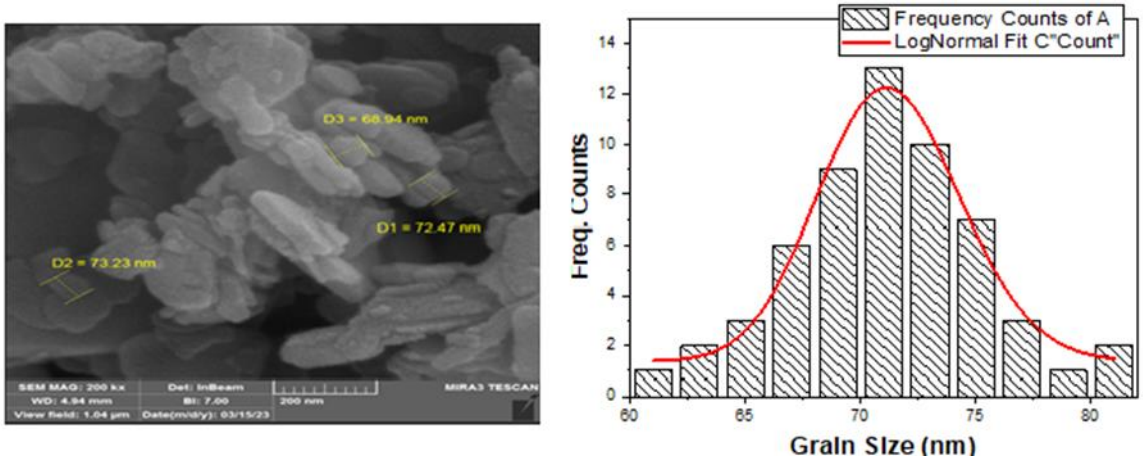

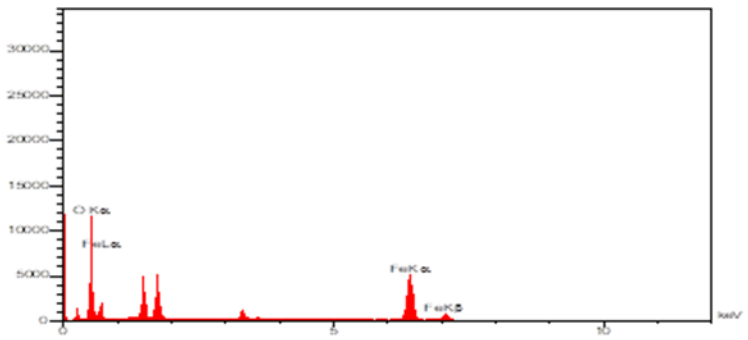

Figure 2. Energy dispersive X-ray analysis (EDX) spectrum of Fe2O3 nanoparticles

2.2. Energy dispersive X-ray analysis(EDX) for Fe_2O_3

Only the iron and oxygen ratio atoms, which indicate the prepared iron oxide's purity and are consistent with the prepared material's weigh ratio, were visible in the EDX result. The information was shown in Figure 2.

2.3 X-ray diffraction analysis for Fe_2O_3

Fe2O3 nanoparticles' XRD pattern revealed multiple peaks at the 2θ position (26.73°, 33.27°, 35.74°, 36.68°, 40.99°, 54.19°, and 62.52°), with corresponding FWHM values of approximately 0.1726, 0.3023, 0.5421, 0.1842, 0.1692, 0.3239, and 0.2835 2θ. The results are consistent with earlier research [13, 14], which validates the iron oxide Fe2O3 compound that was prepared. Using the Debye-Sherrer equation, the average crystal size was determined to be 48.17 nm. Fig. 3 displays the X-ray diffraction pattern.

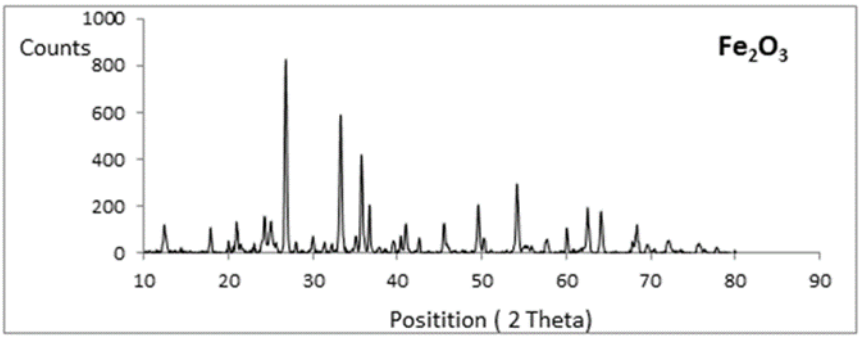

Figure 3. The X-ray diffraction pattern of Fe2O3 nanoparticles

1.4 Détermination of Zeta potentiel for Fe2O3

The aqueous solution of iron oxide (Fe2O3) shows instability and a negative surface charge. At -13.4 mV, the mean zeta potential was measured. Figure 4 displays the results of the zeta potential.

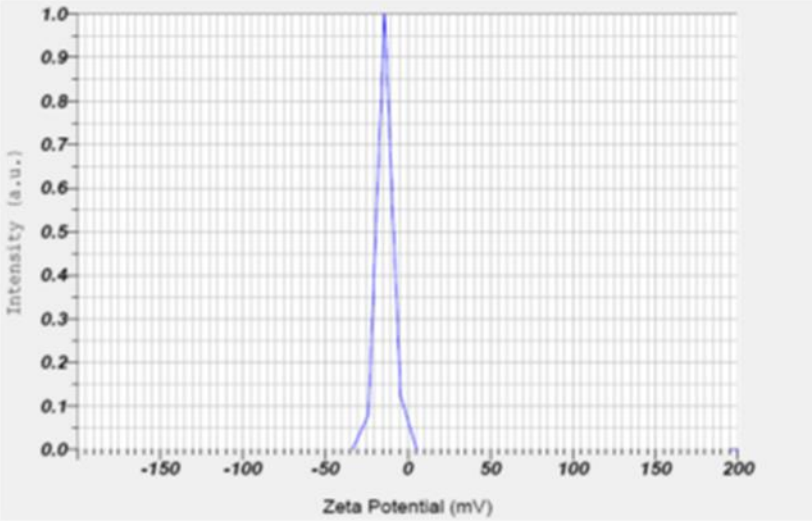

Figure 4. Zeta potential diagram of Fe2O3 nanoparticles

2.5 Surface area and porosity analyses

The functional groups and pore structures on an adsorbent surface essentially determine its adsorption efficiency [15]. However, there are three categories of structural pores: macro, mesoporous, and micro pores [16]. Many techniques, including Barrett Joyner Halenda (BJH), Brunauer Emmett Teller (BET), T-Plot, and Langmuir, are used to determine a material's surface value. These techniques involve the occupation of all active sites on the material's outer surface by inert gases, such as nitrogen, and a temperature of 77 K, at which the molecules of the inert gas are formed [16]. For adsorbent surfaces, the BET and BJH methods were utilized to determine the pore structure type and surface area. Fe2O3 nanoparticle results showed a surface area of 2.93 m2/g and an apparent pore diameter of 7.98 nm. Given its larger surface area compared to the other oxides, Fe3O4 might be a more effective adsorbent for eliminating heavy metal contamination from aqueous solutions. Although the iron oxide Fe2O3 had the lowest surface area value when compared to the other oxide adsorbents, the agglomeration process may occasionally be to blame for the surface area decline. When compared to iron and zinc oxide, titanium oxide also demonstrated a good surface area value; therefore, the chosen synthesis method was regarded to be a significant factor in the material's preparation. Table 2 presents the results of the mesoporous category, where the pore structures of all the adsorbents were found.

Table 2. Surface area and porosity analyses for nanoparticles

Nanoparticles	Surface area (m^2/g)	Pore structure type (nm)
Fe_3O_4	35.89	Mesopores

2.6 Treatment processes

3. Toxic heavy metals, which are introduced into the environmental system through a variety of pathways and pose numerous risks to human health and ecology, particularly through the food chain, must be removed from an aqueous solution [17]. In the current study, we used simulated polluted water by using a water sampler instrument to collect three real samples from Shatt Al-Arab sub-channels, such as Al-Rebat, Al-Ashar, and Al-khora, at a depth of 15 cm on surface water. The samples that were gathered are regarded as waste water because a variety of contaminants, including home and industrial waste, are discharged into the channel without any kind of treatment. In order to achieve the highest removal ratio possible using four nano adsorbent surface Fe2O3 nanostructure, the samples were first contaminated by using stock solutions for four metals: lead, cadmium, copper, and zinc. The samples were then further contaminated by choosing the optimal conditions for contact time, temperature, and acidic function.

4. 2.7 Selecting the affecting parameters on the adsorption efficiency

5. Numerous factors can influence the adsorption process and change the percentage of pollutants removed, either positively or negatively. This chapter examined the removal of various contaminants, including zinc, lead, cadmium, and copper, from their aqueous solutions by identifying the ideal parameters for contact time, temperature, and pH.

6. 2.8 Effect of contact time

7. Under certain fixed parameters, such as concentration of approximately 10 ppm for each heavy metals solution, mixing speed of 120 rpm, volume of 10 ml of the heavy metals solution, and amount of 50 mg of nanoadsorbent under the solution's natural pH, the equilibrium time between the contaminated solution and the solid phase was studied for a duration ranging from 5min to 120 min. The following relation can be used to calculate the removal percentage of heavy metals from four nano adsorbent surfaces [18]:

8. $\%R = [(Co - Ce) / Co] \times 100$

9. Where $Co, Ce,$ are in unit of mg/l, are the initial and residual concentrations of the heavy metals solution, respectively. Following the use of four elements—zinc, lead, cadmium, and copper—to contaminate three actual waste water samples, these elements were removed using four nanoadsorbent surfaces, such as iron oxides (Fe2O3). The findings indicate that, following the removal of four heavy metals from the zinc oxide surface, the contact time required to extract zinc ions from the solution ranged from 15 to 30 minutes, with the AlKhora and AlAshar stations recording the shortest contact times. In contrast, the AlRebat station recorded the longest contact times, which could be explained by the presence of a naturally occurring active site on the zinc oxide surface and competition between zinc ions and other ions in the solution for occupancy of the vacant active site. Due to the obvious of salt content in this station solution, Al-Khora station showed a high removal percent of 88.3%, while Al-Rebat station showed a low removal percent of 25.2% [19]. Table 3 contains a list of the data.

10. In addition, a short time was recorded in the Al-Ashar station while a high removal percent was recorded in the Al-Rebat station. Iron oxide Fe2O3 nanoparticles were utilized as the adsorbent surface for the removal of four heavy metals. The adsorption ratio was calculated as a time function and it recorded a high ratio to remove zinc ions from aqueous solution at contact times of 30 and 60min. More so than the other stations, the Al-Rebat station has observed that lead ions have the shortest contact time and the highest removal ratio when iron oxide Fe2O3 nanoparticles are used as the adsorbent surface. For the purpose of adsorbing cadmium ions, a low removal percent onto Fe2O3 was observed.

11. Three polluted stations recorded the same contact time, with Al-Khora station recording a higher ratio than the other two stations. For the purpose of eliminating copper ions by iron oxide Fe2O3 surface, Al-Ashar and Al-Rebat stations recorded a short contact time of 30 minutes, whereas Al-Kkhora station recorded a long contact time. However, Al-Ashar station recorded a higher removal ratio than the other stations, at 92.79Due to the presence of channels and grooves on the outside of Fe2O3, as well as a strong binding between the adsorbent surface and lead and copper ions, lead and copper ions were found to have the highest removal percentage onto Fe2O3. The contact time effect results for copper, zinc, lead, and cadmium that adsorbed onto the Fe2O3 surface are shown in Table 3.

Table 3. Effect of contact time for Removal of some heavy metals onto Fe_2O_3

Station	Contact time (min)	Zinc	Lead	Cadmium	Copper
		C_e ppm (%R)	C_e ppm (%R)	C_e ppm (%R)	C_e ppm (%R)
Al-Khora	5	2.3312 (76.68)	1.0547 (89.45)	9.4941 (5.05)	2.4586 (75.41)
	15	2.3124 (76.87)	0.9698 (90.30)	8.4859 (15.14)	2.2083 (77.91)
	30	2.2029 (77.97)	0.8677 (91.32)	7.7712 (22.28)	2.0941 (79.05)
	60	1.6425 (83.57)	0.8091 (91.90)	7.2015 (27.98)	1.6292 (83.70)
	120	1.3139	0.6511	7.1670	1.3277

		(86.86)	(93.48)	(28.33)	(86.72)
Al-Ashar	5	1.4787 (85.21)	1.0309 (89.69)	9.0049 (9.95)	0.8918 (91.08)
	15	1.4278 (85.72)	0.7470 (92.53)	8.0315 (19.68)	0.8204 (91.79)
	30	1.3379 (86.62)	0.6875 (93.12)	7.7236 (22.76)	0.7204 (92.79)
	60	1.2126 (87.87)	0.6311 (93.68)	7.4196 (25.80)	0.6079 (93.92)
	120	1.1345 (88.65)	0.6311 (93.68)	7.3932 (26.06)	0.5548 (94.45)
Al-Rebat	5	2.2981 (77.01)	0.4718 (95.28)	9.4491 (5.50)	3.8119 (61.88)
	15	2.1697 (78.30)	0.4014 (95.98)	9.0929 (9.07)	3.4191 (65.80)
	30	2.0427 (79.57)	0.3679 (96.32)	8.7977 (12.02)	3.0164 (69.83)
	60	1.1115 (88.88)	0.3581 (96.41)	8.5811 (14.18)	2.9945 (70.05)
	120	1.0352 (89.64)	0.3438 (96.56)	8.4833 (15.16)	2.9730 (70.27)

2.10 Effect of temperature

All stations recorded the closed values for the removal percentage of zinc ions from the ferric oxide surface; however, the percentage varied depending on the temperature, with Al-Rebat recording the highest percentage at 30 ºC and Al-Ashar recording the second-highest percentage at 50 ºC. An increase in the percentage of zinc ions removed from ferric oxide at a higher temperature could indicate the formation of chemical adsorption between the two. At the lowest temperature of 40 ºC, Al-Rebat polluted station recorded the highest removal percent of lead ions using iron oxide nanoparticles, 97.06%. This was followed by Al-Ashar station at 40 ºC, 94.74%, and Al-Khora station at 20 ºC, 94.26%. An increase in the removal percentage could be caused by the salts in the collected waste water. The ions of cadmium and copper had the highest removal values in Al-Ashar station compared with all stations at low temperatures of 20 and 30 ºC respectively, while Al-Rebat and Al-khora station recoded a low removal values.

For cadmium ions onto ferric oxide at 30 ºC, compared to other ions. Additionally, the following is the order of the percentage of copper ions removed from all stations onto the ferric oxide surface: At low temperatures, Al-Ashar > Al-Khora > Al-Rebat, which could be caused by ion competition and the surface morphology of iron oxide. Table 4 lists every outcome of the removal percentage for copper, zinc, lead, and cadmium ions onto Fe2O3 nanoparticles.

Table 4. Effect of temperature for Removal of some heavy metals onto Fe_3O_4

Station	Temperature (ºC)	Zinc	Lead	Cadmium	Copper
		C_e ppm (%R)	C_e ppm (%R)	C_e ppm (%R)	C_e ppm (%R)
Al-Khora	20	0.6 (94)	0.601368 (93.98)	0.912858 (90.87)	0.63756 (93.62)
	30	0.6 (94)	0.61146 (93.88)	0.91856 (90.81)	0.797274 (92.02)
	40	0.6 (94)	0.608397 (93.91)	1.164952 (88.35)	0.769503 (92.30)
	50	0.6 (94)	0.612312 (93.87)	1.065942 (89.34)	0.819336 (91.80)

Al-Ashar	20	0.6 (94)	0.604617 (93.95)	1.086479 (89.13)	0.657011 (93.42)
	30	0.6 (94)	0.60725 (93.92)	0.891647 (91.08)	0.709819 (92.90)
	40	0.6 (94)	0.604405 (93.95)	1.133094 (88.66)	0.700133 (92.99)
	50	0.6 (94)	0.607985 (93.92)	1.243881 (87.56)	0.741119 (92.58)
Al-Rebat	20	0.6 (94)	0.6 (94)	1.011232 (89.88)	0.662714 (93.37)
	30	0.6 (94)	0.604968 (93.95)	0.921504 (90.78)	0.674442 (93.25)
	40	0.6 (94)	0.603558 (93.96)	1.498761 (85.01)	0.761095 (92.38)
	50	0.6 (94)	0.604857 (93.95)	1.070433 (89.29)	0.702227 (92.97)

2.11 Effect of pH

One of the key elements influencing adsorption efficiency is the acidic function, which increases the removal of certain pollutants by causing a change in charge between the heavy metal ions and the outer surface of the adsorbent [20]. The zeta potential analyses of the four adsorbent surfaces used in this study indicate that they are all negatively charged, with the exception of the zinc oxide surface, which has a positively charged outer surface. The removal percentage was chosen using three solutions with varying pH values (3, 6, and 9).

At pH 9, the stations of Al-Rebat and Al-Khora recorded the highest values, 99.79 and 99.67%, respectively, for the removal of zinc ions from an aqueous solution using iron oxide Fe2O3 as an

adsorbent surface. Although the pH levels at stations 3 and 6 were recorded, the removal percentage convergence across all stations fell between 82.05 and 86.16%.

The best adsorption value for removing lead ions onto Fe2O3 surface was found at pH level 6, and Al-Rebat had the highest removal percentage (100%)—possibly because there was less competition for lead ions' active sites on the outer adsorbent surface from salts.

The behavior of the Fe2O3 surface in eliminating cadmium ions is similar to that of the TiO2 surface, where the removal percentage in the Al-Rebat station reached its highest value of 78.92% when the basic medium was increased. In addition, the ideal pH ranges for adsorbing copper ions increase as the hydrogen concentration levels decrease toward the basic medium, with Al-Rebat having the lowest hydrogen concentration level (98.43%) compared to the other stations. Table 5 lists every outcome of the removal percentage for copper, zinc, lead, and cadmium ions onto Fe2O3 nanoparticles.

Table 5. Effect of the pH level for Removal of some heavy metals onto Fe_2O_3

Station	pH	Zinc	Lead	Cadmium	Copper
		C_e ppm (%R)	C_e ppm (%R)	C_e ppm (%R)	C_e ppm (%R)
Al-Khora	3	1.754694 (82.45)	6.85342 (31.46)	2.368125 (76.31)	2.63263 (73.67)
	6	1.594886 (84.05)	0.534202 (94.65)	2.396226 (76.03)	2.40445 (75.95)
	9	0.032761 (99.67)	0 (100)	2.227619 (77.72)	0.173987 (98.26)
Al-Ashar	3	1.790651 (82.09)	6.495114 (35.04)	2.360096 (76.39)	6.078152 (39.21)
	6	1.518977 (84.81)	0.143322 (98.56)	2.340024 (76.59)	2.296064 (77.03)
	9	0.524171	0	2.275793	0.362236

		(94.75)	(100)	(77.24)	(96.37)
Al-Rebat	3	1.746704 (82.53)	7.407166 (25.92)	2.380169 (76.19)	2.621221 (73.78)
	6	1.38314 (86.16)	0 (100)	2.327981 (76.72)	2.102111 (78.97)
	9	0.020775 (99.79)	0 (100)	2.107186 (78.92)	0.156874 (98.43)

Conclusions

In conclusion, Fe2O3 nanocrystals were successfully prepared using a straightforward co-precipitation technique. Heavy metal removal from wastewater was tested using the synthetic sample. The adsorption activities of Fe2O3 nanocrystals towards heavy metal ions were investigated under various experimental conditions. In the process of heavy metal ion adsorption, pH was crucial. Cu^{2+}, Zn^{2+}, Cd^{2+} , and Pb^{2+} ion removal were studied different temperature, contact time, and at pH 3, 6, and 9. Adsorption is a physico-chemical process that significantly influences the electrostatic attractions between heavy metal ions and Fe2O3 nanocrystals. The findings demonstrate that as contact time and initial metal ion concentration increased, so did the capacity of heavy metal ions. The monolayer adsorption of the metal ions under study onto the surface of Fe2O3 nanocrystals was confirmed by the higher linear regression coefficient values of the Langmuir adsorption isotherm model, which fit the data better than the Freundlich model. The . Cu^{2+}, Zn^{2+}, Cd^{2+} , and Pb^{2+} ions showed Langmuir reasonable adsorption capacities. As demonstrated by the current study's results, Fe2O3 nanocrystals are effective adsorbents for removing heavy metal ions from wastewater.

Acknowledgements The author thanks Dr. Hashim Jabbar from Department of Physics, College of Science, University of Basrah for his kind assistance.

Disclaimer: None

Conflict of interest: There are no conflicts of interest to declare.

Funding disclosure: Funded by University of Basrah.

References

[1] Kafia M. Shareef Surchi, Agricultural Wastes as Low Cost Adsorbents for Pb Removal: Kinetics, Equilibrium and Thermodynamics, International Journal of Chemistry, Vol. 3, No. 3 (2011).
[2] Rozada F, Otero M, Morán A, García AI. Adsorption of heavy metals onto sewage sludge-derived materials. Bioresour Technol. 2008 Sep;99(14):6332-8.
[3] Yingchao Li, Hua Yin, Yuhao Cai, Haoyu Luo, Caiya Yan, Zhi Dang, Regulating the exposed crystal facets of α-Fe2O3 to promote Fe2O3-modified biochar performance in heavy metals adsorption, Chemosphere, Volume 311, Part 1, 2023.
[4] Bagbi Y, Sarswat A, Mohan D, Pandey A, Solanki PR. Lead and Chromium Adsorption from Water using L-Cysteine Functionalized Magnetite (Fe3O4) Nanoparticles. Sci Rep. 2017 Aug 9;7(1):7672.
[5] B. Tripathy, A. Dash, A.P. Das, Detection of environmental microfiber pollutants through vibrational spectroscopic techniques: recent advances of environmental monitoring and future prospects, Crit. Rev. Anal. Chem., 1–11 (2022).
[6] M.A. Ahmed, S.M. Ali, S.I. El-Dek, A. Galal,, Magnetite–hematite nanoparticles prepared by green methods for heavy metal ions removal from water, Materials Science and Engineering: B, Volume 178, Issue 10, 2013.
[7] A.A. Abdelhafez , Feasibility of biochar manufactured from organic wastes on the stabilization of heavy metals in a metal smelter contaminated soil Chemosphere (2014).
[8] M.R. Abraham et al. Water contamination with heavy metals and trace elements from Kilembe copper mine and tailing sites in Western Uganda; implications for domestic water quality, Chemosphere (2017).
[9] Grzegorz Izydorczyk, Katarzyna Mikula, Dawid Skrzypczak, Konstantinos Moustakas, Anna Witek-Krowiak, Katarzyna Chojnacka, Potential environmental pollution from copper metallurgy and methods of management, Environmental Research, Volume 197, 2021.
[10] Elouear Z, Bouzid J, Boujelben N, Feki M, Jamoussi F, Montiel A. Heavy metal removal from aqueous solutions by activated phosphate rock. J Hazard Mater. 2008 Aug
[11] Wenjun Jiang, Miguel Pelaez, Dionysios D. Dionysiou, Mohammad H. Entezari, Dimitra Tsoutsou, Kevin O'Shea, Chromium(VI) removal by maghemite nanoparticles, Chemical Engineering Journal, Volume 222, 2013.
[12] Hassan Karami, Heavy metal removal from water by magnetite nanorods, Chemical Engineering Journal, Volume 219, 2013
[13] Rabindra Bhowmik, A. Saravanan, Surface magnetism, Morin transition, and magnetic dynamics in antiferromagnetic α-Fe2O3 (hematite) nanograins, JOURNAL OF APPLIED PHYSICS 107, 053916 2010
[14] Zhong Liu, Baoliang Lv, Dong Wu, Yuhan Sun, Yao Xu, Magnetic and electrochemical behavior of rhombohedral α-Fe2O3 nanoparticles with (104) dominant facets, Particuology, Volume 11, Issue 3, 2013.
[15] Mizhir AA, Abdulwahid A A, Al-Lami H S. Adsorption of carcinogenic dye Congo red onto prepared graphene oxide-based Composites, Des. Wat. Treat.2020; 202: 381–395.

[16] Abdulnabi Z A. Synthesis and Characterization of some Selenazone Complexes and Nanoadsorbent Surfaces from Industrial Waste for Removing some Carcinogenic Dyes and Heavy Metals from Water, PhD. Thesis .2021; University of Basra.
[17] Mamta Pujari, Dhriti Kapoor, Heavy metals in the ecosystem: Sources and their effects, Heavy Metals in the Environment, Elsevier, 2021.
[18] Zaimee, M.Z.A.; Sarjadi, M.S.; Rahman, M.L. Heavy Metals Removal from Water by Efficient Adsorbents. Water 2021, 13, 2659.
[19] Staszak, K.; Regel-Rosocka, M. Removing Heavy Metals: Cutting-Edge Strategies and Advancements in Biosorption Technology. Materials 2024.
[20] Mirea, Cristina & Diaconu, Ioana & Ruse, Elena & Serban, Ecaterina Anca & Clej, Dumitra & Popa, George & Nechifor, Gheorghe. (2016). THE REMOVAL OF HEAVY METALS USING THE BULK LIQUID MEMBRANE TECHNIQUE.. Progress of Cryogenics & Isotopes Separation. 19. 45-54.

Thermoelectric properties of zintl phase antimonite compounds, $Eu_{0.6}Yb_{0.4}Zn_2Sb_2$, $YbCd_{1.6}Zn_{0.4}Sb_2$, $YbZn_{1.6}Mn_{0.4}Sb_2$ prepared by microwave-assisted solid-state technique

IBRAHIM MAJEED JASIM*, A. HMOOD

Physics Department, College of Science, University of Basrah, Basrah, Iraq.
*Corresponding author: *E-mail address*: ibraheem.m.jasim1982@gmail.com

Abstract

In a relatively short duration (10 minutes) under a microwave irradiation method prepared the chemical Zintl compounds $Eu_{0.6}Yb_{0.4}Zn_2Sb_2$, $YbCd_{1.6}Zn_{0.4}Sb_2$, $YbZn_{1.6}Mn_{0.4}Sb_2$ by using an active carbon as a susceptor material. These samples were then analyzed by the XRD, SEM . The XRD revealed that the compounds crystallized in the hexagonal structure where ZnSb precipitated as a secondary phase in almost all the compounds. Thermoelectric characterizations have been performed for three obtained samples a maximum power factor of 2.62 $\mu W/cmK^2$ at 523K was noticed for $Eu_{0.6}Yb_{0.4}Zn_2Sb_2$ sample with carrier concentration of 5.11×10^{21} cm^{-3} at 300K. And the compound $YbCd_{1.6}Zn_{0.4}Sb_2$ is found the power factor of 8.20 $\mu Wcm^{-1}k^{-2}$ at 523K with carrier concentration of

3.04× 10^{21} cm^{-3} at 300K. The compound $YbZn_{1.6}Mn_{0.4}Sb_2$ the power factor of 1.78 µW/cm k^2 at 523 K with carrier concentration of 4.8 × 10^{21} cm^{-3} at 300 K.

Keywords: microwave irradiation, zintl phase, active carbon, power factor

1. Introduction

Thermoelectricity refers to a phenomenon of thermal and electrical energies can be converted to each other under varied temperatures and different voltages [1-4]. According to the current development in the industrial material fields, ingots have emerged associated with much attention due to their use in many thermal and electrical applications[5]. High thermoelectric figure of merit $ZT=(S^2\sigma/k)T$, where S, σ , K, and T are Seebeck coefficient, electrical conductivity, thermal conductivity, and absolute temperature, respectively [6-9]. The power factor ($S^2\sigma$) is considered as the most important part in the study of thermoelectric materials (TEMs). To reach the high value in the figure of merit (ZT), higher value of power factor and lower thermal conductivity are required [10]. Zintl phase compounds have been prepared by direct solid state technique and found taking a long time under heating for example: $YbZn_{2-x}Mn_xSb_2$ was synthesized at 1323k for 30h[11] ,$Ca_{16}Sb_{11}$ was synthesized at 1423k for several hours [12], $YbCd_{2-x}Mg_xSb_2$ at 1273k for 72h [13], $Ca_{1-x}Yb_xZn_2Sb_2$ at 1273k for 48h[14], $YbZn_2Sb_2$ at 1323k for 30h[15], $SrZn_2Sb_2$ at 1073k for 5days[16]. $Ca_{1-x}Eu_xZn_2Sb_2$ at 1273k for 3 days[17], $Yb_xEu_{1-x}Cd_2Sb_2$ at 1200 °C for 24 h[18]. While in our work the Zintl compounds $Eu_{0.6}Yb_{0.4}Zn_2Sb_2$, $YbCd_{1.6}Zn_{0.4}Sb_2$, $YbZn_{1.6}Mn_{0.4}Sb_2$ are synthesized in short time 10 mins under a microwave-assisted solid state. Microwave irradiation is an efficient method employed to prepare the thermoelectric materials in short time. In comparison with bulk samples, metal powders can feasibly couple under microwave fields at 2.45 GHz and heating reach to 1273 K without causing visible electric discharges[19]. The Zintl phase families like 1-2-2-family which includes $EuZn_2Sb_2$,$YbZn_2Sb_2$, $YbCd_2Sb_2$, $YbMn_2Sb_2$ are considered as important TEMs[11,13,17]. The Zintl compounds crystal structure consist of layered structures with a triangle lattice formed by cation vacancies A^{+2} between two dimensional $(B_2Sb_2)^{-2}$ network is covalently bounded slabs separated by cationic layers [20]. Importantly, a microwave-assisted solid state provides high energy, easy work up and eco-friendly methodology than other traditional techniques[21].

2. Experimental

The rapid microwave synthesis was used to prepare the Zintl phase antimonite compounds from pure elements (Eu, Yb, Zn, Cd, Mn and Sb > 99.99%) semiconductor compounds were weighted 2 g according to the stoichiometric $Eu_{0.6}Yb_{0.4}Zn_2Sb_2$, $YbCd_{1.6}Zn_{0.4}Sb_2$, $YbZn_{1.6}Mn_{0.4}Sb_2$. The powder is mixing into an agate mortar and pestle to create a homogenous mixture for 20 mins, and put it inside a clean quartz ampoule and sealed under high vacuum of 10^{-5} mbar. The ampoule was irradiated with a maximum power of 1000W microwave oven (LG) (MS2147C 1000 W) at 2.45 GHz. An ctive carbon (susceptor) was surrounded the quartz ampoule to absorb microwave irradiation and initiate heating

under a microwave-assisted solid state synthesis. The active carbon helps to raise reaction temperature to reach 1123K for 10 mins (2on:2off) as shown in Fig.1. The temperature of ampoule was measured using an infrared thermometer (S-CA-1168), temperature range 223-1123 K. The fusing materials were further cooled to room temperature to obtain ingot. The morphological, and stoichiometric ratio, structural and were measured . The polycrystalline selected portions of the ingots were imaged using field emission scanning electron microscopy (FESEM), after grinding, the powders were then measured to determine their crystal structure using X-ray diffraction (XRD, PANalytical X'Pert PRO MRD PW3040-Netherlands). The Seebeck coefficient (S) of polished disks was measured by the slope of the linear relationship between the thermoelectromotive force and the temperature difference between the two ends of each sample, more detail in previous report [22].The four-point probe method was using to measure the electrical conductivity (σ) in a vacuum at 10-3 mbar at a temperature range of 298K -523K. The carrier concentration (n) was determined at room temperature from the Hall voltage measurement with an applied magnetic field of 1 T using a PHYWE electromagnetic (model: 6480, Germany).

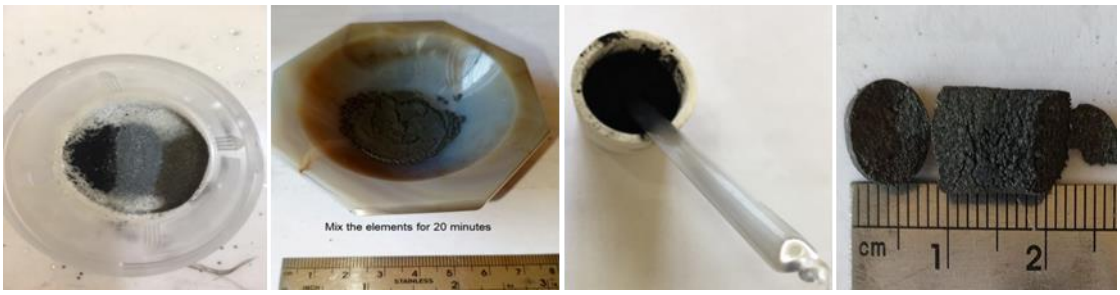

Fig.1: Synthesize the ingots of the compounds

3. Results and discussion

X-ray diffraction (XRD) of $Eu_{0.6}Yb_{0.4}Zn_2Sb_2$, $YbCd_{1.6}Zn_{0.4}Sb_2$, $YbZn_{1.6}Mn_{0.4}Sb_2$ are shown in fig.2. The XRD revealed that the compounds crystallized in the hexagonal structure where ZnSb precipitated as a secondary phase in compounds. The appearance of the secondary phase in the X-ray diffraction results of zintl compounds is consistentwith published works in this field[23].

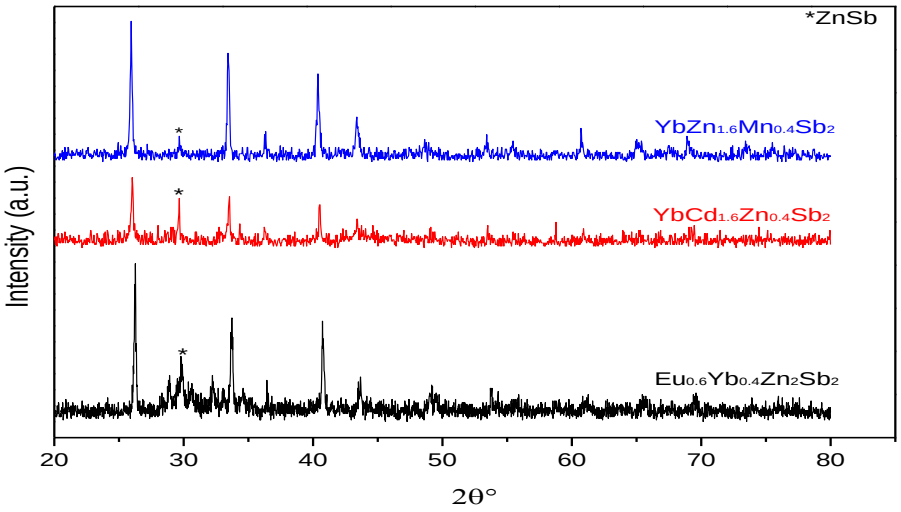

Fig.2: XRD patterns of $Eu_{0.6}Yb_{0.4}Zn_2Sb_2$, $YbCd_{1.6}Zn_{0.4}Sb_2$, $YbZn_{1.6}Mn_{0.4}Sb_2$

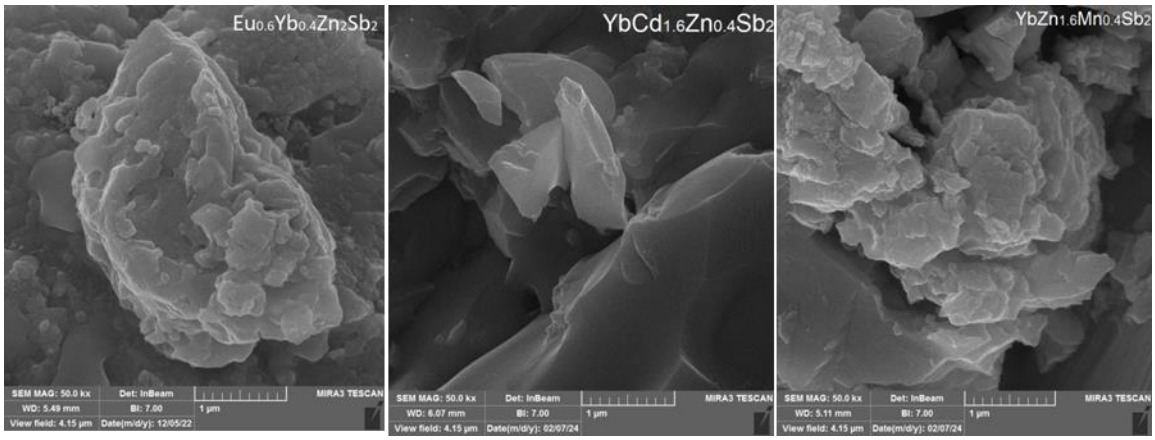

Fig.3: SEM image of $Eu_{0.6}Yb_{0.4}Zn_2Sb_2$, $YbCd_{1.6}Zn_{0.4}Sb_2$, $YbZn_{1.6}Mn_{0.4}Sb_2$

The electrical conductivity (σ) of the $YbCd_{1.6}Zn_{0.4}Sb_2$ decreased when the temperature was increased and this behavior was in agreement with degenerate semiconductor behavior of while the compounds $Eu_{0.6}Yb_{0.4}Zn_2Sb_2$, $YbZn_{1.6}Mn_{0.4}Sb_2$ have relatively little change as shown in Fig.4 .

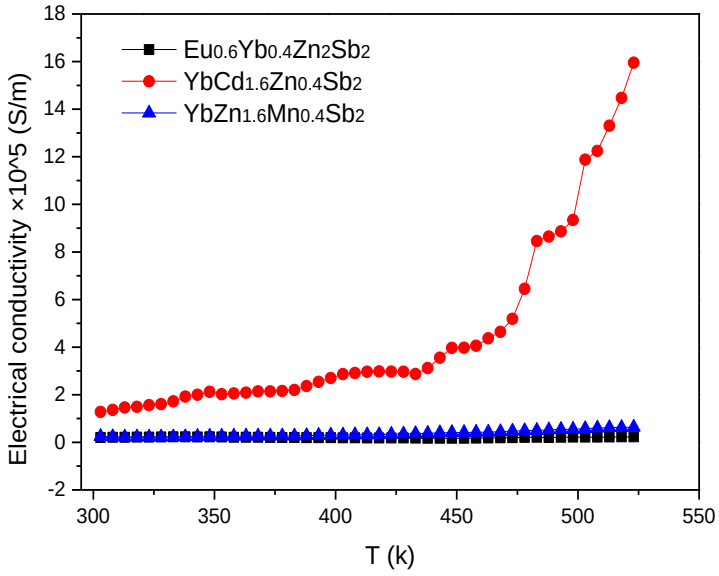

Fig.4 : Electrical conductivity (σ) of the $Eu_{0.6}Yb_{0.4}Zn_2Sb_2$, $YbCd_{1.6}Zn_{0.4}Sb_2$, $YbZn_{1.6}Mn_{0.4}Sb_2$

The Fig.5 shows the dependent temperature of the Seebeck coefficient for $YbCd_{1.6}Zn_{0.4}Sb_2$, $YbZn_{1.6}Mn_{0.4}Sb_2$. The measured values of Seebeck coefficient for are a negative value n-type conductivities which means that the majority of carriers are electrons, while the compound $Eu_{0.6}Yb_{0.4}Zn_2Sb_2$ is p-type as the holes which are represented the majority of carriers of electrical transports.

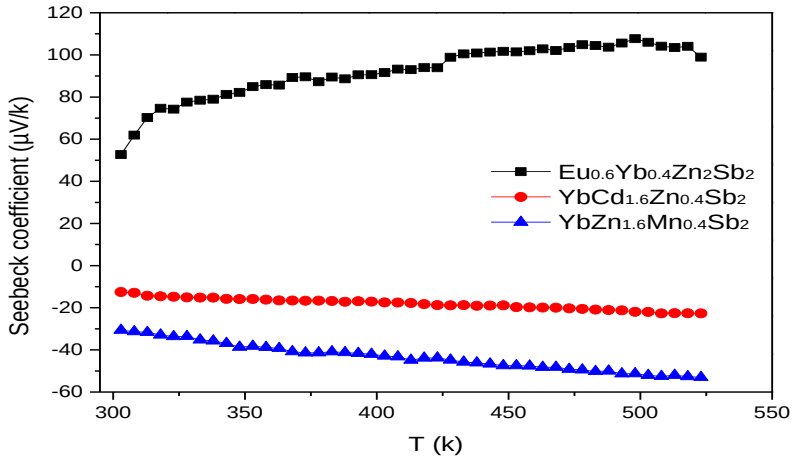

The dependent temperature of the power factor ($S^2\sigma$) of Zintl compounds the $Eu_{0.6}Yb_{0.4}Zn_2Sb_2$, $YbCd_{1.6}Zn_{0.4}Sb_2$, $YbZn_{1.6}Mn_{0.4}Sb_2$ that were prepared under microwave assisted solid state as shown in Fig.6. The high calculated value of power factor ($S^2\sigma$) for the prepared sample $Eu_{0.6}Yb_{0.4}Zn_2Sb_2$ was 2.62 µW/cmk^2 at 518 K .

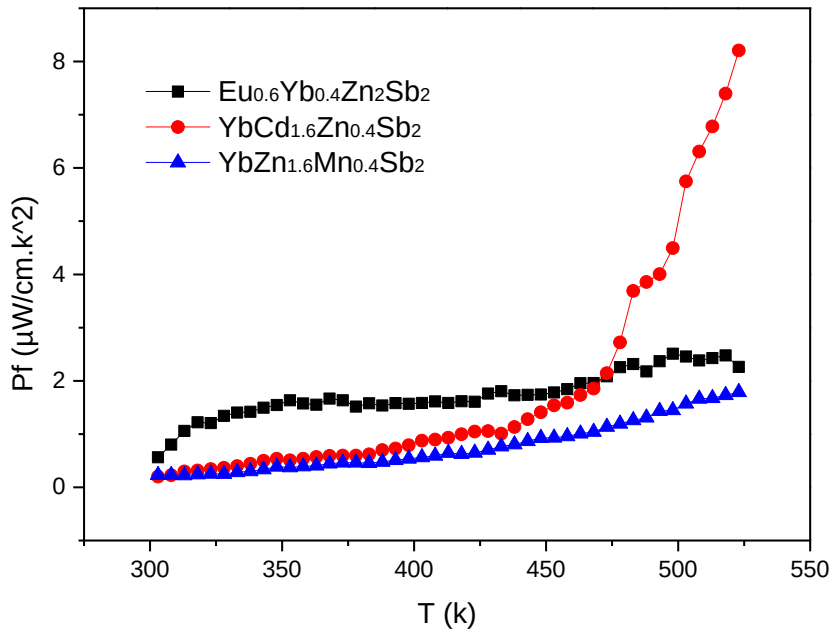

4. Conclusions

$Eu_{0.6}Yb_{0.4}Zn_2Sb_2$, $YbCd_{1.6}Zn_{0.4}Sb_2$, $YbZn_{1.6}Mn_{0.4}Sb_2$ are Zintl chemical compounds have been successfully produced using microwave assisted solid state at short time . The XRD analysis detects that prepared compounds has a hexagonal structure where ZnSb precipitated as a secondary phase in almost all the compounds. The $YbCd_{1.6}Zn_{0.4}Sb_2$ sample reveals moderate electrical conductivity and a higher Seebeck coefficient with maximum power factor of 8.20 µW/cmK^2 at 523 K.

Acknowledgements

The authors gratefully acknowledge support from department of Physics, College of Science, University of Basrah, Iraq.

Ethical Approval: The study protocol was approved by local ethics committee.
Disclaimer: None
Conflict of interest: There are no conflicts of interest to declare.
Funding disclosure: support by ourselves.

References

[1] G. S. Nolas et al., *Thermoelectrics Basic Principles and New Materials Developments*, (*Springer-Verlag Berlin Heidelberg New York*) 2001: p73

[2] L. Chen, R. Liu and X. Shi, *Thermoelectric Materials and Devices*, (*China Science Publishing & Media Ltd, Published by Elsevier Inc.*) 2021: p2

[3] Y. X. Gan, *Nanomaterials for Thermoelectric Devices* (*Pan Stanford Publishing Pte. Ltd*)2018: p. 3.

[4] W. He, G Zhang, X Zhang, J Ji, G Li and X Zhao, *Appl. Energy* **143** 1(2015)

[5] A. Hmood, A. Kadhim and H. Abu Hassan, *Superlattices and Microstructures*. **54** 204(2013)
[6] X. Du, R. Shi, Y. Ma, F. Cai, X. Wangc and Z. Yuanc, *RSC Adv.* **5** 31004 (2015)

[7] A. Kadhim, A. Hmood and H. Abu Hassan, *Mater. Lett.* **97** 24 (2013)

[8] M. W. Gaultois, T. D. Sparks, C. K. H. Borg, R . Seshadri, W.D. Bonificio and D. R . Clarke, *Chem. Mater.* **25** 2911(2013)

[9] A. Hmood, A. Kadhim and H. Abu Hassan, *Adv. Mater. Research* **501** 126 (2012)

[10] X. Zhang et al, *Chem. Eng.* **374** 589 (2019)
[11] T.J. ZHU, C. YU, J. HE, S.N. ZHANG, X.B. ZHAO, and TERRY M. TRITT, Thermoelectric Properties of Zintl Compound YbZn2Sb2 with Mn Substitution in Anionic Framework, J. ELE. MATER., 38(2009)1068-1071, DOI: 10.1007/s11664-009-0667-9.

[12] V. Ponnambalam , X . Gao, S. Lindsey, P. Alboni, Z. Su, B. Zhang, F. Drymiotis, M.S. Daw, T. M . Tritt, Thermoelectric properties and electronic structure calculations of low thermal conductivity Zintl phase series $M_{16}X_{11}$ (M = Ca and Yb; X = Sb and Bi), J. of Alloys and Compounds 484 (2009) 80–85. http://doi:10.1016/j.jallcom.2009.04.131.
[13] Q . Cao, J . Zheng , K . Zhang, G . Ma, Thermoelectric properties of $YbCd_2Sb_2$ doped by Mg , J. of Alloys and Compounds 680 (2016)278-282. http://dx.doi.org/10.1016/j.jallcom.2016.04.118.
[14] F. Gascoin, S. Ottensmann, D. Stark, M. S. Haile and G. Snyder, Zintl Phases as thermoelectric Materials Tuned transport properties of compounds $Ca_xYb_{1-x}Zn_2Sb_2$,J. Adv. Funct. Mater.15(2005)1860–1864. https://doi.org/10.1002/adfm.200500043.
[15] Xiong Zhang, Bin Zhang, Kun-ling Peng , Xing-chen Shen, Gui-tai Wu , Yan-ci Yan , Shi-jun Luo, Xu Lu, Guo-yu Wang, Hao-shuang Gu, Xiao-yuan Zhou, Spontaneously promoted carrier mobility and strengthened phonon scattering in p-type $YbZn_2Sb_2$ via a Nano compositing approach, J .Nano Energy 43(2018)159-167. https://doi.org/10.1016/j.nanoen.2017.11.019

[16] H . Zhang, M. Tang, W. Schnelle, M. Baitingerv, Z. Man ,H. Chen ,X. Yang, J. Zhao, Y. Grin, Thermoelectric Properties of Polycrystalline SrZn2Sb2 Prepared by Spark Plasma Sintering , J. Electron. Mater. 39 (2010)1772–1776. https://doi.org/10.1007/s11664-010-1151-2.

[17] T. A. Wubieneh, P. We, C. Yeh, S. Chen, Y. Yuan Chen , Thermoelectric Properties of Zintl Phase Compounds of $Ca_{1-x}Eu_xZn_2Sb_2$ $(0 \leq x \leq 1)$, J. Electron. Mater 45(2016)1942-1946. https://doi.org/10.1007/s11664-015-4303-6.

[18] H. Zhang, L. Fang, M.-B. Tang, Z. Y. Man, H. H. Chen, X. X. Yang, M. Baitinger, Y. Grin, and J.-T. Zhao, Thermoelectric properties of $Yb_xEu_{1-x}Cd_2Sb_2$, J. Chem. Phys. 133 (2010) 194701 http://dx.doi.org/10.1063/1.3501370.

[19] A. G. Whittakera , D. M. P. Mingos, Microwave-assisted Solid-state Reactions involving Metal Powders, J. Chem. Soc. Dalton Transaction(1995) 2073-2079 . https://doi.org/10.1039/DT9950002073.

[20] A. Zevalkink, W.G. Zeier, E. Cheng, G.J. Snyder, J.-P. Fleurial, S. Bux, Nonstoichiometry in the Zintl Phase $Yb_{1-\delta}Zn_2Sb_2$ as a Route to Thermoelectric Optimization, J. Chem. Mater. 26 (2014) 5710-5717. http://dx.doi.org/10.1021/cm502588r.

[21] A. Kadhim, A. Hmood, H. Abu Hassan, Physical properties of Bi2 (Te, Se)3 and Bi2Se1.2Te1.8 prepared using solid-state microwave synthesis ,J. Mater. Lett. 65 (2011) 3105–3108. http://dx.doi.org/10.1016/j.matlet.2011.06.069.

[22] Gorgory S. Pomrehn, Alex. Zevalkink, Wolfgang G. Zeier, Axel. van de Walle and G. Jeffrey Snyder, J. Ang. Chem. **126** 3490 (2014)

[22] A. Hmood, A. Kadhim and H. Abu Hassan, *Mater. Chem. and Phys.* **136** 1148(2012)

[23] Y. Takagiwa, Y. Sato , A. Zevalkink, I. Kanaza , K. Kimura , Y. Isoda , Y. Shinohara, Thermoelectric properties of $EuZn_2Sb_2$ Zintl compounds: ZT enhancement through Yb substitution for Eu , J. of Alloys and Compounds 703(2017)73-79. http://dx.doi.org/10.1016/j.jallcom.2017.01.350.

Computer scope

Classification of supervised deep learning models for Covid-19 tweets sentiment analysis

Rusul Mohammed alkhafaji[a] shaymaa awad kadhim[b],Humam Adnan Sameer[C],Doaa hadi abid muslim[d]

University of Kufa

ABSTRACT

Social media provided a successful management of human societies in light of global crises. Social media platforms have been considered the central authority in guiding society, receiving information and conducting business in many countries during the COVID-19 pandemic period in March 2020. The social platform has seen an increase in use of 45% for public platforms and 35% for the use of messages. This study suggests An AI-based model for predicting the likelihood of infection with COVID-19 through sentiment analysis and early detection using a Natural Language Processing library with deep learning techniques CNN. The model performed improved the distinction between patients who are 'positive' and patients who are 'natural' and unaffected are 'negative'. The performance of the model was tested using publicly available databases on Twitter for the period from March 16, 2020 to April 14, 2020.The achieved accuracy percentage was (~9%9.8)) and based on the four measures Accuracy, Recall, Precision and F1-score.
Keywords: Sentiment Classification ,Deep Learning ,Convolutional Neural Networks , COVID-19 , Natural language processing

1.Introduction

Deep learning models, specifically Convolutional Neural Networks (CNNs), have become effective tools for sentiment analysis tasks in recent years[1]. CNNs are particularly adept at learning spatial hierarchies of features, making them well-suited for processing sequential data such as text[2]. By combining CNN architectures with NLP methodologies, researchers can create robust sentiment classification models that accurately categorise COVID-19 tweets into positive, negative, or neutral sentiment classes[3]. This study aims to investigate the use of NLP and CNN techniques in sentiment analysis of COVID-19-related tweets on Twitter[4]. By examining sentiment patterns over time, geographic regions, and topical themes, we aim to uncover nuanced insights into public attitudes, emotions, and perceptions surrounding the pandemic[4].

The results of this study have the capacity to provide valuable insights for public health strategies, crisis communication initiatives, and social policy interventions that try to tackle the complex issues presented by the COVID-19 pandemic[8].

The Coronavirus (COVID-19) outbreak has not only emerged as a worldwide health disaster but also as a substantial social and psychological phenomenon, impacting people's behaviours, emotions, and perceptions on a global scale. Twitter and other social media platforms have become influential avenues for individuals to promptly share their ideas, concerns, and responses to the pandemic in the digital era[9].

Sentiment analysis, a subfield of natural language processing (NLP), provides a valuable method for comprehending and examining the emotions conveyed in COVID-19-related messages on Twitter[9]. Researchers can utilise NLP approaches to analyse large volumes of text data and gain valuable insights. This allows them to identify patterns, trends, and changes in public sentiment towards the

virus, government actions, healthcare measures, and social effects[10].
The subsequent sections of this study provide a detailed examination of the methodology, dataset, experimental setup, and results of our sentiment analysis. We emphasise the importance and consequences of utilizing natural language processing (NLP) and convolutional neural network (CNN) approaches to comprehend the changing public sentiment during the Coronavirus pandemic[11].
This analysis aims to elucidate the predominant emotion against COVID-19 on Twitter, offering significant insights for public health authorities, politicians, and researchers[14]. Analysing the changes in people's emotions can provide valuable insights for implementing specific actions, developing effective crisis communication plans, and implementing public health measures to address the social and psychological consequences of the pandemic[15].
The aim of the current study is to reach our findings as a contribution to the first understanding of analyzing individuals' feelings and anxiety during the Covid-19 crisis in order to develop a healthcare system that can effectively deal with human behavior and provide optimal guidance to society through social media platforms. Ensuring the safety of citizens by disseminating accurate information related to the pandemic, linking them with health authorities, and providing support and health updates.

2. Methodology

There are basic steps to be relied upon within the methodology of studying the introduction in this research and:
Collect the data set to train and test the deep learning model.
Preprocessing the dataset for post processing.
Convert text data to vector form using NLP.
Divide the data set into training and test groups.

3. NLP Techniques

Natural Language Processing (NLP) is type of function can be defined as a group of computational techniques that are characterized by their theoretical nature in automatic analysis and representation of human languages. NLP research has evolved from the age of punch cards and batch processing (with a sentence parsing time of about 7 minutes) to the age of Google and other platforms with millions of pages (which can be processed in less than a second).
The idea of this technique was created in the 1950s, and initial research in NLP focused on limited tasks such as machine translation, information extraction/retrieval, text summarization, answering questions, topic analysis, and modeling [16].
The majority of previous NLP implementations were hand-coded rule-based systems that were only able to perform some tasks related to natural language processing. The challenge came when these systems had to be expanded to account for the endless flow of exceptions or ever-increasing volumes of text and audio data.

Provides a statistical NLP, which automatically extracts, categorizes, and labels text and audio input items before each possible interpretation of these items is given a statistical probability. Convolutional Neural Networks (CNNs) and others are combined to create Natural Language Processing (NLP) systems that "learn" as they work and extract more precise meaning from massive amounts of unstructured text. Such as computer algorithms, machine and deep learning models as well as statistical NLP techniques and audio datasets that are not categorized or ordered. Natural language processing is the driving force behind machine intelligence in many modern real-world applications. Here are a few examples:

Spam detection, Machine translation, Virtual agents and chatbots, Social media sentiment analysis and Text summarization.

Most of the research at the time focused on syntax, due to the necessity of grammatical processing at that time and partly through implicit or explicit support for syntax-based processing despite the presence of semantic problems and NLP needs from the beginning [17].

More generally, NLP targets computer programs that translate text from one language to another, respond to spoken commands, and summarize large amounts of text quickly - even in real time. There are many examples now using this, such as voice-operated GPS systems, digital assistants, speech-to-text dictation software, chatbots for customer service, and other consumer conveniences. In business organizations, NLP provides solutions that help simplify critical business processes and increase employee productivity [17].

3.1. NLP tasks

Natural language generation is the process of converting structured data into human language; it is frequently referred to as the opposite of voice recognition or speech-to-text. Figure 1 shows Popular NLP Tasks

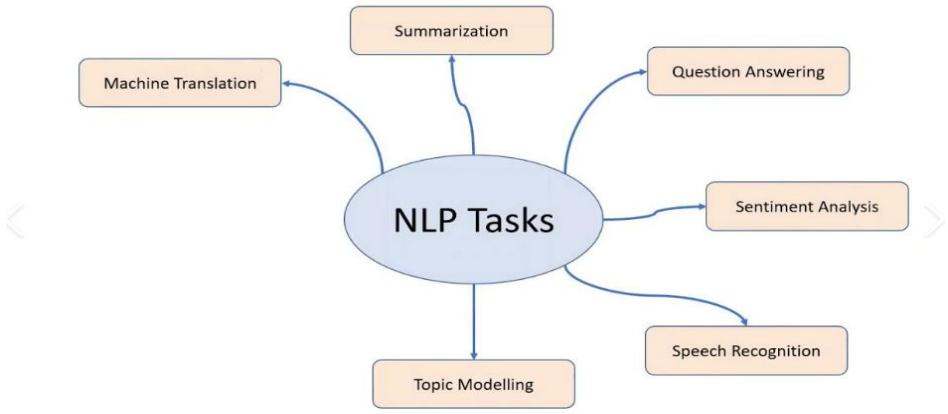

Figure 1 Popular NLP Tasks

4.Proposed System

The system proposed in this study consists of a set of steps for analyzing messages during the Covid-19 epidemic. Figure 2 represents the proposed flow chart for the system architecture. The dataset represents Twitter COVID-19. In order to initialize the data and facilitate the work of the advanced stages of the proposed system, texts are processed in the third stage and refers to the cleaning and preparation of tweets data for modeling. This stage includes: Remove all barriers, links and numbers, Remove Stop words (common words like "the", "a" etc.), Remove Retweets, HTML, Stemming, Tokenization. Then the coding stage begins (the third stage) The words are encoded and routed. Converting tweet words into numbers. In the fourth stage, the data is divided into two groups: training and testing. Extracting the model and training the neural network is the last stage of the proposed system.

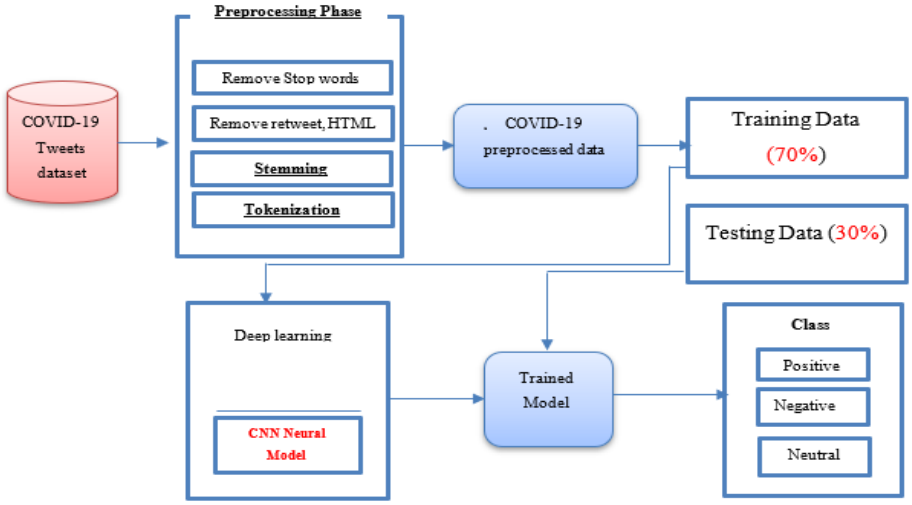

Figure 2 *The proposed system of deep learning*

4. Data Set Features and Description

The dataset used in this study can be found on kaggle, a machine/deep learning database. There are 129,570 samples distributed over two data sets. The training data set includes 118,174 entries, accounting for 70% of the total data. 12386 for testing at 30%. Table 1 shows a sample of the data set

London	16-03-2020	@MeNyrbie @Phil_Gahan @Chrisitv https://t.c…	Neutral
UK	16-03-2020	advice Talk to your neighbours family to ex…	Positive
Vagabonds	16-03-2020	Coronavirus Australia: Woolworths to give e…	Positive
nan	16-03-2020	PLEASE, don't panic, THERE WILL BE ENOUGH F… Stay calm, stay safe.	Positive
nan	16-03-2020	Not because I'm paranoid, but because my fo…	Negative
Ã T: 36.319708,-82.363649	16-03-2020	As news of the regionÂ s first confirmed COV…	Positive
35.926541,-78.753267	16-03-2020	Cashier at grocery store was sharing his in…	Positive
Austria	16-03-2020	was at the supermarket today. Didn't buy to… #toiletpapercrisis #covid 19 https://t.co/e	Neutral

Table 1*: Dataset sample and Features Description*

5.Preprocess Step

Numerous symbols (including !, #, @, and others), numbers, punctuation, and stop words are permitted in tweets. Stop words are described as words that lack emotion. like that, he, she, and he. Sentiment analysis is not appropriate for this set of data. So that it could be processed further, we cleaned the data by eliminating punctuation, numbers, and symbols, and changing all of the characters to lowercase. The stop words were then taken out of the list of tokens after dividing the tweet into tokens. The basic shapes of each tweet after cleaning and pre-processing are stored in a list called vocabulary. Table (2) provides an illustration of the reprocessing results.'

Table (2) Shows the Pre-processing of stop words and special characters

Tweet 1	#Delicious #Beef #Cheese #Burger @McDonald Testing CheeseBurger and Hamburger
After Pre-processing	[delicious, beef, cheese, burger, mcdonald, taste, cheeseburger, hamburger]
Tweet 2	#Late Service @McDonald Delicious Hamburger but slow service
After Pre-processing	[late, service, mcdonald, delicious, hamburger, slow]
Vocabulary	[delicious, beef, cheese, burger, mcdonald, taste, cheeseburger, hamburger, late, service, slow]

The text cleaning process was carried out in four stages shown in figure (3) and based on the NLTK library of NLP for Natural Language Processing. The NLTK (Natural Language Toolkit) library provides a set of libraries and software for statistical language processing. NLTK is one of the most powerful NLP libraries, having packages that make machines understand and respond to human languages with appropriate responses.

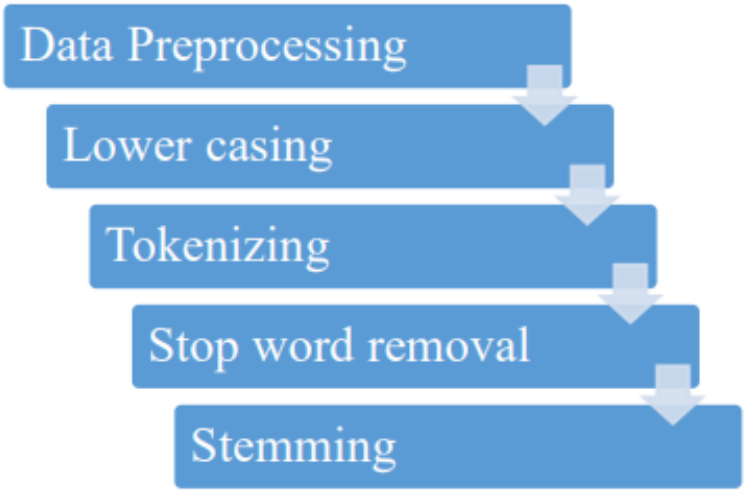

Figure(3): The steps in data pre-processing.

6.Evaluation Metrics

The last phase of this work is the three-evaluation metrics that have been used for experimental results.

1- Accuracy measure

Classification when we use the term accuracy, we typically imply accuracy. The number of correct predictions divided by the total number of input samples is the ratio. It is mandatory to calculate the confusion matrix which include True Positive (TP), True Negative (TN), False Positive (FP), False Negative (FN).

Accuracy = (TP+TB) / (TP+TN+FN+FP) …. (1)

2- Recall

It is calculated by dividing the number of accurate positive findings by the total number of relevant samples (all samples that should have been identified as positive).

$$recall = \frac{TP}{TP + FN} \quad \dots \quad (2)$$

3- Precision

It is the number of correct positive outcomes divided by the classifier's expected number of positive findings.

$$precsion = \frac{TP}{TP + FP} \quad \ldots \quad (3)$$

4- F1-score

The Harmonic Mean of accuracy and recall is the F1 Score. F1 Score has a range of [0, 1]. It informs you how exact and robust your classifier is (how many occasions it properly classifies). High precision but low

recall offers an extremely accurate result, but it also misses a huge number of occurrences that are difficult to classify. The higher the F1 Score, the better our model's performance.

$$F1 - Score = \frac{2 * precsion}{precsion + recall} \quad \ldots \quad (4)$$

Where,

TP : True Positive is the number of times the attack traffic was correctly classified.

FN : False Negative is the number of times attack packets was classified as normal packets.

FP : False Positive is the number of times the normal packets was classified as attack packets. From the confusion matrix, The following performance measures can be identified: Accuracy

7.RESULTS AND DISCUSSIO

In this section, we present the results of sentiment analysis for Twitter tweets using a hybrid approach combining Natural Language Processing (NLP) techniques and Convolutional Neural Networks (CNNs). The sentiment of tweets was classified into four categories: positive, negative, neutral.

We discuss the findings and implications of our analysis in understanding public sentiment dynamics amidst the Coronavirus (COVID-19) pandemic.

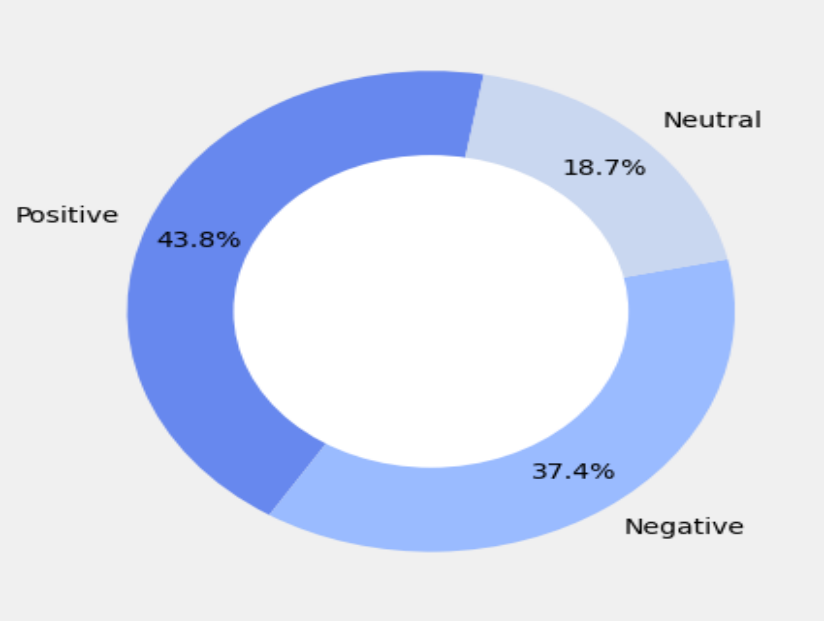

Figure (4) shows the structure of Twitter Covid-19 dataset

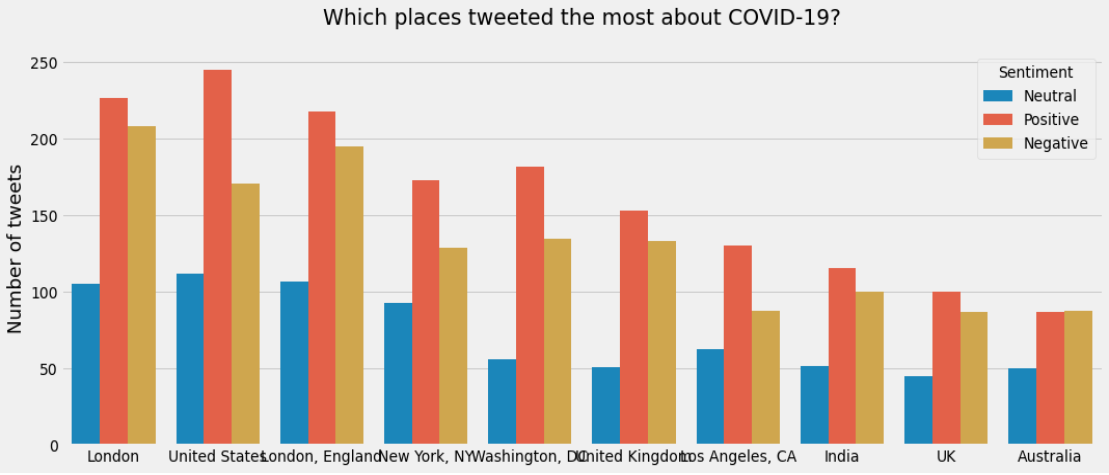

Figure (5) shows Twitter's COVID-19 sentiment classification by country geographic location

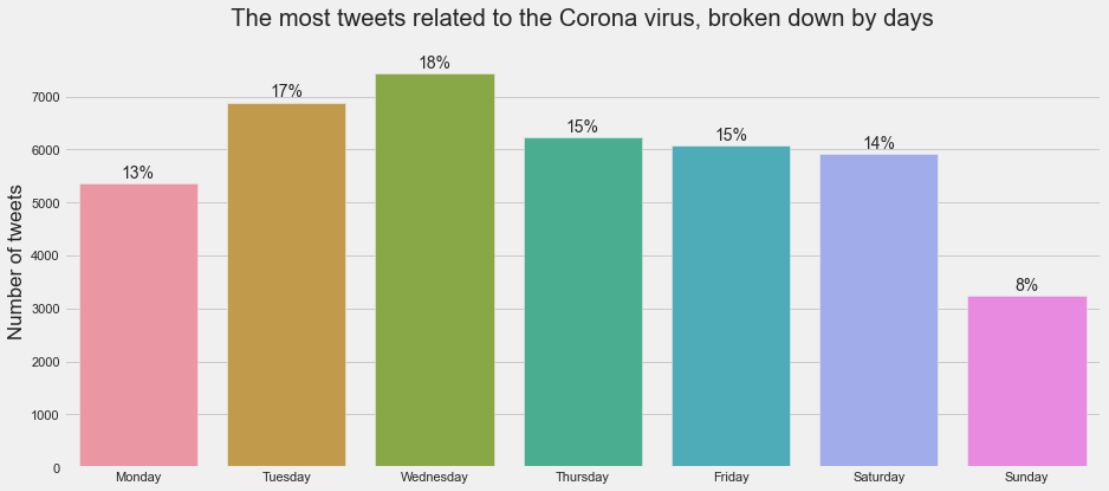

Figure (6)shows Twitter's COVID-19 sentiment classification by days of week

Figure (4) shows the percentage of Twitter analysis according to its status (normal, positive and negative). While the figure (5) and (6) shows the distribution of tweets classification according to geographical location and days.

8. Sentiment Classification Performance

The NLP and CNN-based sentiment analysis model achieved promising results in classifying the sentiment of COVID-19-related tweets. The model demonstrated high accuracy, precision, recall, and F1-score across all sentiment categories, indicating its robustness in capturing nuanced sentiment expressions in Twitter data.

The table (3) shows the behavior of deep learning algorithms on Twitter Covid-19 dataset by used the four scales (Accuracy, Precision,, Recall, F1 score) where the results showed the superiority of the CNN algorithm in performance efficiency and detection accuracy.

Figures (5,6) also show the behavior of the deep learning algorithms that have undergone training, where the training accuracy was compared with validation accuracy using random samples from the test samples.

Table (3).the performance of models on Twitter Covid-19 dataset

No,	Models name	Accuracy	Precision	Recall	F1 score:

2.	CONVOLUTIONAL Neural Networks (CNN)	99.80%	81.683%	87%	84%

The table (3) shows the behavior of deep learning algorithms on Twitter Covid-19 dataset by used the four scales (Accuracy, Precision,, Recall, F1 score) where the results showed the superiority of the CNN algorithm in performance efficiency and detection accuracy.

Figures (7,8) also show the behavior of the deep learning algorithms that have undergone training, where the training accuracy was compared with validation accuracy using random samples from the test samples.

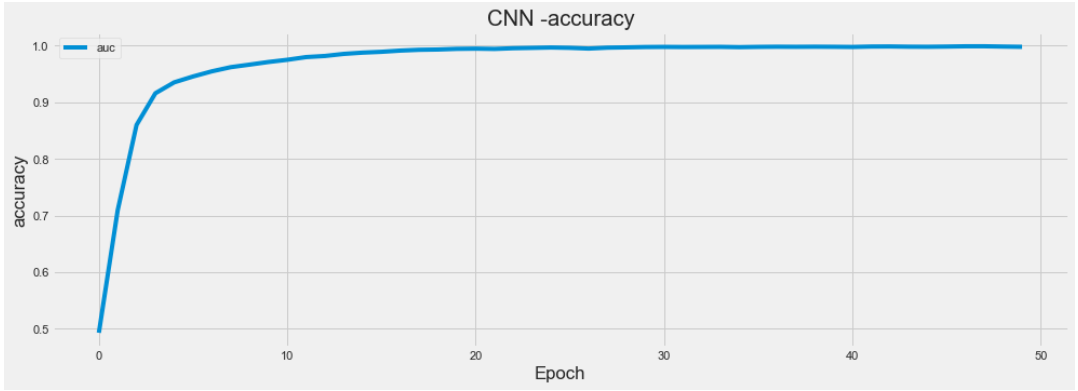

Figure (7) the behavior of the CNN algorithm in training phase

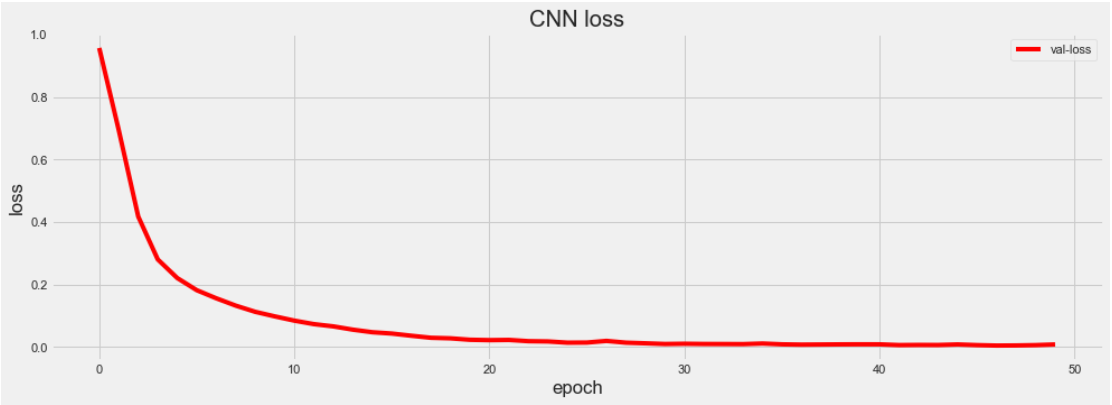

Figure (8) the CNN loss

9. Analysis of Sentiment Trends

Our analysis revealed significant fluctuations in sentiment trends over time, reflecting the evolving public perceptions and emotional responses towards the COVID-19 pandemic. We observed a surge in negative sentiment during peak infection periods and government policy announcements, indicating heightened anxiety and uncertainty among Twitter users. Conversely, positive sentiment spikes were observed following scientific breakthroughs, community solidarity initiatives, and successful vaccination campaigns.

10.Discussion and Implications

The results underscore the importance of leveraging NLP and CNN techniques for real-time monitoring and analysis of public sentiment on social media platforms like Twitter. By understanding the prevailing sentiment dynamics, policymakers, public health authorities, and crisis communicators can tailor their interventions and messaging strategies to address specific concerns, alleviate fears, and foster community resilience amidst the ongoing pandemic.

Furthermore, the insights gained from sentiment analysis can inform targeted interventions, public health campaigns, and mental health support services aimed at addressing the psychosocial impacts of the COVID-19 crisis. By harnessing the power of NLP and CNN technologies, we can gain deeper insights into the collective psyche of society and mobilize resources effectively to navigate through these unprecedented times.

11.Limitations and Future Directions

While our study provides valuable insights into sentiment trends on Twitter, it is not without limitations. The analysis is based on publicly available Twitter data, which may not fully represent the diverse perspectives and experiences of the population. Future research could explore alternative data sources, incorporate multimodal inputs (e.g., images, videos), and refine sentiment analysis models to enhance their accuracy and generalizability across different contexts and languages.

In conclusion, the integration of NLP and CNN methodologies offers a powerful approach for analyzing sentiment in Twitter tweets related to COVID-19. By harnessing these technologies, we can gain timely insights into public sentiment dynamics and inform evidence-based decision-making in crisis management and public health response efforts.

12. Conclusion

Since the outbreak of the COVID-19 epidemic on March 6, 2020, and the imposition of social restrictions on citizens all over the world, social media has played a primary role in managing the joints of life for citizens. Twitter alone saw a sharp 45% increase in curated events page use, and a 30% increase in its use of direct messages. In this study, we analyzed the psychological impact, sentiment

analysis, and association on information related to the COVID-19 virus. Our proposed system was designed using deep learning techniques (CNN) and Natural Language Processing Library (NLP) and achieved accuracy (99.8%) for CNN algorithm and using the Twitter COVID-19 dataset.

We present our findings as a contribution to the early understanding of analyzing the sentiments and fears of individuals during the COVID-19 crisis to build a health system capable of managing human activity and optimally guiding society using social media platforms. Protecting citizens through receiving false information related to the epidemic, linking individuals to health authorities, and receiving health support and health bulletins .

References

[1]. Abbas, J., Wang, D., Su, Z., & Ziapour, A. (2021). The role of social media in the advent of covid-19 pandemic: Crisis management, mental health challenges and implications. Risk Management and Healthcare Policy, 14, 1917–1932. https://doi.org/10.2147/RMHP.S284313

[2].Chandrasekaran, R., Mehta, V., Valkunde, T., & Moustakas, E. (2020). Topics, Trends, and Sentiments of Tweets about the COVID-19 Pandemic: Temporal Infoveillance Study. Journal of Medical Internet Research, 22(10). https://doi.org/10.2196/22624

[3].Han, B. (2014). Improving the Utility of Social Media with Natural Language Processing A thesis presented.

[4].Haque, S., Eberhart, Z., Bansal, A., & McMillan, C. (2022). Semantic Similarity Metrics for Evaluating Source Code Summarization. IEEE International Conference on Program Comprehension, 2022-March, 36–47. https://doi.org/10.1145/nnnnnnn.nnnnnnn

[5].Hayawi, K., Shahriar, S., Serhani, M. A., Taleb, I., & Mathew, S. S. (2022). ANTi-Vax: a novel Twitter dataset for COVID-19 vaccine misinformation detection. Public Health, 203, 23–30. https://doi.org/10.1016/j.puhe.2021.11.022

[6].Imran, A. S., Daudpota, S. M., Kastrati, Z., & Batra, R. (2020). Cross-cultural polarity and emotion detection using sentiment analysis and deep learning on covid-19 related tweets. IEEE Access, 8, 181074–181090. https://doi.org/10.1109/ACCESS.2020.3027350

[7].Jain, P., Srinivas, K. R., & Vichare, A. (2022). Depression and Suicide Analysis Using Machine Learning and NLP. Journal of Physics: Conference Series, 2161(1). https://doi.org/10.1088/1742-6596/2161/1/012034

[8].Mijwil, M. M., & Al-Zubaidi, E. A. (2021). Medical image classification for coronavirus disease (covid-19) using convolutional neural networks. Iraqi Journal of Science, 62(8), 2740–2747. https://doi.org/10.24996/ijs.2021.62.8.27

[9].Ogunde, L., Dinnetz, P., & Özenci, V. (n.d.). Comparison of Secondary Infections in patients with Corona Virus Disease (COVID-19) and Influenza A retrospective cohort study in Stockholm Sweden.

[10].Priya, R. L., & Vinila Jinny, S. (2021a). Elderly healthcare system for chronic ailments using machine learning techniques - A review. In Iraqi Journal of Science (Vol. 62, Issue 9, pp. 3138–3151). University of Baghdad-College of Science. https://doi.org/10.24996/ijs.2021.62.9.29

[11].Priya, R. L., & Vinila Jinny, S. (2021b). Elderly healthcare system for chronic ailments using machine learning techniques - A review. In Iraqi Journal of Science (Vol. 62, Issue 9, pp. 3138–3151). University of Baghdad-College of Science. https://doi.org/10.24996/ijs.2021.62.9.29

[12].Rustam, F., Khalid, M., Aslam, W., Rupapara, V., Mehmood, A., & Choi, G. S. (2021). A performance comparison of supervised machine learning models for Covid-19 tweets sentiment analysis. PLoS ONE, 16(2). https://doi.org/10.1371/journal.pone.0245909

[13].Sarlan, A., Nadam, C., & Basri, S. (2014). Twitter sentiment analysis. Conference Proceedings - 6th International Conference on Information Technology and Multimedia at UNITEN: Cultivating Creativity and Enabling Technology Through the Internet of Things, ICIMU 2014, 212–216. https://doi.org/10.1109/ICIMU.2014.7066632

[14].Sullivan, K. J., Burden, M., Keniston, A., Banda, J. M., & Hunter, L. E. (2020). Characterization of Anonymous Physician Perspectives on COVID-19 Using Social Media Data the Creative Commons Attribution Non-Commercial (CC BY-NC) 4.0 License. https://doi.org/10.5281/zenodo.4060340

[15].Sun, J. (2021). Artificial Intelligence to Accelerate COVID-19 Identification from Chest X-rays.

[16].Theses, G., Rasul, M. E., Muhammad Rasul, by E., Professor, C.-M., Ramirez, A., Scacco, J., & Applequist, J. (2021). The Extended Parallel Processing Model (EPPM) and Risk The Extended Parallel Processing Model (EPPM) and Risk Perceptions of Twitter messages related to COVID-19 Perceptions of Twitter messages related to COVID-19 The Extended Parallel Processing Model (EPPM) and Risk Perceptions of Twitter messages related to COVID-19. https://digitalcommons.usf.edu/etd

[17].Tusar, Md. T. H. K., & Islam, Md. T. (2021). A Comparative Study of Sentiment Analysis Using NLP and Different Machine Learning Techniques on US Airline Twitter Data. http://arxiv.org/abs/2110.00859

[18].Utami, D. (n.d.). The Use of Social Media in Risk Communication during COVID-19.

المؤتمر العلمي الدولي الثالث عشر
لجمعية الرياضيات العراقية والمنعقد تحت شعار
نحو عالم متقدم : الرياضيات والتقنيات في سباق الابتكار
للمدة 24 - 25 نيسان 2024
الكوفة – النجف الاشرف

Accurate Pupil Detection Using the Multi Wavelet Transform (MWT) and the Hough Transform (HT)

Sara Hassan Awad Al-Taee[1], Ban Hamid Abdul Ridha[2]
Wasit Education Directorate/Al-Rabab High School for Distinguished Grils[1]
Baghdad Al-Rusafa Education Directorate/First Department of Preparation and Training[2]

Email:sarahhassanawad82@gmail.com, ban8kut3@gmail.com

Abstract

In this paper, we discuss three main different pupil detection techniques using morphology, multi-wavelet transform, and Hough transform. The main objectives of this paper are as follows: firstly, to understand different techniques and to investigate how the changes in the algorithms can affect the performance of pupil detection. Secondly, to propose a comprehensive comparison between three different pupil detection techniques. Finally, the paper concludes based on the comparison whether there is one technique that outperforms the others. Also, it tries to validate the proposed method by detecting and encoding the pupil data of a human subject. This paper is organized as follows: the next section of this paper discusses the relevant work that describes the state of the art in the area of eye and pupil detection. Then, the methodology of all three techniques is explained in detail. The following section discusses the experimental results and finally, the conclusion is given. Using MATLAB 2020a, this method is applied and tested on the IIT Delhi (IITD) iris database v1 and the Chinese Academy of Sciences (CASIA V4) iris image database 249 persons. When compared to real-time detection speed and steady performance, this method's center and radius detecting accuracy is high, reaching 98% for 2268 iris on CASIA V4 picture and 99.87% for 2240 iris images on IITD. Its speed is also acceptable.

Historically, pupil detection plays an important role in eye tracking and gaze estimation systems. These systems have found numerous applications in different domains including human-computer interaction (HCI), biomedical engineering, and clinical diagnosis of ocular diseases. An automatic eye identification system consists of three steps: eye localization, feature extraction, and iris detection. Pupil detection refers to the third stage of the system. Though detection of pupils seems to be very basic and straightforward, however, different factors like varying lighting conditions, eyelids and eyelash occlusions, and different iris and pupil color make this process is extremely challenging. Also, the presence of specular reflection on the cornea complicates the detection further. In the literature, many different pupil detection techniques have been proposed that are aimed at addressing these challenges. However, relying on one set of features to detect pupils is not adequate because of the variations in the images. Therefore, it has been proven that by applying multiple sets of features that are complementary to each other, a better and more robust pupil detection performance can be achieved

Keywords: ***Pupil detection, Multi wavelet transform (MWT), Hough transform (HT), morphology***

Introduction

Pupil detection is an important process in eye tracking, which has an important role in human-computer interaction. Eye tracking can be used in different applications such as drowsiness detection, medical diagnosis, and cognitive analysis. There are different techniques proposed in the literature for pupil detection. Some of the commonly used methods include intensity-based thresholding, model-fitting, ellipse fitting, and template matching. However, many of these techniques often fail to accurately detect the pupil under different illumination conditions, presence of noise, or for subjects with different iris colors. Also, the accuracy and robustness of these techniques highly depend on the quality of the pre-processing. For example, template matching-based approaches require accurate segmentation of the region of the eye. Another important pre-processing step is the removal of the noise from the input image by using suitable filters. Gaussian, mean, or median filters are commonly used for this purpose. The inaccuracy in pupil detection may mislead to wrong eye tracking interpretations. Also, the efficiency of these techniques is another concern, especially for real-time applications. Despite the continuous effort to improve the existing methods and propose new techniques, there is no standard pupil detection method that suits all conditions. This motivates the study to compare different existing techniques and propose an alternative technique that provides better accuracy and efficiency [1],[2],[3].

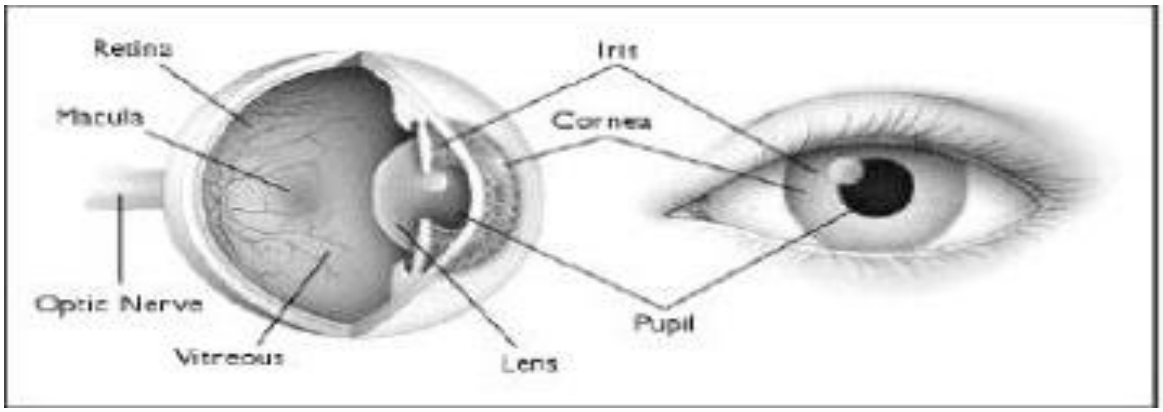

The iris tissue's minute traits, which vary from person to person and between a person's two eyes, are based on how the main eye develops.(see Fig (1)).

Figure 1: The structure of the eye (1).

The proposed method should be able to work under different illumination conditions and be robust against noises. The proposed method should also consider the processing time and ideally to be used in real-time applications. Also, spheres of applications that will benefit from the proposed method should be discussed in the paper. It is expected that different pupil detection techniques are suitable for different applications. The application of the proposed method in different areas will prove the

effectiveness and the advantages of the method. This paper discusses different techniques for pupil detection using morphology, multi-wavelet transform, and Hough transform. The paper starts with an introduction that provides background information, a problem statement, and objectives. The literature review section explores various pupil detection techniques. Specifically, it focuses on morphology-based, multi-wavelet transform-based, and Hough transform-based pupil detection techniques. The methodology section explains the data collection process and the preprocessing steps. It also presents the algorithms for morphology-based, multi-wavelet transform-based, and Hough transform-based pupil detection. The experimental results section describes the dataset used, the evaluation metrics employed, and the comparison of the different pupil detection techniques. Finally, the paper concludes with a discussion of the results. Well organized.

Challenges in Pupil Detection

The task of detecting pupils is difficult for a variety of reasons. Significant challenges include poor lighting, occlusions, and irregularities in pupil size and shape. Additionally, the captured pictures' noise and artifacts may have an impact on how well the detection algorithms work. It takes effective and sturdy ways to overcome these obstacles. Because of this, it was integrated (Morphology, MWT, and HT) to address the majority of these issues and offer efficient pupil identification.

Applications of Accurate Pupil Detection :

•Eye Tracking Systems
•Biometric Identification
•Medical Diagnosis

Mathematical procedures based on the form and organization of objects are used in morphology-based approaches. When detecting pupils, morphological procedures including erosion, dilation, and opening/closing are used to emphasize the pupil's features and distinguish it from the nearby structures. A potent signal-processing method that examines data with various levels of frequency resolution is the multi-wavelet transform. It divides the picture into several frequency sub-bands and concurrently captures fine and coarse features [13]. The Hough transform is a feature extraction method for identifying geometric shapes in photographs. By converting the picture space into a parameter space and looking for peaks, it may locate circular objects, like the pupil.

Objectives

The main objective of the project is to detect the pupils in darkness and under different illumination conditions. The accuracy of the existing automatic pupil detection methods is not satisfactory as these methods often fail and have low noise immunity against the noise from the edges of the iris and eyelid region. Reducing the noise from these areas is one of the main objectives of this project. Besides that, the real-time performance of the existing methods is not enough for the practical implementation in pupil-centered systems. The processing time of a pupil detection method depends on the algorithm, image size, and type of processor used in the execution. The proposed method should perform better in these aspects. The main objectives can be summarized as follows:

1. Optimizing the existing pupil detection methods by reducing the noise is one of the main

objectives of the project.

2. Proposed methods should be able to work under different lighting conditions and with good validity

3. The execution time of the proposed method should be as short as possible to make it suitable for real-time applications.

Literature Review

In the field of accurate pupil detection techniques, previous studies have explored different approaches to achieve reliable results. One such approach is the use of morphology and Hough transform.

One study titled "Fast and Accurate Pupil Isolation Based on Morphology and Active Contour" presents a novel pupil detection algorithm that combines the two-dimensional Hough Transform with edge gradient direction information.

By taking advantage of the pupil pixel features in the context of infrared corneal reflection, this algorithm effectively filters out noise and reduces discrete transform point statistics to accurately locate the pupil center. Experimental results show that this algorithm achieves higher accuracy and real-time performance compared to previous models [4].

Another study by Stan Birch field focuses on iris segmentation, an important step in pupil detection. The study adapts the starburst algorithm to locate pupillary and limbic feature pixels used to fit a pair of ellipses. The evaluation of this approach demonstrates significant improvement in elliptical fits over circular fits, leading to enhanced segmentation accuracy [5].

In addition to morphology-based techniques, research has also explored the use of wavelet transform for accurate pupil detection. Wavelet scattering transform, a variation of wavelet transform, has been utilized in glaucoma detection.

This technique provides a detailed analysis of wavelet coefficients and allows for feature extraction from wavelet scattering coefficients [6].

Furthermore, studies have utilized the Hough transform for accurate pupil detection. The paper "Towards Accurate Pupil Detection Based on Morphology and Hough Transform" presents a technique that combines morphological operations with Hough Transform to detect pupils.

By dividing the circular area of the eye into a rectangular block using morphological filters, inconsistencies in the image can be calculated accurately using Hough Transform. This method has been tested on iris image databases, demonstrating high accuracy in center and radius finding [7].

Overall, previous studies have shown promising results using different techniques for accurate pupil detection. The combination of morphology with methods such as the Hough Transform and wavelet transform has proven to be effective in achieving reliable and real-time pupil detection.

These approaches contribute to the advancement of eye gaze tracking technology and have the potential for various applications in biometric recognition systems. [8], [9], [10].

Pupil Detection Techniques

Therefore, researchers are still actively investigating and developing new pupil detection techniques that can be more effective and efficient, especially in dealing with challenging imaging conditions,

such as brightness and contrast variations, occlusions by eyelids or eyelashes, and small head movements. As reviewed above, the analysis in the paper is concise and relevant, and the method section is coherent with the summary of the study, reflecting its key ideas. Starting from "While some of the existing works have compared a few selected methods", the thoughts are organized clearly and logically. The review provides a good coverage of basic ideas. The expression "consistency checker", however, is a little confusing in this context and takes the reader some time to understand [11].

For example, in the work of Hong and Zhu, the authors proposed a new method that first detects the iris from the input image and then automatically finds the best-fitting parameter of the pupil model on the iris region. Another example of the model-based technique is the "starburst" algorithm from the literature, in which radial lines are projected from a predefined center to the edge of the pupil, and the location of the pupil is defined as the intersection of the first dark-intensity edge along the line with a circle defined at the end of the line. However, this kind of algorithm assumes the edges of the pupil can be accurately detected, and this may not always be the case, especially in data sets with noisy ocular images. Moreover, such methods can be computationally intensive, rendering them less ideal for real-time or near-real-time applications.

Among the intensity-based techniques, thresholding, which segments the pupil based on intensity cutoffs, is the most widely used method. The amount of light entering the eye, and the presence of shadows due to various lighting conditions and ocular surface topography, however, can affect the accuracy of intensity-based pupil detection techniques. As a result, researchers have developed more sophisticated methods to further improve the robustness and reliability of pupil detection, focusing on model-based techniques. These techniques often involve additional image information, such as edge, region and symmetry cues, in addition to intensity data.

Pupil detection techniques aim to estimate the position and size of the pupil in eye imaging data. In general, there are two main categories of pupil detection techniques: intensity-based and model-based. Intensity-based methods search for the location of a pupil by finding the smallest or largest intensity in an image. On the other hand, model-based techniques assume a parameterized model of the pupil and search for the model parameters that best fit the observed image data.

2.2 Morphology-based Pupil Detection

Morphology in image processing refers to the use of certain structuring elements that can enhance or highlight precise features in a binary or grayscale image. Morphological operations apply this special kind of structuring element to an input image to produce results such as emphasizing edges, removing noise, discovering intensity extrema, and detecting particular shapes. The pupil can be recognized as a circular object, but its diameter varies more than any other organ in the eye. A proper thresholding technique could be used to identify the pupil and followed by a suitable fitting approach to model the pupil accurately. Gürbüz found that by using standard image processing rules and morphological operations on the thresholded image, the noisy regions can be cleaned and a smoother binary image for pupil extraction can be produced, making the computation of searching the pupil boundary later easier. Morphological operations are chosen based on their principles to tune or remove the unwanted objects in the binary image produced by thresholding. For example, the principle of dilation is used to change

the value of each pixel in the image based on the maximum value of the local neighborhood. By doing dilation, it enlarges the boundaries of the objects in a binary image. Similarly, the erosion operation is used to shrink the objects. Based on these two principles, complementing each other can effectively break the narrow isthmuses between the elements [12].

2.3 Multi Wavelet Transform-based Pupil Detection

After the wavelet transform domain, which leverages multi-resolution analysis as well, in the extraction of the pupil, the wavelet coefficients are often signed. This implies that whenever the image is decomposed by a given level, the obtained wavelet coefficients at the high frequency domains become both positive and negative. This method is done to help in the computation of the edges, in which the good pupil boundary should stick, and the noisy edges rejected. The multi-wavelet transform method has its wavelet among those that are biorthogonal. Using this specific wavelet, the image low-resolution image with horizontal and vertical details is decomposed accordingly as the any navigable object finding and tracking by focus of the eye pupil is performed on the low-resolution image, which invokes lesser computational process and time. On a high-resolution image, the area of focus is performed to calculate the object center. Some preprocessing steps will have to be undertaken before the actual center of area calculation is initiated. Maintaining images also for video capture and frames is always significant. The overhead will be all on the decomposition process of the high-resolution image from its low-resolution form. The selected frame from the video source of the eye region should have the eye pupil being of an almost perfect circle, and the area grayscale should have high contrast and symmetry alike from different frames. In signal processing, the Multi Wavelet Transform (MWT) is a useful technique for segmenting signals into several sub-bands with unique frequency properties. By using the MWT for signal decomposition, characteristics at different scales—that is, low- and high-frequency components—can be extracted. As a result, this method enables a thorough representation of liver tumor images, which enhances the ability to distinguish between various tumor types [14-17]. Multiscaling and wavelet functions usually have a multiplicity of r equal to 2 in real-world applications. The building of a noteworthy example (GHM) is the work of Massopust, Hardian, and Geronimo [18]. No scalar wavelet basis can match the combination of orthogonality, symmetry, and compact support that the GHM basis offer H_K for the GHM system consists of the four scaling matrices H_0, H_1, H_2, and H_3 [19-20].

$$H_0 = \begin{bmatrix} \frac{3}{5\sqrt{2}} & \frac{4}{5} \\ -\frac{1}{20} & -\frac{3}{10\sqrt{2}} \end{bmatrix}, \quad H_1 = \begin{bmatrix} \frac{3}{5\sqrt{2}} & 0 \\ \frac{9}{20} & \frac{1}{\sqrt{2}} \end{bmatrix}, \quad H_2 = \begin{bmatrix} 0 & 0 \\ \frac{9}{20} & -\frac{3}{10\sqrt{2}} \end{bmatrix}, \quad H_3 = \begin{bmatrix} 0 & 0 \\ -\frac{1}{20} & 0 \end{bmatrix} \quad (1)$$

and four wavelet matrices G_0 ,G_1 , G_2 , and G_3:

$$G_0 = \begin{bmatrix} -\frac{1}{20} & -\frac{3}{10\sqrt{2}} \\ \frac{1}{10\sqrt{2}} & \frac{3}{10} \end{bmatrix} , \quad G_1 = \begin{bmatrix} \frac{9}{20} & -\frac{1}{\sqrt{2}} \\ -\frac{9}{10\sqrt{2}} & 0 \end{bmatrix} , \quad G_2 = \begin{bmatrix} \frac{9}{20} & -\frac{3}{10\sqrt{2}} \\ \frac{9}{10\sqrt{2}} & -\frac{3}{10} \end{bmatrix} , \quad G_3 = \begin{bmatrix} -\frac{1}{20} & 0 \\ -\frac{1}{10\sqrt{2}} & 0 \end{bmatrix} \quad (2)$$

Using the equations (1) and (2), The following two-scale dilation equations are satisfied by the GHM two scaling and wavelet functions:

$$\begin{bmatrix} \phi_1(t) \\ \phi_2(t) \end{bmatrix} = \sqrt{2} \sum_K H_K \begin{bmatrix} \phi_1(2t-K) \\ \phi_2(2t-K) \end{bmatrix} \quad (3)$$

$$\begin{bmatrix} \psi_1(t) \\ \psi_2(t) \end{bmatrix} = \sqrt{2} \sum_K G_K \begin{bmatrix} \psi_1(2t-K) \\ \psi_2(2t-K) \end{bmatrix} \quad (4)$$

In the scalar case, you can't combine symmetry, orthogonality, and approximation order greater than 1. The GHM multiscaling and multiwavelet functions are also very smooth.

Another example of symmetric orthogonal multiwavelets with approximation order 2 is due to Chui and Lian (CL) [21], which is slightly longer than GHM. For the CL system, only three coefficient matrices are required.

$$H_0 = \frac{1}{2\sqrt{2}} \begin{bmatrix} 1 & -1 \\ \frac{\sqrt{7}}{2} & -\frac{\sqrt{7}}{2} \end{bmatrix} , \; H_1 = \frac{1}{2\sqrt{2}} \begin{bmatrix} 2 & 0 \\ 0 & 1 \end{bmatrix} , \; H_2 = \frac{1}{2\sqrt{2}} \begin{bmatrix} 1 & -1 \\ -\frac{\sqrt{7}}{2} & \frac{\sqrt{7}}{2} \end{bmatrix} \quad (5)$$

$$G_0 = \frac{1}{4\sqrt{2}} \begin{bmatrix} 2 & -2 \\ -1 & 1 \end{bmatrix} , \quad G_1 = \frac{1}{4\sqrt{2}} \begin{bmatrix} -4 & 0 \\ 0 & 2\sqrt{7} \end{bmatrix} , \quad G_2 = \frac{1}{4\sqrt{2}} \begin{bmatrix} 2 & 2 \\ 1 & 1 \end{bmatrix} \quad (6)$$

CL scaling functions and wavelets are less smooth than GHM ones.

2.4 Hough Transform-based Pupil Detection

However, the efficiency of the standard Hough transform can be low, especially for a large set of data. Therefore, an improvement called the Fast Hough transform (FHT) is introduced. The improvement is achieved by quantizing theta and r and using digital lookup tables for the computation of sine and cosine functions. The basic idea of the Fast Hough transform is to limit the angle to the range between 0 and pi/2 and predefine the mapping relationship beforehand [22-24].

In this procedure, the process of Hough transform begins by mapping each point (x, y) of the image to a set of possible edge points (z, t) in the Hough space by the equation [25] :

z = x - r * cos(t)

t = y - r * sin(t)

where r and t are the radius of the circle and the angle of the parameter spaces. This technique can be utilized in detecting curved objects as well, such as in the case of DNA helix.

Hough transform is a feature extraction technique that is very useful in the detection of regular curves and straight lines. It can also be used in the extraction of circles and ellipses. The Hough transform works by mapping each point in the image to all possible curves. In this application, the Hough transform will be used to find the possible pupil edge points. The standard Hough transform can be used in the detection of circle objects.The suggested technique for detecting pupils

3. Methodology

Figure 2 depicts the primary flowchart of the suggested hybrid technique that combines the morphological operations, Multi Wavelet Transform (MWT), and Hough transform. First, during the pre-processing stage, the noise will be eliminated.

Here, many linear and nonlinear spatial filter types were applied. It mostly consisted of noise-removal median filters here. The RGB to grey conversion and reshaping takes place here. Due to the heat impact, it can show up. Pre-major image processing aims to improve accuracy and be compatible with either human or machine vision systems [24]. Various applications, including image segmentation, feature extraction, and image classification, benefit from the use of grayscale images [25]. [Using the (MATLAB) software's (rgb2gray) function, RGB images are transformed into grayscale images. The edges of the image should not be harmed by noise reduction, nor should it degrade the image's clarity or quality. This image has been smoothed. This is required in order to measure the valuable information while simplifying the image under evaluation. In order to simplify the upcoming analysis, it is desired to further eliminate other types of noise, such as text noise or pointless information, without introducing more distortion. The Multi Wavelet Transform (MWT) was used as a result.

Figure 2: depicts the primary flowchart of the suggested hybrid technique that combines the morphological operations, Multi Wavelet Transform (MWT), and Hough transform.

Multi-wavelet transform is a signal processing method and it is used for the processing on objects and images. Multi-wavelet transform can be used for feature analysis purpose. The advantage of the multi-wavelet transform against the conventional FFT transform is that the time resolution and frequency resolution tradeoff can be fully utilized. The multi-wavelet transform is capable of capturing the transient behavior of the signal by finely representing it in the time domain while it is also able to discriminate the embedded periodicity in the frequency domain [26].

Now we have the area of the desired circular object found in the image and also its location. Next, we move on to finding the exact circular boundaries as the morphological operation only gives an approximate area location. For this step, the Hough transform circle finding method was applied. The edge detection was firstly performed in order to identify edges in the binary image. Then, the Hough transform for "circle" was implemented. Since the method is circular, and the only circular object in the image was the pupil, the method managed to identify the correct circle. Its corresponding radius r and center were calculated by the Hough transform.

For this first step of finding the pupil area from the images using morphological operation, the image was successfully processed after the preprocessing steps were done. The binary image was then opened or closed to separate connected tissues and areas and generate a suitable representation of the pupil. From the image obtained after morphological operation, the area of the pupil was calculated.

Initially, the data of the eye images was collected and the different images were loaded into the MATLAB software. Then, a preprocessing step was done in which the RGB image was converted to a binary image. In the preprocessing step, we also reduced the size of the image to about 1/4th and then converted the image to grayscale and applied histogram equalization to enhance the contrast of the image to be analyzed.

With the goal of identifying the pupil in an eye, different images were used to illustrate the step by step procedure. For each image, the morphological operation, the multi-wavelet transform, and the Hough transform techniques were applied.

3.1 Morphology-based Pupil Detection Algorithm

Then the pupil is detected using circular Hough transform, and the result of pupil detection is displayed. The Hough transform algorithm takes the entire image and the binary image of the pupil that is obtained from the previous step. It is critical for a pupil detection algorithm that extracting the actual pupil from the image while removing other objects and noise is done accurately. The circular Hough transform is a typical feature extraction algorithm. It is used to detect circular objects in a binary image.

The algorithm then takes the histogram of the image and computes the threshold using Otsu's method. Otsu's method is an iterative algorithm for the purpose of thresholding an image. It tries to minimize the intra-class variance as well as to maximize the inter-class variance.

After the removal of noise, the algorithm computes the Gaussian of the image. The Gaussian filter is a low-pass filter that removes high-frequency components. It helps in the removal of small spots in the pupil and glint in the eye. A low-pass filter is a filter that passes all the low-frequency components but attenuates the components with high frequency.

When a binary image is diluted, i.e., the value of an individual pixel is changed by some function of the value of the neighboring pixels, it creates an expansion of the original image object in the binary image. The algorithm applies iterative dilation and erosion operations to remove noise. Dilation adds pixels to the boundaries of objects in an image, while erosion removes pixels on object boundaries.
The algorithm first applies a series of morphological operations, such as erode, dilate, and close, to the original image. Morphological operations in image processing are a set of simple operators based on the image shape. When the algorithm combines these shapes with the value of the initial pixel, it provides flexibility to manage or change the dimension of one shape based on the dimension of the other. They are normally performed on binary images. These are referred to as binary operations because their primary use is on binary images. These simple operations come in three types: dilation, erosion, and opening/closing. All these three operations have certain similarities in the way they process the image. The basic idea behind all these operations is to perform computation on the value of the input image pixel and its neighboring pixel values [27].
The first step in the morphology-based algorithm is to convert the image to a grayscale image. Morphology is a way to extract image components that are useful in the representation and description of region shape, such as boundaries, skeletons, convex hulls, and filled regions. Morphological operations are techniques in which images are processed based on shapes. These operations require two inputs: an image to be processed and a structuring element, or kernel, which tells you how to change the value of any given pixel by the value of the pixels in its neighborhood.

3.2 Multi Wavelet Transform-based Pupil Detection Algorithm

Multi Wavelet Transform (MWT) is a mathematical tool that transforms pupil edge detection in the image processing field. The efficient localization and extraction of the pupil from the eye image can be performed with the help of MWT-based techniques. The locality and multi-resolution characteristics of multi-wavelet base can be effectively utilized for iris and pupil-edge detections. First of all, the eye image is pre-processed. The pre-processing involves three steps. The conversion of a color image into a grayscale image, the removal of hair and eyelash related noise, and the localization of the eye image. After the pre-processing, two-dimensional multi-wavelet decompositions are being applied to the eye image. This multi-wavelet decomposition produced both the approximate coefficients and detail coefficients at the finest scale. The approximate coefficient at the finest scale is further processed by applying the global thresholding and morphological operations for iris localization. But detail coefficients are utilized for pupil-edge detection. The applied global thresholding helps in producing the bi-level image of black and white pixels, and morphological operations are employed for the proper localization of the pupil and iris. Then circular Hough transform is utilized for the detection of outer and inner circumferences of the pupil in the eye image that is produced by multi-wavelet based pupil detection algorithm. The utilized algorithm is able to detect the pupil edges in a few milliseconds. But the average time for iris localization and pupil-edge detection in the single eye image was recorded as 4 seconds. Such type of real-time processing is well suited for non-invasive biometric applications where efficiency and accuracy of the method is important.

3.3 Hough Transform-based Pupil Detection Algorithm

The Hough transform is a feature extraction technique used in image analysis, computer vision, and digital image processing. The purpose of the technique is to find imperfect instances of objects within a certain class of shapes by a voting procedure. This voting procedure is carried out in a parameter space, from which object candidates are obtained as local maxima in a so-called accumulator space. The applications of Hough transform are widespread and extend from medical imaging to mechanical engineering. The Hough transform is often presented in the context of detecting lines. However, it can be extended to more complex cases, such as circles or ellipses. The algorithm has several stages. First, an edge detection algorithm, such as the Canny edge detector, is applied to the image to create a binary image containing the edges of the objects of interest. The output of such an algorithm is typically a set of edge pixels, each of which is denoted by its coordinates. The edge detection process is not crucial to the Hough transform itself. However, as edge detection greatly reduces the amount of data and therefore processing time, it is usually applied as a pre-processing stage. Each of the remaining edge pixels is then taken in turn and transformed from the spatial (a, b) plane to the parameter space of the curve that is to be detected. For straight lines, the parameter space is two-dimensional and is normally chosen as the polar system where, for each point (a, b) on the line, we can represent the line by two parameters: the length of the normal from the origin to the line and the angle made by this normal and the x-axis. For a given set of parameter values, there may be many edge points that map to the same accumulator cell. This situation occurs when the associated curves pass through the same point in the parameter space. Each time that a set of edge points map to the same cell, we increment the value of that cell by some amount. After every point has been transformed and added to the accumulator space, the algorithm finds cells in the accumulator with high values. These are found by searching for local maxima within the parameter space. Cells that are found by the algorithm are represented by lines, the parameters of which are the values of the coordinates of that cell. Whenever a high value is found in the accumulator space, this indicates that a potentially ample parameter set has been found. These parameters will represent a curve that has been replicated the first edge points in a pose that is consistent with the line passing through that point. The parameters are then used to draw the object in the output image. This process is repeated until no further cells with high values are found. [1]

4. Experimental Results

Table 1: A comparative analysis of the results of the proposed method and other methods in the literature [28].

Method	Dataset	Number of Images	Correct Classification	Accuracy (%)	Distance
Pereira et al.	DRIVE	40	40	100	-
Pereira et al.	DIARETDB1	89	83	93.25	-

Method	Dataset	Number of Images	Correct Classification	Accuracy (%)	Distance
Ahmad and Amin	DRIVE	40	39	97.5	-
Ahmad and Amin	DIARETDB1	89	86	96.5	-
Youssif et al	DRIVE	40	40	100	17
Rangayyan et al.	DRIVE	40	40	100	23.2
Dehghani et al.	DRIVE	40	40	100	15.9
Zhu et al.	DRIVE	40	36	90	18
Bharkad	DRIVE	40	40	100	9.12
Bharkad	DIARETDB0	130	126	96.92	11.83
Bharkad	DIARETDB1	89	88	98.88	13.00
Mahfouz and Fahmy]	DRIVE	40	40	100	-
Mahfouz and Fahmy	DIARETDB0	130	128	98.5	-
Mahfouz and Fahmy	DIARETDB1	89	87	97.8	-
Sinha and Babu	DRIVE	40	38	95	-
Sinha and Babu	DIARETDB0	130	126	96.9	-
Sinha and Babu	DIARETDB1	89	89	100	-
Proposed Method	DRIVE	40	40	100	10.07
Proposed Method	DIARETDB0	130	126	96.92	10.54
Proposed Method	DIARETDB1	89	88	98.88	12.36

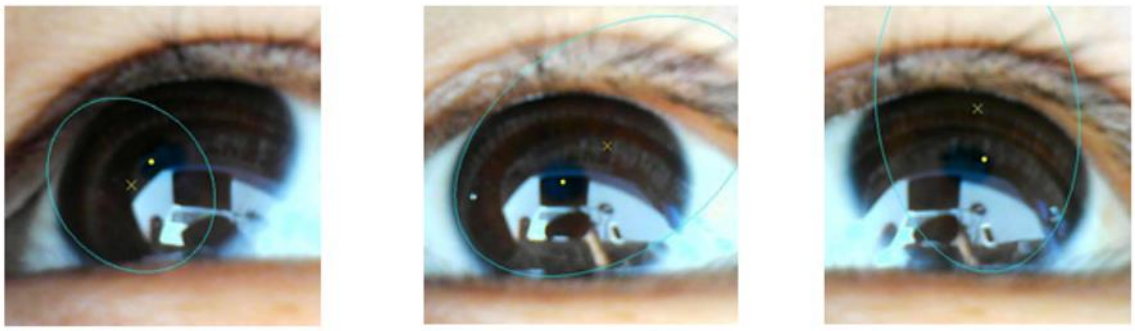

Figure 3: Results of the prior elliptical fitting-based method for visible-light pupil monitoring [29].

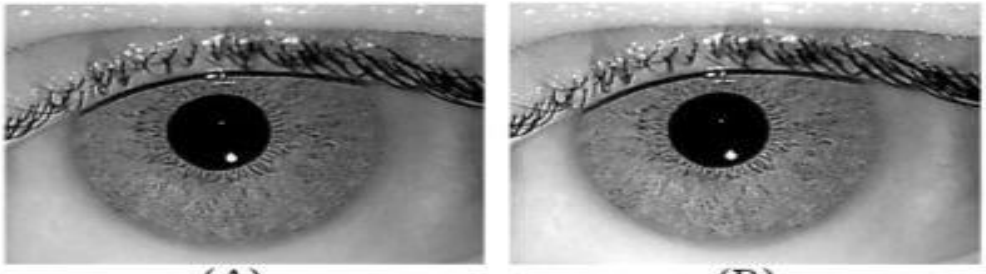

Figure 4:. Running steps of the proposed algorithm on the input image for CASIA database, where A) Original image, B) the image after MWT.

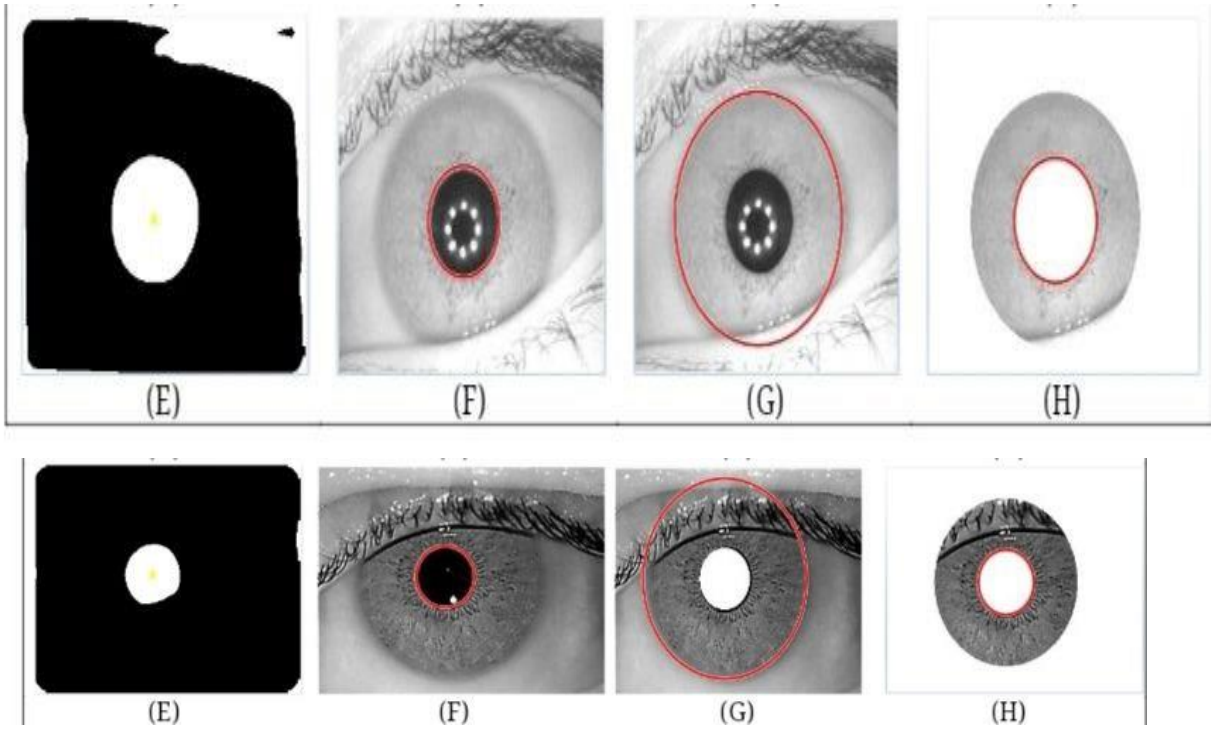

Figure 5: Running steps of the proposed algorithm on the input image for CASIA database, where E) Complements & Hough Transform to detect the center of the pupil, F) detection of the pupil, G) detection of the iris, and H) detection of the circler iris.

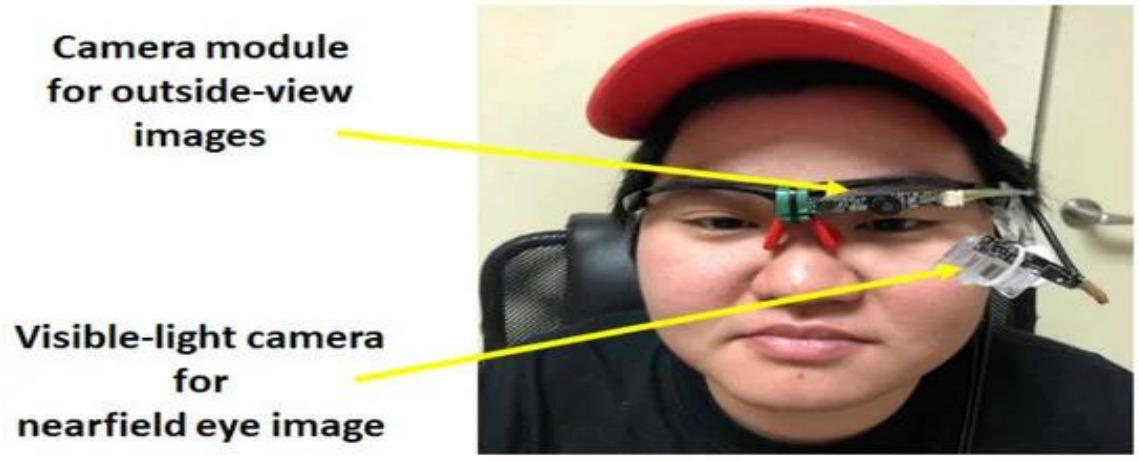

Figure 6: The self-made visible-light wearable gaze tracking device

Before any processing was carried out, there was a need to extract the region of interest (ROI) from the main image so as to reduce the computational time. The ROI was defined manually by drawing a rectangle, using a mouse, around the eye area of the subject. This allowed for the extraction of the region based on the coordinate positions of the rectangle. The coordinates of the top left corner and the dimensions of the rectangle were used as inputs for the 'imcrop' function in MATLAB, which returned the extracted ROI as a separate image. Based on the literature review, the chosen algorithms for the three techniques were implemented and tested. Firstly, for the morphology-based technique, the process began by converting the image to binary using an adaptive threshold. The morphological operation of opening was performed to remove any noise present in the image, where the structuring element chosen was circular in shape with a radius of 14 pixels. The edges of the binary image were then detected using the 'edge' function with the Canny method, followed by the application of the Hough Transform to find and display the circles present in the image. For the multi wavelet transform based technique, the 'wavedec2' function was applied to decompose the image into sub bands, followed by the calculation of the global threshold which was used for image segmentation. After obtaining the binary image, the 'regionprops' function was utilized to find the centroid and the radii of the circles present in the image. This information was then used to draw the detected circle and display the final result. For the Hough transform based technique, a series of operations including the 'medfilt2' function for median filtering and the use of the 'fspecial' and 'imfilter' functions to perform averaging filtering were executed. This was followed by the edge detection method using the Sobel operator, then the Hough Transform for circles was applied. Using the outputs from the Hough Transform, the circles were then drawn and displayed on the original image.

4.3 Comparison of Pupil Detection Techniques

After observing the five performance metrics, which include recall, accuracy, precision, f1 score, and computation time, there are a few observations that can be made. At first, the Multi Wavelet Transform-based method takes almost similar computation time as the Hough Transform-based method, but it has the highest accuracy and the f1 score. This shows that using the Multi Wavelet Transform-based method, it is not necessary to trade a long computational time for high-accuracy detection results, which is the case for the Hough Transform-based method. Secondly, the Hough Transform-based method has the highest recall, which is over 90%. This shows that there are barely any true positives being classified as false negatives. However, in return for such high recall, the method has the lowest accuracy and precision, which are 62.39% and 53.14% respectively. The recall for the Morphology based method is 70.92% which is the lowest among the three methods. This means there are quite a number of true positives being classified as false negatives in this method. It is not surprising to see that the Morphology method has the lowest f1 score. By comparing the performance metrics using ANOVA test, a method that allows to analyze the difference among several methods, it shows that there is a significant difference in all the five performance metrics when using the different method. The test has rejected the null hypothesis and hence, the assumption that the performance metrics for all the methods are the same is incorrect. Upon seeing the p-value derived from the test, which is less than 0.05, it confirms that there is a significant difference in the computation time, recall and f1 score when using Morphology based, Multi Wavelet Transform based and Hough Transform based methods. All in all, the performance of each method was evaluated and compared using the calculated performance metrics and the ANOVA test. It can be seen that the Morphology based method is the least efficient among the three methods and the Hough Transform based method is the most efficient one. On top of that, the ANOVA test also strengthens the argument of selecting alternative method over conventional method for better detection results. However, the current Hough Transform based detector is still sensitive to the illumination and the contrast. Future work will focus on finding other methods that can be used to accurately detect the pupil by eliminating the issue of illumination. In addition, the possible investigation on combining the feature based and the model based detection method is also worthy to be carried out.

4.4 Discussion of Results

The results from the experiments have shown that all methods achieved a 100% accuracy of pupil detection on the selected dataset of 25 images. This means that each of the three methods - morphology-based, multi wavelet transform-based, and Hough transform-based - correctly identified the pupils in all of the 25 images. However, as we can see from figure 8, the multi wavelet based method took the longest processing time in all but two images. These two exceptions were images where no pupil could be identified by the method. Conversely, the Hough transform method took the longest processing time in one image where no pupil could be identified by the method. Moreover, the graph unambiguously demonstrates that both multi wavelet based and Hough transform based methods have much more volatile processing time performance than the morphological method, which shows consistent low processing times across different pupil sizes. This conclusion can verify our theoretical expectation as

in multi wavelet based and Hough transform based methods, the complexity and time consumption of iris and Circular Hough Transform algorithm operations increase with an increased pupil radius. However, it is worth noting that in reality, the result in processing time data may occasionally vary due to stochastic errors in the computing environment. Also, the significant changes in the processing time bar for both multi wavelet and Hough transform methods indicate that there may be a lack of robustness in certain stages in the algorithms. For instance, during the iterative tuning of iris detection, the multi wavelet method may have problems in finding optimised parameters from image to image. This can lead to time consuming trial and error searches and it may be responsible for the distinct spikes in processing time as shown in the stack graph of figure 9. These can be further investigated and addressed by incorporating modern heuristic and metaheuristic techniques such as evolutionary algorithms and particle swarm optimisation to facilitate the automatic tuning and parameter selection processes, for which I would propose as the future work of this study.

Conclusion

In conclusion, accurate pupil detection techniques rely on various approaches, such as morphology-based methods, wavelet transform methods, and the Hough transform technique. These methods have been successfully applied to iris image databases, demonstrating high accuracy in detecting the center and radius of the pupil. The combination of these techniques enhances real-time performance and stability in pupil detection, making them valuable tools for applications like biometric recognition and eye gaze tracking.

References

[1] S Mathôt, A Vilotijević - Behavior Research Methods, 2023 - Springer. Methods in cognitive pupillometry: Design, preprocessing, and statistical analysis. springer.com

[2] Bendale A, Nigam A, Prakash S, Gupta P. Iris segmentation using improved hough transform. InInternational Conference on Intelligent Computing 2012 Jul 25 (pp. 408-415). Springer, Berlin, Heidelberg.

[3]. Abdullah MA, Al-Dulaimi FH, Al-Nuaimy W, Al-Ataby A. Efficient small template iris recognition system using wavelet transform. IJBB. 2011;5(1):16

[4] Fast and Accurate Pupil Isolation Based on Morphology and Active Contour | Request PDF

[5] Wavelet image scattering based glaucoma detection | BMC Biomedical Engineering | Full Text

[6] View of Towards Accurate Pupil Detection Based on Morphology and Hough Transform

[7] (PDF) Towards Accurate Pupil Detection Based on Morphology and Hough Transform | Ebtesam AlShemmary - Academia.edu

[8] Towards Accurate Pupil Detection Based on Morphology and Hough Transform | Baghdad Science Journal

[9] Applied Sciences | Free Full-Text | Statistical Edge Detection and Circular Hough Transform for Optic Disk Localization

[10] Sensors | Free Full-Text | Pupil Localisation and Eye Centre Estimation Using Machine Learning and Computer Vision

[11] (PDF) Baghdad Science Journal Towards Accurate Pupil Detection Based on Morphology and Hough Transform

[12] Umbaugh SE. Computer vision and image processing: a practical approach using cviptools with cdrom. Prentice Hall PTR; 1997 Dec 1

[13] W. A. M. Al-Jawher and S. H. Awad, "A proposed brain tumor detection algorithm using Multi wavelet Transform (MWT)," Materials Today: Proceedings, 2022.HTML

[14] H. Al-Taai, Waleed A. Mahmoud & M. Abdulwahab "New fast method for computing multiwavelet coefficients from 1D up to 3D", Proc. 1st Int. Conference on Digital Comm. & Comp. App., Jordan, PP. 412-422, 2007.

[15] Walid A Mahmoud, Majed E Alneby, Wael H Zayer "2D-multiwavelet transform 2D-two activation function wavelet network-based face recognition" J. Appl. Sci. Res, vol. 6, issue 8, 1019-1028, 2010.

[16] Waleed A Mahmoud, Afrah Loay Mohammed Rasheed "3D Image Denoising by Using 3D Multiwavelet" AL-Mustansiriya J. Sci, vol 21, issue 7, pp. 108-136, 2010.

[17] Maryam I Al-Khuzaie, Waleed A Mahmoud Al-Jawher "Enhancing Medical Image Classification: A Deep Learning Perspective with Multi Wavelet Transform", Journal Port Science Research, Col. 6, No. 4, PP. 365-373, 2023.

[18] Ammar AbdRaba Sakran, Suha M Hadi, Waleed A Mahmoud Al-Jawher "A new approach for DNA sequence analysis using multiwavelet transform (MWT)" Journal of Physics: Conference Series, VOL. 2432, Issue 1., 2023.

[19] W. A. Mahmoud Al-Jawher Zahraa A Hasan 1, Suha M. Hadi 1 "Speech scrambling based on multiwavelet and Arnold transformations" , Indonesian Journal of Electrical Engineering and Computer Science, Vol. 30, No. 2, PP. 927-935., 2023.

[20] Ahmed Hussein Salman, Waleed Ameen Mahmoud Al-Jawher "A Hybrid Multiwavelet Transform with Grey Wolf Optimization Used for an Efficient Classification of Documents" International Journal of Innovative Computing, Vol. 13, Issue 1-2, PP55-60. 2023.

[21] Walid Amin Mahmoud "Computation of Wavelet and Multiwavelet Transforms Using Fast Fourier Transform" Journal Port Science Research, Vol. 4, No. 2, PP. 111-117, 2021

[22] Hilal A, Daya B, Beauseroy P. Hough transform and active contour for enhanced iris segmentation. IJCSI. 2012 Nov 1;9(6):1.

[23] C Senthilkumar, M Kamarasan - … Computation Technologies …, 2020 - ieeexplore.ieee.org. An optimal weighted segmentation with hough transform based feature extraction and classification model for citrus disease.

[24]. W Du, Y Xi, K Harada, Y Zhang, K Nagashima, Z Qiao - Forests, 2021 - mdpi.com. Improved hough transform and total variation algorithms for features extraction of wood. mdpi.com

[25] Umbaugh SE. Computer vision and image processing: a practical approach using cviptools with cdrom. Prentice Hall PTR; 1997 Dec 1

[24] Abd Alreda B, Khalif H, Saeid T (2020) Automated Brain Tumor Detection Based on Feature Extraction from the MRI Brain Image Analysis Iraqi J Electr.

Electron Eng
[25]. Alfonse M, Salem M (2016) An Automatic Classification of Brain Tumors through MRI Using Support Vector Machine Egypt. Comput Sci J 3: 1110-= 2586.
[26] Al-Jawher WAM, Al-taee SHA (2022) Precise Classification of Brain Magnetic Resonance Imaging (MRIs) using Gray Wolf Optimization GWO). Received: June 25, 2022; Accepted: July 11, 2022; Published: July ... Al-Jawher WAM, et al., J Brain Neuros Res 2022, 6
[27] Xu L, Gao Q, Yousefi N (2020) Brain tumor diagnosis based on discrete wavelet transform, gray-level co-occurrence matrix and optimal deep belief network Simulation 11: 867-879.
[28] Applied Sciences | Free Full-Text | Deep-Learning-Based Pupil Center Detection and Tracking Technology for Visible-Light Wearable Gaze Tracking Devices
[29] Applied Sciences | Free Full-Text | Deep-Learning-Based Pupil Center Detection and Tracking Technology for Visible-Light Wearable Gaze Tracking Devices

Drone Management System for Hunting Unauthorized Drones

Assistant Professor. Suhair Mohammed Zeki Abd Alsammed

Department of Computer Science, University of Technology, Baghdad, Iraq.
E-mail: suhiar.m.abdllsammed@uotechnology.edu.iq

Abstract
Drones, with their unauthorized path, threaten aircraft and airport systems, emergency procedures, and passenger safety. Therefore, an idea can be made that helps detect and monitor unauthorized drones, which are radars that monitor aircraft, where the aircraft is captured and its information is stored in a database. The information is the aircraft number and the name of the aircraft. And the name of the radar that captured the plane, the radar number, and the time the plane was captured with a picture of the plane. 4 radars can be used, each containing its own hard drive-in which information is stored, and the special hard drive for each radar is linked to the database of the main site, which in turn is linked to a special network for this purpose and to make a connection between it and the institution's website. Overall, this drone photo capturing system presents a valuable tool for improved security and efficiency in airspace management. However, addressing privacy concerns and ensuring robust cybersecurity are crucial for successful implementation.

Keywords: unauthorized Drones, monitor aircraft, threaten aircraft, radar, captured

1. Introduction:

The flow of drones in our current area in the airspace has raised great concerns in countries, as their illegal use has led to an increase in danger and breach of safety meanings, and the development in the challenges of detection and identification of these aircraft has become very important for the advanced detection of unauthorized drones By entering countries for fear of reaching sensitive institutional areas.[1] Therefore, determining the identity of the plane and the legality of its entry, either through jamming or hunting according to a specific system, seemed to be an issue that occupies the interest of most countries in the world.[3]

Unauthorized drones refer to drones that are not legal or permitted for use in specific areas or under certain circumstances.

This can include flying drones in restricted airspace, such as near airports or government facilities, or using drones without the necessary permits of licenses. [5]

2. Related Works:

The search term "A Review on Software-Based and Hardware-Based Authentication Mechanisms for the Internet of Drones" touched Emmanouel T. Michailidis in 2022. Each component of the heterogeneous air as well as ground network is linked together and outfitted with cutting-edge sensors, communication modules, and processing power. IoD network evolution presumes mitigation of numerous privacy and security concerns. Therefore, for achieving secure operation within the IoD, strong authentication methods should be established. Yet, developing lightweight and effective authentication solutions is a difficult task because of the intrinsic characteristics of the IoD and the power, computational, and memory limitations of unmanned aerial vehicles (UAVs). Setting up sophisticated sensors that are connected to a communications device, an air and ground network, and an approach of elliptical encryption, public key encryption, or machine learning for reducing privacy and security risks.

The article "On the Detection of Unauthorized Drones - Techniques and Future Perspective" by Hamid Menouar, Muhammad Asif Khan, Adnan Abu-Dayya, Aisha Eldeeb, and Flora D. Salim originally appeared in 2022. In order to safeguard individuals' privacy from drones, drone detecting systems are essential. A system for detecting drones that is accurate, reliable, strong, and affordable is required. Owing to the significance of the issue, numerous drone detection techniques were put out over time. Because of the intrinsic shortcomings of the underlying detecting technology, none of them offer adequate performance. Numerous performance criteria exist, including robustness against environmental conditions, accuracy, detection range, and more. This encourages a thorough examination and critical evaluation of current methods, stressing both their advantages and

disadvantages. This study presents a critical analysis regarding the state of the art and provides a comprehensive overview of current drone detection technology. We offer important insights into upcoming drone detection systems based on the review. We think that such revelations will enable researchers and engineers in the field a thorough understanding of the larger environment around the drone detection problem.

In 2015 Chris Sandbrook" The social implications of using drones for biodiversity conservation " Unmanned aircraft and their contribution to mitigating problems, and for the conservation sector to agree on a reasonable framework for self-regulatory use of unmanned aircraft without authorization to fly in the air. Until such research and regulation is done, it would be wise to avoid spreading the widespread use of non-conservation-authorized drones.

3. Drone Management System (DMS)

A drone management system (DMS) for hunting unauthorized drones involves using a combination of hardware and software tools to detect, track, and neutralize unauthorized drones. One common tool used in such systems is the drone detection sensor, which can be either radar or a camera-based system. Those sensors are capable of detecting if there is a drone in the airspace and present real-time data about its speed, location, and altitude [18]

Usually, DMS is based upon UAV Tracking and Management System that utilizes the data that had been obtained by the detection sensors of theradarfor tracking the movements of thedroneand providing alerts to system operators. The software may be programmed as well for automatically taking action to neutralize the drone, for example, jamming its control signals or using an anti-drone system to physically intercept and disable itand after that, the DMS systems may be utilized in various settings, such as event securityandborder security.[17] It should be noted that the use of the anti-drone technology is conditional on strict regulations in several countries and it is of high importance to make sure that any DMS system operates according to the local rules and regulations.

4. Unauthorized drones

There aremany common systems fordrone control that are utilized in the DMS for neutralizing the unauthorized drones, examples include: [14]

Radio Frequency (RF) Jamming: This system ofdroneneutralization works through cutting off communications between the drone and the operator. The jamming system transmits signal on a similar frequency to the control signal of thedrone's, which is effective in blocking the ability of thedrone in receiving commands from the operator.

GPS spoofing: Some of theantidrone systems utilize the GPS spoofing for tricking a drone into thinking that it’s somewhere else or flying at an altitude that is not actually precise. Which might cause the drone to lose its bearings and crashing or plummeting.

Laser systems: those can be utilized for disablingdronesthroughtargeting their electronic mechanisms, like navigation systems orcamera. Lasers can be utilized as well for blinding the pilot of thedrone, which makes it quite difficult for them to control the drone. [10]

Net Cannon: which can be defined as anti-drone system involving shooting a net at the drone for the purpose of disabling it. The web can get entangled with the propellers of thedrone, which causes it to lose the power and fall down.

5. Some local laws and regulations of the use of the counter-drone technology

Lawsandregulationsofutilizing the counter-drone technology range from one country to another and those could get complicated. On other hand, here are a few examples of the local laws and regulations in various locations:[16]

US: where the FAA (i.e.,Federal Aviation Administration) is responsible for the regulation of theuseof the drones and counter-drone technology. This administration established guidelines for counter-drone technologyoperation, which included the restrictions on utilizing specific counter-drone systemtypes near the other sensitive locations such asairports.

European Union: In the EU, using counter-drone technology is regulated byGDPR(i.e., General Data Protection Regulation) as well as other laws concerned withprivacy. Those laws require that any data that are collected by the anti-drone systems should be lawfully and transparently processed and that the individuals have rights of accessing and controlling their private data.

UK: where CAA (i.e., Civil Aviation Authority) is responsible for the regulation of theuse of drones and counter-drone technology. CAA established the rules for counter-drone technologyuse, which included the restrictions on using specific types of systems near the airports as well as other sensitive locations. [15]

Canada:TransportCanadais responsible for the regulation ofcounter-drone technology uses, it had set upguidelines for counter-drone technology uses, and thatincludesrestricting the use ofspecificsystemtypes near some locations like the airports.

6. Counter-drone TechnologyGuidelines

There are many differences concerning counter-drone technology guidelines, as thosedifferby different countries and the technologyapplication itself. On the other hand, some general instructionsarerecommended,often in cases of the DMS implementationswiththe counter-drone technology:
Abiding by the local laws: It should be ensured that any DMS system is operated based on the local drone operation and counter-drone technologyregulations. This could be including obtaining the important permissions from the authorities. [11]

Minimizing collateral damage risks: Counter-drone technologies must be designed for minimizing collateral damages to properties, people, and other aircraft. Using kinetic counter-drone systems, like the laser systemsornet guns, must be considered carefully in order to avoid accidental consequences.
Risk assessment: which should be performed for the identification of the possible threats from the unauthorized drones and for the determination of appropriate counter-drone technologies formitigatingsuch threats.
Privacy considerations: Counter-drone technology must be designed forrespectingtherights to privacy andhave to be utilized only for purposesitwas intendedfor. Data that is collected by the counter-drone systems must be transparentlyandlawfully processed, and people must have the right of accessing and controlling their own data.
Coordination with the local authorities: and that includes aviation authorities andlaw enforcement, which could be highly important for ensuring the safety and effectiveness of counter-drone technology uses.
Training and proficiency: counter-drone technology operators need to undergo the necessary training and must be skillful in using the technology for ensuring effective andsafe operations.

7. Drone Regulations

Several countries implemented regulations for governing droneuses, which includerequirements related toregistration, restricteddesignationsofairspaces, anda penalty for operating drones with no proper authorizations. [16]Such regulations have the aim of deterring the unauthorized drone operations and facilitating drone ownertracking.

8. Radar (Radio Detection and Ranging)

Radar(which is referred to as the radio detection and ranging as well) operates through transmitting microwave radio waves that reflect back to radar antenna when colliding with some object, such as another aircraft. Subsequently, the radar system computes the object's velocity and distance by measuring the time it takes for the waves to return. The shape and size of the item could be ascertained by the radar system using the strength of reflected signal. After that, this data is shown on a screen for operators to review. Pulsed radar and continuous wave radar are the two main aircraft detection technologies used by radar systems. [21] Pulsed radar emits brief radio wave bursts, or pulses, and after that pauses until the signal is reflected before emitting another pulse. The distance to the item is determined by measuring the interval between the pulse's transmitting and receiving. The drone's direction and speed could be ascertained by the radar system by sequentially sending out several pulses. Furthermore, the continuous wave radar constantly generates radio waves while monitoring for variations in the frequency of reflected signal brought on by the Doppler Effect. The shift in frequency that happens as a drone target moves in relation to a wave source, like radar, is known as the Doppler

Effect. The radar system measures the Doppler shift to ascertain the direction and speed of an object. [12]

Modern radar systems often use a combination of these technologies, as well as other advanced signal processing techniques, to achieve higher resolution and better target discrimination. In addition, many radar systems are now equipped with computer algorithms and machine learning techniques that can help identify and track multiple targets simultaneously and without interference.

9. Materials and Methods:

In this section include proposed system design, suggested drone detection model.

9.1. Proposed System Design

The major idea of the system refers to dividing the area that we want to monitor in to four sections. Each section has its own radar to monitor the drones pass through its sky.

Each radar contains a hard disk that stores information about the drones.

The hard disk is connected to the system database where the database imports data from the radar when picking up any new drone.

When any new drone is captured, notifications will appear including that anew drone has been captured.

9.2. The Suggested Drone Detection Model:

In this section involves many steps, send data from radar, show a pop-up to information, and inter to condition yes or no. show in Figure 1., Figure 2., and Figure 3.

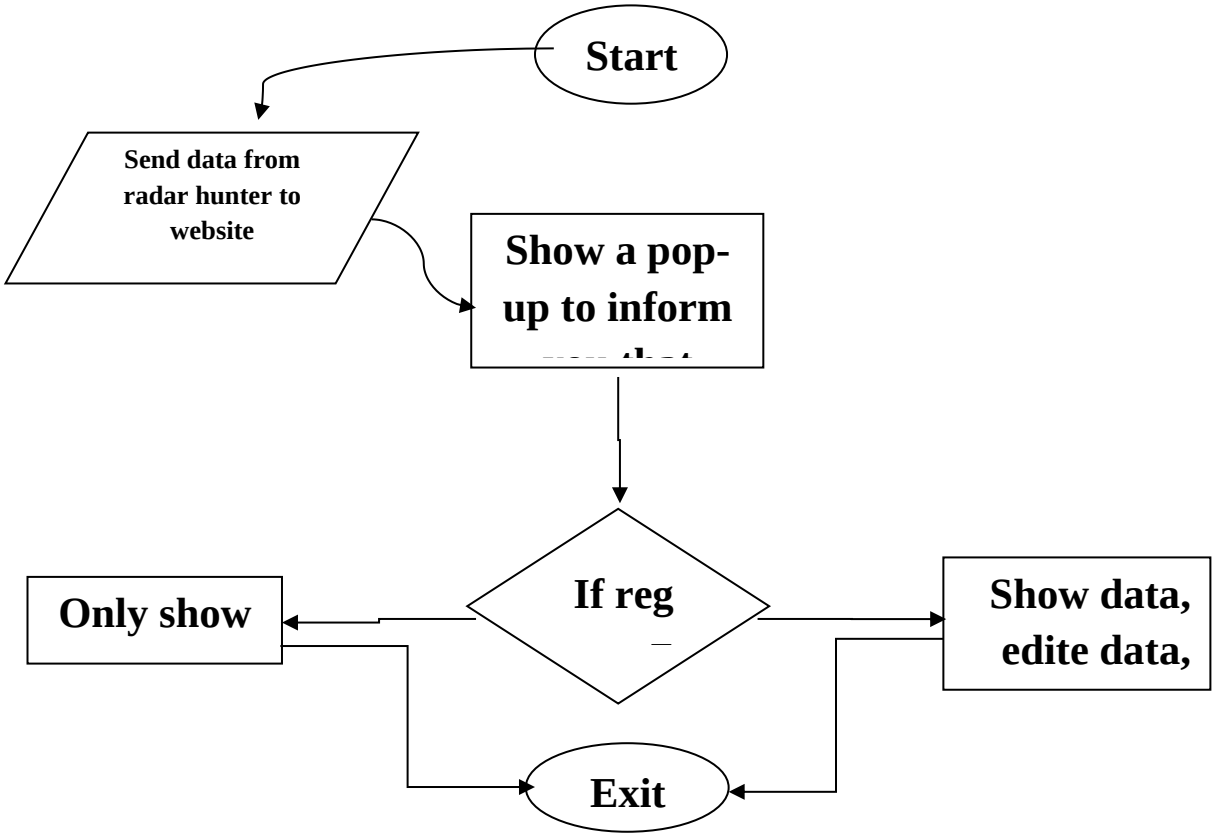

Figure 1. Proposed Drone Detection Model flowchart

Algorithm 1: Proposed system Algorithm.

```
Data: capture image drone
Result: Drone information
Initialization;
Perform drone detection and classification and payload recognition;
If capture image do not equals to the data in database program then
Perform perceived Threat Analysis;
Check Drone Data status
else
If object status harmful then
Show data;
Edit data;
Remove data;
Else
 Just show data;
Show a pop-up that a new Drone;
end
```

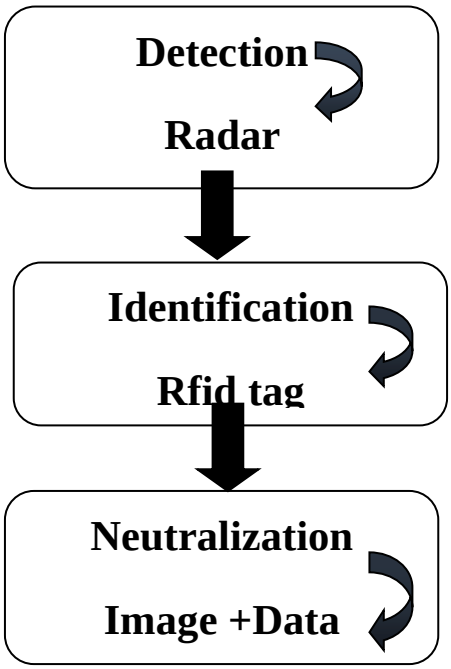

Figure 2. Components of an anti-drone system

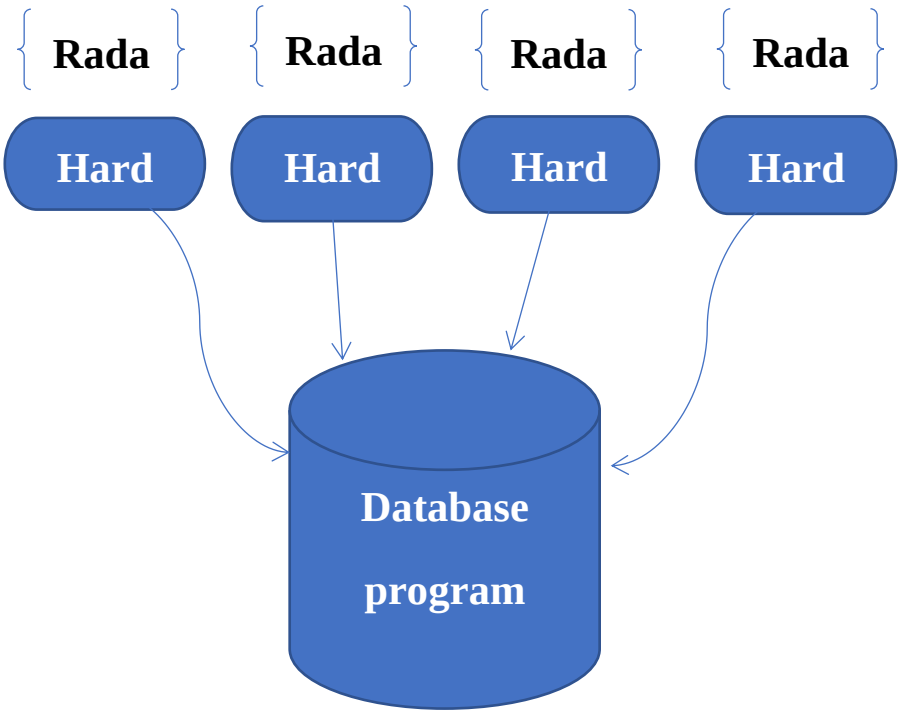

Figure 3. flowchart database program

9.3 Capture drone information

To capture drone information for use in radar chart, will need data on multiple variables that want to compare that could be relevant for a drone: as shown in Figure 4., Figure 5., Figure 6., Figure 7., Figure 8., and Figure 9.

ID drone			
Radar name	*Image*	*Number*	*Name drone*

Figure4.Information table

Figure5.Captured drone information

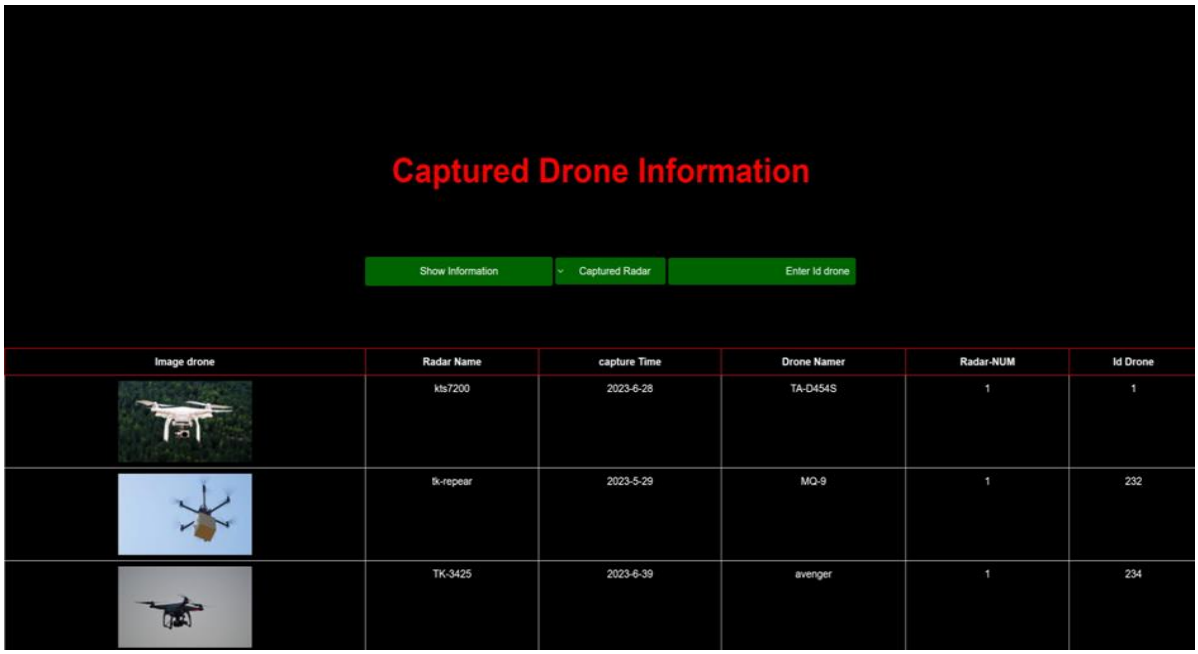

Figure 6. Information for Drones

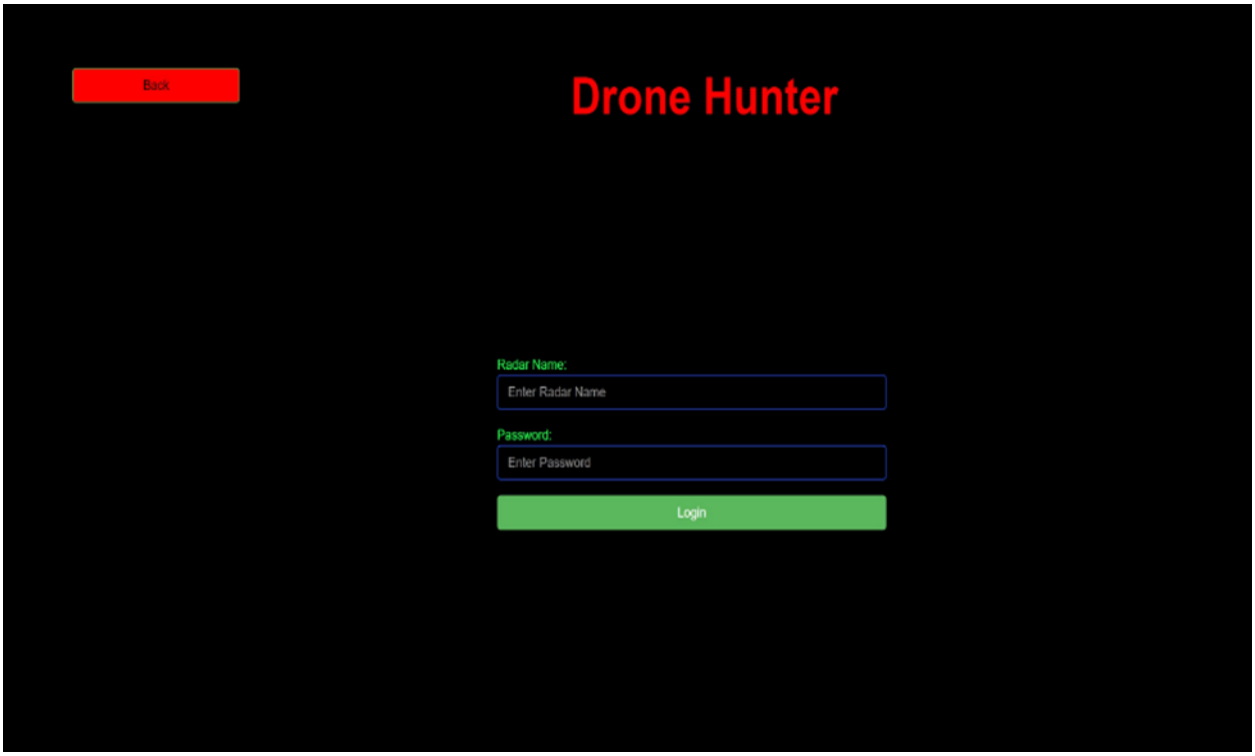

Figure7.Login system

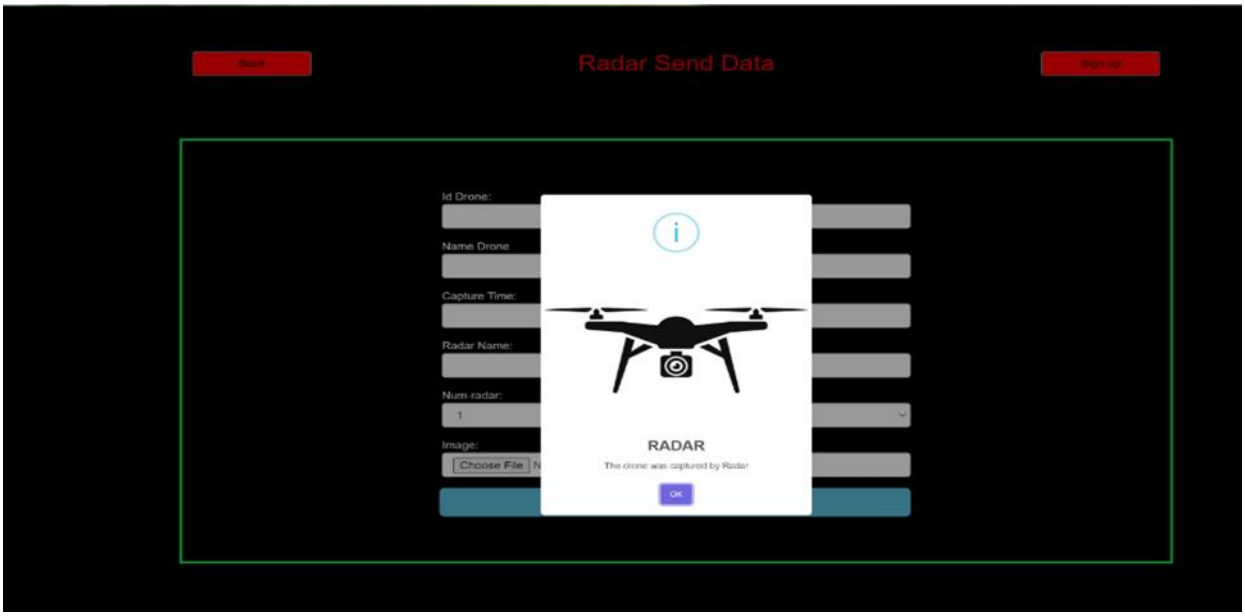

Figure 8 Radar send data

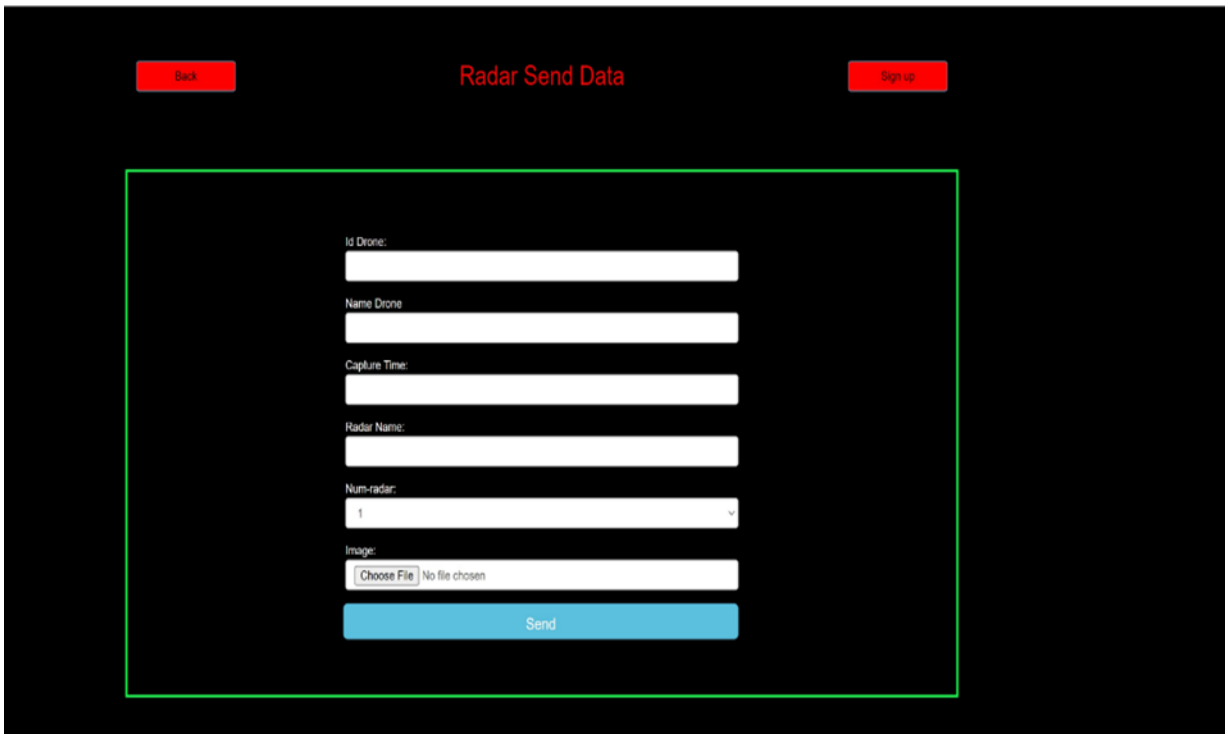

Figure 9 Radar saved data

9.4 Gather Data for the "Radar Hunter"

1- Manufactures 'Website by visiting the official website of the drone who captured by radar

2- Customer Reviews who have purchased and used the radar hunter

3- Check online drone retailers to find product descriptions and

Specifications

4- Join drone enthusiasts and users to find discussions about the radar hunter

- Figure 10 as shown how the Radar Hunter saved data.

Figure 10 Radar saved data

10 Test and Result Methods:

In this section include the output of proposed drone management system radar hunter.

10.1 Output:

The output includes: sign up, how radar works, show data in system, analysis of system, challenges, improvements, value add, and author contributions.

10.1.1 Sign up

Authentication is essentially the process of verifying someone or something is who or what they claim to be. In the digital world, it's most commonly used to confirm a user's identity when trying to access a system or online account.

10.1.2 How a radar works

Detect drones When the radar senses a drone entering the area it is responsible for, it takes pictures of it and stores them on its hard drive.

Radar send data When the radar sends the captured drone data to the system database, the system will display notifications to the user that a new drone has been captured.

Data structuring The data is structured in tables containing the drone's name, its ID number, the time it was captured, the radar that captured it, and its ID number.

10.1.3 Show data in system

The data in the system is displayed in a table format. It is also possible to search for the data of each radar by its ID number.

10.1.4 Analysis of system

System Features:

- ✓ **Data Collection**: The system collects vital information about drones, such as their name, ID number, the ID number of the radar that captured the images, and photos of the drone.
- ✓ **Tracking**: The system allows for tracking the movements of drones within its designated airspace.
- ✓ **Security**: The system aids in monitoring the airspace and preventing unauthorized activities.
- ✓ **Data Analysis**: The collected data can be used to analyze drone traffic patterns and identify potential risks.

10.1.5 Challenges:

- **Privacy**: Collecting drone data may raise privacy concerns.
- **Cybersecurity**: The system must be secured against hacking and cyberattacks.
- **Integration**: Integrating the system with other systems, such as air traffic control systems, can be challenging.
- **Cost**: The cost of installing and maintaining the system can be high.

10.1.6 Improvements:

- **Integration of Artificial Intelligence Techniques: AI can be used to analyze images automatically and identify suspicious drones.**
- **Developing an Interactive User Interface: A user interface can be developed to allow users to view and analyze data easily.**
- **Enhancing Integration with Other Systems: The system can be integrated with other systems, such as air traffic control systems, to enhance security and efficiency.**

10.1.7 Value Added:

- **Improved Security: The system helps improve security and prevent unauthorized activities.**

- **Increased Efficiency: The collected data can be used to enhance the efficiency of aerial operations.**
- **Decision Support: The collected data aids in better decision-making.**

A drone photo capturing system is a valuable system that can be used to improve security and efficiency in various domains. However, certain challenges, such as privacy and cybersecurity, need to be addressed.

10.1.8 Author Contributions

Conceptualization,
Data creation,
Formal analysis,
Funding acquisition,
Investigation,
Methodology,
Project administration,
Resources,
Validation,
Writing—original draft
Writing—review and editing,

Conclusions

To close such gap in current anti-drone system designs which concentrate only on drone detection with minimal effort for harmful screening, a 4-radar designed program for the purposes of attachment object identification, drone detection, and a secure channel neutralization model are presented in this work. Four radars have been utilized to upload drone images and capture several drone models of varying sizes in cloudy circumstances in order to provide superior detection and extensive coverage for

identification. The image of the drone, its number, and the radar number that detected it are also recorded in a database along with other relevant information about the intended drone. This information is after that compared to the database that has been stored to ascertain whether or not the drone is listed as authorized to enter the airspace. Those results set important new standards for the development and design of anti-drone systems, which serve as a defensive mechanism to maintain safety and order in both international and domestic airspace and to restrict the use of drones for illicit purposes without permission or entry authorization.

However, there are still issues such as inaccurate identification associated with Drone identification ofDrone and other objects camouflaged in their surrounding environment, and identification of Drone in international airspace so the need to address remains for robust performance of spot-based counter vision and trapping Within unmanned aircraft systems.

References

1. Tao, J.; Han, T.; Li, R. Deep-Reinforcement-Learning-Based Intrusion Detection in Aerial Computing Networks. *IEEE Netw.* **2021**, *35*, 66–72. [Google Scholar] [CrossRef]
2. Taha, B.; Shoufan, A. Machine Learning-Based Drone Detection and Classification: State-of-the-Art in Research. *IEEE Access* **2019**, *7*, 138669–138682. [Google Scholar] [CrossRef]
3. Shi, X.; Yang, C.; Xie, W.; Liang, C.; Shi, Z.; Chen, J. Anti-Drone System with Multiple Surveillance Technologies: Architecture, Implementation, and Challenges. *IEEE Commun. Mag.* **2018**, *56*, 68–74. [Google Scholar] [CrossRef]
4. Floreano, D.; Wood, R.J. Science, Technology and the Future of Small Autonomous Drones. *Nature* **2015**, *521*, 460–466. [Google Scholar] [CrossRef] [PubMed][Green Version]
5. Park, S.; Kim, H.T.; Lee, S.; Joo, H.; Kim, H. Survey on Anti-Drone Systems: Components, Designs, and Challenges. *IEEE Access* **2021**, *9*, 42635–42659. [Google Scholar] [CrossRef]
6. Haviv, H.; Elbit, E. Drone Threat In addition, CUAS Technology: White Pape. *Elbit Syst.* **2019**, *1*, 1–20. [Google Scholar]
7. Ripley, W. Drone with Radioactive Material found on Japanese Prime Minister's Roof. CNN.com. 2015. Available online: https://edition.cnn.com/2015/04/22/asia/japan-prime-minister-rooftop-drone/index.html (accessed on 31 January 2022).
8. Reuters. Greenpeace Slams Superman-Shaped Drone into Nuclear Plant. *New York Post*, 3 July 2018; Volume 1, 1–2. [Google Scholar]
9. Phillips, C.; Gaffey, C. Most French Nuclear Plants 'should be shutdown' over Drone Threat. *Newsweek Magazine*, 24 February 2015; Volume 1, 1–3. [Google Scholar]
10. Hubbard, B.; Karasz, P.; Reed, S. Two Major Saudi Oil Installations Hit by Drone Strike, and US Blames Iran. *The New York Times*, 14 September 2019. [Google Scholar]

11. Akter, R.; Doan, V.S.; Lee, J.M.; Kim, D.S. CNN-SSDI: Convolution Neural Network Inspired Surveillance System for UAVs Detection and Identification. *Comput. Netw.* **2021**, *201*, 108519. [Google Scholar] [CrossRef]
12. Gopal, V. Developing an Effective Anti-Drone System for India's Armed Forces. *Obs. Res. Found. Issue Brief* **2020**, *1*, 1–20. [Google Scholar]
13. Çetin, E.; Barrado, C.; Pastor, E. Counter a Drone in a Complex Neighborhood Area by Deep Reinforcement Learning. *Sensors* **2020**, *20*, 2320. [Google Scholar] [CrossRef][Green Version]
14. Bhatnagar, S.; Gill, L.; Ghosh, B. Drone Image Segmentation Using Machine and Deep Learning for Mapping Raised Bog Vegetation Communities. *Remote Sens.* **2020**, *12*, 2602. [Google Scholar] [CrossRef]
15. Bemposta Rosende, S.; Sánchez-Soriano, J.; Gómez Muñoz, C.Q.; Fernández Andrés, J. Remote Management Architecture of UAV Fleets for Maintenance, Surveillance, and Security Tasks in Solar Power Plants. *Energies* **2020**, *13*, 5712. [Google Scholar] [CrossRef]
16. Sun, H.; Yang, J.; Shen, J.; Liang, D.; Ning-Zhong, L.; Zhou, H. TIB-Net: Drone Detection Network With Tiny Iterative Backbone. *IEEE Access* **2020**, *8*, 130697–130707. [Google Scholar] [CrossRef]
17. Carrio, A.; Tordesillas, J.; Vemprala, S.; Saripalli, S.; Campoy, P.; How, J.P. Onboard Detection and Localization of Drones Using Depth Maps. *IEEE Access* **2020**, *8*, 30480–30490. [Google Scholar] [CrossRef]
18. Shi, Z.; Chang, X.; Yang, C.; Wu, Z.; Wu, J. An Acoustic-Based Surveillance System for Amateur Drones Detection and Localization. *IEEE Trans. Veh. Technol.* **2020**, *69*, 2731–2739. [Google Scholar] [CrossRef]
19. Dogru, S.; Marques, L. Pursuing Drones with Drones Using Millimeter Wave Radar. *IEEE Robot. Autom. Lett.* **2020**, *5*, 4156–4163. [Google Scholar] [CrossRef]
20. Alnuaim, T.; Mubashir, A.; Aldowesh, A. Low-Cost Implementation of a Multiple-Input Multiple-Output Radar Prototype for Drone Detection. In Proceedings of the 2019 International Symposium ELMAR, Zadar, Croatia, 23–25 September 2019; pp. 183–186. [Google Scholar]
21. Guvenc, I.; Koohifar, F.; Singh, S.; Sichitiu, M.L.; Matolak, D. Detection, Tracking, and Interdiction for Amateur Drones. *IEEE Commun. Mag.* **2018**, *56*, 75–81. [Google Scholar] [CrossRef]

Survey of Verification Communication Protocol Security using Computational Models

Ghadeer Ibrahima
Technical Institute of Al-Diwaniyah, Al-Furat Al-Awsat Tehnical University (ATU), Al-Diwaniyah, Iraq

المؤتمر العلمي الدولي الثالث عشر
لجمعية الرياضيات العراقية والمنعقد تحت شعار
نحو عالم متقدم : الرياضيات والتقنيات في سباق الابتكار
للمدة 24 - 25 نيسان 2024
الكوفة – النجف الاشرف

ABSTRACT

Nowadays, as a result of the rapid advancement of technology and the development of new communication concepts between people like the Internet of Things (IoT) and Social Media, it is now crucial to protect the privacy and security of those communications from unauthorized access. The process of interpersonal communication requires the use of protocols that provide mutual authentication and encryption of transmitted data. In this paper, the most commonly used models are presented to prove the security of the protocol. In addition to how to achieve authentication between the parties, it may give an overview of these models such as reductionist and Simulatability, types, and how they are used in the analysis of protocols.

Keywords: Protocols, Computational Models, Authenticated Key Exchange, Random Oracle Model, Secure Channels.

Introduction

Protocols are a set of rules agreed upon between two or more parties to transfer data between the parties correctly without tampering [1]. The security objectives that these protocols seek to achieve are represented in two parts, the first being the exchange of authentication and the secondly generating a shared secret key to encrypt and decrypt messages. Where authentication takes different forms for the parties to prove their identity to each other, these forms include [2]:

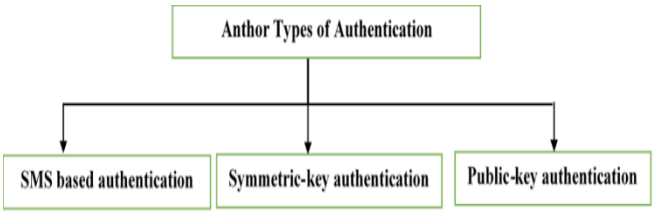

Fig. 1. Types of Authentication

It is possible to build such protocols to establish a session and exchange information between the parties, but there is a fundamental problem represented by the adversary that has the possibility of interference between the parties [2]. The adversary can be worked changes the messages (deleting, adding, modifying, ... etc.) or can enter the session as one of the parties participating in it or impersonate one of the parties such as the individual responsible for the session or the other parties, and this is a big problem. Therefore, when a protocol is designed, it must prove the safety feature, as we prove that the adversary cannot break the security of this protocol. To achieve this, one must first choose the concepts of security that correctly diagnose the adversary's objectives and how much information it possesses. Secondly, a suitable security model must be identified with the protocol that helps in proving the safety feature, which is the area currently covered by the research [3]. As the tools and techniques that lead to protocol analysis are growing faster, and the reason for this is due to the adversary's ability, which

is limited or unlimited, in breaking the security of the protocol. The adversary can be classified into several types according to the capabilities of corruption:

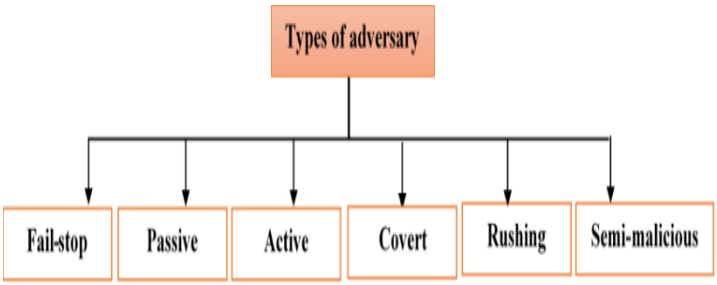

Fig. 2. Types of Adversary

It is necessary to limit the adversary's ability. This can be done by building a safety protocol against his attacks. It is possible to know whether the protocol achieves the security objectives or not through mathematical models that depend on the random oracle model [4]. There are no common high-level criteria used to evaluate these models. According to reality, the models should be just a meaning that does not depend on any assumptions or definitions [3]. In addition, the form must be preserved, meaning no parameters whose specification is not defined within the model or depends on certain assumptions beyond it. Having this feature of models makes it easy to design independent protocols that do not link with each other. The form must be clear and accurate, not subject to false or ambiguous interpretation. Therefore, in this paper, we will deal with some security models that include protocols for exchanging keys between two, three, or a group of participants.

2. RANDOM ORACLE MODEL

How can an adversary break the security of the protocol and how does it know the information about the keys? In order to be able to analyze the protocol, we must first determine the opponent's hostile capabilities on the protocol. This is represented by queries made by the opponent to obtain information. In each model, it is assumed that the opponent has complete control over all sessions (communications) in the network, so he interacts with them through inquiries that are sent to Oracle, and he gets an appropriate response. Those inquiries must be acceptable to Oracle [4].

It can be expressed as a closed, protected black box that gives a correct response to every query (input) that is within this box but gives a random response to non-existent queries, and the type of response is within its output. It gives the same response every time a query is requested from it. Work of the function can thus be summarized [5]:

1. If the entered query is not found in the box, the response will be a random output from its potential output. It generates an output for every query entered into it. Then add this query that does not exist and output it to the box.

2. If the entered query exists, it gives the result (response) that was previously saved.

Oracle Random was added by Bellare and Rogaway for the first time [6]. It differs from the hash function in that the result of the function cannot be calculated by the adversary or the people participating in a communication session (when adversary requests a random oracle query that is through a secure channel, the output is calculated inside Oracle, and then the response is returned through the same channel). The oracle model has been used to prove the security of protocols on a large scale, but it is not considered completely perfect because it does not mean that when the hash function is used to substitute the random oracle, the system remains secure. but the oracle model remains better than others. Informal description of the oracle queries [7]:

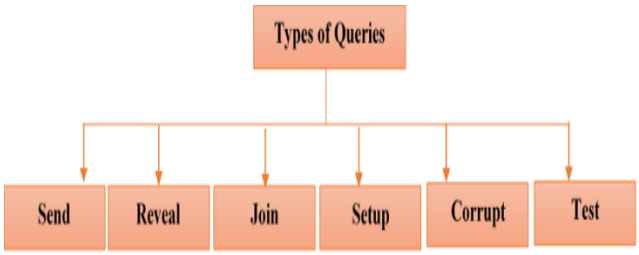

Fig. 3. Types of Queries

Table 1- Types of queries.

Queries	Definition
Send	The Adversary makes this query as a start to accept the Adversary as a member without giving him the information. When he sends this query, it must be acceptable to Oracle for the opponent. It is possible through this query to return Oracle or accept or reject.
Join	When the protocol is being executed this query is used for eavesdropping. This query is intended only for the Adversary, because the members participating in the session do not inquire, so a copy of the implementation of the Adversary is given.
	When the protocol is being executed this query is used for eavesdropping. This query is intended only for the Adversary, because the members participating in the session do not inquire, so a copy of the implementation of the Adversary is given.

Setup	
Corrupt	This query is used to obtain long-term keys and corrupt the session by impersonating the Adversary as one of the participants in the session.
Test	This is a kind of comparison query that an Adversary can request from Oracle at any time. Oracle generates a random bit and it is compared with the Adversary bit. If the result is one, the keys are given to the Adversary, and if it is zero, the attacker will return a random string. This query is requested by the attacker only once.

There are several models used to prove the safety of protocols and measure their analysis. We will discuss them. The chart below shows the models used, their families and types:

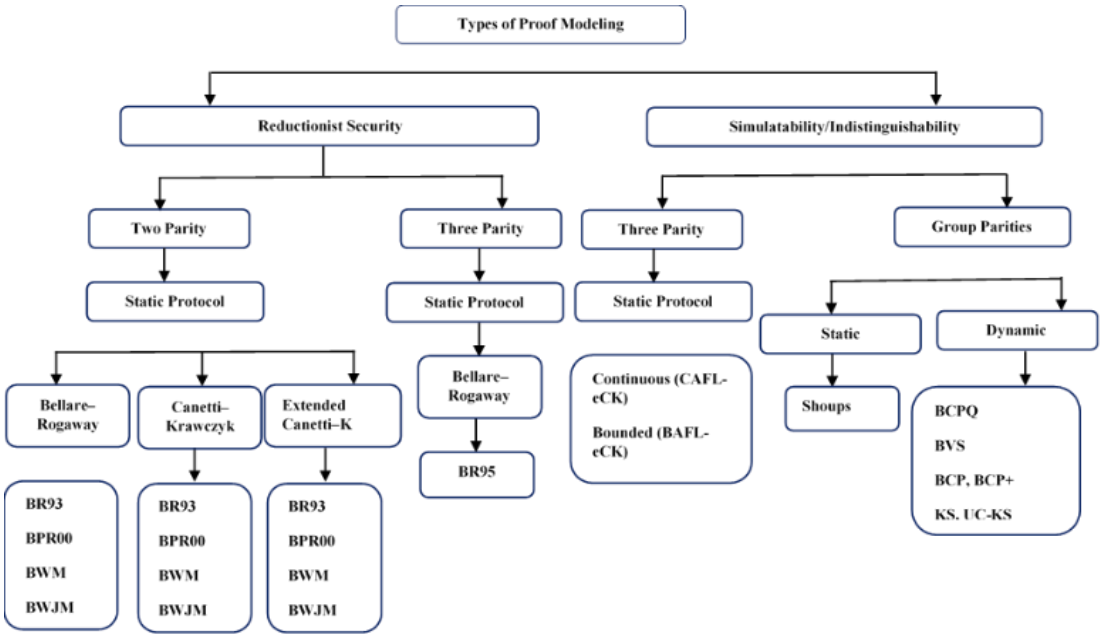

Fig. 4. Types of proof modeling.

3. OVERVIEW OF MODELS

What are the models and why do we use them? Models are functions that are applied to protocols that assume an environment contains both session subscribers and the attacker. They give the attacker a variety of different information depending on the model from the session to see how well the protocol can resist the attacker. These models are used to analyze and break protocols [8].

The information varies from one model to another. There is information that enables the attacker to know the session key, and information that is weak. Here the measure is the quality of the information, not the quantity [9, 10].

A) The models are divided into two main parts: Reductionist Security Proofs and Proofs Based on Simulatability/Indistinguishability.

1) Reductionist Security Proofs

Security of protocols or called security game which played between the adversary and its environment. The game starts with public keys and other parameters, if the adversary stops and gives its output then the game end, specified condition, and security based on the success of the adversary in the game.

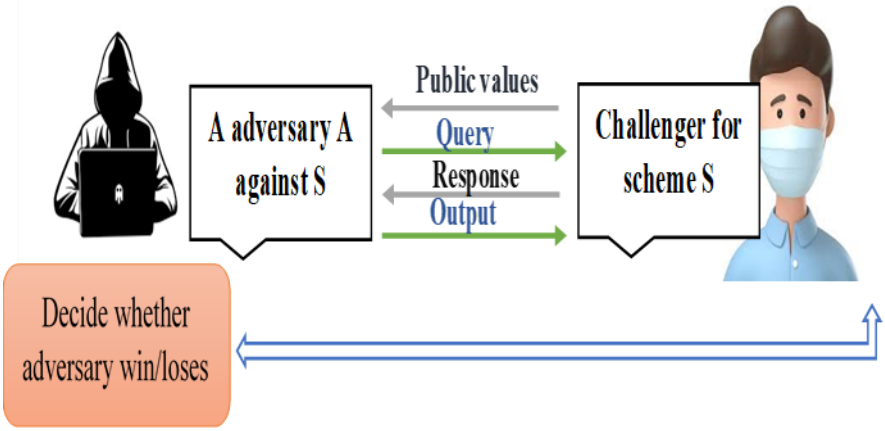

Fig. 5. Example of security model.

2) Proofs Based on Simulatability/Indistinguishability

Type of modeling:

1. Bellare–Rogaway Model (BR)

It was proposed by Bellare & Rogaway and is considered the first model that demonstrates opponent capabilities with the definition of security. Scientific research began to move towards this goal since then and resulted in the presentation of many protocols and security computational models. Include of many types [6, 7, 11]:

Can be considered as a particular kind of computational security strategy, where the security of a cryptographic construction is derived from the indistinguishability of the ideal and real executions.

Table 2- Description of Br93 Model.

Definition	Actions
BR93 model	Bellare and Rogaway started the study of entity authentication and key distribution in 1993. BR93 uses matching conversations to define partners. Transitions between two party in the BR93 model are small events. A conversation is a finite sequence of events, where form event (p; q; y) for a time p, an input message q and an output message y. if two users $C_A = (\tau 0\ ,\ 'start',\ \alpha 1),\ (\tau 2\ ,\ \beta 1\ ,\ \alpha 2)$ and $C_B = (\tau 1\ ,\ \alpha 1\ ,\ \beta 2),\ (\ \tau 3\ ,\ \alpha 2\ ,\ *\ ),\ for\ \tau 0\ <\ \tau 1\ <\cdots$
Properties that determine the security	Mutual Authentication and Key Establishment or authenticated key exchange
Drawbacks	1. every party has a long-term key shared with every other party. 2. There is a strong conjugation between key exchange and authentication. 3. There are limited adversarial capabilities.

Table 3- Description of BR models.

Model	Setting	Partnering mechanism	Gap
BR93	Two-party shared key	Matching Conversations	coupling authentication with key exchange
BR95	Server-based	Partner function	Unpair the previous model, but there is no authentication for the reason for using partner function
BPR2000	Password-based	Session identifiers	Use password for authentication is considered weak method so not provide forward secrecy.

BWM	Public key	Matching Conversations	It is a good model for relying on encryption and signature.
BWJM	Key agreement	Matching Conversations	It is a good model for relying on AK and AKC.

2 . Canetti–Krawczyk (CK)

The second family of models includes

Table 4- Description of Ck Models

Model	Setting	Partnering mechanism	Gap
BCK98	Two-party shared key	• authenticated links (AM). • unauthenticated links (UM)	Problems the opponent obtains session keys and long-term keys by corruption query, Shoup called this strong adaptive corruption.
CK01	Two-party shared key	Session identifiers	**1. Session identifiers:** no concrete definition of how they are obtained. **2. Session state query:** It does not provide a perceptual definition of a session's state. **3. Restrictions on queries:** If there is a current session, a new session cannot be queried.
HMQV	Two-party shared key	Session identifiers	Principal B with partner C has a session identifier (IDB; IDC; MO; MI) where MO and MI are messages received and sent by the session.

3) Extended CK (eCK)

It based on long-term secret and an ephemeral secret. sessions identifiers are (role; IDA; IDB; Out; In) and (role'; IDB; IDA; In; Out) with role' ~= role. Queries in eCK are (send, reveal, ephemeral, long-term, test) [12, 13].

Table 5- Description of Eck Models

Model	Setting	Powerful
MU08	Two-party shared key	This model provides poor security that prevents an opponent from submitting a long-term query. It crosses weaker than eCK and stronger in other models
eCKw	Two-party shared key	allows the opponent to replay the message and obtain the long-term key.
eCK-PFS	Two-party shared key	opponent obtain on the long-term key
seCK	Two-party shared key	it provides the opponent with space to obtain intermediate information on session keys.

4) The Generic After-the-fact Leakage-eCK ((·) AFL-eCK) Model

This includes both types of security models continuous after-the-fact leakage eCK (CAFL-eCK) model and the bounded after-the-fact leakage eCK (BAFL-eCK) model. The first type of forms gives the opponent the power to obtain specific information from long-term secret keys, as well as knowledge of the session key and temporary keys. The second type allows the opponent to obtain continuous large information about the long-term key and the session key [14].

Continuous After-the-fact Leakage-eCK (CAFL-eCK)	Bounded After-the-fact Leakage-eCK (BAFL-eCK)
Here, information about the keys can be leaked continuously during the session between the parties, but the main determinant of this model is that obtaining the session keys depends on the	The information that may be available to the adversary through this form is specific and primitive. Therefore, the total rate of long-term key leakage and the session proposal is restricted according to the information obtained. In short, the strength point depends on the amount of information obtained, as well as its importance. If this information is important and sufficient to break the protocol, the session has been hacked,

parameters that the adversary can obtain.	otherwise, the opponent will find it difficult to penetrate the session.

Table 6- Description of Models.

5. Shoup's Simulation Model

This model is considered a starting point, different from the above models, as it provides two systems, one of them the ideal system and the other the real system. Shoup's model allowing three different powers to corrupt principals (Static corruptions, Adaptive corruptions, Strong adaptive corruptions). The table below shows the difference between the two systems [15, 10].

TABLE 7- Description of the types shoup Model.

Real System	Ideal System
1. The adversary controls the networks 2. Adversary has no information about the keys and random values 3. A trusted third party TTP is defined, and the principals can interact with this part to obtain the long-term key.	1. The adversary runs the protocol by initializing users, where their tasks are • starting and ignoring sessions. • reactive with applications. 2. The adversary in this case will decide which sessions will be connected. 3. Session keys are not chosen traditionally but rather independently and randomly of other parameters.

6.Group key exchange Modelling

Protocols consist of two types [16]:

1. Dynamic-group key-exchange protocols: In order to deal with dynamic group changes in following protocol sessions more efficiently, participants must generally store more auxiliary information.

Dynamic GKE protocol consists of:

- Each party in the protocol execute an initialization algorithm.
- A setup protocol used to initialize the group members and initial session key computation.
- A joint protocol between the current-group members and a set of joining members.
- A remove protocol is executed over the remaining group members after a subset of group members has been excluded.

2 . Static protocols: the auxiliary information is chosen fresh for each new protocol execution. Therefore, strong corruption attacks against dynamic protocols become much more critical

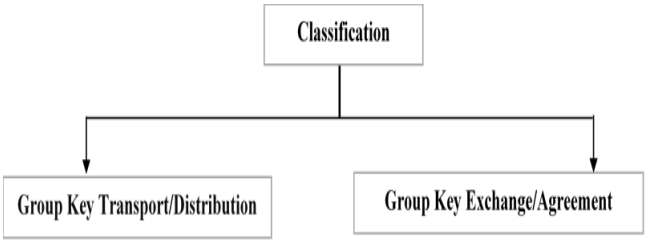

Fig. 6. Types of key group.

1. Group Key Transport/Distribution

In this type, one of the group members creates the session keys and sends them securely to the rest of the parties participating in the session. The transfer process must be confidential and honest through secret transmission channels. The person responsible for generating this key may be either a person belonging to the group or a trusted third party (TTP) that chooses keys instead of subscribers [17].

2. Group Key Exchange/Agreement

In this type, the shared key is generated through the participation of more than one party in its derivation, so the key information is shared so that the value of these keys cannot be predetermined. Therefore, all members must interact with each other in order to calculate this value [17, 18]. The table 7shows some of the models used in the analysis of mass protocols [19, 20].

Table 8-Example protocol for each model.

Model	Type Key Exchange	Protocol Example
BR93	Two-Party Key Exchange	Diffie and Hellman
BR95	Three-Party Key Exchange	Joux
BPR2000	Two-Party Key Exchange	Diffie and Hellman

BWM	Two-Party Key Exchange	Diffie and Hellman
BWJM	Two-Party Key Exchange	Diffie and Hellman
BCK98	Two-Party Key Exchange	Diffie and Hellman
CK01	Two-Party Key Exchange	Diffie and Hellman
HMQV	Two-Party Key Exchange	Diffie and Hellman
MU08	Two-Party Key Exchange	Diffie and Hellman
eCKw	Two-Party Key Exchange	Diffie and Hellman
eCK-PFS	Two-Party Key Exchange	Diffie and Hellman
seCK	Two-Party Key Exchange	Diffie and Hellman
BAFL-eCK	Two-Party Key Exchange	Diffie and Hellman
CAFL-eCK	Two-Party Key Exchange	Diffie and Hellman
BCPQ	Group Key Exchange	(Burmester and Desmedt), (Steiner, Tsudik, and Waidner)
BCP	Group Key Exchange	(Ateniese, Steiner, and Tsudik), (Barua, Dutta, and Sarkar)
BCP+	Group Key Exchange	Lee, Kim, Kim, and Ryu
KS	Group Key Exchange	Ingemarsson, Tang, and Wong
UC-KS	Group Key Exchange	Ateniese, Steiner, and Tsudik
BVS	Group Key Exchange	Becker and Wille

TABLE 9- Compression between models from where queries.

Models	Send	Reveal	State Reveal	Corrupt	Test
BR93	Yes	Yes	No	Yes	Yes
BR95	Yes	Yes	No	Yes	Yes
BPR2000	Yes	Yes	No	No	Yes
BWM	Yes	Yes	No	Yes	No
BWJM	Yes	Yes	No	Yes	No
BCK98	Yes	Yes	No	Yes	No
CK01	Yes	Yes	Yes	Yes	Yes
HMQV	Yes	Yes	Yes	No	Yes
MU08	Yes	Yes	No	No	Yes
eCKw	Yes	Yes	No	No	Yes
eCK-PFS	Yes	Yes	No	No	Yes
seCK	Yes	Yes	No	No	Yes
BAFL-eCK	Yes	Yes	No	Yes	No
CAFL-eCK	Yes	Yes	No	Yes	No
BCPQ	Yes	Yes	No	Yes	Yes
BCP	Yes	No	No	Yes	Yes
BCP+	Yes	Yes	No	Yes	Yes
KS	Yes	Yes	Yes	Yes	Yes

Models	Send	Reveal	State Reveal	Corrupt	Test
BR93	Yes	Yes	No	Yes	Yes
BR95	Yes	Yes	No	Yes	Yes
BPR2000	Yes	Yes	No	No	Yes
BWM	Yes	Yes	No	Yes	No
BWJM	Yes	Yes	No	Yes	No
BCK98	Yes	Yes	No	Yes	No
CK01	Yes	Yes	Yes	Yes	Yes
HMQV	Yes	Yes	Yes	No	Yes
MU08	Yes	Yes	No	No	Yes
eCKw	Yes	Yes	No	No	Yes
eCK-PFS	Yes	Yes	No	No	Yes
seCK	Yes	Yes	No	No	Yes
BAFL-eCK	Yes	Yes	No	Yes	No
CAFL-eCK	Yes	Yes	No	Yes	No
BCPQ	Yes	Yes	No	Yes	Yes
BCP	Yes	No	No	Yes	Yes
BCP+	Yes	Yes	No	Yes	Yes
KS	Yes	Yes	Yes	Yes	Yes

TABLE 10- Description of group key exchange models

Models	Definition	Powerful	Drawbacks
Model by Bresson, Chevassut, Pointcheval, and Quisquater (BCPQ)	The first protocol designed for collective key exchange protocols is the opposite of previous models that occur between two parties. Includes an expansion of the BR methodology	It allows the opponent to send multiple queries to the Oracle and reveal the session key and long-term suggestion Using this adversarial setting the. The partnering in BCPQ model depends on two security goals, authenticated key exchange (AKE) and mutual authentication.	1. there are GKE protocols that enable an active adversary to be able to impersonate a participant through an oracle. 2. The second problem is the GKE protocols that accept each subscriber's Id hash when there are no more than two participants in the session. 3. this models that depend on the exchange of conversations is that they only become available after the implementation of the protocol.
Models by Bresson, Chevassut, and Pointcheval (BCP)	It is an expansion of the BCPQ model, with additional property to deal with dynamic group key exchange protocols. During the execution of the protocol, the group membership can be change, this property makes the adversary confused.	Use queries, Setup, Join, and Remove. The BCP model defines AKE-security and MA-security as in the BCPQ model.	similar to those in BCPQ model concerning the security of the protocol against attacks.
Models by Bresson, Chevassut, and Pointcheval (BCP+)	This model overcomes the weaknesses in the previous model, to get the strongest security against the opponent attacks	1. Using secure coprocessor and smart card has been used where the relevant internal state information is stored and saved in the secure coprocessor, and the long-lived keys of participants are stored within a smart card. 2. BCP+ model defines two types of forward secrecy, first type is weak forward secrecy (wfs), which is a weak corruption model that all BCP model's queries can be used by the adversary as well as Send, Sends, and Corrupts queries.	Expensive in terms of time and cost
Models by Katz and Shin (UC-KS)	Describing the implementation of the ideal protocol. In each model, security proofs are used to prove its characteristics.	These proofs in this model are based on the simulation approach (the opponent's inability to distinguish) while the rest of the models depend on the reductionist approach. Katz and Shin suggested a compiler to convert any GKE protocol which is secure in the BCPQ model into a protocol that is secure in their UC-	1. main problem is that Katz and Shin have not provided reductive evidence that this compiler is capable of counteracting internal attacks that are specific in their model.

		based model and provided simulatability/indistinguishability-based security proofs for this case	This leaves the field open for an answer to find out whether the definitions of the agreement it contains and the security against the opponent who impersonates the identity from within in their mathematical model is sufficient to build reductionist security proofs. 2. This model is that the definitions for this model were not strong enough due to a lack of consideration of the issues related to key control and contributive.
Model by Bohli, Vasco, and Steinwandt (BVS)	New model but rather a development of the BCPQ model by Katz and Yung. To achieve integrated security protocols against strong hostile attacks.	this model is its focus on two objectives, the first of which should not provide the ability for the opponent to distinguish between the session key and the random values that the oracle returns, as well as the focus on forward secrecy to build an integrated secure session for all participants in the session. Its second goal is to provide strong authentication that allows undamaged people who have the same session ID and session key.	1. The opponent must adhere to a certain formula π_(i,j)^s that is not uncorrupted by which the session key is calculated and the extent of its influence on it. Because the opponent does not have enough freedom to choose that formula at the attack stage. 2. The opponent in this form cannot detect the internal parameters of the oracle (strong corruption). 3. There is no clarity in defining the algorithm xk in the sense of criteria by which people can distinguish between the real key generated during the implementation of the protocol and the random key affected by the adversary.

7. Conclusion

In this paper, we have referred to protocols, their types and objectives, as well as mutual authentication, and the most prominent methods used for authentication and encryption. Providing a secure connection has become a necessary and urgent need at the present time, so it is necessary to prove the security of the protocols used in communication before applying them. In this paper, we discussed the oldest and

most recent models, especially in protocols that contain a large number of participants in the communication (session). For each model there are advantages and disadvantages that led to the emergence of other models, where it turns out that the strongest model is BCP+. It provides powerful information to the attacker but is costly in terms of computation and time. The model must be used according to the protocol produced. For each protocol, there are characteristics, for example, two, three or more parties, and the appropriate model is determined for them.

REFERENCES

[1] K.-K. R. Choo, C. Boyd, and Y. Hitchcock, "Errors in Computational Complexity Proofs for Protocols", In Advances in Cryptology – ASIACRYPT'05, volume 3788 of Lecture Notes in Computer Science, pages 624–643. Springer, (2005, December).

[2] C. Boyd, A. Mathuria, and D. Stebila, "Protocols for authentication and key establishment", (Vol. 1), Heidelberg: Springer, 2003.

[3] M. Bellare, D. Pointcheval, and P. Rogaway, "Authenticated key exchange secure against dictionary attacks", In International conference on the theory and applications of cryptographic techniques, (pp. 139-155). Springer, Berlin, Heidelberg, (2000, May).

[4] D. K. Kala, and V. Sharma, "Public Key Encryption Algorithm and the Random Oracle", 2009.

[5] S. A. Kurtz, S. R. Mahaney, and J. S. Royer, "Average dependence and random oracles" University of Arizona, Department of Computer Science, 1991.

[6] C. Boyd, K. K. R. Choo, and A. Mathuria, "An extension to Bellare and Rogaway (1993) model: resetting compromised long-term keys", In Australasian Conference on Information Security and Privacy (pp. 371-382). Springer, Berlin, Heidelberg, (2006, July).

[7] K. K. R. Choo, and Y. Hitchcock, "Security requirements for key establishment proof models: Revisiting Bellare–Rogaway and Jeong–Katz–Lee protocols", In Australasian Conference on Information Security and Privacy (pp. 429-442). Springer, Berlin, Heidelberg, (2005, July).

[8] M. A. Alia, A. A. Tamimi, and O. N. AL-Allaf, "Cryptography based authentication methods", In Proceedings of the World Congress on Engineering and Computer Science (Vol. 1), 2014.

[9] V. Shoup, "Sequences of Games: A Tool for Taming Complexity in Security Proofs", Cryptology ePrint Archive, Report 2004/332, 2004. http://eprint.iacr.org/ 2004/332.pdf. 42, 59, 60, 206, 209.

[10] K. K. R. Choo, C. Boyd, and Y. Hitchcock, "Examining Indistinguishability-Based Proof Models for Key Establishment Protocols", In Advances in Cryptology – ASIACRYPT'05, volume 3788 of Lecture Notes in Computer Science, pages 585–604. Springer, 2005. 69, 72, 78.

[11] K. K. R. Choo, "A proof of revised Yahalom protocol in the Bellare and Rogaway (1993) model", The Computer Journal, 50(5), 591-601, 2007.

[12] C. Cremers, "Examining indistinguishability-based security models for key exchange protocols: the case of CK, CK-HMQV, and eCK", In Proceedings of the 6th ACM Symposium on Information, Computer and Communications Security (pp. 80-91), (2011, March).

[13] X. Jinyue, W. Jiandong, F. Liming, R. Yongjun, and B. Shizhu, "Formal Proof of Relative Strengths of Security between ECK2007 Model and other Proof Models for Key Agreement Protocols", *Cryptology ePrint Archive*, 2008.

[14] J. Alawatugoda, D. Stebila, and C. Boyd, "Modelling after-the-fact leakage for key exchange (full version)", In Proceedings of the 9th ACM symposium on Information, computer and communications security, (pp. 207-216), (June, 2014).

[15] J. Katz and M. Yung, "Scalable Protocols for Authenticated Group Key Exchange", In Advances in Cryptology - CRYPTO'03, volume 2729 of Lecture Notes in Computer Science, pages 110–125. Springer, 2003. 13, 37, 42, 48, 80, 82, 83, 85, 99, 100, 101, 102, 103, 109, 110, 111, 116, 129, 130.

[16] E. Bresson, O. Chevassut, and D. Pointcheval, "Dynamic group Diffie-Hellman key exchange under standard assumptions" In International conference on the theory and applications of cryptographic techniques (pp. 321-336). Springer, Berlin, Heidelberg., (2002, April).

[17] E. Bresson, O. Chevassut, and D. Pointcheval, "Provably authenticated group Diffie-Hellman key exchange—the dynamic case", In International Conference on the Theory and Application of Cryptology and Information Security (pp. 290-309). Springer, Berlin, Heidelberg, (2001, December).

المؤتمر العلمي الدولي الثالث عشر
لجمعية الرياضيات العراقية والمنعقد تحت شعار
نحو عالم متقدم : الرياضيات والتقنيات في سباق الابتكار
للمدة 24 - 25 نيسان 2024
الكوفة – النجف الاشرف

Static scope

Estimating the Gini index from Beta-Normal distribution

Waleed Ahmed Hassen Al-Nuaami

purecomp.waleed.hassan@uodiyala.edu.iq

Department of Biology, College of Education for Pure Sciences, University of Diyala

Abstract

This paper introduces the idea for estimating the Gini index from the beta-normal distribution. The value of the Gini coefficient depends depend on the value of the parameters. By comparing the results obtained from the simulated Gini coefficient, it can be concluded that in general, as the amount of sample size increases, the Gini coefficient increases. The results revealed that, when the amount of the coefficient is close to zero, it approaches the balance between the distribution of wealth and income in the society.

Keywords: Beta distribution; Cumulative distribution function; Gini coefficient; Normal distribution

1. Introduction

Various numerical indicators such as Solow's coefficient Soltow [1], Broun's coefficient of change [2], Theil's index [3], Atkinson's ratio [4], and Nelson's ratio [5] exist to express the inequality or variability of incomes among members of a given community. Indicators based on Lorenz curves, however, are among the most used indicators. The Gini coefficient is one of the most widely used indicators based on the Lorenz curve in measuring income inequality. The Gini coefficient is also used to study inequalities in health [6] and inequality over the lifetime of various age groups in tables [7] and [8]. Although some recent methods for estimation of variance have been developed, very common indicators such as the Gini coefficient are employed, for comparative purposes and trend analysis without taking the sampling changes into account, because point estimates can be easily obtained through these coefficients.

The Gini coefficient which can be achieved from the Gini Mean Difference [9] is widely regarded as one of the most well-known income inequality measurement methods. The Gini coefficient is also shown in the area between the 45° line and the Lorenz curve. The Lorenz curve proposed by Lorenzo [10] is another method of measuring the inequality. The Gini coefficient of zero (line 45 degrees) represents a perfect equality, so that all values are equal (for example, everyone has the same income), while the Gini coefficient of one (or 100) represents the maximum inequality between values (For example, among many people, only one is capitalist, while the rest do not have any income, in this case

the Gini coefficient will be close to 1). The existence of widespread inequalities in income distribution leads to poverty and increases in its domestic level, as well as growing class gaps in societies. The income distribution describes the degree of inequality in individuals' income within a country. The phenomenon of income inequality is not only a major cause of poverty in developing countries, but also slows down the economic growth. Hence, discussions and judgments about the reciprocal effects of economic growth and income distribution along with the expansion of growth models are so important.

In statistics, there are many distributions that are used to model the distribution of random variables, but among all probability distributions, continues distributions with non-negative values that are generally skewed, are used to model income distributions. As few economic characteristics, such as income, take just non-negative values, it is necessary to use distributions which work with just positive values. In this regard, generalized distributions are used as families of such high-flexibility distributions to examine these economic characteristics. generalized beta distribution is located at the head of these distributions.

Several papers have made valuable contributions to the understanding of income distribution and economic inequality. Sarabia and Castillo (2005) [11] focus on max-stable families and their applications to income distributions, highlighting their significance in modeling extreme events.

.

2. Gini Coefficient and beta-normal Distribution

2.1 ***Gini Coefficient***

The Gini coefficient is derived from the name Gini [19]–[21]. In the past years, the Gini coefficient has gradually become the main indicator of inequality in the economy. Statisticians use this index in many empirical studies and political research.

Anand [22] and Chakravarty [23] provided understandable research on the inequality measure that included the Gini coefficient. Other authors, such as Lambert [24], Silber [25], Atkinson and Bourguignon [26], provided understandable references to income inequality and poverty using a Gini coefficient as a measure of inequality. The Gini coefficient is used to measure the dispersion of income distribution, consumption distribution, distribution of wealth or distribution of other types of economic indicators.

Gini coefficient has different forms and interesting interpretations. For example, it can be expressed as the ratio of the two regions defined by the 45° line and the Lorenz curve in a single unit, as the different mean Gini function, as the covariance between earnings and their ranks, or as a particular type of matrix form.

The Gini index is one of the most common statistical indicators of diversity and inequality to measure the distribution of dispersion in Allison's sociology and social sciences. Furthermore, the Gini index is widely used in econometrics as a standard measure of inequality between individuals or between individuals in terms of income and wealth; Atkinson [4], Sen [27] and Anand [22].

The Gini coefficient is a complex inequality criterion that measures the inequality through the Lorenz curve. Figure (1) shows the Lorenz curve defined on (0,1) and continuously increases from (0, 0) to (1, 1).

To draw the Lorenz diagram, data are ranked from small to large, and then their cumulative distributions are calculated and finally are put against the cumulative ratio. In the Lorenz curve, the Gini coefficient (G) is the area between the Lorenz curve and the steady gradient.

$$G = \frac{A}{A+B} = 2A = 1 - 2B$$

It ranges from 0, in which all measurements are equal and represents perfect equality to $\frac{n-1}{n}$, with n representing a sample size and all measurements except one is 0. For a large sample, the final value of 1 represents the maximum possible inequality. Full reviews of the Gini coefficient can be found in Gini [21] and Bellu and Liberati [28].

The concept of the Gini index or "Gini coefficient" is closely related to the concept of the Lorenz curve. The Gini coefficient is a number between zero and one equal to the "enclosed area" between the Lorenz curve and the "perfect equality distribution line". Whenever resources and wealth of a society are distributed "quite fair" among all individuals, Lorenz curve reaches to "perfect equality line", and the Gini coefficient becomes zero. Conversely, in the case of an "absolutely unequal distribution of wealth" in a society or absolute monopoly (all the wealth of the community is handed to one person, while others have a zero-sum wealth), the Gini coefficient will be equal to one.

2.2 Beta-Normal Distribution

Eugene et al. [29] presented the beta-normal distribution by combining the beta distribution and the normal distribution. This distribution extends the normal distribution and offers more versatility in terms of its shapes, making it applicable to various scenarios. Subsequently, numerous authors have generalized similar distributions to the beta-normal.

Beta-normal distribution with parameters $\alpha > 0,\ \beta > 0,\ \mu \in \mathbb{R},\ \sigma > 0$, the probability density function (pdf) is given as follows:

$$f(x) = \frac{1}{B(\alpha,\beta)}\left[\Phi\left(\frac{x-\mu}{\sigma}\right)\right]^{\alpha-1}\left[1-\Phi\left(\frac{x-\mu}{\sigma}\right)\right]^{\beta-1}\sigma^{-1}\phi\left(\frac{x-\mu}{\sigma}\right), x \in \mathbb{R}$$

In this regard, $\Phi(.)$ and $\phi(.)$ are respectively cumulative distribution function and density function of the probability of standard normal distribution, and $B(.,.)$ is a Beta function. α and β are shape parameters that describe skewness, kurtosis, and bimodal state of equation (1). μ is a location parameter and σ is a scale parameter which indicates the amount of expansion and contraction of the shape. Beta-Normal distributions can be unimodal or bimodal to skew distributions.

A category of generalized Beta distribution were first introduced from its cumulative distribution function by [30]. Cumulative distribution function of a category of generalized beta distributions is defined using the following function:

$$F(x) = \frac{1}{B(\alpha,\beta)} \int_0^{G(x)} t^{\alpha-1}(1-t)^{\beta-1} dt, \alpha > 0, \beta > 0$$

where, $G(x)$ is a cumulative distribution function of a family of random variables, and $B(\alpha,\beta) = \int_0^1 x^{\alpha-1}(1-x)^{\beta-1}dx.$

Barreto et al. [31], presented an important extension to beta Frechet (BF) distribution to conclude some general properties of this category. Suppose that, β is a real non integer number and $|x| < 1$. Consider the extension of power series as follows:

$$(1-x)^{\beta-1} = \sum_{j=0}^{\infty} \frac{(-1)^j \Gamma(\beta)}{\Gamma(\beta-j)j!} x^j . \beta$$

As a result, the incomplete beta function can be expressed as follows:

$$B_x(\alpha,\beta) = x^{\alpha} \sum_{j=0}^{\infty} \frac{(-1)^j \Gamma(\beta) x^j}{\Gamma(\beta-j)j!\,(j+\alpha)}$$

In the above formula, $\beta - 1$ will be the upper limit of j, if β is defined as an integer. Defining the constant,

$$w_j(\alpha,\beta) = \frac{(-1)^j \Gamma(\beta)}{\Gamma(\beta-j)j!\,(j+\alpha)}$$

and using the relations (3) and (4), the cumulative distribution function of the β-Gamma distribution is expressed as follows:

$$F(x) = \frac{1}{B(\alpha,\beta)} \sum_{r=0}^{\infty} w_r(\alpha,\beta) G(x)^{\alpha+r}$$

Deriving (5), $f(x)$ is extended as follows:

$$f(x) = \frac{1}{B(\alpha,\beta)} g(x) \sum_{r=0}^{\infty} (\alpha+r) w_r(\alpha,\beta) [G(x)]^{\alpha+r-1} \qquad (6)$$

Using the relation (2) twice, the expansion $[G(x)]^{\alpha}$ for non-integer α, is obtained as follows:

$$G(x)^{\alpha} = \Big(1 - \big(1 - G(x)\big)\Big)^{\alpha} = \sum_{j=0}^{\infty} \frac{(-1)^j \Gamma(\alpha+1)}{\Gamma(\alpha-j+1)j!} \big(1 - G(x)\big)^j$$

$$= \sum_{j=0}^{\infty} \sum_{r=0}^{j} \frac{(-1)^{j+r} \Gamma(\alpha+1)}{\Gamma(\alpha-j+1)(j-r)!\, r!} \big(G(x)\big)^r$$

$$= \sum_{j=0}^{\infty} \sum_{r=0}^{\infty} \frac{(-1)^{j+r} \Gamma(\alpha+1)}{\Gamma(\alpha-j+1)(j-r)!\, r!} \big(G(x)\big)^r$$

We assume that

$$S_r(\alpha) = \sum_{j=r}^{\infty} \frac{(-1)^{j+r} \Gamma(\alpha+1)}{\Gamma(\alpha-j+1)(j-r)!\, r!}$$

Consequently, using relation (8), the extension (7) is expressed as follows:

$$G(x)^{\alpha} = \sum_{r=0}^{\infty} S_r(a) (G(x))^r$$

If α is not an integer, then the equation (9) of the distribution function (5) can be obtained as follows:

$$F(x) = \frac{1}{B(\alpha,\beta)} \sum_{r=0}^{\infty} t_r(\alpha,\beta) G(x)^r$$

where $t_r(\alpha,\beta) = \sum_{l=0}^{\infty} w_l(\alpha,\beta) s_r(\alpha+l)$. By a simple derivation of (10), an extension $f(x)$ for a non-integer number, α is as follows:

$$f(x) = \frac{1}{B(\alpha,\beta)} g(x) \sum_{r=0}^{\infty} (r+1) t_{r+1}(\alpha,\beta) G(x)^r. \qquad (11)$$

The purpose of this period is to formulate a density expansion, when an integer α is unstable to obtain power series with $G(x)$, which is expressed only for the correct powers. This proposition follows the main result of the paper [32].

In general, exacting first moments of a beta-normal distribution cannot be obtained. However, for some selected values of α and β, some exact first moments are obtained which are shown in the Table 2.1 [33].

Table 2.1: Exact first moments of a beta-normal for some values of α and β

β	α	μ_{BN}	σ_{BN}	Skewne	Kurtos	Shape
0.05	0.05	0.000	5.948	0.000	2.209	Bimoda
	0.10	2.285	4.881	-0.088	2.422	Bimoda
	0.20	3.689	4.045	0.002	2.749	Unimod
	0.50	4.652	3.395	0.296	3.004	Unimod
	1.00	5.034	3.147	0.477	3.117	Unimod
	10.00	5.701	2.798	0.747	3.417	Unimod
	100.00	6.162	2.616	0.872	3.655	Unimod
0.10	0.05	-2.289	4.881	0.088	2.422	Bimoda
	0.10	0.000	4.032	0.000	2.352	Bimoda
	0.20	1.658	3.295	0.020	2.555	Unimod
	0.50	2.763	2.614	0.188	2.889	Unimod
	1.00	3.263	2.322	0.401	3.067	Unimod
	10.0	4.133	1.915	0.784	3.546	Unimod
	100.00	4.707	1.725	0.956	3.922	Unimod
0.20	0.05	-3.689	4.045	-0.002	2.749	Unimod
	0.10	-1.658	3.295	0.020	2.555	Unimod
	0.20	0.000	2.679	0.000	2.558	Bimoda
	0.50	1.340	2.054	0.108	2.811	Unimod
	1.00	1.955	1.748	0.300	3.018	Unimod
	10.0	3.048	1.303	0.776	3.659	Unimod
	100.00	3.741	1.116	0.997	4.182	Unimod
0.50	0.05	-04.652	3.395	-0.296	3.004	Unimod
	0.10	-2.763	2.614	-0.188	2.889	Unimod
	0.20	-1.340	2.054	-0.108	2.811	Unimod
	0.50	0.000	1.525	0.000	2.861	Unimod
	1.00	0.704	1.247	0.137	2.983	Unimod
	10.0	2.080	0.803	0.617	3.573	Unimod
	100.00	2.930	0.631	0.877	4.154	Unimod
1.00	0.05	-5.034	3.147	-0.477	3.117	Unimod
	0.10	-3.362	2.322	-0.401	3.067	Unimod
	0.20	-1.955	1.748	-0.300	3.018	Unimod
	0.50	-0.704	1.247	-0.137	2.983	Unimod
	1.00	0.000	1.000	0.000	3.000	Unimod
	10.0	1.538	0.586	0.409	3.331	Unimod
	100.00	2.057	0.429	0.655	3.765	Unimod
10.0	0.05	-5.701	2.798	-0.747	3.417	Unimod

	0.10	-4.133	1.915	-0.784	3.546	Unimod
	0.20	-3.048	1.303	-0.776	3.659	Unimod
	0.50	2.080	0.803	-0.617	3.573	Unimod
	1.00	-1.538	0.586	-0.409	3.331	Unimod
	10.0	0.000	0.284	0.000	3.013	Unimod
	100.00	1.354	0.169	0.1303	3.043	Unimod
100.0	0.05	-6.162	2.616	-0.872	3.655	Unimod
	0.10	-4.707	1.725	-0.956	4.182	Unimod
	0.50	-2.930	0.631	-0.877	4.154	Unimod
	1.00	-2.507	0.429	-0.655	3.765	Unimod
	10.0	-1.354	0.169	-0.130	3.043	Unimod
	100.00	0.000	0.088	0.000	3.001	Unimod

From Table 2.1, we can see that the shape of the beta-normal distribution would be left skewed, symmetric or right skewed, unimodal or bi-modal depends on the values of the parameters α and β. For example, if $\alpha < \beta$, then the shape of beta-normal will be left skewed, if $\alpha = \beta$, then the shape of beta-normal will be left symmetric, and if $\alpha > \beta$, then the shape of beta-normal will be right skewed.

2.4 Calculate the Gini coefficient of the beta-normal distribution.

To compare income distribution inequality, various indices are used, many of which are derived from the Lorenz curve. However, the classic Gini coefficient and its variations are commonly used to measure income inequality. In this section, the Gini coefficient will be obtained for the beta-normal distribution. The Gini coefficient can be calculated directly from the cumulative distribution function $F(x)$. While the $F(x)$ is zero for all negative values and μ represents the mean distribution, so the Gini coefficient is equal to:

$$G = 1 - \frac{1}{\mu}\int_0^{\infty}\big(1 - F(x)\big)^2 dx = \frac{1}{\mu}\int_0^{\infty} F(x)\big(1 - F(x)\big)dx. \qquad 2(1$$

to calculate the Gini coefficient for the beta-normal distribution with the cumulative distribution function (5) for integers α and β.

$$\int_0^{\infty} F(x)dx = \frac{1}{B(\alpha,\beta)}\sum_{j=0}^{\infty}\frac{(-1)^j\Gamma(\beta)}{\Gamma(\beta-j)j!}\frac{1}{(\alpha+j)}\int_0^{\infty} G(x)^{\alpha+j}dx \qquad 3(1$$

Since $G(x)$ is a cumulative normal distribution function, we have,

$$\int_0^{\infty} G(x)^{\alpha+j}dx = \int_0^{\infty}\{\Phi(\frac{x-\mu}{\sigma})\}^{\alpha+j}dx. \qquad 4(1$$

By placing $z = \frac{x-\mu}{\sigma}$, $dx = \sigma dz$ and applying binomial expansion we have,

$$\int_0^\infty G(x)^{\alpha+j} dx = \sigma \int_0^\infty \{\Phi(z)\}^{\alpha+j}\, dz = \sigma \sum_{k=0}^{\alpha+j} (-1)^k \binom{\alpha+j}{k} \int_0^\infty \{1-\Phi(z)\}^k$$

$$= \sigma \sum_{k=0}^{\alpha+j} (-1)^k \binom{\alpha+j}{k} \delta_k \qquad 5(1$$

From the relations (13) and (14), the relation (12) is obtained as follows:

$$\int_0^\infty F(x)dx = \frac{\sigma}{B(\alpha,\beta)} \sum_{j=0}^{\beta-1} \frac{(-1)^j \Gamma(\beta)}{\Gamma(\beta-j)j!} \frac{1}{(\alpha+j)} \sum_{k=0}^{\alpha+j} (-1)^k \binom{\alpha+j}{k} \delta_k \qquad 18)$$

To get $\int F(x)^2\, dx$:

$$F(x)^2 = \left[\frac{1}{B(\alpha,\beta)} \sum_{j=0}^{\beta-1} \frac{(-1)^j \Gamma(\beta)}{\Gamma(\beta-j)j!} \frac{G(x)^{\alpha+j}}{(\alpha+j)}\right]\left[\frac{1}{B(\alpha,\beta)} \sum_{l=0}^{\beta-1} \frac{(-1)^l \Gamma(\beta)}{\Gamma(\beta-l)l!} \frac{G(x)^{\alpha+j}}{(\alpha+l)}\right]$$

$$= \frac{1}{B(\alpha,\beta)^2} \sum_{j=0}^{\beta-1} \sum_{l=0}^{\beta-1} \frac{(-1)^{j+l} \Gamma(\beta)^2}{\Gamma(\beta-j)\Gamma(\beta-l)j!\, l!} \frac{G(x)^{2\alpha+j+l}}{(\alpha+j)(\alpha+l)} \int_0^\infty F(x)^2 dx$$

$$= \frac{1}{B(\alpha,\beta)^2} \sum_{j=0}^{\beta-1} \sum_{l=0}^{\beta-1} \frac{(-1)^{j+l} \Gamma(\beta)^2}{\Gamma(\beta-j)\Gamma(\beta-l)j!\, l!} \frac{1}{(\alpha+j)(\alpha+l)} \int_0^\infty G(x)^{2\alpha+j+l}\, dx$$

$$= \frac{\sigma}{B(\alpha,\beta)^2} \sum_{j=0}^{\beta-1} \sum_{l=0}^{\beta-1} \frac{(-1)^{j+l} \Gamma(\beta)^2}{\Gamma(\beta-j)\Gamma(\beta-l)j!\, l!} \frac{1}{(\alpha+j)(\alpha+l)} \int_0^\infty \{\Phi(z)\}^{2\alpha+j+l}\, dz$$

$$= \frac{\sigma}{B(\alpha,\beta)^2} \sum_{j=0}^{\beta-1} \sum_{l=0}^{\beta-1} \frac{(-1)^{j+l} \Gamma(\beta)^2}{\Gamma(\beta-j)\Gamma(\beta-l)j!\, l!} \frac{1}{(\alpha+j)(\alpha+l)} \sum_{m=0}^{2\alpha+j+l} (-1)^m \binom{2\alpha+j+l}{m} \int_0^\infty \{1 - \Phi(z)\}^m\, dz$$

From the relation (13) we have,

$$\int_0^\infty \{1-\Phi(z)\}^m\, dz = \delta_m$$

so,

$$\int_0^{\infty} F(x)^2 dx$$
$$= \frac{\sigma}{B(\alpha,\beta)^2} \sum_{j=0}^{\beta-1} \sum_{l=0}^{\beta-1} \sum_{m=0}^{2\alpha+j+l} \frac{(-1)^{j+l+m}\Gamma(\beta)^2}{\Gamma(\beta-j)\Gamma(\beta-l)j!\, l!\, (\alpha+j)(\alpha+l)} \binom{2\alpha+j+l}{m} \delta_m \quad (19)$$

By placing the relationships (12) and (18) and (19) in (14), the Gini coefficient for the beta-normal distribution is obtained as follows,

$$G = \frac{1}{\mu}\int_0^{\infty} (F(x) - F(x)^2)dx = \frac{\frac{\sigma}{B(\alpha,\beta)} \sum_{j=0}^{\beta-1} \frac{(-1)^j \Gamma(\beta)}{\Gamma(\beta-j)j!} \frac{1}{(\alpha+j)} M}{\mu + \frac{\sigma}{B(\alpha,\beta)} T}$$

where

$$M = \sum_{k=0}^{\alpha+j} (-1)^k \binom{\alpha+j}{k} \delta_k - \frac{1}{B(\alpha,\beta)} \sum_{l=0}^{\beta-1} \sum_{m=0}^{2\alpha+j+l} \frac{(-1)^{l+m}\Gamma(\beta)}{\Gamma(\beta-l)l!\,(\alpha+l)} \binom{2\alpha+j+l}{m} \delta_m$$

and

$$T = \sum_{j=0}^{\beta-1} \left\{ \sum_{k=0}^{\alpha+j-2} \frac{(-1)^{j+k}}{(k+1)} \binom{\beta-1}{j} \binom{\alpha+j+l}{k} \delta_{k+1} + \frac{(-1)^{\alpha-1} - (-1)^j}{\alpha+j} \binom{\beta-1}{j} \delta_{\alpha+j} \right\}.$$

3. Simulation Study

Using software R, we have conducted a simulation study in this section. The Gini coefficient of the beta-normal distribution for various parameters, α, β, μ and σ for 10, 20, 30, 35, 50, and 100 samples with 100000 iterations, was calculated continuously, then it was compared to the actual Gini coefficient of the beta-normal distribution calculated in Maple software. The simulation results are summarized in the Table 3.1. In Table 3.1, we have two Gini coefficients, (i) the simulation of the beta-normal distribution in which the parameters of the beta-normal distribution have been estimated and (ii) the population Gini coefficient of the beta-normal distribution. By comparing the results obtained from the real and simulated Gini coefficients using R and Maple software respectively, it can be concluded that in general, as the amount of sample size increases, the Gini coefficient also increases, plus the value of the Gini coefficient depends on the value of the parameters. Table 3.1 points out that as the Gini coefficient is between 0 and 1, it cannot be calculated when the mean of the beta-normal is 0 or negative. As we mentioned above, when the amount of the coefficient is close to zero, it approaches the balance between the distribution of wealth and income in the society. These results can be obtained for any distribution of the combination.

Table 3.1: The actual Gini coefficient of the beta-normal distribution

α	β	μ	σ	n	Gini S	Mse	Bias	Gini R
1	0.5	0.7	1.25	10	0.26681	0.0000	0.0017	0.2685

				20	0.3546	0.0074	0.0861	
				30	0.3951	0.0160	0.1266	
				35	0.4242	0.0243	0.1558	
				50	0.5730	0.0927	0.3045	
				100	0.8563	0.3455	0.5878	
2	1	0	1	10	0.2597	0.0323	0.1796	0.4393
				20	0.3454	0.0088	0.0940	
				30	0.4358	0.0000	0.0035	
				35	0.5500	0.0122	0.1107	
				50	0.6502	0.0445	0.2109	
				100	0.8458	0.1652	0.4065	
4	1	0	1	10	0.1222	0.0527	0.2295	0.3517
				20	0.2693	0.0068	0.0823	
				30	0.3223	0.0009	0.0293	
				35	0.2119	0.0195	0.1398	
				50	0.3905	0.0015	0.0388	
				100	0.6593	0.0947	0.3077	
5	1	1	1	10	0.1619	0.0001	0.0118	0.1737
				20	0.1929	0.0004	0.0192	
				30	0.1579	0.0002	0.0158	
				35	0.2119	0.0015	0.0382	
				50	0.3369	0.0266	0.1632	
				10	0.3397	0.0276	0.1660	
1	2	1	1	20	0.2237	0.0450	0.2121	0.4358
				30	0.2617	0.0303	0.1741	
				35	0.5870	0.0229	0.1512	
				50	0.4123	0.0006	0.0235	
				100	0.5840	0.0219	0.1481	
				10	0.6687	0.0542	0.2329	
1	5	1	1	20	0.2094	0.0022	0.0470	0.2565
				30	0.2139	0.0018	0.0425	
				35	0.3528	0.0093	0.0964	
				50	0.3296	0.0053	0.0731	
				100	0.6683	0.1696	0.4118	
				10	0.7900	0.2846	0.5335	
3	2	0	1	20	0.2321	0.0327	0.1810	0.4131
				30	0.3368	0.0058	0.0763	

				35	0.2857	0.0162	0.1273	
				50	0.4711	0.0034	0.0581	
				100	0.5356	0.0150	0.1225	
				10	0.5399	0.0161	0.1268	
4	2	1	1	20	0.1460	0.0041	0.0638	0.2098
				30	0.1462	0.0040	0.0636	
				35	0.1203	0.0080	0.0895	
				50	0.1453	0.0042	0.0645	
				100	0.2055	0.0000	0.0043	
				10	0.2318	0.0005	0.0220	
2	3	1	1	20	0.1997	0.0320	0.1789	0.3786
				30	0.2308	0.0218	0.1478	
				35	0.2600	0.0141	0.1186	
				50	0.2792	0.0099	0.0994	
				100	0.4898	0.0124	0.1112	
					0.6976	0.1017	0.3190	

Continue Table 3.1

α	β	μ	σ	n	Gini S	Mse	Bias	Gini R
4	3	0	1.5	10	0.1988	0.0000	0.0028	0.2015
				20	0.2251	0.0006	0.0235	
				30	0.3103	0.0118	0.1088	
				35	0.4293	0.0519	0.2278	
				50	0.5985	0.1576	0.3969	
				100	0.6622	0.2122	0.4607	
2	4	1	1	10	0.0746	0.1120	0.3347	0.4093
				20	0.1740	0.0554	0.2353	
				30	0.2252	0.0339	0.1841	
				35	0.3363	0.0053	0.0730	
				50	0.4658	0.0032	0.0565	
				100	0.5741	0.0272	0.1648	
1	0.24	0	1	10	0.4037	0.0004	0.0208	0.4246
				20	0.5693	0.0209	0.1447	
				30	0.5496	0.0156	0.1251	
				35	0.6594	0.0552	0.2349	
				50	0.7079	0.0803	0.2833	

				100	0.7681	0.1180	0.3435	
0.5	1	0	1	10	0.5466	0.1613	0.4016	0.9482
				20	0.6001	0.1212	0.3481	
				30	0.6093	0.1148	0.3389	
				35	0.7154	0.0542	0.2328	
				50	1.0691	0.0146	0.1209	
1	0.5	0	1	10	0.3491	0.0071	0.0845	0.4336
				20	0.3771	0.0032	0.0565	
				30	0.5512	0.0138	0.1176	
				35	0.5910	0.0248	0.1574	
				50	0.7298	0.0878	0.2963	
				100	0.7635	0.1089	0.3300	
100	1	0	1	10	0.0509	0.0019	0.0441	0.0950
				20	0.0662	0.0008	0.0289	
				30	0.0709	0.0006	0.0241	
				35	0.0822	0.0002	0.0128	
				50	0.0836	0.0001	0.0114	
				100	0.0930	0.0000	0.0021	
10	0.5	0	1	10	0.1536	0.0037	0.0612	0.2149
				20	0.1837	0.0010	0.0311	
				30	0.2598	0.0020	0.0450	
				35	0.2864	0.0051	0.0715	
				50	0.3773	0.0264	0.1625	
				100	0.4800	0.0703	0.2652	
100	0.5	0	1	10	0.0506	0.0046	0.0679	0.1185
				20	0.0868	0.0010	0.0317	
				30	0.1415	0.0005	0.0231	
				35	0.1164	0.0000	0.0021	
				50	0.1131	0.0000	0.0053	
				100	0.1165	0.0000	0.0020	
1	0.2	0	1	10	0.3250	0.0078	-0.0884	0.4134
				20	0.3930	0.0004	-0.0204	
				30	0.4224	0.0001	0.0090	
				35	0.7870	0.1396	0.3736	
				50	0.8463	0.1875	0.4330	
				100	0.8652	0.2041	0.4518	

4. Some Concluding Remarks

The Gini index is one of the most common statistical indicators of diversity and inequality to measure the distribution of dispersion. There are many distributions in statistics that are used to model the income distributions. The four-parameter distribution is called beta-normal distribution, which is a generalization of normal distribution which is widely used to model the skewed distribution. This paper discusses the estimation of the Gini index from Beta-Normal distribution. To illustrate the findings of the paper, a simulation study has been conducted. From simulation results, it is concluded that in general, as the amount of sample size increases, the Gini coefficient increases. Moreover, the value of the Gini coefficient depends on the value of the parameters.

References

[1] L. Soltow, "Patterns of Wealthholding in Wisconsin since 1850," *(No Title)*, 1971.

[2] D. Braun, "Multiple measurements of US income inequality," *Rev. Econ. Stat.*, pp. 398–405, 1988.

[3] H. Theil, "Economics and information theory," *Econ. Inf. Theory*, vol. 7, 1967.

[4] A. B. Atkinson, "On the measurement of inequality," *J. Econ. Theory*, vol. 2, no. 3, pp. 244–263, 1970, doi: 10.1016/0022-0531(70)90039-6.

[5] J. I. Nelson, "Income inequality: the American states," *Soc. Sci. Q.*, vol. 65, no. 3, p. 854, 1984.

[6] R. Illsley and J. Le Grand, "The measurement of inequality in health," in *Health and Economics: Proceedings of Section F (Economics) of the British Association for the Advancement of Science, Bristol, 1986*, Springer, 1987, pp. 12–36.

[7] S. Anand, F. Diderichsen, T. Evans, V. M. Shkolnikov, and M. Wirth, "Measuring disparities in health: methods and indicators," *Challenging inequities Heal. from ethics to action*, pp. 49–67, 2001.

[8] V. M. Shkolnikov, E. E. Andreev, and A. Z. Begun, "Gini coefficient as a life table function: Computation from discrete data, decomposition of differences and empirical examples," *Demogr. Res.*, vol. 8, pp. 305–358, 2003, doi: 10.4054/demres.2003.8.11.

[9] C. Gini, "Variabilità e mutabilità Reprinted in Memorie di Metodologica Statistica ed E Pizetti and T Salvemini (Rome: Libreria Eredi Virgilio Veschi) Go to reference in article." 1912.

[10] M. O. Lorenz, "Methods of measuring the concentration of wealth," *Publ. Am. Stat. Assoc.*, vol. 9, no. 70, pp. 209–219, 1905.

[11] J. M. Sarabia and E. Castillo, "About a class of max-stable families with applications to income distributions," *Metron*, vol. 63, no. 3, pp. 505–527, 2005.

[12] Yan He, "A Review of Personal Income Distribution," *Adv. Stud. Theor. Appl. Econom.*, vol. 42, pp. 79–91, 2005, doi: 10.1007/0-387-24344-5_6.

[13] M. Langel and Y. Tillé, "Variance estimation of the Gini index: Revisiting a result several times published," *J. R. Stat. Soc. Ser. A Stat. Soc.*, vol. 176, no. 2, pp. 521–540, 2013, doi:

10.1111/j.1467-985X.2012.01048.x.

[14] S. Mirzaei, G. R. Mohtashami Borzadaran, M. Amini, and H. Jabbari, "A new generalized Weibull distribution in income economic inequality curves," *Commun. Stat. - Theory Methods*, vol. 48, no. 4, pp. 889–908, 2019, doi: 10.1080/03610926.2017.1422754.

[15] B. P. Singh and U. D. Das, "On an Induced Distribution and its Statistical Properties," pp. 1–14, 2020, [Online]. Available: http://arxiv.org/abs/2010.15078

[16] M. I. Ekum, O. M. Akinmoladun, and A. S. Ogunsanya, "Stochastic Modelling of COVID-19 Closed Cases in Nigeria Transactions of the Nigerian Association of Mathematical Physics STOCHASTIC MODELLING OF COVID-19 CLOSED CASES IN NIGERIA," no. February 2022, 2020.

[17] M. I. Ekum, M. O. Adamu, and E. E. Akarawak, "T-Dagum: A Way of Generalizing Dagum Distribution Using Lomax Quantile Function," *J. Probab. Stat.*, vol. 2020, 2020, doi: 10.1155/2020/1641207.

[18] N. Rasheed, "Topp-Leone Leone Dagum Distribution Distribution : Properties and its Applications," no. September 2019, 2021.

[19] C. Gini, *Variabilità e mutabilità: contributo allo studio delle distribuzioni e delle relazioni statistiche.[Fasc. I.]*. Tipogr. di P. Cuppini, 1912.

[20] C. Gini, "Sulla misura della concentrazione e della variabilità dei caratteri," *Atti del R. Ist. veneto di Sci. Lett. ed arti*, vol. 73, pp. 1203–1248, 1914.

[21] C. Gini, "Measurement of inequality of incomes," *Econ. J.*, vol. 31, no. 121, pp. 124–125, 1921.

[22] S. Anand, *Inequality and poverty in Malaysia: Measurement and decomposition*. The World Bank, 1983.

[23] S. R. Chakravarty, "Why Measuring Inequality by the Variance Makes Sense from a Theoretical Point of View," *J. Income Distrib.*, vol. 10, no. 3–4, p. 6, 2001.

[24] P. J. Lambert, "True Distribution and Redistribution of Income: A Mathematical Analysis." Basil Blackwell, 1989.

[25] J. Silber, "Factor components, population subgroups and the computation of the Gini index of inequality," *Rev. Econ. Stat.*, pp. 107–115, 1989.

[26] A. B. Atkinson and F. Bourguignon, "Introduction: Income distribution and economics," *Handb. income Distrib.*, vol. 1, pp. 1–58, 2000.

[27] A. Sen, *On economic inequality*. Oxford university press, 1997.

[28] L. G. Bellu and P. Liberati, "Inequality analysis: the gini index. EASYPol Module 40," *UN Food Agric. Organ. Rome*, 2006.

[29] N. Eugene, C. Lee, and F. Famoye, "Beta-normal distribution and its applications," *Commun. Stat. methods*, vol. 31, no. 4, pp. 497–512, 2002.

[30] F. Famoye, C. Lee, and N. Eugene, "Beta-normal distribution: Bimodality properties and application," *J. Mod. Appl. Stat. Methods*, vol. 3, no. 1, p. 10, 2004.

[31] W. Barreto-Souza, G. M. Cordeiro, and A. B. Simas, "Some results for beta Fréchet distribution," *Commun. Stat. Methods*, vol. 40, no. 5, pp. 798–811, 2011.

[32] L. C. Rêgo, R. J. Cintra, and G. M. Cordeiro, "On some properties of the beta normal distribution," *Commun. Stat. - Theory Methods*, vol. 41, no. 20, pp. 3722–3738, 2012, doi: 10.1080/03610926.2011.568156.

[33] R. C. Bose and S. S. Gupta, "Moments of order statistics from a normal population," *Biometrika*, vol. 46, no. 3/4, pp. 433–440, 1959.